

Gonçalo Fernando Ferreira de Sá

PHOTOACOUSTIC WAVES FOR TRANSDERMAL DRUG DELIVERY

2012



UNIVERSIDADE DE COIMBRA

Gonçalo de Sá



**PHOTOACOUSTIC WAVES FOR
TRANSDERMAL DRUG
DELIVERY**



Tese orientada por:

Luís Guilherme da Silva Arnaut Moreira

Universidade de Coimbra



Tese apresentada à Universidade de Coimbra
para obtenção do grau de Doutor em Química
na especialidade de Química Médica

Coimbra 2012

Aos meus pais, irmão e avó

O meu núcleo de vida...

À Lara

Pelo amor e perseverança...

Acknowledgments

A finalização dos estudos de doutoramento compreende um desafio intelectual que ultrapassa o esforço individual de um qualquer candidato. O rigor e trabalho exigidos para este fim ampliam e amadurecem a sua visão de Ciência, enquanto disciplina interdisciplinar do conhecimento humano. Com estas palavras agradeço a todas as pessoas que contribuíram para o meu caminho, enquanto homem de Ciência.

Ao Professor Doutor Luís G. Arnaut recupero as palavras de Thomas Huxley: “Um mundo de factos estende-se para além do mundo das palavras”. O seu contributo para o sucesso desta tese é inquestionável. As inúmeras discussões científicas definiram a minha visão de trabalhar, pensar e liderar. Não me ocorrem melhores elogios.

Ao Doutor Carlos Serpa atribuo um papel fulcral na orientação do meu doutoramento. Nos momentos decisivos dos desafios científicos, a visão analítica dos factos permitiu o atingir dos objectivos propostos. O meu reconhecimento para toda a vida.

Ao Professor Doutor Sebastião Formosinho relembro a pergunta que mudou a minha vida: “Existe um trabalho científico para realizar? Queres participar?”. A resposta a essa pergunta definiu um percurso de licenciatura, mestrado e doutoramento.

À Prof. Doutora Maria Minguéns Pereira e ao Doutor Sérgio Simões reconheço o papel determinante no início deste trajecto.

À Doutora Maria João Moreno agradeço a introdução no mundo dos processos biológicos e a possibilidade de iniciarmos a resolução de uma questão científica pertinente.

Aos meus colegas de laboratório, Elsa, Rui e Paulo Gomes, um muito obrigado pelo acolhimento e orientação nos detalhes laboratoriais.

Ao Renato Cardoso, Hélder Tão e aos meus primos Renata e Ivan, a minha apreciação pela amizade e revisão dos detalhes de inglês desta tese.

A toda a minha família (Pereira Ferreira e de Sá), aos amigos de Coimbra e Leiria reconheço-vos o contínuo apoio nesta etapa. O vosso contributo tornou possível...

À família Cabrita Pereira, um muito obrigado por me terem recebido e tratado excepcionalmente bem.

Um bem-haja a todos.

Table of Contents

Resumo.....	i
Abstract.....	iii
List of Patents, Book Chapters, Papers and Prizes.....	v
List of Abbreviations.....	vii
Definition of Terms.....	ix
List of Figures and Graphics.....	xi
List of Tables.....	xxiii
I. Objectives and Outline	1
1. Objectives.....	3
2. Outline.....	3
II. Essential Properties of Skin	5
1. Introduction.....	7
2. Skin Functions.....	7
3. Anatomy and Physiology of the Skin.....	8
3.1 Stratum Corneum.....	9
3.2 Epidermis.....	10
3.3 Dermis.....	13
4. Drug Diffusion Routes in the Skin.....	14
5. The Stratum Corneum Role in the Barrier Function.....	14
6. Desquamation Process in the Stratum Corneum.....	17
7. Hydration of the Stratum Corneum.....	18
8. References.....	20
III. Basic Concepts in Transdermal Drug Delivery	25
1. Introduction.....	27
2. Historical Landmarks in Transdermal Drug Delivery.....	29
3. Advantages of Transdermal Delivery versus other Drug Delivery Systems....	30
4. Drawbacks of Transdermal Drug Delivery Systems.....	32
5. Transcutaneous Absorption in the Skin.....	32
6. Events governing Transdermal Drug Delivery.....	33
6.1 Drug Lipophilicity.....	33
6.2 Drug Mobility.....	33
6.3 Passive Drug Diffusion.....	34

6.4 Drug-Skin Interactions	36
6.5 Skin Pharmacokinetics	36
6.6 Cutaneous Pharmacokinetics.....	37
6.7 Cutaneous Clearance.....	38
6.8 Skin Metabolism.....	39
6.9 Stratum Corneum Reservoir.....	39
6.10 Transdermal Studies in Human and Animal Skin: Physiology and Anatomy Correlation.....	39
7. References.....	42

IV. Transdermal Drug Delivery Technologies 45

1. Introduction.....	47
2. Passive Drug Diffusion.....	48
2.1 Creams for Topical Delivery.....	49
2.2 Gels for Topical Delivery.....	50
2.3 Absorption Enhancers.....	51
2.3.1 General Characterization of the Absorption Enhancers.....	52
2.4 Transdermal Patches.....	55
3. Active Drug Diffusion.....	57
3.1 Electroporation.....	57
3.2 Iontophoresis.....	58
3.3 Jet Inject.....	59
3.4 Skin Ablation.....	60
3.5 Microneedles.....	61
3.6 Sonophoresis.....	62
3.7 Photomechanical Waves.....	64
4. Comparison of the Transdermal Drug Delivery Technologies.....	65
5. References.....	66

V. Laser Generation of Acoustic Waves 69

1. Introduction.....	71
2. Mechanisms for Acoustic Waves Generation.....	71
3. Physics of Acoustic Wave Propagation.....	74
3.1 Hooke's Law for Acoustics.....	75
3.2 Newton's Law for Acoustics.....	76
3.3 Acoustic Wave Equation.....	77
3.4 Heat Equation.....	78

4. Theory for Laser induced Acoustic Waves.....	78
4.1 The Grüneisen Coefficient.....	79
5. Generation of Photoacoustic Waves by the Thermoelastic Process.....	80
6. References.....	84
VI. Development of a Photoacoustic Waves based TDD System	89
1. Introduction.....	91
1.1 Background.....	91
2. Photoacoustic Calorimetry Pathway to the Photoacoustic Waves Generation..	92
2.1 Photoacoustic Calorimetry Cells.....	94
2.2 Photoacoustic Calorimetry with Solid Samples.....	94
3. Laser System Suitable for PA Waves Generation.....	96
4. Construction of the Piezophotonic Materials.....	97
4.1 Photoacoustic References.....	98
4.1.1 Porphyrins as Photocalorimetric References.....	99
4.1.1.1 UV-Visible Absorption Spectroscopy.....	99
4.1.1.2 Fluorescence Spectroscopy.....	100
4.1.2. Graphite as Photoacoustic References.....	101
4.1.3 Near Dyes as Photoacoustic References.....	102
4.1.4 Strongly Absorbing PAC References.....	102
5. Development and Optimization of the Piezophotonic Materials.....	103
5.1 Metalloporphyrins and Carbon based Thin Films.....	103
5.2 Metalloporphyrins and Activated Carbon based Thin Films.....	105
5.3 Metalloporphyrins and Near-Infrared based Thin Films.....	106
5.4 Metalloporphyrins and NIR based Thin Films in Polystyrene and TiO ₂ ..	107
5.5 Metalloporphyrin based Thin Films <i>versus</i> Thick Black Polystyrene....	109
5.6 Bandwidths of the Piezophotonic Films based upon Metalloporphyrins..	110
5.7 Water Based Piezophotonic Films	111
6. Summary of the Best Piezophotonic Materials.....	112
7. Characterization of Acoustic Waves Generated by Explosive Polymer Films.	113
8. Comparison between PA Waves, Ultrasound Waves and Shock Waves.....	115
9. Design of a PA Waves System based on Piezophotonic Materials.....	117
10. References.....	118

VII. Understanding the Interaction between Photoacoustic Waves and the Skin	121
1. Introduction.....	123
2. Lipids Biophysical Nature.....	123
2.1 Model Membranes.....	124
2.1.1 Liposomes.....	124
2.2. Lipids Dynamics: Phase Transition.....	125
3. Fluorescence Anisotropy Studies in the DPPC:DPH System.....	126
3.1 DPPC:DPH System at 40 °C subject to the PA Waves.....	128
3.2 DPPC:DPH System at 41 °C subject to the PA Waves.....	129
3.3 DPPC:DPH System at 42 °C subject to the PA Waves.....	129
4. Conclusions.....	130
5. References.....	133
VIII. Safety Issues of the Photoacoustic Waves Transdermal System	135
1. Introduction.....	137
2. PA Waves Application in Animal Models.....	138
2.1 Conclusions for the Animal Studies.....	141
3. PA Waves Application in Human Volunteers.....	141
4. Overall Conclusions.....	143
5. Rationalization of the PA Waves Interaction with the SC Intercellular Lipids.....	144
6. References.....	147
IX. Transdermal Drug Delivery Experiments	149
1. Introduction.....	151
2. Formulation Optimization of Photosensitizers.....	152
2.1 Results and Discussion.....	153
3. <i>Ex-Vivo</i> Transdermal Sensitizer Delivery by the PA Waves.....	160
3.1 Qualitative Study of the Best Energy in the PA Waves Delivery.....	161
3.2. Transdermal Delivery by the PA Waves using TiO ₂ Substrate.....	162
4. <i>Ex-Vivo</i> Transdermal Sensitizer Delivery by PA and Shock Waves.....	163
4.1 Qualitative Analysis of the Transdermal Sensitizer Delivery.....	164
5. <i>In Vivo</i> Transdermal Sensitizer Deliver by the PA Waves.....	165
5.1 Results and Discussion.....	165
5.2. Conclusion.....	170
6. <i>Ex-Vivo</i> and <i>In Vivo</i> Topical Delivery of GFP by the PA Waves.....	171
7. References.....	172

X. Prospects in Gene Delivery	175
1. Introduction.....	177
2. Gene Transfer with Acoustic Waves.....	178
2.1 Background	178
3. Cellular Viability Experiments.....	180
4. <i>In Vitro</i> Gene Transfer with Photoacoustic Waves.....	181
5. References.....	185
XI. Concluding Remarks	187
1. Conclusion.....	189
2. PA Waves Vision in Transdermal Drug Delivery.....	191
3. References.....	193
XII. Instrumentation, Materials and Methods	195
1. Instrumentation.....	197
1.1 Absorption Spectroscopy.....	197
1.2 Emission Spectroscopy.....	197
1.3 Photoacoustic Calorimetry.....	197
1.4 Microscopy Analysis.....	198
2. Materials.....	199
3. Methods.....	199
3.1 Production of Piezophotonic Materials.....	199
3.2 Generation of Photoacoustic Waves.....	200
3.3 Large Unilamellar Vesicles Preparation.....	200
3.4 Transepidermal Water Loss (TEWL) Experiments.....	201
3.5 Tissue Preparation.....	202
3.6 Preparation of the Transdermal Formulations.....	203
3.7 Transdermal Drug Delivery Studies.....	203
3.8. Extraction Procedure.....	203
3.9. Transdermal Delivery in Minipigs.....	204
3.10. Cell Viability and Cell Transfection Experiments.....	205
4. References.....	207

Resumo

A pele funciona como barreira protectora contra a difusão de fármacos e patógenos, o que delimita a administração transdérmica a um conjunto reduzido de moléculas. A aplicação de metodologias passivas e activas, tal como, formulações tópicas, promotores de absorção, *patches* transdérmicos e métodos físicos não constituem ainda opções clinicamente válidas, para a larga maioria dos medicamentos, à utilização de agulhas hipodérmicas, pelo que estas permanecem a principal alternativa à entrega oral de fármacos, independentemente das questões relacionadas com a dor, contaminações e reciclagem. A maioria destes sistemas transdérmicos não cumpre as necessidades de segurança, eficácia e de dor requerente na administração transdérmica de fármacos. A utilização de ondas fotoacústicas enquanto sistema transdérmico consiste na conversão rápida e eficiente da energia de um pulso de laser, numa onda de pressão intensa e de larga banda de frequências, capaz de transientemente permeabilizar as camadas exteriores da pele ou da membrana celular. As ondas fotoacústicas apresentam as seguintes características físicas: curta duração (cerca de 1000 vezes mais curto do que um microssegundo), banda de frequências até 200 MHz e amplitude máxima de dezenas de atmosferas. A geração destas ondas assenta na utilização de pulsos de laser curtos (< 8 ns), fluências de laser moderadas (< 50 mJ/cm²), de modo a gerar ondas com rápidos tempos de crescimento (> 1 bar/ns) e pressões máximas até 50 bar, o que as coloca nos limites mínimos de perturbação efectiva de barreiras biológicas (de 1 a 50 bar/ns). A eficiência da transdução da luz laser em pressão pode ser conseguida através de um material de espessura reduzida, com um coeficiente de Grüneisen elevado e pela incorporação de um corante, tal como uma molécula com as propriedades das referências fotoacústicas, que respeite as seguintes relações: i) uma absorção linear, u_a , superior a 100 cm⁻¹, e ii) um decaimento não-radiativo para o estado fundamental inferior a < 1 ns. A interacção das ondas fotoacústicas com tecidos biológicos aumenta a perda de água transepidérmica (TEWL), por um factor de 3, em pele humana, de forma indolor e reversível (2 minutos). A utilização destas ondas na administração transdérmica de fármacos emprega ondas de 12 bar, com frequências de 100 MHz, pelo que o seu mecanismo de interacção com os tecidos baseia-se na força acústica da radiação. Em particular, estas ondas produzem gradientes de pressão superiores a 15 bar, através de 5 corneócitos da pele (cada corneócito apresenta 5 μ m de largura). A sonoforese e ultra-sonografia (com frequências entre de 0,2-20 MHz) não interagem com os tecidos por este mecanismo, uma vez que geram gradientes de pressão diminutos, se compararmos com a largura da camada córnea da pele (comprimento de onda típico de um ultra-som de 1 MHz é de 150 μ m, enquanto que a espessura do estrato córneo é de 15 μ m).

Os resultados experimentais de entrega transdérmica com ondas fotoacústicas mostram que a pele de minipigs permanece intacta após a entrega intra-epidérmica de fotossensibilizadores (> 1000 Da) e de uma proteína de elevada massa molecular (proteína de fluorescência verde, GFP de 27000 Da). A interação das ondas fotoacústicas com a membrana celular e a concomitante expressão de GFP demonstra o potencial desta técnica na permeabilização de membranas biológicas.

Palavras-Chave: Ondas Fotoacústicas · Entrega Transdérmica de Fármacos ·
Materiais Piezofotônicos · Expansão Termoelástica ·

Abstract

The remarkable protection against drugs and pathogens provided by the skin limits transdermal delivery to a very small set of the medicines. Topical formulations, absorption enhancers, transdermal patches and physical methods with therapeutic purposes have added more to popular folklore than to the clinical armamentarium, and hypodermic needles remain the most relevant alternative to oral delivery regardless of pain, contaminations and waste/recycling. These alternative transdermal systems have not yet fulfilled the need for safe, painless, efficient and affordable transdermal delivery of drugs. The photoacoustic waves (PA) transdermal system consists in the rapid and efficient conversion of the energy of a laser pulse into a broadband and intense pressure wave capable of transiently permeabilizing the outer layers of the skin or of the cellular membrane. Each photoacoustic wave is of very short duration (almost 1000 times shorter than a microsecond), covers a broad band of frequencies (up to 200 MHz), and its maximum amplitude is of tens of atmospheres. Short laser pulses (< 8 ns) with modest laser fluences (< 50 mJ/cm²) can generate PA waves with very high rise times (> 1 bar/ns) and moderate peak pressures (< 50 bar), within the limits required to perturb biological barriers (1-50 bar/ns). Efficient light-to-pressure transduction can be achieved with a thin material with a large Grüneisen coefficient and by incorporating a dye, such as a molecule with the properties of photoacoustic references, that respect the following relations: i) $\mu_a > 100$ cm⁻¹ at the incident laser light, ii) ultrafast radiationless decays to the ground state (< 1 ns). Such PA waves increase the transepidermal water loss (TEWL) by a factor of 3 in human skin in a painless and reversible manner (2 minutes). The enhancement of drug delivery employed 12 bar of photoacoustic waves and center frequencies of 100 MHz and follows the acoustic radiation force mechanism. Indeed, we produced a 12 bar pressure gradients across 5 skin corneocytes (approx. 5 μ m wide). Sonophoresis and ultrasonography (with center frequencies of 0.2-20 MHz) cannot operate through this mechanism because they generate small pressure gradients across the stratum corneum (the typical wavelength of ultrasound at 1 MHz is 150 μ m whereas the thickness of the stratum corneum is 15 μ m). We also show that the skin of minipigs remains intact after intraepidermal delivery of photosensitizers (> 1000 Da) and a large protein (Green Fluorescence Protein, GFP of 27000 Da) with this method. The photoacoustic waves interaction with the cellular membrane and the concomitant GFP expression demonstrates this technique potential to effectively permeabilize biological barriers.

Keywords: Photoacoustic waves · Transdermal Drug Delivery · Piezophotonic Materials · Thermoelastic Expansion

List of Patents, Book Chapters, Papers and Prizes

Patents

“Device for the efficient delivery of compounds to or through the skin or biological barriers, using light-absorbing thin films”.

Gonçalo F. F. Sá, Carlos A. L. Serpa Soares, Luis. G. S. Arnaut Moreira, Universidade de Coimbra. PT Patent Application number 105635, 19 de Abril de 2011 (pedido PCT 19/04/2012).

Book Chapters

“Dermal drug delivery with photoacoustic waves generated by piezophotonic materials”

Gonçalo F.F. Sá, Carlos Serpa, Luis G. Arnaut, *Percutaneous penetration enhancers. The new Percutaneous penetration enhancers (in preparation)*

Papers

“Dermal drug delivery with photoacoustic waves generated by piezophotonic materials”.

Gonçalo F.F. Sá, Carlos Serpa, Luis G. Arnaut, *submitted* to Journal of Controlled Release.

“Intense, high-frequency pressure waves produced with low laser fluences”.

Carlos Serpa, Gonçalo F. F. Sá, Luis G. Arnaut, *Proc. SPIE*, Number 8207A, volume 12, **2012**, Pages 1-6.

“Multi-spectral photoacoustic mapping of the diffusion of bacteriochlorins through the skin: exploring a new PAT contrast agent”.

F. A. Schaberle, L. A. F. Reis, Gonçalo F. F. Sá, C. Serpa, A. R. Abreu, M. M. Pereira, L. G. Arnaut, *Proc. SPIE*, Volume 8089, **2011**, 80890 Q1-7.

“Synthesis and photophysical characterization of a library of photostable halogenated bacteriochlorins: An access to near-infrared chemistry”

M. M. Pereira, C. J. P. Monteiro, A. V. C. Simões, S. M. A. Pinto, A. R. Abreu, Gonçalo F. F. Sá, E. F. F. Silva, L. B. Rocha, J. M. Dabrowski, S. J. Formosinho, S. Simões, L. G. Arnaut, *Tetrahedron*, Volume 66, **2010**, Pages 9545-9551.

“Synthesis and photophysical properties of amphiphilic halogenated bacteriochlorins: New opportunities for photodynamic therapy of cancer”.

Mariette M. Pereira, Carlos J. P. Monteiro, Sara M. A. Pinto, Ana V. Simões, Gonçalo F. F. Sá, Elsa F. F. Silva, Luís G. Arnaut, Sebastião J. Formosinho, Sérgio Simões e Luís Rocha, *Journal of Porphyrins and Phthalocyanines*, Volume 13, **2009**, Pages 567-573.

“Synthesis of amphiphilic sulfonamide halogenated porphyrins: MALDI-TOFMS characterization and evaluation of 1-octanol/water partition coefficients”.

Carlos J. P. Monteiro, Mariette M. Pereira, Sara M. A. Pinto, Gonçalo F. F. Sá, Luís G. Arnaut, Sebastião J. Formosinho, Sérgio Simões e Mark F. Wyatt, *Tetrahedron*, Volume 64, **2008**, Pages 5132-5138.

Prizes

BES® Innovation Prize, 2008.

Agency for the Valuation and Commercialization of Research Results (AVCRI) da Red Universitaria Ibero-americana de Incubación de Empresas (RedEmprendia/Santander), 2010.

List of Abbreviations

Abs	Absorbance
BBG	Brilliant Blue G®
CAC	Critical Aggregation Concentration
CMC-NA	Carboxymethylcellulose – sodium as counter ion
CO ₂	Carbon Dioxide
CPP	Critical Packing Parameter
CuTMeOHPP	Copper (II) 5,10,15,20-tetramethoxyphenylporphyrin
DMPC	1,2-dimyristoyl phosphocholine
DMSO	Dimethyl Sulfoxide
DNA	Deoxyribonucleic Acid
dopa	Dihydroxyphenylalanine
DPH	Diphenylhexatriene
DPPC	Dipalmitoylphosphatidylcholine
EF	Enhancement Factor
FDA	Federal Drug Administration, United States
FFT	Fast Fourier Transform
GFP	Green Fluorescence Protein
GUV	Giant Unilamellar Vesicles
h	Thickness
HOMO	Highest Occupied Molecular Orbitals
HPLC	High Pressure Liquid Chromatography
I_L	Laser Optical Power Density
LPP	Long Periodicity Phase
LUMO	Lower Unoccupied Molecular Orbitals
LUV	Large Unilamellar Vesicles
MI	Mechanical Index
MLV	Multilamellar Vesicles
Mn-TPP	Mn ^{III} 5,10,15,20-tetraphenylporphyrinate (with chloride as counter ion)
Mn-TPPS	Mn ^{III} 5,10,15,20-tetrakis(4-sulphonylphenyl)porphyrinateacetate (with chloride as counter ion)
Mn-TUP	Mn ^{III} 5,10,15,20-tetraundecylporphyrinate (with chloride as counter ion)
MRayl	Unit of Acoustic Impedance (One million Rayl = kg/(s m ²))
NC	New Coccine ®
NIR	Near-Infrared

NMF	Natural Moisturizing Factor
NMR	Nuclear Magnetic Resonance
O/W	Oil/Water
OA	Oleic Acid
P	Pressure
PA	Photoacoustic
PAC	Photoacoustic Calorimetry
PBS	Phosphate Buffer Solution
PDMS	Polydimethylsiloxane
PG	Propylene Glycol
p_{\max}	Maximum Pressure
PMMA	Polymethylmetacrylate
POPC	1-palmitoyl-2-oleoyl phosphocholine
PP	Peak Pressure
PS	Polystyrene
PTT	Phase Transition Temperature
r	Anisotropy
SC	Stratum Corneum
SCCE	Stratum Corneum Chymotryptic Enzyme
SCTE	Stratum Corneum Tryptic Enzyme
SEM	Standard Error of the Mean
SPP	Short Periodicity Phase
SUV	Small Unilamellar Vesicles
SWNT	Single wall nanotubes
T_c	Transmission Coefficient
T	Temperature
TDD	Transdermal Drug Delivery
TDDS	Transdermal Drug Delivery Systems
TEWL	Transepidermal Water Loss
TiO ₂	Titanium dioxide
TP	Transdermal Patches
TPP	Tetraphenylporphyrinate
UMT	Ultrasound-Mediated Transfection
US	United States
USW	Ultrasound Waves
UV	Ultraviolet
V	Volume
W/O	Water/Oil
WHO	World Health Organization

Definition of Terms

Percutaneous Absorption	A general term which describes the passage of a compound through the skin but does not necessarily indicate its eventual fate. The process can be subdivided into the following steps:
1. Penetration	The entry of a compound into a particular layer.
2. Permeation	The diffusion of a compound through a particular layer.
Transcutaneous absorption	Phenomenon that describes the diffusion of drugs and/or metabolites through the intercellular spaces rather than through a skin cell.
Transdermal delivery	Defined as the passage of a substance, such as a drug, from the outside of the skin through its various layers, into the bloodstream.
Topical delivery	Defined as the application of a formulation containing the drug to the first layers of the skin to directly treat cutaneous disorders or the cutaneous manifestations of a general disease with no drug reaching the systemic circulation.
Intradermal delivery	Defined as the delivery of a compound to the skin itself, i.e., to a specific layer within the skin.
Transdermal Formulation	A formulation which after local application to the skin surface allows active drug to reach the systemic circulation.
Topical formulation	A formulation designed for local delivery i.e., after local application to the skin no drug should reach the systemic circulation.
Laser fluence	The laser energy per unit area on the work material, expressed in units of J/cm^2 .

Laser pulse duration	τ_L is the full width at 1/e level of the laser pulse, and is conveniently expressed in units of nanosecond, <i>ns</i> .
Optical power density	The power density of a laser beam, where the power density is the power of the laser by unit irradiation area, expressed in W/cm ² or more conveniently in MW/cm ² .
Acoustic transient	Employed to describe both hypersonic and sonic acoustic waves.
Impulse of an acoustic transient	Defined as the rate of pressure increase per unit of time, expressed in units of bar/s.
Rise time of an acoustic transient	Defined as the time from 10% to 90% of the peak pressure.
Broadband	Wide frequency band that covers a continuous frequency spectrum and when used to qualify a pressure wave designates an acoustic emission with significant frequency components of tens of MHz.
Optical penetration depth	δ is the depth at which the intensity of the radiation inside the material falls to 1/e, conveniently expressed in cm.
Photoacoustic reference compound	Compound that absorbs the radiative energy of a laser pulse and rapidly transforms that energy into heat by radiationless processes, while returning to its ground electronic state. As it is known in the art, a PAC reference compound produces the photoacoustic wave of the highest possible intensity by the absorption of a laser pulse of a given energy and in a given configuration in the absence of net chemical reactions, within the duration of the laser pulse.
Linear decadic absorption coefficient	μ_{as} , or linear absorption coefficient, is the absorbance divided by the optical path length through the sample, and is expressed in cm ⁻¹ .

List of Figures and Graphics

Fig. 2.1 - Cross-sectional illustration of human skin.....	7
Fig. 2.2 - Intercellular coupling between corneocytes cells by corneodesmosomes.....	9
Fig. 2.3 - The viable epidermis and the process of keratinization.....	11
Fig. 2.4 - Schematic representation of the drug diffusion routes across human skin.....	14
Fig. 2.5 - The orthorhombic lipid lateral organization in the SC.....	15
Fig. 2.6 - Biological interpretation of the SC membrane arrangement. Intercellular regions with long alkyl chains ceramides connected to polar head groups and then to the keratinocytes (protein envelope).....	16
Fig. 2.7 - The keratinocytes division in the stratum basale with the migration process to the SC. The corneocytes loose the cohesive properties on contact with the proteolytic enzymes (SCTE and SCCE)	17
Fig. 3.1 - Historical landmarks in transdermal drug delivery.	29
Fig. 3.2 - Ideal limits for the physico-chemical properties for candidates to TDD ($K_{O/W}$ represents for partition coefficient oil/water).....	31
Fig. 3.3 - Pharmacokinetic compartment model of skin layers and the processes involved in transcutaneous permeation.	38
Fig. 4.1 - The effect of different absorption enhancers in the stratum corneum structure. The left side image represents the biological action of skin occlusive conditions as swelling takes place in the intracellular keratin of the corneocytes, which creates polar channels. The right image symbolizes the biological consequence of the SC fluidization, as it develops in the corneodesmosomes.....	55
Fig. 4.2 - Basic structure of transdermal patches: drug-in-adhesive (left) and reservoir type (right).	56
Fig. 4.3 - Schematic view of electroporation. The proposed mechanism of action [108-110] is based on the application of electrical pulses that crosses the lipid lamellae (open spaces) vacuuming it, so that a water influx arises to it (black circles)	58
Fig. 4.4 - A schematic representation of a typical iontophoresis application to the skin. Two electrodes are placed in contact to	

	the skin surface and a drug reservoir is positioned between the skin and the electrode of the same electric charge.....	59
Fig. 4.5 -	Schematic microneedle based technology. The microneedle array (black triangles) pierces the skin promoting drug diffusion (black dots).....	62
Fig. 4.6 -	Three possible modes of ultrasound waves to permeabilize the stratum corneum intercellular lipids.....	63
Fig. 4.7 -	Schematic representation of the photomechanical waves based technology. The 10 J <i>per</i> pulse laser light is impinged and absorbed by a target material (black polystyrene, 1mm). The resulting pressure wave crosses a drug reservoir that also acts as a coupling medium and permeabilizes the upper skin layers. In consequence, the drug entrance in the skin is facilitated and a concentration gradient sustains the TDD, until the barrier function is fully recovered.	64
Fig. 5.1 -	Principal mechanisms for laser generation of acoustics transients: (a) thermoelastic expansion and (b) ablation regime.....	72
Fig. 5.2 -	Plasma produced by a CO ₂ laser after detonating a graphite medium.....	73
Fig. 5.3 -	A typical photoacoustic wave: PP represents the peak pressure of the wave, RT symbolizes its rise time (10 to 90% of the PP) and λ_L the acoustic wavelength.....	74
Fig. 5.4 -	Material represented as rectangles that are disturbed by the action of an acoustic wave. The lower left depicts the rarefaction of the wave where the surrounding medium pushes the material into a larger volume, diminishing its density. The lower right depicts the compression of the material into a smaller volume, increasing the system pressure	75
Fig. 6.1 -	Nanosecond laser flash photolysis for: left) Mn-TPP film in cellulose acetate; right) CuTMeOHPP film in cellulose acetate.....	95
Fig. 6.2 -	Left) transient absorption decay for CuTMeOHPP in cellulose acetate (450 nm); Right) PAC signals for CuTMeOHPP in cellulose acetate, with Mn-TPP in cellulose acetate as reference.....	95

Fig. 6.3 - Simulated laser pulses of 1 μ s, 8 ns and 1 ps time width (left) and respective bandwidths (right).....	96
Fig. 6.4 - Absorption spectrums of MnTPP dissolved in toluene ($\epsilon_{480 \text{ nm}} \geq 10^5 \text{ M}^{-1} \text{ cm}^{-1}$), Mn-TUP dispersed in polystyrene and Mn-TPPS adsorbed in TiO_2	100
Fig. 6.5 - Chemical structure of the porphyrins used: TPP, <i>Mn-TPP</i> , <i>Mn-TUP</i> and <i>Mn-TPPS</i> are the tetraphenylporphyrinate, $\text{Mn}^{\text{III}}5,10,15,20$ -tetraphenylporphyrinate, $\text{Mn}^{\text{III}}5,10,15,20$ -tetraundecylporphyrinate and $\text{Mn}^{\text{III}}5,10,15,20$ -tetrakis (4-sulphonylphenyl) porphyrinateacetate.....	101
Fig. 6.6 - Absorption spectrum of graphite in a TiO_2 substrate and single wall nanotubes dispersed in carboxyl methyl cellulose (Na) ...	101
Fig. 6.7 - Absorption spectrum of Epilight TM 1178 in a polystyrene substrate.....	102
Fig. 6.8 - Chemical structures of the water based photoacoustic references: Allura red®, Amaranth®, New Coccine® and brilliant black G®.....	102
Fig. 6.9 - PAC adapted arrangement for the irradiation of the piezophotonic films. The laser pulse first traverses a quartz window and the contact transducer is protected from the laser by a mirror. The film is between the window and the mirror. Good acoustic contact is maintained by adding silicone or ultrasound gel.....	103
Fig. 6.10 - Representative photoacoustic waves as function of time. PA waves produced by [A1] with 400 μ m, [A2, A3] with 50 μ m, [A4] with 100 μ m and [A5], upon pulsed laser excitation at 532 nm, with 10 mJ/cm^2 and measured by a 225 MHz contact transducer.....	104
Fig. 6.11 - Representative photoacoustic waves as function of time. PA wave produced by [B2, B3] upon pulsed laser excitation at 505 nm, with laser energy of 76 mJ/cm^2 and measured by a 10 MHz contact transducer.....	105
Fig. 6.12 - Representative photoacoustic waves as function of time. PA wave produced by [C1] with a thickness of 200 μ m upon pulsed laser excitation at 1064 nm, with laser energy of 50 mJ/cm^2 and measured by a 15 MHz contact transducer.....	106

Fig. 6.13 -	Representative photoacoustic waves as function of time. PA wave produced by [D1] with a 37 μm of thickness, [D5] with a thickness of 5 μm , [D7] with a thickness of 33 μm upon pulsed laser excitation at 478 nm, with laser energy of 31 mJ/cm^2 and measured by a 15 MHz contact transducer.....	107
Fig. 6.14 -	Left) Absorption spectrum of Mn-TUP dissolved in Sylgard® - silicone elastomer. Right) Photoacoustic wave generated [D6] film upon laser excitation at 478 nm with 31 mJ/cm^2	108
Fig. 6.15 -	Representative photoacoustic waves as function of time. PA wave produced by [A1] upon pulsed laser excitation at 355 nm, with laser energy of 10 mJ/cm^2 , and measured by a 225 MHz contact transducer.....	109
Fig. 6.16 -	Left) Representative photoacoustic waves as function of time. PA wave produced by [F1] upon pulsed laser excitation at 484 nm, with laser energy of 50 mJ/cm^2 and measured by a 225 MHz contact transducer. Right) Respective bandwidth analysis of [F1, F2, F3] films.....	110
Fig. 6.17 -	Measured photoacoustic waves as function of time. Normalized and representative PA waves produced by [G1, G3, G4] upon pulsed laser excitation at 532 nm, with laser energy of 50 mJ/cm^2 and measured by a 20 MHz needle hydrophone.....	111
Fig. 6.18 -	Representative photoacoustic wave as function of time. The wave was produced by irradiating a polystyrene film containing Mn-TPP, with $\mu_a = 644 \text{ cm}^{-1}$, $\Gamma=0.7$, $c_L= 2400 \text{ m/s}$, laser pulse duration of 8 ns, laser energy density of 32 mJ/cm^2 , optical power density of 4MW/ cm^2	112
Fig. 6.19 -	Chemical structure of aryltriazene.....	113
Fig. 6.20 -	Pressure wave amplitudes measured with a 15 MHz contact piezoelectric transducer following the excitation of a triazene polymer films with increasing laser fluences (squares) compared with the amplitude measured with another triazene film at a higher energy (circle, only a lower limit for the shock wave amplitude could be measured in this experiment because it exceeded the range of the oscilloscope).....	113

Fig. 6.21 - Thermoelastic generation of an acoustic wave by a thin polymer film containing a photoacoustic reference, compared with the shock wave generated by a thin triazene film.....	114
Fig. 6.22 - Same as previous figure but using additional triazene polymer films and a polystyrene film doped with a Mn-TUP (red).....	114
Fig. 6.23 - Left) FFT analysis of the pressure waves generated with Mn-TUP in polystyrene substrate versus the pressure wave generated by a black polystyrene disk (red and blue lines measured with a 225 MHz contact transducer. Mn-TUP in a polystyrene substrate measured by a 20 MHz needle hydrophone. Right) Dependence of the photoacoustic signal intensity on the thickness of the series of films of titanium dioxide with Mn-TUPS (matched absorbances) at the pulsed laser excitation wavelength of 472 nm, as measured by a 100 MHz contact transducer.....	116
Fig. 6.24 - Schematic cross representation of the assembled PA waves transdermal system A- formulation, B – biological barrier, 1 – laser pulse, 2 – laser box, 3 –window, 4 – piezophotonic material, 5 – mirror, 6 – structural element, 7 – optical guide...	117
Fig. 7.1 - Chemical structure of DPPC.....	124
Fig. 7.2 - Chemical structure of DPH.....	127
Fig. 7.3 - Laser assembly (1) for the irradiation of the polymer film. The laser pulse (green) impinges into the piezophotonic material (2), which produces a PA wave that traverses a quartz cell (3) until it reaches the DPPC:DPH solution. The anisotropy signal is followed by a Cary Eclipse fluorescence spectrophotometer (4) equipped with a thermostatic multicell holder (3). Acoustic contact is maintained by an ultrasound gel.....	128
Fig. 7.4 - Changes in DPH fluorescence anisotropy after PA waves application on the DPPC:DPH system (100:1) at 40 °C. Vesicles were exposed to PA waves for 0.5 minutes (gray) and 1 minute (blue) in the left image and 2 minutes (red) and 5 minutes (black) in the right image. The PA waves were produced by irradiating a polystyrene film containing tetraphenyl porphyrin of manganese, with $\mu_a = 640 \text{ cm}^{-1}$, $\Gamma = 0.7$, $c_L = 2400 \text{ m/s}$, laser pulse duration of 8 ns, laser energy density of 50 mJ/cm^2 , optical power density of 6.25 MW/cm^2 ..	128

- Fig. 7.5 -** Changes in DPH fluorescence anisotropy after PA waves application on the DPPC:DPH system (100:1) at 41°C. Vesicles were exposed to PA waves for 0.5 minutes (gray) and 1 minute (blue) in the left image and 2 minutes (red) and 5 minutes (black) in the right image. The PA waves were produced by irradiating a polystyrene film containing tetraphenyl porphyrin of manganese, with $\mu_a = 640 \text{ cm}^{-1}$, $\Gamma = 0.7$, $c_L = 2400 \text{ m/s}$, laser pulse duration of 8 ns, laser energy density of 50 mJ/cm^2 , optical power density of 6.25 MW/cm^2 . 129
- Fig. 7.6 -** Changes in DPH fluorescence anisotropy after PA waves application on the DPPC:DPH system (100:1) at 42 °C. Vesicles were exposed to PA waves for 0.5 minutes (gray), 1 minute (blue) and 2 minutes (red)) in the left image and 5 minutes in the right image. The PA waves were produced by irradiating a polystyrene film containing tetraphenyl porphyrin of manganese, with $\mu_a = 640 \text{ cm}^{-1}$, $\Gamma = 0.7$, $c_L = 2400 \text{ m/s}$, laser pulse duration of 8 ns, laser energy density of 50 mJ/cm^2 , optical power density of 6.25 MW/cm^2 130
- Fig. 7.7 -** Change in anisotropy after PA waves application (left). The DPPC:DPH was exposed to 2 minutes of PA waves at 41°C. Anisotropy recovery was fitted with a single exponential represented by the red line with $\tau = 1.70 \times 10^2 \text{ s}$ (right)..... 130
- Fig. 8.1 -** Schematic representation of Mexameter® MX 18. The melanin and hemoglobin content is determined at 568, 660 and 870 nm, respectively..... 137
- Fig. 8.2 -** Schematic representation of the Tewameter® TM 300..... 138
- Fig. 8.3 -** Changes in transepidermal water loss after PA waves application (black) and after occlusion (gray) in different minipigs skin sites. The minipig skin was exposed for 20 seconds of PA waves produced upon laser irradiation (50 mJ/cm^2 , 6.25 MW/cm^2) in Mn-TUP incorporated in polystyrene, and the change is the TEWL after the exposure to the PA waves minus the initial TEWL..... 138
- Fig. 8.4 -** **Left)** Transepidermal water loss ($\pm \text{SEM}$) in normal skin (black) and after occlusion (gray) without the PA waves. **Right)** Transepidermal water loss ($\pm \text{SEM}$) after in normal skin (black) and after (gray) 30 seconds PA waves application.

	SEM symbolizes the standard error of the mean.....	139
Fig. 8.5 -	Changes in transepidermal water loss after PA waves application (black) and after occlusion (gray) in different minipigs skin sites. The minipig skin was exposed for 1 minute of PA waves produced upon laser irradiation (50 mJ/cm ² , 6.25 MW/cm ²) in Mn-TUP incorporated in polystyrene, and the change is the TEWL after the exposure to the PA waves minus the initial TEWL.....	139
Fig. 8.6 -	Left) Transepidermal water loss (\pm SEM) in normal skin (black) and after occlusion (gray) without the PA waves. Right) Transepidermal water loss (\pm SEM) after in normal skin (black) and after (gray) 1 minute of PA.....	140
Fig. 8.7 -	Changes in transepidermal water loss after PA waves application (black) and after occlusion (gray) in different minipigs skin sites. The minipig skin was exposed for 5 minutes of PA waves produced upon laser irradiation (50 mJ/cm ² , 6.25 MW/cm ²) in Mn-TUP incorporated in polystyrene, and the change is the TEWL after the exposure to the PA waves minus the initial TEWL.....	140
Fig. 8.8 -	Left) Changes in transepidermal water loss after (in gray) and before (in black) occlusion in different minipigs skin sites. Basal TEWL recovery in 20 minutes. Right) Changes in transepidermal water loss after (in gray) and before (in black) 5 minutes of PA waves application in different minipigs skin sites. Basal TEWL recovery in 55 minutes.....	141
Fig. 8.9 -	Changes in transepidermal water loss (average \pm s.e.m.) of the right (in red) and left (in blue) ventral forearms of volunteers. The right ventral forearms were exposed for 2 minutes to PA waves generated by Mn-TUP piezophotonic films in polystyrene although subject to 50 mJ/cm ² laser pulses at 20 Hz, and the change is the TEWL after the exposure to the PA waves minus the initial TEWL. The TEWL of the left ventral forearms was measured with the same protocol but with the laser off. The transient change in this case comes from near-surface water trapped by occlusion.....	142
Fig. 8.10 -	Box chart graphic describing the pain felt by the volunteers after the PA waves application.....	143

Fig. 8.11 -	Rationalization of the increased skin permeability following the application of photoacoustic waves with frequencies above 100 MHz. Top: unperturbed stratum corneum, shown as 14 layers of tightly packed corneocytes with hydrophilic domains (blue) separated by intercellular lipid lamellae (green), where the diameter of the corneocytes (40 μm) is not represented to the scale. Middle: Compressive front and rarefaction tail of a high-impulse photoacoustic wave traversing the stratum corneum and producing very fast pressure changes. Bottom: perturbed stratum corneum with expansion of the lacunar spaces where the organization of the lipid matrix is changed but takes some time to relax to the original structure, which facilitates the diffusion of drugs through the expanded spaces..	145
Fig. 9.1 -	Representative fluorescence microscopy images of the sensitizer distributed in the minipig epidermis for 2 hours, when various formulations containing DMSO as absorption enhancer is used.....	154
Fig. 9.2 -	Representative fluorescence microscopy images of the sensitizer distributed in the minipig epidermis for 2 hours, when various formulations containing oleic acid as absorption enhancer is used.....	155
Fig. 9.3 -	Representative fluorescence microscopy images of the sensitizer distributed in the minipig epidermis for 2 hours, when various formulations containing Azone as absorption enhancer is used.	155
Fig. 9.4 -	Estimated response surface illustrating the effect of water, sensitizer and propylene glycol concentrations in the accumulation of the sensitizer in the minipig epidermis when a formulation containing DMSO is used. EF stands for enhancement factor.	156
Fig. 9.5 -	Estimated response surface illustrating the effect of water, sensitizer and propylene glycol concentrations in the accumulation of the sensitizer in the minipig epidermis when a formulation containing oleic acid is used.....	157
Fig. 9.6 -	Estimated response surface illustrating the effect of water, sensitizer and propylene glycol concentrations in the accumulation of the sensitizer in the minipig epidermis when a	

	formulation containing Azone is used.....	157
Fig. 9.7 -	Left) Fluorescence calibration curve of the sensitizer in dichloromethane. Right) Amount of sensitizer extracted from the 1 cm ² of minipig skin after 2 hours for the formulations containing DMSO, oleic acid and Azone. All essays were repeated 4 times.	159
Fig. 9.8 -	Left) Passive delivery of the sensitizer with formulation D and an incubation time of 30, 60 and 120 minutes repeated 6 times. Right) Amount of sensitizer extracted from the minipig skin with formulation D when passive delivery and PA waves delivery experiments were done in collinear skin sites for reporting the same SC barrier. The laser impinged in a Mn-TUP piezophotonic material of polystyrene with 290 cm ⁻¹ for 2 minutes at 532 nm. All essays were repeated 4 times.....	160
Fig. 9.9 -	Representative confocal fluorescence images for the passive delivery of the sensitizer (top) and PA waves active delivery (down). The confocal fluorescence images have a transmission (left) and a fluorescence (right) image. The incubation time was 20 minutes after the laser impinged in a Mn-TUP piezophotonic material of polystyrene with $\mu_a = 290 \text{ cm}^{-1}$, at 532 nm with 50 mJ/cm ² and for 2 minutes.....	161
Fig. 9.10 -	Representative microscopy fluorescence images for the passive delivery of the sensitizer (left) and PA waves active delivery (right). The PA delivery was produced with Mn-TPPS piezophotonic film in TiO ₂ ($\mu_a = 670 \text{ cm}^{-1}$ – thickness of 7.5 μm) with 12 laser pulses at 355 nm with laser fluences of 10 mJ/cm ² , and an incubation time of 20 minutes. In the extraction figure (right), the essays were repeated 4 times.....	162
Fig. 9.11 -	Sensitizer extraction after passive delivery with formulation D at incubation time of 20 minutes compared with 20 minutes of incubation time of PA waves and shock waves essays. All essays were repeated 4 times. The PA waves were generated upon irradiation of Mn-TUP incorporated in polystyrene with $\mu_a = 368 \text{ cm}^{-1}$, with light of 355 nm for 2 minutes. The shock waves used the aryltriazenes polymers with $\mu_a = 2200 \text{ cm}^{-1}$ and with laser light of 355 nm for 2 minutes.....	163

Fig. 9.12 - Representative fluorescence microscopy images of the 20 minutes sensitizer distributed in the minipig epidermis after passive delivery with formulation D.....	164
Fig. 9.13 - Representative fluorescence microscopy images of the 20 minutes sensitizer distributed in the minipig epidermis after active delivery with PA waves using formulation D. Laser energy at 50 mJ/cm ² with 355 nm.....	164
Fig. 9.14 - Representative fluorescence microscopy images of the 20 minutes sensitizer distributed in the minipig epidermis after active delivery with shock waves using formulation D. Laser energy at 10 mJ/cm ² at 355 nm.....	164
Fig. 9.15 - Fluorescence calibration curve, in dichloromethane, for the sensitizer used in the <i>in vivo</i> experiments.....	165
Fig. 9.16 - Quantification by fluorescence of the sensitizer extracted from minipig following passive permeation, when oleic acid was employed as absorption enhancer.....	167
Fig. 9.17 - Mass of sensitizer extracted from minipig following PA waves (average data of the sum for 0.5 and 5% formulation – 15 to 60 minutes) or passive permeation, when oleic acid was employed as absorption enhancer. PA waves were generated with Mn-TUP in polystyrene ($\mu_a = 640 \text{ cm}^{-1}$) upon laser irradiation with 532 nm light of 25 and 50 mJ/cm ² for 2 minutes.....	167
Fig. 9.18 - Sensitizer extracted from the skin after PA waves application and passive delivery when Azone is used as absorption enhancer. PA waves were generated with Mn-TPP in polystyrene ($\mu_a = 230 \text{ cm}^{-1}$) upon laser irradiation with 532 nm light of 50 mJ/cm ² for 2 minutes.....	169
Fig. 9.19 - Representative confocal microscopy images of sensitizer located in the SC of the minipig following a 2hours passive permeation when oleic acid is employed as absorption enhancer.....	169
Fig. 9.20 - Representative fluorescence microscopy images of sensitizer located in the SC of the minipig following a 30 minutes incubation time with PA waves application ($\mu_a = 640 \text{ cm}^{-1}$, 532 nm light of 50 mJ/cm ² for 2 minutes), when oleic acid is employed as absorption enhancer.....	170

Fig. 9.21 -	Representative fluorescence image for the <i>in vivo</i> passive delivery of GFP (left). <i>In vivo</i> topical delivery of GFP with 12 PA waves active delivery (middle) and <i>ex-vivo</i> 6 PA waves GFP delivery (right). Experimental conditions of the piezophotonic materials PA waves generation: $\lambda_{exc} = 355$ nm, $\mu_a = 640$ cm ⁻¹ and $\mu_a = 330$ cm ⁻¹ for the Mn-TUP incorporated in a polystyrene substrate.....	171
Fig. 10.1 -	Typical set-up conditions for the cellular viability and gene transfection essays. A fiber optic guide 532 nm nanosecond laser light into the piezophotonic material that produces the photoacoustic waves. The PA waves are transmitted to the culture well using silicone as an acoustic coupling medium and its application is exerted from the bottom of the well.....	180
Fig. 10.2 -	A – Representative image for negative controls essays performed for both plasmids. B – Representative image for the positive control with gwizGFP DNA delivered with lipofectamine. C – Representative image for the positive control with pEGFPC3 DNA delivered with lipofectamine.....	183
Fig. 10.3 -	A – Representative image of the pEGFPC3delivery by the PA waves with an application time of 1.5 minutes. B – Representative image of PA waves essays for an application time of 3 minutes with gwizGFP plasmid.....	184
Fig. 12.1 -	Representative fluorescence images of the sensitizer permeation used for constructing the visual analogue scale in the factorial design experiments. These images typify an evaluation of the amount of sensitizer and its distribution across the minipig epidermis (0 – no permeation; 5 – maximum permeation).....	198

List of Tables

Table 2-1 - Characteristics of human skin layers.....	13
Table 2-2 - Procedures for recovering hydric balance in the skin.....	19
Table 3-1 - Transdermal drug delivery versus oral and intravenous administration of drugs.....	30
Table 3-2 - Physico-chemical and pharmacokinetics data for current market drugs in TDD. Abbreviations: M_r , molecular weight in Daltons (Da); M_p , melting point; $\log K_{o/w}$, logarithm of the oil–water partition coefficient; S_{aq} , aqueous solubility; K_p , permeability coefficient; Cl , clearance; $t_{1/2}$, elimination half-life; Oral BA, oral bioavailability; Therap. BL, therapeutic blood level.....	35
Table 3-3 - Thicknesses of skin layers in rat, mice, pig and human	41
Table 4-1 - Commercially available drugs in the form of transdermal patches.....	47
Table 4-2 - Transdermal drug delivery technologies sorted by physical principal.....	48
Table 4-3 - The effect, the diagrammatic representation and applications of the different genders of absorption enhancers	54
Table 4-4 - Comparative features of transdermal patches.....	57
Table 4-5 - Parameters affecting skin electroporation.....	58
Table 4-6 - Histological consequence of various lasers impinging in the skin.....	61
Table 4-7 - Transdermal drug delivery technologies characteristics.....	65
Table 6-1 - Thermal and acoustic properties for the piezophotonic materials substrates. PDMS stands for polydimethylsiloxane, PMMA for polymethylmethacrylate and PS for polystyrene. * Not applicable.....	98
Table 6-2 - Piezophotonic films characteristics and PA waves amplitude generated upon laser excitation. $I_{Abs}/I_0 = (1-10^{-Abs})$: I_{Abs} represents the fraction of incident light absorbed; I_0 represents the energy of incident light. * Not applicable.....	105
Table 6-3 - Piezophotonic films characteristics and PA waves amplitude generated upon laser excitation. $I_{Abs}/I_0 = (1-10^{-Abs})$: I_{Abs} represents the fraction of incident light absorbed; I_0 represents the energy of incident light. * Not applicable.....	106

Table 6-4 - Piezophotonic films characteristics and PA waves amplitude generated upon laser excitation at 1064 nm.....	107
Table 6-5 - Piezophotonic films characteristics and PA waves amplitude generated upon laser excitation. $I_{Abs}/I_0 = (1-10^{-Abs})$: I_{Abs} represents the fraction of incident light absorbed; I_0 represents the energy of incident light. * Not applicable.....	108
Table 6-6 - Piezophotonic films characteristics and PA waves amplitude generated upon laser excitation at 532 nm. $I_{Abs}/I_0 = (1-10^{-Abs})$: I_{Abs} represents the fraction of incident light absorbed; I_0 represents the energy of incident light. * Not applicable.....	109
Table 6-7 - Piezophotonic films characteristics and PA waves amplitude generated upon laser excitation. $I_{Abs}/I_0 = (1-10^{-Abs})$: I_{Abs} represents the fraction of incident light absorbed; I_0 represents the energy of incident light. * Not applicable.....	110
Table 6-8 - Piezophotonic films characteristics and PA waves amplitude generated upon laser excitation.....	111
Table 6-9 - Summary of the best piezophotonic materials characteristics	112
Table 6-10 - Shock, ultrasound and photoacoustic waves physical characterization.....	115
Table 7-1 - Recovery kinetic parameters for a single exponential decay..	131
Table 9-1 - Excipients percentage in the sensitizer formulations (A to H) produced for the factorial design experiments.....	152
Table 9-2 - Dependent and independent variables and respective levels used in the construction of a partial 3^2 factorial design.....	154
Table 9-3 - <i>Ex-vivo</i> transdermal sensitizer delivery by the PA and shock waves.....	163
Table 9-4 - Quantification of the sensitizer by steady-state fluorescence after extraction from the minipigs, using oleic acid as absorption enhancer. <i>TS</i> stand for tape-stripping. <i>NO</i> symbolizes passive delivery. Each essay was repeated 2 times or performed without repetition. PA waves were generated with Mn-TUP in polystyrene ($\mu_a = 640 \text{ cm}^{-1}$) upon laser irradiation with 532 nm light of 50 mJ/cm^2 for 2 min...	166
Table 9-5 - Quantification by fluorescence of the sensitizer extracted after biopsy punches in minipigs, using Azone as absorption enhancer. PA waves were generated with Mn-TPP in polystyrene ($\mu_a = 230 \text{ cm}^{-1}$) upon laser irradiation with 532	

	nm light of 50 mJ/cm ² for 2 minutes.....	168
Table 10-1 -	Gene transfection efficiency in ultrasound-mediated systems.....	179
Table 10-2 -	Cellular viability essays: piezophotonic materials, PA waves contact time, linear absorption (μ_a) and determined cell viability (CV). * Not applicable.....	181
Table 10-3 -	Experimental design for the application of PA waves in gene transfection essays. The gwizGFP and pEGFPC3 are notations for DNA plasmids used in different concentrations (5, 10, 50, 100 μ g/ml). The PA waves exposure time ranged from 1.5 to 3 minutes.....	182

I

Objectives and

Outline

1. Objectives

The subject of this thesis is to exploit the thermoelastic expansion phenomenon for the generation of high impulse photoacoustic (PA) waves, which can transiently disturb a biological barrier. This work describes the physical principles and rationalizes the use of photoacoustic waves with moderate peak pressures, but high impulses (pressure over time) to overcome the barrier function of biological barriers, such as the skin.

The emphasis of the experimental work relied in on the development of materials, which maximize the conversion of light into pressure, by modulating specific parameters, such as the materials thickness, their thermoelastic properties and the characteristics of laser pulses. Secondly, the safety issues derived from the use of the PA waves as a transdermal system are evaluated concerning the biophysical mechanism of drug permeation and the possibility of permanent damage in the tissues (i.e., recovery of the skin barrier function and erythema measurements). Finally, the optimized materials for the PA waves generation are used in the transdermal and cellular delivery of molecules with different physico-chemical properties, namely the molecular weight and lipophilicity.

2. Outline

The scope of this thesis is subordinated to the interconnection of four scientific disciplines: Chemistry, Physics, Pharmacy and Medicine. The amplitude of these themes suggests a thorough description of the key contributes of these disciplines, to the overall understanding of the novelty presented by the application of photoacoustic waves to biological barriers.

Chapter II consists on a literature review about the main functions of skin as a regulatory organ, as well as a detailed description about the physiology and anatomy of the main skin layers. The unique physiological composition and architecture of skin, if compared to other biological barriers, results in specific features, such as drug diffusion routes, barrier function, desquamation process and the relevance of hydration. Chapter III addresses basic concepts related to skin as a drug delivery target, focusing in the ideal characteristics of drugs and its connection to the main features arising from the skin barrier function. Chapter IV presents an overview of the current transdermal technologies developed to overcome the skin barrier, their definitions and mechanisms of action.

Chapter V reviews the physics of the processes responsible for the laser generation of photoacoustic waves focusing in their mechanisms of interaction with matter. The propagation of acoustic waves can be rationalized by the heat conduction and the acoustic wave equations. The latter equation highlights the Grüneisen coefficient, an important parameter relating the

pressure peak of the PA wave with the thermal properties of the material. Chapter VI clarifies the theoretical and practical development of the transdermal system from the photoacoustic calorimetry in liquids to solids and its consequence, as the first step to produce the piezophotonic materials (*piezo* – mechanical stress/pressure, *photonic* – light) capable of generating acoustic transients with high pressure and short rise times, within the duration of the laser pulse.

Chapter VII discusses new insights about the unknown biophysical mechanism concerning the interaction of the acoustic transients with the skin. Our work is based on a lipid model resembling the lipids within the intercellular spaces of the skin, and on measurements of phase transition temperature by fluorescence anisotropy following application of PA waves application. Chapter VIII presents the safety tests performed in animal models, minipigs, and prior to the application of PA waves in a group of volunteers. Variations in transepidermal water loss (recovery of the barrier function), erythema (skin damage) and associated pain are shown to demonstrate the safe use of photoacoustic waves.

Chapter IX describes transdermal drug delivery experiments regarding the *ex-vivo* and *in vivo* skin delivery of photosensitizers, before and after the application of PA waves. It emphasizes the development of different formulations containing different absorption enhancers using factorial design to optimize the formulation process. The size limitation of the PA waves transdermal system was addressed by the *ex-vivo* and *in vivo* delivery of a large protein, Green Fluorescence Protein (GFP). Chapter X illustrates the potential of PA waves in disturbing the cellular membrane and its concomitant effectiveness in delivering DNA plasmids that express GFP.

Chapter XI summarizes the highlights of the thesis regarding the experimental results and the impact of the work in the development of an effective and safe transdermal drug delivery system. Chapter XII describes the materials and methods employed throughout the experimental work. The position of this section in the end of the thesis, instead on the beginning of each experimental chapter allows additional emphasis, clarity and conciseness on the subject discussed in the chapter. Nevertheless, the essential experimental aspects of each chapter are described briefly.

II

Essential Properties of Skin

1. Introduction

Understanding the skin structure, especially its barrier function and routes of drug diffusion, is critical to rationalize the interaction between photoacoustic (PA) waves and the living tissues and, consequently, to enhance the transdermal delivery of a wider range of drugs. The exact nature of lipid organization within the skin generates enormous debate in the scientific literature. An outline of the current knowledge in the field is described below.

2. Skin Functions

The human skin (figure 2.1¹) is the most extensive organ of the human body with an area of 2 m², accounting for roughly 16% of the total body weight [1-3]. It guarantees a homeostatic relation between the body and the external surroundings while assuring sensory, protective and metabolic functions [1-3]. An effective barrier function against the entrance of drugs and pathogens arises from the skin unique multilayered structure (figure 2.1) [3].

The outlined functions associated with the anatomy of the skin layers protect the body against harsh physico-chemical, microbial, electrical and thermal aggressions. Additionally, the skin physiology controls the rate of water evaporation preventing dehydration [4, 5]. The multilayered structure represents the distinctive characteristic in avoiding the entrance in the human body of microorganisms, but other processes contribute to an unfavorable environment for microbial proliferation. Such as, special glands, sebaceous and sweat ones, which produce a superficial acidic mantle (*sebum* with pH around 5) composed by a complex mixture of lipids with bacteriostatic and fungistatic activities [6-8].

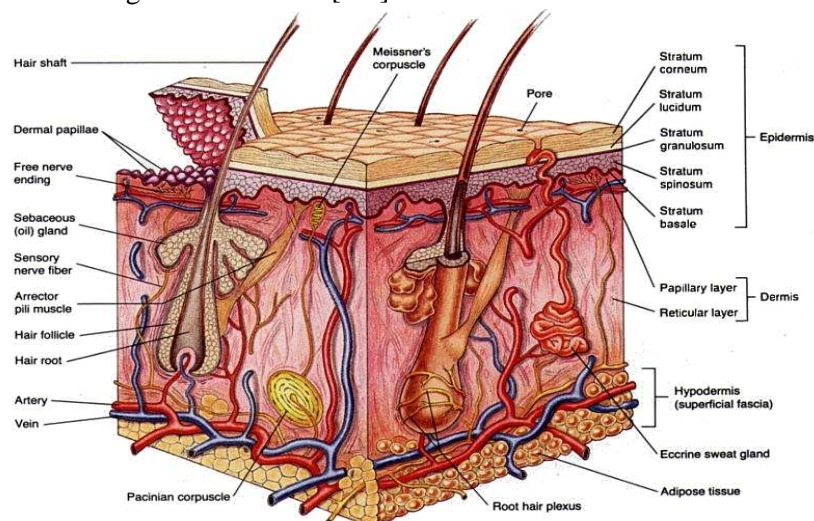


Fig. 2.1 – Cross-sectional illustration of human skin.

¹ Image available at the http://www.lhsc.on.ca/Health_Professionals/Wound_Care/intro/structur.htm, from *London Health Sciences Centre* website (downloaded 19/02/2012).

The skin also plays a protective role against ultraviolet (UV) radiation because of the melanin high content in the epidermis, which has the ability to absorb and diffract the UV rays reducing the sun induced injuries [1, 4, 8]. Nevertheless, the UV rays are indispensable for the vitamin D synthesis, an antioxidant molecule, which is critical to the calcium absorption in the gastrointestinal tract and to the normal growth of bones and teeth [3, 7, 8].

The thermoregulation mechanisms of the skin involve the evaporation of sweat and water in the skin surface, as well as the vasodilatation of blood vessels, which leads to a rapid cooling [6]. Oppositely, the vasoconstriction of superficial vessels prevents heat loss from the human body [6, 8]. The perception and communication of external stimuli, such as pain and thermal trauma, represents a process by which the skin transmits the information throughout the body by a complex network of nerve endings, for interpretative analysis by the human brain [4, 8]. Finally, if the disruption of the barrier function occurs, the skin represents an advanced outpost of immunologic surveillance because of the high content in specialized immune cells that convey information from antigen invasion, to the body immunologic system [4, 8].

3. Anatomy and Physiology of the Skin

The key limitations to the success of transdermal drug delivery technologies lie in the skin itself and result from its excellent physical barrier to the ingress of drugs or foreign entities. Passive delivery methodologies (for instance, transdermal patches), electrical and acoustically assisted technologies demonstrate ineffective therapeutic flow for small and lipophilic drugs, due to the tortuous diffusion pathways across the stratum corneum layers [1]. Mechanical technologies simply promote the removal of skin barrier for further nonrestricted deliver of drugs [1].

These latter technologies may unchain the impasse for transdermal drug delivery technological development, though the skin as a tissue sets other limitations namely contamination, epidemic and intradermal transport issues because the systemic bloodstream is readily available [3]. Or even mechanical concerns to address the anatomical differences between skin sites [1-3]. The relations between flexibility, strength and ease of use must be sought to achieve a full and complete regulatory authorization.

This chapter will examine the skin physiology and its unique architecture, which results on a remarkably effective barrier and the main contributor to the skin's impermeability to drugs [9]. The skin's outermost layer, the stratum corneum (SC), is only 10 to 20 μm thick and its composition exhibits a dozen layers of hardly packed nonliving skin cells (corneocyte), embedded in a mixture of lipids with high spatial organization [9, 10]. The penetration of most

molecules through the skin occurs by the intercellular spaces [9] around the corneocytes, which display structural constraints (diminished areas) and solubility requirements. Beneath the SC, there is the viable epidermis, which is 50 to 100 μm thick and consists of constantly renewing, outward moving cells called keratinocytes [10]. Additionally, immune Langerhans' and somatosensory Merkel cells appears in this layer. The dermis represents the next layer, with an average thickness of 1-2 mm and typically constituted by collagen and elastin fibers [1]. This fibrous network represents the bulk of the skin, and its characteristic tensile strength and elasticity arise from it. Furthermore, it is rich in capillaries, capable of clearing most penetrants within minutes [11]. The dermis rests on the hypodermis, which composition hoards loose fatty connective tissue, and, consequently, considerable variation on its thickness occurs over the surface of the body, as well as between individuals [8].

The sum of these various layers together with their appendages – follicular, sweat and sebaceous glands - and underlying microvasculature constitute a living envelope surrounding the human body.

3.1 Stratum Corneum

The stratum corneum is the final product of epidermal differentiation that forms a highly resistant, compact, horny layer made up of approximately 15-25 cell layers [9, 11]. Each day, roughly one layer of the SC is lost in a process termed desquamation and another layer synthesized by the underlying epidermis.

The main elements of the SC are the corneocytes - flat polyhedral-shaped, enucleated, dehydrated, keratinized cells - which are embedded in a matrix of lipid bilayers, often described using the analogy of the bricks and mortar model [1, 10]. The corneocytes measure 20-40 μm in diameter and differ in thickness depending on the body site, but 0.5-0.8 μm correspond to stated values [7, 11]. The enucleated corneocytes exhibit keratin filaments (very dense protein) in its cytosol, which result in a chemically resistant, yet flexible shell. The physical actors responsible for maintaining attachment between corneocytes and singular cells are called corneodesmosomes (figure 2.2) [13].

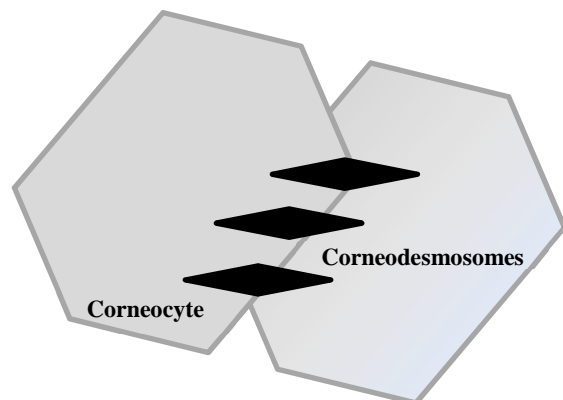


Fig. 2.2 – Intercellular coupling between corneocytes cells by corneodesmosomes.

These junctions are crucial to the structural integrity of the SC barrier and its constitution includes plaque proteins, such as plakoglobin, desmoglein-1 and desmocollin-1, which infiltrate the plasma membrane of the corneocyte and anchor it to the keratin filaments [13, 14]. The lower stratum corneum (stratum compactum) physiological characteristics show the presence of several corneodesmosomes and a superimposed structure [15]. Towards the skin surface, the characterization of the corneocytes shows a decrease of corneodesmosomes number. The cells detach at these regions forming a much looser SC structure, stratum disjunctum, where the corneocytes are in desquamation process [15, 16].

The stratum corneum physiological composition consists of 70% protein, 15% lipid and 15% water, compared to the 70% of water in the viable epidermis [16, 17]. Environmental conditions and the evaporative water flux from deeper layers control the SC water content [17]. The SC is an extremely hygroscopic membrane: it can absorb up to 500% of its dry weight, in less than 1h after immersion in water [18]. This membrane has vertical swelling, in a degree of 4 to 5 times its original width [18]. The intercellular regions correspond to 5-21% of the entire SC volume [1-3] and its composition comprises of neutral lipids (mainly, ceramides) originated in the membrane-coating granules (Odland bodies) of the stratum granulosum (viable epidermis) [19, 20]. These ceramides represent the main constituents of the intercellular regions (12 ceramides detected at this point) [20]. The ceramides composition includes sphingosine, phytosphingosine or 6-hydroxysphingosine base linked to a hydroxy fatty acid by an amide connection. The fatty acid is normally of 20 to 22 carbon atoms in length, with saturation and nonbranched. The saturation of these acids enables high order in the lateral packing of the intercellular lipids, which reduces the permeability of the stratum corneum [6, 17, 19]. The intercellular region has a high content in cholesterol, which suggests an enhancement in the fluidity of the overall skin structure. Additionally, cholesterol may be a factor in regulating the process of desquamation [21].

3.2 Epidermis

The stratum corneum cells originate and migrate from the viable epidermis, where extensive cellular division takes place [22]. Moreover, various stages of epidermal keratinization may occur (figure 2.3²).

² Image available at <http://www.virtualmedicalcentre.com/anatomy/oral-mucosa/59>, from *Virtual Medical Centre* (downloaded at 7/03/2012).

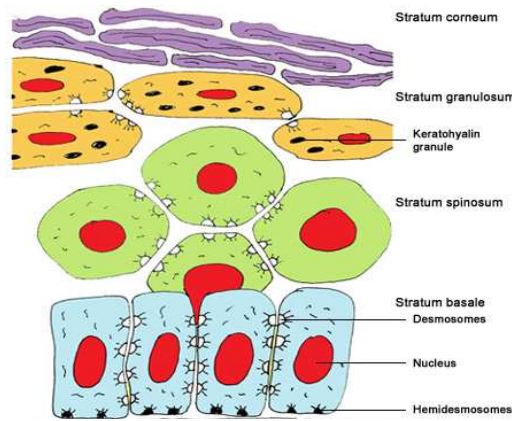


Fig. 2.3 – The viable epidermis and the process of keratinization.

The presence of the stratum lucidum only appears where the skin is exceptionally thick, mainly in palms and soles. Its composition includes five layers of dead, flattened keratinocytes filled with eleidin, an intermediate form of keratin [1-18]. The rate of mitosis in the stratum basale controls the thickness of the lucidum. In addition, the skin pigmentation (melanin content) determines the darkness of this stratum [19].

In the stratum granulosum, the keratinocytes lost their nuclei and the cytoplasm appears of granular shape because of keratohyalin accumulation. The keratohyalin granules contain profilaggrin, a precursor of the protein filaggrin, which promotes the aggregation and alignment of the keratin filaments. Additionally, Odland bodies can be found in this structure, and their function is the production of lipidic lamellar subunits, as well as some hydrolytic enzymes (proteases, lipases, glycosidases) [17-23]. These bodies fuse with the plasma membrane and release their content into the intercellular matrix, as the cells in the stratum granulosum progress into the SC [22, 23]. The lipid subunits are precursors of the SC's intercellular lipids: phospholipids, cholesterol and glucosylceramides. The released content also has enzymes, which can break down the phospholipids and convert the glucosylceramides into ceramides: the lipids that form the final epidermal barrier [20, 23]. The absence of phospholipids, one of the principal physiological features of the SC, occurs in this layer, where they transform into fatty acids [24, 25].

The connection between keratinocytes and corneodesmosomes appears in the stratum spinosum [20, 21]. Also, the immune Langerhans cells originate in this stratum. The scientific literature states that these cells derive from circulating blood monocytes because they share common marker characteristics [4, 6]. Considerable evidence shows that their dendritic appendages capture cutaneous antigens and deliver them to lymphocytes, which are responsible for the initiation of the immune response [4, 6].

Finally, the stratum basale or germinativum is a continuous monolayer situated above the basement membrane. This specialized membrane separates the epidermis from the dermis and controls the nourishing and traffic of a variety of cytokines and growth factors (active in the epidermal remodeling and repair processes) [26, 27]. The stratum basale consists of cuboidal keratinocytes, in constant mitotic division that feeds the outward migration of cells to the overlying layers: stratum spinosum, granulosum, lucidum and finally the stratum corneum. The basal cells exhibit large nuclei, cell organelles, diminished keratin filaments and melanocytes responsible for skin pigmentation. Additionally, cells responsible for touch-sensitive processes can be found in large numbers - Merkel cells [6, 11].

A summary of the keratinization process in the viable epidermis highlights the loss of cellular organelles [27-30]:

- Mitochondria and the endoplasmic reticulum decrease in quantity, until they are entirely absent by the level of the stratum lucidum;
- Large, dense and irregularly shaped masses (keratohyalin granules, precursor of keratin) appear in stratum granulosum cells;
- In the stratum granulosum, keratin filaments accumulate in the cells in a filamentous structure. Cells of the stratum lucidum consist exclusively of this altered ("keratinized") variety;
- Soluble interfibrillar material is lost in the stratum corneum, so the lower layers (stratum compactum) consist almost exclusively of a homogeneous mass of keratin;
- In the SC, corneodesmosomes comprise approximate regions of about 300 Å (Angstroms) adjacent to cell membranes, to promote keratin attachment. These corneodesmosomes appear in the same number in all cell layers until the stratum lucidum. Here, the intercellular lipids form a denser band stating an apparent loss of connection between corneocytes.

The pigmentation of the skin is a fundamental characteristic on protecting it from the UV radiation that can cause mutagenic effects in the keratinocytes DNA [1, 4, 8, 28]. The enzyme content of the melanocytes is responsible for the UV absorption by the following reactions: tyrosinase converts tyrosine to dihydroxyphenylalanine (*dopa*) and the latter to dopaquinone with the subsequent formation of melanin [28]. In detail, tyrosinase synthesis occurs in the rough endoplasmic reticulum and, afterwards, the Golgi body produces vesicles containing tyrosinase. These vesicles are the melanosomes, the melanin-synthesizing apparatus of the cell. The melanin transportation to the keratinocytes results from the action of dendrites and become especially prominent in the stratum basale [29, 30].

Essential Properties of Skin

The epidermis is an avascular layer, where its living cells receive needed nutrients by diffusion from the underlying dermal capillaries, through the basement membrane and then into the cells. Metabolic products of the cells enter the circulation by diffusion in the opposite direction. The basement membrane guarantees the support of the epidermis and serves as an attachment to underlying tissues. Moreover, it also represents an effective barrier to drug diffusion [29]. Along its surface, the basal cells exhibit many hemidesmosomes [21, 25], which increase the adherence of the basal cells (and therefore of the entire epidermis) to the basement membrane (and therefore to the dermis). The contact between the epidermis and dermis is an undulating surface with upward projections of the dermal papillae and complementary downward insertions of the epidermis, to increase surface area of contact and also the attachment process.

3.3 Dermis

The dermis corresponds to a water based tissue of connective collagen and elastin fibers embedded in glycosaminoglycans grids [1]. From the chemical nature of its constituents, this layer determines the characteristic strength and elasticity of the skin [4]. The predominant cells are fibroblasts (responsible for the production of connective tissue) and mast cells (specialized in the immune and inflammatory response). In diminished number, melanocytes can be found, as well as hair follicles (root hair plexus) and sweat ducts (figure 2.1), which originate deep in the dermis. Additionally, in the dermis, extensive blood flow system and others members of skin physiology, namely skin nutrition and repair systems can be found [4, 6]. Table 2-1 summarizes the main characteristics of the human skin layers.

Table 2-1 – Characteristics of human skin layers.

Skin layer	Thickness	pH	Principal cells	Vasculature	Function
SC	10-20 μm	4-5	Corneocytes	Not present	Barrier
Epidermis	50-150 μm	< 7.4	Keratinocytes Melanocytes Langerhans Merkel	Not present	Biosynthetic factor Metabolic barrier
Dermis	1-2 mm	7.4	Fibroblast Mast Endothelial Immune	Blood vessels Lymphatic Nutrition Repair system	Connective tissue Support tissue

4. Drug Diffusion Routes in the Skin

Drug diffusion through the skin favors the intercellular route because the transcellular pathway is highly inaccessible due to extensive pseudo-crystalline keratin filaments within the corneocytes [1, 10, 11, 16] – figure 2.4. The flow rate of drug diffusion across the intercellular spaces is conditional to the molecule lipophilicity, but also to other physicochemical properties, such as molecular weight, solubility and hydrogen bonding ability [1, 10]. However, the free movement of macromolecules in the lipidic structure presents physical restrictions because the available spaces are smaller than 50 Å [31, 32]. For such molecules, this suggests that the SC represent an additional barrier for drug diffusion, which is not the case for small molecules [32].

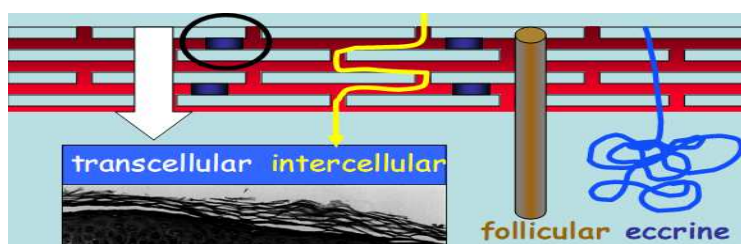


Fig. 2.4 – Schematic representation of the drug diffusion routes across human skin.

Another possibility for skin drug diffusion is the use of the skin appendages, i.e., hair follicles and sweat glands, which form shunt pathways through the intact epidermis [32-34]. These shunts could embody an alternative to overcome the difficulties in drug diffusion across the skin, but they only occupy 0.1% and 0.001 % (follicular and eccrine, respectively) of the entire human skin surface. This results in diminished contribution to the overall diffusion (eccrine are the most common sweat glands, but apocrine glands can also be found).

In conclusion, the main route for drug diffusion is the intercellular one because of the low diffusivity in the transcellular regions filled with pseudo-crystalline keratin filaments [1]. This route might be available for only small and polar compounds, although it is 100 times longer than the route through the skin lipids [32].

5. The Stratum Corneum Role in the Barrier Function

The intercellular lipids constitute the only continuous area across the SC, which means that the lipid organization of the skin is a defining factor in the barrier function. The detail structure and physical state of the intercellular lipids is rationalized by two biophysical models. The first model clearly states that the lipids organize in highly packed lamellar bilayer structures [35, 36].

Several studies added that the lipid lamella orientation is almost parallel to the corneocyte surface with repetitive distances of approximately 6.0-6.4 nm and 13.2-13.4 nm [37, 38].

X-ray diffraction studies [24] reveal that these lipid domains could be found in a coexistence of crystalline, gel and liquid phases. The lipid lateral packing in a crystalline phase exhibits an orthorhombic orientation (figure 2.5³), the gel phase a hexagonal orientation and the liquid phase a non-specific one [39]. The predominant lateral orientations, orthorhombic and hexagonal, differ in the distances between the lipids head groups. Hexagonal packing has a distance between lipids of 0.41 nm (nanometers), whereas orthorhombic is 0.37 nm. This means that the latter organization is tighter packed, thereby reducing the open spaces for drug diffusion [39].

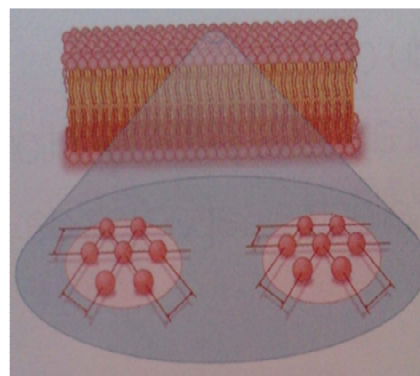


Fig. 2.5 – The orthorhombic lipid lateral organization in the SC.

The stratum disjunctum has a hexagonal lateral packing and the inner regions of the stratum compactum possess the tightly packed orthorhombic lipid lamellae [40]. At physiological temperatures, the SC lipids of humans, pigs and mice arrange in a lamellar structure with two repeating units: a long periodicity phase (LPP) with a repeat length of ca. 134 Å and a short periodicity phase (SPP) with a repeat length of ca. 60 Å [38, 39, 40-46]. The LPP does not exist in other biological barriers, and its occurrence in the SC reflects its crucial relevance for the barrier function [40-42]. The LPP formation depends on the presence of long chain ceramides, although, free fatty acids can promote the formation of the SPP by inducing the transition from a hexagonal lateral organization to the orthorhombic lateral matrix and to increase the fraction of SC lipids forming a liquid phase [40-46]. The probable existence of SC lipids in a more fluid phase should be responsible for the normal rates of transepidermal water loss (100-150 mL per day and square meter of healthy skin [42]). Furthermore, it may increase skin elasticity (in addition to elastin fibers in the dermis) and allow the existence of enzymatic activity that otherwise was unlikely in a fully developed crystalline phase [43].

The works of Norlén *et al* [47-49] introduce the second model of lipid structure, which advocates that the SC's intercellular lipids organize as a single gel phase model. From an organizational and packing point of view, it considers that the SC intercellular regions exist as a single and repetitive lamellar gel phase. This model represents a clear opposition to the previous one because it does not consider phase separation structures in the unperturbed stratum corneum structure.

³ Image available at the market report *Expression Cosmétique – The global information on cosmetics and fragrances*, N° 15, 2012 (ISSN 2108-1956).

The different rationalizations of the stratum corneum organization reveal ambiguous characterization of the barrier function [40, 45]; nevertheless this feature must be related to its constituents (figure 2.6⁴). The water permeability in the SC is three orders of magnitude lower than all the other biological membrane [50]. Clearly, this relates to the components therein or their lack, namely the phospholipids that typically provides flexibility and exchange pathways between two membrane environments [50, 51]. The lipid matrix production occurs in the stratum granulosum, where hydrolytic enzymes synthesize the ceramides (41%), free fatty acids (9%), cholesterol (27%), cholesteryl esters (10%) and colesteryl sulfate (2%) [51]. The essential role of the SC lipids reveals itself after physical removal by solvent extraction procedures, which lead to significant increases in water loss or drug diffusion rates [49, 50].

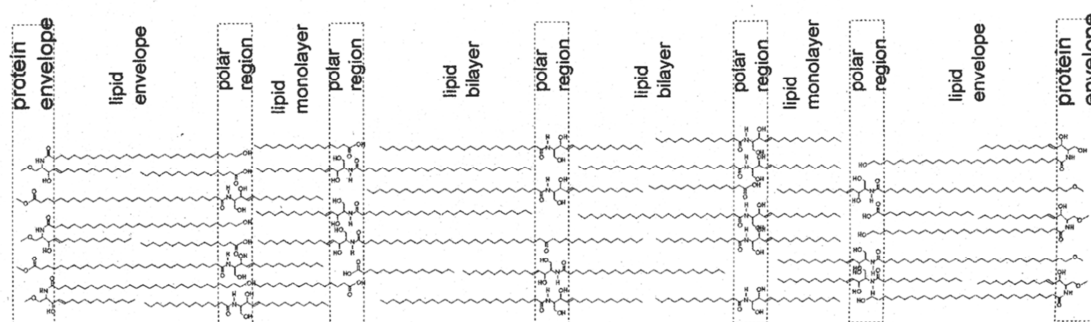


Fig. 2.6 – Biological interpretation of the SC membrane arrangement. Intercellular regions with long alkyl chains ceramides connected to polar head groups and then to the keratinocytes (protein envelope).

Ceramides play a crucial role in both organizational models, and many classes (12) can be identified in the human stratum corneum. Ceramides are sphingolipids that consist of a long amino alcohol chain, where a non-hydroxy fatty acid or a α -hydroxy fatty acid links itself *via* an amide bond [39, 46]. The literature refers that the least polar of these ceramides, ceramide 1 or acylceramide [40], plays a decisive role in the lipid organization, or more accurately, leads the system to a molecular arrangement typical of a stable lipid association [40].

The saturated free fatty acids vary the chain length between C16 and C24 [51]. The long carbon chain lengths of these molecules contribute to the tight lateral packing resulting in a less fluid and less permeable lipid domains, than the liquid crystalline organization of phospholipids in others biological membranes [11].

⁴ Image available at the market report *Expression Cosmétique – Guide des ingrédients cosmétiques*, 2011 (ISSN 2108-1956).

6. Desquamation Process in the Stratum Corneum

The desquamation process of the stratum corneum maintains an unceasing renewal of the barrier function as it loses its protective function, in correspondence to the replacement of its outermost layer of corneocytes [51, 52]. The desquamation involves a two stage process: (1) release of intact corneocytes, presumably after the degradation of all the corneodesmosomes, and (2) loss of the intercellular adhesive structures between the corneocytes.

An explanation to the decrease of SC cohesion relates with a decrease in the number of corneodesmosomes across the SC [54]. Suzuki *et al* [53, 55] revealed that corneodesmosomes degradation occurs by proteases present in the extracellular spaces of the SC, the SC tryptic enzyme (SCTE) and the SC chymotryptic enzyme (SCCE). These proteins specialize in the proteolysis of the corneodesmosal proteins, desmoglein I, desmocollin and corneodesmosin (figure 2.7⁵) [57, 58]. Additionally, environmental conditions and biochemical factors, such as humidity, cholesterol sulfate, calcium ion concentration and pH may also play a pivotal role in desquamation; however the role of these factors remain unclear [56].

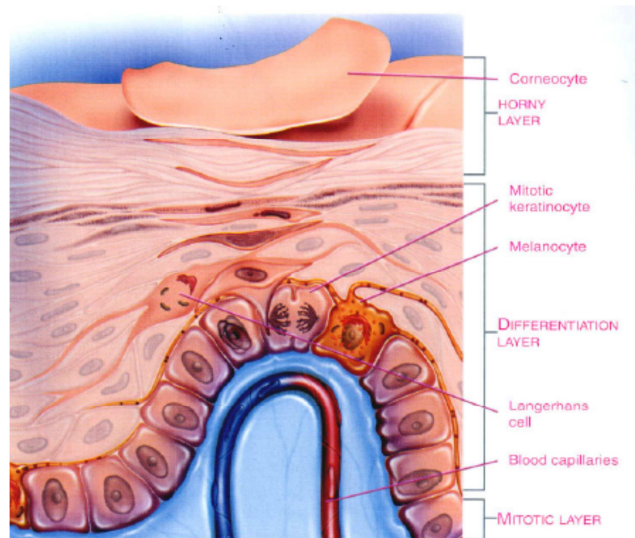


Fig. 2.7 – The keratinocytes division in the stratum basale with the migration process to the SC. The corneocytes loose the cohesive properties on contact with the proteolytic enzymes (SCTE and SCCE).

A normal desquamation is of crucial importance for the maintenance of the SC barrier function and a normal skin appearance. The total turnover in one day corresponds to a loss of about 40 milligrams (mg) of horny cells [17].

In a normal health conditions, the loss of desquamated monolayers corresponds to the rate of epidermal cell production. Additionally, the body has emergency mechanisms to reply to a systemic failure in the SC renewal, namely the increase of the overall keratinization process (increased SC thickness) by epidermal growth factors [17, 52-58].

⁵ Image available at the market report *Monographic Supplement Series of Household and Personal Care Today: Anti-aging and Beauty inside*, N° 1, 2012 (ISSN 2035-4614).

7. Hydration of the Stratum Corneum

An equilibrium state between the human body and its surroundings requires that all skin structures and their secretions converge in a homeostatic state. Conservation of the skin homeostasis thus results from regulations of the hemodynamic and thermal properties of the skin barrier [59].

Stratum corneum water content plays a key role in the skin hydration. In this layer, the ability to set water from deeper tissues depends on the lipid retention, and thus a disruption in the SC barrier enhances perspiration processes [60-62].

The water retention within the stratum corneum depends on three aspects [60]:

- Presence of natural hygroscopic agents within the corneocytes (collectively referred to as Natural Moisturizing Factor - NMF);
- Presence of unperturbed intercellular lipids, which forms a barrier against transepidermal water loss (TEWL) [63];
- A tortuous pathway across the intercellular domains that inhibits the exiting of water (inducing a slow rate process).

The natural moisturizing factor refers to a complex mixture of water soluble compounds with low molecular weight, resulting from the degradation of filagrine by the corneocytes. The keratinization process induces the breakdown of this protein that otherwise provides structural integrity of SC cells in a linear structure [64].

The NMF composition results from a mixture of the histidine amino acids of filagrine, organic acids and their salts, urea and inorganic ions [59, 64]. These substances promote the setting of water in the stratum corneum because of the hygroscopic effect and by their moisturizing properties. Among them, sodium lactate and the sodium salt of 2-pyrrolidone-5-carboxylic acid appear to have the most hygroscopic capacity [59].

The water content of the stratum corneum is required for its own renewal process, thus an increase in the TEWL may lead to structural damage in the functional enzymes (loss of the quaternary structure) involved in the desquamation process. This results in the formation of small granules visible on the surface of the skin, which causes the appearance of dehydrated skin and the consequent loss of pronounced biomechanical properties [62, 63]. The regulation of water content in the skin arises from an endogen or an external source. The endogen source results from the diffusion of water from the dermis to the SC surface that produces insensible

Essential Properties of Skin

perspiration or normal sweating [59]. The external contribution result from environmental moisture or aesthetic hydrophilic formulations that interact with NMF components of the corneocytes [65].

The cutaneous senescence follows the association of two natural processes [59-64]: (1) the decrease in the hydrolipidic emulsion that covers the skin (13% to 7%, in percentage of SC water content), which is a mantle formed by the secretion products of the sebaceous and sweat glands and (2) the decrease in the glycosaminoglycans concentration (factors of tissue elasticity) and electrolytes in dermal tissue. The promotion of skin senescence and dehydration increases upon the action of external conditions, such as the wind, temperature rise and dry air. Additionally, chemical substances can extract NMF components, such as surfactants, and certain diseases, such as ichthyoses, dermatitis, psoriasis and/or eczemas can disrupt the SC organization, thus eliminating the capacity of water retention. The maintenance of skin homeostatic state achieved by a hydric balance has external mechanisms depicted in table 2-2 [59]:

Table 2-2 – Procedures for recovering hydric balance in the skin.

Correction Mechanism	Compounds
Passive mechanism	Occlusive formulations e.g., vaseline
Active Mechanism	Hygroscopic and humectants e.g., glycerin, and hyaluronic acid
Aesthetic hydrophilic formulations	Protective and emollient action e.g., vegetable triglycerides, lanoline and cholesterol
Essential fatty acids	Vitamin F, arachidonic acid, linolenic linoleic acid.
Substances similar to NMFs'	Urea, sodium lactate, pyrrolidone, sodium carboxylate)
Substances with anti-oxidative power	Retinoic acid, alpha-hydroxy acids

8. References

- [1] B.W. Barry, Novel mechanisms and devices to enable successful transdermal drug delivery. *Eur. J. Pharm. Sci.*, 14, (2001) 101-114.
- [2] R. Wickett, M. Visscher, Structure and function of the epidermal barrier. *Am. J. Infect. Control*, 34 (2006) 98-110.
- [3] R. Paus, What is the 'true' function of the skin? *Exp. Dermatol.*, 11 (2002) 159-187.
- [4] K.A. Walters, *Dermatological and transdermal formulations*, Marcel Dekker, New York, 2002.
- [5] M. Brown, G. Martin, S. Jones, F. Akomeah. *Dermal and transdermal drug delivery systems: Current and future prospects*. *Drug Delivery*, 13 (2006) 175-187.
- [6] J.E. Riviere, *Dermal absorption models in toxicology and pharmacology*. CRC Press, Boca Raton, 2006.
- [7] R. Marks, The stratum corneum barrier: the final frontier. *J. Nutr.*, 134 (2004) 2017-2021.
- [8] P.M. Elias, Stratum corneum defensive functions: an integrated view. *J. Invest. Dermatol.*, 125 (2005) 183-200.
- [9] R.J. Scheuplein, Percutaneous absorption after twenty-five years: or "old wine in new wineskins". *J. Invest. Dermatol.*, 67 (1976) 31-38.
- [10] M.R. Prausnitz, R. Langer, Transdermal drug delivery. *Nature Biotechnology*, 26 (2008) 1261-1268.
- [11] G.K. Menon, New insights into skin structure: scratching the surface. *Adv. Drug Deliv. Rev.*, 54 (2002) 3-17.
- [12] E. Berardesca, Disorders of skin barriers: clinical implications. *J. Eur. Acad. Dermatol. Venereol.*, 16 (2002) 559-561.
- [13] J.C.R. Jones, S.B. Hopkinson, L.E. Goldfinger, Structure and assembly of hemidesmosomes. *BioEssays*, 20 (1998) 488-494.
- [14] D.T. Woodley, Importance of the dermal-epidermal junction and recent advances. *Dermatologica*, 174 (1987) 1-10.
- [15] B. Sondell, L.-E. Thornell, T. Egelrud, Evidence that stratum corneum chymotryptic enzyme is transported to the stratum corneum extracellular space via lamellar bodies. *J. Invest. Dermatol.*, 104 (1995) 819-823.
- [16] C.R. Harding, The stratum corneum: structure and function in health and disease. *Dermatol. Therapy*, 17 (2004) 6-15.
- [17] P. Elias, Epidermal lipids, barrier function, and desquamation. *J. Invest. Dermatol.*, 80 (1983) 44-49.

- [18] A.V. Rawlings, P.J. Matts, Stratum corneum moisturization at the molecular level: an update in relation to the dry skin cycle. *J. Invest. Dermatol.*, 124 (2005) 1099-1110.
- [19] A.E. Kalinin, A.V. Kajava, P.M. Steinert, Epithelial barrier function: assembly and structural features of the cornified cell envelope. *BioEssays*, 24 (2002) 789-800.
- [20] F. Chang, D.C. Swartzendruber, P.W. Wertz, C.A. Squier, Covalently bound lipids in keratinizing epithelia. *Biochim. Biophys. Acta* 1150 (1993) 98-102.
- [21] E. Christophers, Cellular Architecture of the Stratum Corneum. *J. Invest. Dermatol.*, 56 (1971) 165-169.
- [22] L. Landmann, Epidermal permeability barrier: transformation of lamellar granule disks into intercellular sheets by a membrane fusion process. *J. Invest. Dermatol.*, 87 (1986) 202-206.
- [23] G.F. Odland, The fine structure of the interrelationship of cells in the human epidermis. *J. Biophys. Biochem. Cytol.*, 25 (1958) 529-538.
- [24] J.A. Bouwstra, G.S. Gooris, J.A. Van der Spek, W. Bras, Structural investigations of human stratum corneum by small-angle x-ray scattering. *J. Invest. Dermatol.*, 97 (1991) 1005-1012.
- [25] I. Brody, Intercellular space in normal human stratum corneum. *Nature*, 209 (1966) 472-476.
- [26] J.R. Hazel, E.E. Williams, The role of alterations in membrane lipid composition in enabling physiological adaptation of organisms to their physical environment. *Prog. Lipid Res.*, 29 (1990) 167-227.
- [27] C.C. Selby, An electron microscope study of thin sections of human skin. *J. Invest. Dermatol.*, 29 (1957) 131-149.
- [28] C.R. Harding, The stratum corneum: structure and function in health and disease. *Dermatol. Therapy*, 17 (2004) 6-15.
- [29] J. Bouwstra, G. Pilgram, G. Gooris, H. Koerten, M. Ponc, New aspects of the skin barrier organization, *Skin Pharmacol. Appl. Skin Physiol.*, 14 (2001) 52-62.
- [30] P.W. Wertz, Stratum corneum lipids and water. *Exog. Dermatol.*, 3 (2004) 53-56.
- [31] G. Cevc, G. Blumeb, A, Schtitzlein, D. Gebauer, A. Paul, The skin: a pathway for systemic treatment with patches and lipid-based agent carriers. *Advanced Drug Delivery Reviews*, 18 (1996) 349-378.
- [32] T.W. Prow *et al*, Nanoparticles and Microparticles for Skin Drug Delivery, *Adv. Drug Del. Rev.*, (2011) doi:10.1016/j.addr.2011.01.012.
- [33] T. Serizawa, T. Onodera, K. Oba, Percutaneous absorption of a drug into hair follicles. *Exog. Dermatol.*, 22 (1995) 195-200.

- [34] L.M. Lieb, B.D. Brown, G.G. Krueger, A.P. Liimatta, R.N. Bryan, Description of the intrafollicular delivery of large molecular weight molecules to follicles of human scalp skin in vitro. *J. Pharm. Sci.*, 86 (1997) 1022-1029.
- [35] G.M. Gray, H.J. Yardley, Lipid compositions of cells isolated from pig, human, and rat epidermis. *Journal of Lipid Research*, 16 (1975) 434-440.
- [36] F. Bonté, A. Saunois, P. Pinguet, A. Meybeck, Existence of a lipid gradient in the upper stratum corneum and its possible biological significance. *Arch. Dermatol. Res.*, 289 (1997) 78-82.
- [37] M. Ponec, A. Weeheim, P. Lankhorst, P. Wertz, New acylceramide in native and reconstructed epidermis. *J. Invest. Dermatol.*, 120 (2003) 581-588.
- [38] I. Hatta, N. Ohta, S. Ban, H. Tanaka, S. Nakata, X-ray diffraction study on ordered, disordered and reconstituted intercellular lipid lamellar structure in stratum corneum. *Biophys. Chem.*, 89 (2001) 239-242.
- [39] J.A. Bouwstra, G.S. Gooris, F.E.R. Dubbelaar, M. Ponec, Phase behaviour of lipid mixtures based on human ceramides: coexistence of crystalline and liquid phases. *J. Lipid Res.*, 42 (2001) 1759-1770.
- [40] J.A. Bouwstra, G.S. Gooris, F.E.R. Dubbelaar, M. Ponec, Phase behaviour of stratum corneum lipid mixtures based on human ceramides: the role of natural and synthetic ceramide 1. *J. Invest. Dermatol.*, 118 (2002) 606-617.
- [41] J.A. Bouwstra, G.S. Gooris, F.E.R. Dubbelaar, M. Ponec, Phase behaviour of lipid mixtures based on human ceramides: coexistence of crystalline and liquid phases. *J. Lipid Res.*, 42 (2001) 1759-1770.
- [42] J.A. Bouwstra, G.S. Gooris, F.E.R. Dubbelaar, A.M. Weerheim, A.P. Ijzerman, M. Ponec, Role of ceramide 1 in the molecular organization of stratum corneum lipids. *J. Lipid Res.* 39 (1998) 186-196.
- [43] T.J. McIntosh, M.E. Stewart, D.T. Downing, X-ray diffraction analysis of isolated skin lipids: reconstitution of intercellular lipid domains. *Biochemistry*, 35 (1996) 3649-3653.
- [44] S.H. White, D. Mirejovsky, G.I. King, Structure of lamellar lipid domains and corneocyte envelopes of murine stratum corneum. An X-ray diffraction study. *Biochemistry*, 27 (1988) 3725-3732.
- [45] C.L. Gay, R.H. Guy, G.M. Golden, V.H.W. Mak, M.L. Francoeur, Characterization of low-temperature (i.e. < 65°C) lipid transitions in human stratum corneum. *J. Invest. Dermatol.*, 103 (1994) 233-239.
- [46] J. Novotný, B. Janůšová, M. Novotný, A. Hrabálek, K. Vávrová, Short-Chain Ceramides Decrease Skin Barrier Properties, *Skin Pharmacol Physiol* 22 (2009) 22-30.

- [47] L. Norlén, Skin structure, function and formation - learning from cryo-electron microscopy of vitreous, fully hydrated native human epidermis. *Int. J. Cosm. Sci.* 25 (2003) 209-226.
- [48] L. Norlén, A. Al-Amoudi, J. Dubochet, A cryotransmission electron microscopy study of skin barrier formation. *J. Invest. Dermatol.*, 120 (2003) 555-560.
- [49] L. Norlén, Skin barrier formation: the membrane folding model. *J. Invest. Dermatol.*, 117 (2001) 823-829.
- [50] R.O. Potts, M.L. Francoeur, Lipid biophysics of water loss through the skin. *Proc. Natl. Acad. Sci. USA*, 87 (1990) 3871–3873.
- [51] A. Weerheim, M. Ponc, Determination of stratum corneum lipid profile by tape stripping in combination with high-performance thin-layer chromatography. *Arch. Dermatol. Res.*, 29 (2001) 191-199.
- [52] S.J. Chapman, A. Walsh, S.M. Jackson, P.S. Friedmann. Lipids, proteins and corneocyte adhesion. *Arch. Derm. Res.*, 283 (1991) 167- 173.
- [53] Y. Suzuki, J. Nomura, J. Hori, J. Koyama, M. Takahashi, I. Horii. Detection and characterization of endogeneous protease associated with desquamation of stratum corneum. *Arch. Derm. Res.*, 285 (1993) 372-377.
- [54] L. Hansson, M. Strömqvist, A. Bäckman, P. Wallbrandt, A. Carlstein, T. Egelrud, Cloning, expression, and characterization of stratum corneum chymotryptic enzyme. *J. Biol. Chem.*, 269 (1994) 19420-19426.
- [55] M. Brattsand, T. Egelrud. Purification, molecular cloning, and expression of human stratum corneum trypsin-like serine protease with possible function in desquamation. *J. Biol. Chem.* 274 (1999) 30033-30040.
- [56] A. Rawlings, C. Harding, A. Watkinson, J. Bank, C. Ackerman, R. Sabin. The effect of glycerol and humidity on desmosome degradation in stratum corneum. *Arch. Derm. Res.*, 287 (1995) 457-464.
- [57] I.A. King, A. Tabiowo, P. Purkis, I. Leigh, A.I. Magee. Expression of distinct desmocollin isoforms in human epidermis. *J. Invest. Dermatol.* 100 (1993) 373-379.
- [58] I.E. Eckholm, M. Brattsand, T. Egelrud, Stratum corneum tryptic enzyme in normal epidermis: a missing link in the desquamation process? *J. Invest. Dermatol.*, 114 (2000) 56-63.
- [59] *Skin and Aging Processes.* Barbara A. Gilchrest. CRC Press, Inc. Boston. 1983.
- [60] I.O. Smirnova, Functional morphology of skin ageing. *Adv. Gerontol.*, 13 (2004) 44-51.
- [61] K.L. Dalziel, Aspects of cutaneous ageing. *Clin Exp Dermatol.*, 16 (1991) 315-23.
- [62] S. Verdier-Sévrain, F. Bonté, Skin hydration: a review on its molecular mechanisms. *J. Cosmet. Dermatol.*, 6 (2007) 75-82.

- [63] S. Meguro, Y. Arai, Y. Masukawa, K. Uie, I. Tokimitsu, Relationship between covalently bound ceramides and transepidermal water loss (TEWL). *Arch. Dermatol. Res.*, 292 (2000) 463-468.
- [64] P. Chandar, G. Nole, A.W. Johnson, Understanding natural moisturizing mechanisms: implications for moisturizer technology. *Cutis*. 84 (2009) 2-15.
- [65] J.M. Crowther, A. Sieg, P. Blenkiron, C. Marcott, P.J. Matts, J.R. Kaczvinsky, A.V. Rawlings, Measuring the effects of topical moisturizers and changes in stratum corneum thickness, water gradients and hydration in vivo. *Br. J. Dermatol.*, 159 (2008) 567-77.

III

**Basic Concepts
in Transdermal
Drug Delivery**

1. Introduction

The past 30 years witnessed an explosion in the discovery, design and establishment of new therapeutic agents and pharmaceuticals. The correspondent innovations in drug delivery systems have not fully empowered successful delivery of many of those novel pharmaceuticals nor developed new treatments for current drugs [66, 67].

Drug delivery is the administration of a pharmaceutical into a human / animal body to achieve a therapeutic effect for a medical condition or disorder. Drugs can be administered into the body through three main routes:

- Enteral (drugs administered through gastrointestinal tract)
 - Oral - through the mouth;
 - Sub-lingual - under the tongue;

- Parenteral (drugs injected into the body)
 - Intravenous – injection into a vein;
 - Subcutaneous - injection beneath the skin;
 - Intramuscular - injection into a muscle;

- Others (drugs administered through mucosal membranes, skin or others)
 - Ocular - instilled in the eye [68];
 - Nasal - absorbed through nasal membranes [69];
 - Rectal and vaginal – absorbed through genital tissue [70];
 - Topical – delivery *in situ* to the skin;
 - Transdermal - delivered through the skin for a systemic purpose.

The common routes for administering drugs are either orally or parenterally being oral the preferred in drug delivery as it is convenient, safe and inexpensive [72]. Nevertheless, it presents several limitations, which include low bioavailability of various drugs due to the hepatic first pass metabolism [1, 4]. In oral delivery, the drug travels to the liver through the intestinal wall before transportation to its target *via* the bloodstream. The intestinal wall and liver may chemically alter (metabolize) many drugs, decreasing the amount of drug reaching the bloodstream. Some orally administered drugs also irritate the digestive tract [1].

Moreover, many of these drugs lose their therapeutic efficiency due to the harsh acidic environment and digestive enzymes of the stomach content [73], or they are either poorly or erratically absorb through the digestive pathway.

Administration of drugs through injections is the next most common route, which includes the intravenous, intramuscular and subcutaneous routes. The use of a hypodermic needle constitutes the traditional method of parenteral administration and an effective way of delivering a drug. A *bolus* delivery of a drug (e.g., a vaccine), may be completed within one minute with essentially no cost, though the World Health Organization estimates that the subsequently disposable accounts for tens of dollars [72].

In the subcutaneous route, a needle inserts into the fatty tissue just beneath the skin. The injected drug moves into small blood vessels and reaches the bloodstream through lymphatic vessels [73]. The subcutaneous route is used in the administration of various drugs, such as vaccines because otherwise these macromolecules would be digested in the gastrointestinal tract, upon oral intake. The application of the intramuscular route instead of the subcutaneous route occurs when a large volume of a drug is necessary.

In the intravenous route, a needle inserts directly into a vein and a solution containing the drug diffuses by a single dose or continuous infusion. The characterization of this route includes a high bioavailability of the drug, the ability to deliver a precise dose immediately and a controlled medical procedure. However, it can produce a negative impact in the symptomatic condition of the patient. Patient lack of compliance due to needle phobia is one of the main drawbacks, but contamination, waste issues and dosing mistakes establish drug injection, as a traumatic experience for millions around the world [72, 73]. Additionally, administration through intravenous injections requires experienced and trained personnel, because it is difficult to insert a needle or catheter into a vein.

Taking in account the public concern with parenteral drug delivery, the American Congress approved the *Needlestick Safety and Prevention Act*, where there is a reference to more than 1 million needle sticks and contaminations each year in the United States (US) alone, which can lead to fatal diseases, such as hepatitis A or C [72]. Moreover, for hepatitis B, as much as 20% of the viral transmissions are estimated to be caused in this way [72]. According to the World Health Organization (WHO), the unsafe injection practice accounts for more than 1.3 million deaths and costs \$535 million annually [72].

In order to overcome the identified drawbacks in traditional drug delivery routes, researchers started to consider alternate routes to deliver drugs into the body, such as the eyes [71], mucosal membranes [69], genitals [70] and skin [1, 5, 10, 73]. Due to the ease of application and large area of surface, transdermal drug delivery (TDD) can be particularly attractive when compared to these other routes.

Basic Concepts in Transdermal Drug Delivery

The development of transdermal drug delivery systems (TDDS) that show efficacy, safety and increase bioavailability over the enteral and parenteral route will certainly impact the everyday life in the medical practice. Additionally, it can produce dramatic changes in the topical application of drugs for treatment of localized skin diseases or nourish the skin for beauty reasons, which is nowadays practiced with hypodermic needles [10, 72]. There are several TDDS and various passive formulations available, which provides alternatives to oral and parenteral route, however, the diminished flow rates of drug diffusion across the skin is limited by restrictive physicochemical properties.

2. Historical Landmarks in Transdermal Drug Delivery

In the last decades, transdermal drug delivery systems accomplished several medical landmarks and developed into a fashionable solution for many diseases (figure 3.1) [72, 73]. Two main routes characterize the TDDS; transdermal permeation defines the passage of a substance, such as a drug, from the outside of the skin through its various layers, into the bloodstream. Topical delivery describes the application of a formulation containing the drug to the first layers of the skin to treat cutaneous disorders (e.g., acne) or the cutaneous manifestations of a general disease (e.g., psoriasis) with no drug reaching the systemic circulation.

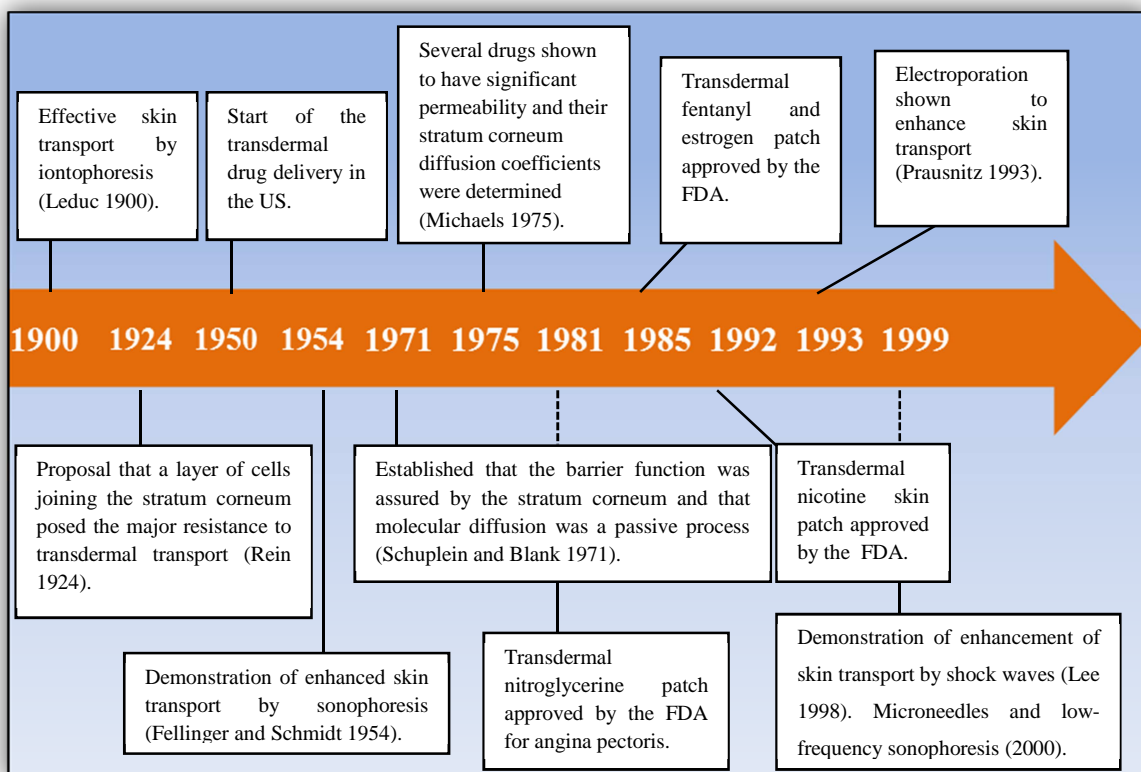


Fig. 3.1 – Historical landmarks in transdermal drug delivery.

3. Advantages of Transdermal Delivery versus other Drug Delivery Systems

Table 3-1 summarizes the main advantages of TDDS with respect to oral and intravenous delivery, which may favor patient compliance to the treatment.

Table 3-1 – Transdermal drug delivery versus oral and intravenous administration of drugs.

Feature	Transdermal	Oral	Intravenous
Reduced first-pass effects	✓	○	✓
Constant drug levels	✓	✓	○
Self-administration	✓	✓	○
Unrestricted patient activity	✓	✓	○
Non invasive	✓	✓	○

This summary shows the enormous potential of TDDS and provides the motivation for intense research in this field. The main advantages for transdermal delivery can be expressed as [5, 73]:

- Large and readily accessible surface area for absorption, 2 m²;
- Avoids the disadvantages of oral drug delivery, such as gastrointestinal distress;
- Avoids the hepatic first-pass effect;
- Allows effective use of drugs with short therapeutic windows;
- Provides controlled maintenance of plasma levels of potent drugs after initial administration;
- The patient-modulated drug delivery improves patient compliance;
- Allows discontinuation of drug delivery in case of adverse reactions.

One of the main features of transdermal drug delivery relates with the reduced first-pass effect [1]. The ingestion of drugs *via* oral delivery corresponds to its passage through the liver, in which they undergo metabolism and degradation reactions with enzymes present therein, before entering the bloodstream. This first-pass effect results in diminished amounts of available drug to reach the site of action and higher doses must be prescribed to compensate it. In comparison, the skin structure provides a direct path to the bloodstream, reducing the first-pass effect and the over dosing effects (concomitant administration of lower doses).

The intravenous introduction of drugs to the body avoids many of the shortfalls described in table 3-1, though its invasive and stressful nature (particularly, for chronic administration) encourages the search for alternative strategies.

Further benefits of TDD systems emerged over the past few years as technologies evolved in its efficacy and safety. These include the potential for sustained release (useful for drugs with short

biological half-lives requiring frequent oral or parenteral administration) and controlled input kinetics, which is essential for drugs with narrow therapeutic indices [73]. The TDD clinical use must be justified therapeutically because drugs with high oral bioavailability and short dosing schedules do not require alternative deliveries. Transdermal administration does not correspond to immediate therapeutic levels of a certain drug; thus its use, is only considered for sustained therapeutics over a relatively large period a time or chronopharmacological management therapies, such as hormone internalization [72, 73].

Nevertheless, a large range of drugs remains of interest for TDD, but their transdermal administration is presently unfeasible [5, 73]. The nature of the SC is, in essence, the key to this problem. The diffusional resistance offered by this membrane results in daily drug doses that do not exceed the $\leq 10 \text{ mg}$ range [72, 73], even for a reasonable transdermal patch area.

This limitation imposes the first criterion for a successful transdermal candidate: transdermal drugs must be pharmacologically potent, requiring therapeutic blood concentrations in the nanograms per milliliter (ng ml^{-1}) range. The second criterion is related to the SC physiology that restricts molecules that can be transported across this outer covering. Not all molecules that pass the 'potency' test will have the necessary physicochemical properties (summarized in figure 3.2) [1, 5, 10, 72, 73]:

Ideal limits of Drugs for TDD	
Characteristics	Value
<input type="checkbox"/> Aqueous solubility	<input type="checkbox"/> $\geq 1 \text{ mg ml}^{-1}$
<input type="checkbox"/> Lipophilicity	<input type="checkbox"/> $1 \leq \log K_{O/W} \leq 3$
<input type="checkbox"/> Molecular weight	<input type="checkbox"/> $< 500 \text{ Da}$
<input type="checkbox"/> Melting point	<input type="checkbox"/> $< 200 \text{ C}$
<input type="checkbox"/> pH	<input type="checkbox"/> 5-9
<input type="checkbox"/> Maximum dose	<input type="checkbox"/> 10 mg day^{-1}

Fig. 3.2 - Ideal limits for the physico-chemical properties for candidates to TDD ($K_{O/W}$ represents for partition coefficient oil/water).

The works of Lipinski *et al* [74] developed a scientific rule of thumb for the solubility and diffusion of drugs across biological barriers based upon experimental data. The Rule of Five predicts suitable drug candidates for body intake, but was developed primarily for oral delivery. However, recent studies concluded that a vast majority of non-oral drugs ($\geq 98\%$) have physico-chemical properties within the limits of this rule [74]. The intrinsic characteristics of skin physiology restrict even further transdermal drug diffusion, which results in the following postulates:

- The logarithm of octanol/water partition coefficient ($K_{O/W}$) ≤ 3 ;
- Molecular weight (MW) < 500 Dalton;
- Not more than 5 hydrogen bonds donors;
- Not more than 10 hydrogen bond acceptors.

4. Drawbacks of Transdermal Drug Delivery Systems

The prospect of combining transdermal delivery with therapeutic efficacy, safety and patient compliance has captured the attention of many pharmaceutical companies and the scientific community. Nevertheless, there are limitations to TDD that must be taken into account, in the design of its applications, namely [75, 76]:

- Narrow range of drugs that can surpass the skin barrier function;
- Difficult to obtain high blood levels of drugs;
- The living skin has several enzymes that might metabolize the drug;
- The fashionable passive delivery, transdermal patches, may be uncomfortable to wear;
- The transdermal technologies may cause skin irritation;
- Transdermal devices may be more expensive than other traditional routes of administration.

5. Transcutaneous Absorption in the Skin

Transcutaneous absorption is a phenomenon that describes the diffusion of drugs and/or metabolites through the intercellular spaces rather than through a skin cell. This definition characterizes the scientific data on transdermal drug diffusion because the intercellular pathway remains the main route for TDD [75]. Consequently, the parameters that govern the absorption of drugs across the skin are similar to those in semipermeable membranes and the passage of the stratum corneum implies that the transcutaneous flow is directly proportional to the concentration gradient of the incoming drug [1, 5].

Fick's diffusion law describes this phenomenon and its modulation may improve drug flow rates [4]. The direct correlation between concentration and diffusion raises difficulties in TDD development because of the importance of the drug physico-chemical properties, such as size, stability or volatility. Drug permeation can be further enhanced by the use of carriers, absorption enhancers or physical delivery devices [1, 73].

6. Events governing Transdermal Drug Delivery

6.1 Drug Lipophilicity

Essentially, the stratum corneum barrier is a lipophilic barrier, with the intercellular lipid domains forming channels through which drugs diffuse in order to achieve the underlying vascular infrastructure and to ultimately access the systemic circulation [75]. Consequently, highly lipophilic molecules with low molecular weight demonstrate the highest flow rate through the stratum corneum [1, 75]. Until it reaches the bloodstream, drug diffusion is a two-step process: first, a molecule releases from the formulation and partitions into the SC, and then, it spreads into the aqueous layer beneath, viable epidermis, which composition contains 70% of water (15% of water in the SC).

Ideally, lipophilic drugs diffuse promptly through the lipid lamellae but are trapped when they reach the aqueous layers. The opposite holds true for hydrophilic compounds as they try to surpass the stratum corneum barrier. Therefore, the drug must have an affinity for both lipid and aqueous environment for an effective transcutaneous absorption ($\log K_{O/W}$ between 1 and 3).

After the passage of the intercellular regions, transdermal drug delivery may be enhanced by the cutaneous blood flow [77]. Mechanisms that maximize the cutaneous blood flow may facilitate drug diffusion through the skin due to the maintenance of a high concentration gradient of the drug in the tissues. Fever, physical exercise, and vasodilators are examples of these mechanisms. Whereas, some systemically administered vasoconstrictors may reduce the transcutaneous absorption of drugs (shutdown of the capillary network in the skin).

6.2 Drug Mobility

The partition into the stratum corneum demands that the drug must be sufficiently mobile to diffuse across this narrow-spaced layer. Diffusion within biological membranes does not obey the Stokes–Einstein equation [78], which describes this process for spherical particles in a continuous Brownian movement. Within the SC, drug diffusion may simultaneously be interrupted by the different physical state of the lipids within the intercellular matrix and the extremely packed arrangement of the corneocyte [73]. Consequently, they must circumnavigate it to access the viable epidermis.

The rationality for such non-Stokesian diffusion is based on the free volume theory because drug diffusion takes place by the dynamic exchange of molecules in regions of free volume within the membranes [73, 78]. The Stokes-Einstein theory, $D_m \propto Mr^{-1/3}$, do not emphasize the

molecular size as a fundamental factor in drug diffusivity. However, in the fragile equilibrium of the intercellular area, the molecular size should have a critical role [79, 80]:

$$D_m = D_0 * \exp(-\beta * Mr) \quad (3.1)$$

where D_m is the drug diffusivity within the SC, D_0 is the membrane diffusivity of a hypothetical molecule of zero molecular volume, β is a constant that is characteristic of the membrane, and Mr is the molecular volume of the drug. Consequently, drug diffusivity decreases exponentially as molecular volume increases (and hence molecular weight), imposing a size limitation on transportation across the skin.

6.3 Passive Drug Diffusion

The passive permeation of a drug across the diffusion rate limiting stratum corneum down to the blood flow can be described by Fick's laws of diffusion [1, 4, 80]. These laws represent a useful tool by which transdermal availability may be modulated. At steady-state equilibrium, Fick's first law determines that the amount of drug entering the membrane is equal to the amount leaving the membrane, so that the flux is defined by [73, 80-84]:

$$J_{SS} = \left(\frac{D_m * K_{SC/veh}}{h} \right) * C_{veh} = K_p * C_{veh} \quad (3.2)$$

where J_{SS} is the steady-state flux ($\text{mg cm}^{-2} \text{h}^{-1}$) across a membrane of thickness, h in centimeters (cm); $K_{SC/veh}$ is the drug's stratum corneum-vehicle partition coefficient; D_m is the drug diffusivity ($\text{cm}^2 \text{h}^{-1}$) in the SC; C_{veh} is the drug concentration (mg cm^{-3}) in the vehicle, and K_p is the formulation-dependent permeability coefficient of the drug [4].

According to this relationship, transcutaneous fluxes can be enhanced by increasing solute diffusivity and partitioning into the SC, and by increasing solute concentration in the applied formulation. Nevertheless and reminding the skin's structure, the lipophilic SC is followed by an aqueous epidermal domain, so that the development of a topical or transdermal formulation must consider the physicochemical nature of all the underlying structures to the overall diffusion process. Hence $K_{SC/veh}$ (governed by drug lipophilicity) must favor both transfers into and out of the SC.

Furthermore, the transdermal formulation should exhibit supersaturation conditions to maximize C_{veh} so that there is a constant flux of the drug into the skin [82]. A saturated formulation of the drug (with a thermodynamic activity of one) will provide the maximal flux, irrespective of the selected vehicle and drug solubility therein [73]. Formulation scientists are familiar with the dictum of Takeru Higuchi [73, 81], which states that, under ideal conditions, all formulations

Basic Concepts in Transdermal Drug Delivery

that are saturated with a drug will yield the same J_{SS} across the skin. In other words, drug X having a solubility of 2 mg ml^{-1} and 20 mg ml^{-1} in vehicles Y and Z, respectively, will penetrate the skin at an equivalent rate (although, for varying periods) when delivered from saturated formulations in either vehicle [73]. In addition, the maximization of C_{veh} occurs by selecting a vehicle with a high affinity for the drug; however, it can result in a $K_{SC/Veh}$ reduction due to increased solubilization in the formulation.

Another relevant aspect in skin diffusion and not addressed in the Fickian theory is that most drugs are weak acids or bases, existing in unionized and ionized forms, in an aqueous environment [4, 78]. The unionized form is usually lipid soluble and diffuses readily across the stratum corneum. The ionized form has smaller lipid solubility and high electrical resistance and thus cannot penetrate membranes easily. The selection of a transdermal formulation considers the principle of enhancement of flow rates, $K_{SC/Veh}$ and C_{veh} , although having stock for cushioning a therapeutic dose. The art of formulation manipulation requires an understanding of all events governing skin diffusion to deliver a therapeutic drug dose. Table 3-2 depicts the current market drugs that meet all these conditions [73]:

Table 3-2 – Physico-chemical and pharmacokinetics data for current market drugs in TDD. Abbreviations: Mr, molecular weight in Daltons (Da); M_p , melting point; $\log K_{o/w}$, logarithm of the oil–water partition coefficient; S_{aq} , aqueous solubility; K_p , permeability coefficient; Cl , clearance; $t_{1/2}$, elimination half-life; Oral BA, oral bioavailability; Therap. BL, therapeutic blood level.

Drug	Mr Da	Mp °C	Log $K_{O/w}$	S_{aq} mg ml^{-1}	K_p cm h^{-1} * 10^3	Cl l h^{-1}	$t_{1/2}$	Oral BA %	Therap. BL ng ml^{-1}	mg day^{-1} delivered
Scopolamine	303	59	1.24	75	0.5	67	2.9	27	0.04	0.15
Clonidine	230	140	0.83	30	35	13	13	95	0.2-2	0.1-0.3
Estradiol	272	176	2.49	<0.1	5.2	700	0.05	<1	0.05	0.05-0.1
Fentanyl	337	83	2.93	0.2	10	51	7.5	32	1	0.6-2.4
Nicotine	162	< -80	1.17	100	3	78	2	30	10-30	7-22
Testosterone	288	153	3.31	<0.1	400	-	0.8	<1	10-100	4-6

This table considers the fashionable transdermal delivery systems, the transdermal patches. The myriad of transdermal patches that maximize the passive drug diffusion relations are limited by size and dose. The transdermal delivered drugs, such as nicotine (162 Da) and fentanyl (337 Da), have therapeutic doses of a maximum of $20 \text{ mg/ day / area}$. The explosion of drug development in the last decades urges the enhancement of TDD application due to poor oral route bioavailability of these drugs [1]. For instance, the mass of insulin is 6000 Da and modern DNA building blocks for vaccines or biotechnological drugs may have molecular weights, in

the order of hundreds of kilounits (kDa). The significance of the physico-chemical parameters in table 3-2 illustrates the relatively confined ranges for currently marketed transdermal agents. Consequently, the drugs that benefit from this mode of delivery are only a limited number due to the lack of possession of the ideal physico-chemical properties. Hence, there exists a clear need to overcome the barrier function in order to increase drug delivery across the skin, and to extend the scope of transdermally delivered drugs.

6.4 Drug-Skin Interactions

Drug-skin interactions examine the solubility of a compound in the stratum corneum and its diffusivity across the intercellular lipids. These interactions are also of interest from the substantivity and corrosivity point of view [4].

Substantivity is a measure of the binding of solutes to the skin sites and its resistance to washing. This requirement is a crucial property of a cosmetic formulation. Some authors report [84-86] that the affinity of various nonionic formulations (from sunscreens to antimicrobial agents) has a linear relation with drug concentration and that the corneocyte affinity to it, relates to their octanol-vehicle partition coefficient ($K_{SC/veh}$). This relation is not valid for saturated binding places (the increase of concentration does not affect the partition). Substantivity is also noteworthy in skin toxicology [85], as it determines the time scale of the adsorption process between the formulation and the skin.

The skin permeability and the formulation development should consider the corrosivity of its excipients (with obvious health implications). There is a molar concentration threshold at which some molecules, such as acids, phenols and other alcohols (methanol) change the skin permeability by destroying its physiological structure. The physicochemical properties of an excipient can induce different reactions, as polar phenols damage the skin due to enhanced skin solubility and nonpolar phenols do not, due to a diminished $K_{SC/veh}$ [4, 86]. Additionally, various authors report that skin irritation relates to the drug's pK_a : for pK_a lower than 4 the molecules exhibits damaging irritation levels, just like above 10 [4, 86].

6.5 Skin Pharmacokinetics

Pharmacokinetics is the active time course of drugs in the body or individual tissues after their entrance into the body. The drug transportation presents two levels: the achievement of a systemic effect arises from the minimum resistance, binding, and local metabolism of skin; on the contrary, local effects involve high cutaneous concentrations and minimal spillover to the systemic circulation (barely detectable plasma levels).

A mathematical model accepted to discuss the key aspects of transcutaneous diffusion is the compartment model [87-89]. The focus of this model is on the interpretation of the formulation excipients effect and the drug itself on the skin pharmacokinetics. Pharmacokinetics principles states that the concentration $C(t)$ of a solute at time t at any site is defined by the input flux to the site J_{SS} and the transfer time $tr(t)$ to that site:

$$C(t) = J_{SS} * tr(t) \quad (3.3)$$

in this case the symbol $*$ represents a convolution. In the compartment model, this equation can be applied to define plasma concentration (C_p) at the sites of action and solute concentrations in different parts of the skin because they are considered independently. Consequently, concentrations in different skin compartments, such as viable epidermis (C_{ve}) and the transfer time for this layer ($tr(t)_{ve}$) can be determined:

$$C_{ve}(t) = J_{ve} * tr_{ve} \quad (3.4)$$

However, the mathematical description must take into account the differences in skin physiology and the physico-chemical properties of the formulation excipients. After the topical application ($C_{topical}$), the systemic plasma concentrations are defined by the convolution of the skin flux time profile for the solute to reach systemic circulation ($J_{skin}^{circ}(t)$), which allows determining the plasma concentration-time profile:

$$C_p^{topical}(t) = J_{skin}^{circ}(t) * C_p^{iv}(t) \quad (3.5)$$

6.6 Cutaneous Pharmacokinetics

In cutaneous pharmacokinetics, the objective is to target a region within the skin, figure 3.3 [4]. The first approach is to determine skin target concentrations based on the knowledge of the flux to the site and clearance from it [87-89]. Nakashima *et al* [90] reported the validation of these relations by the use of skin target-site free-drug concentration (C^*) from the *in vitro* flux data to predict topical *in vivo* delivery. The compartment model examines the relations mentioned to predict bioavailability [91]. Steady-state determinations of free concentration (C_{SS}^*) at different skin sites relate to the total concentration at that site (C_{SS}) by the fraction of free solute in that position (f_u^*):

$$C_{SS}^* = f_u^* C_{SS} = \frac{f_u^* k_p' C_{veh}}{\left(\frac{Cl^*}{A}\right) + k_p' \left(\frac{K^*}{K_m}\right)} \quad (3.6)$$

where k_p' is the apparent permeability coefficient to the site, C_{veh} is the concentration of solute in the vehicle, Cl^* is the clearance from the site divided by the area of application (A), k^* is the

SC-site partition coefficient ($k^* = C_{SC}/C_{SS}$) and K_m is the stratum corneum-vehicle partition coefficient ($k_m = C_{SC}/C_v$).

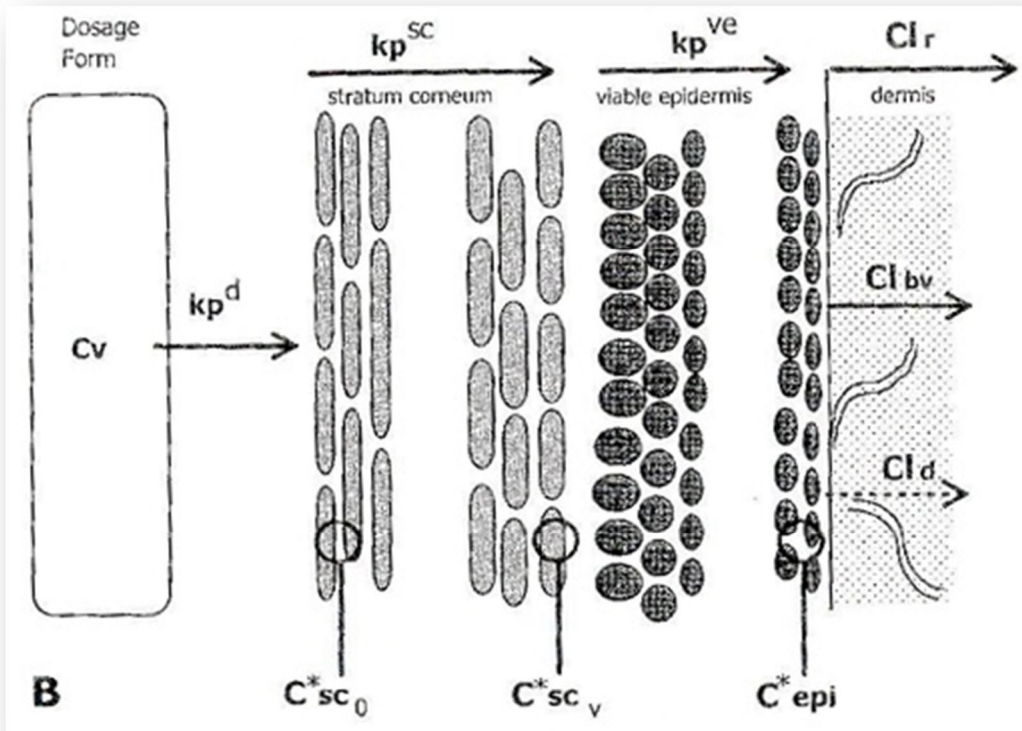


Fig. 3.3 – Pharmacokinetic compartment model of skin layers and the processes involved in transcutaneous permeation.

6.7 Cutaneous Clearance

Moreover, there is a question about the drug clearance in skin layers as depicted in the figure 3.3. In this figure, solutes may either be transport away by the local capillaries on the dermis or diffuse to deeper tissues [92]. The lymphatic transport may be relevant to large molecular weight molecules [93]. The steady-state concentration in each tissue is described as:

$$C_{SS}^i = \frac{k_p^i C_v A}{Cl^i + k_p^i A \left(\frac{K^i}{K_m} \right)} \quad (3.7)$$

According to this equation, the C_{SS}^i enhancement occurs by reducing the clearance from the tissue. This effect can arise from the application of vasoconstrictors that undermine the local blood supply or by the recirculating solutes ascending from the capillaries [94].

6.8 Skin Metabolism

The metabolism of solutes in the skin classifies as a clearance mechanism because it affects the local drug concentration, which represents the final therapeutic target. The site of action of skin enzymes is unclear and not fully understood [4, 91, 92]. The key enzymes are aryl hydrocarbon hydroxylase, deethylases, hydrolases, monooxygenases, esterases, peptidases, and aminopeptidases. The major outcome of skin first-pass effect is that the proportion of metabolized drug concentration is significantly small if compared to the levels from the gastrointestinal first-pass effect [94].

6.9 Stratum Corneum Reservoir

The original proposal of the stratum corneum reservoir role was presented after studies with radiolabeled corticosteroids [93]. The application of a skin formulation induces an occlusion effect, which maximizes the drug retention on the stratum corneum layer (also water retention) and produces vasoconstriction [93]. Some authors suggest that the phenomenon results from the high solubility and low diffusivity of the drugs contained in the formulation (table 3-2), which apparently retains the drugs in the upper layers of the epidermis [94].

The obstruction of skin surface allied to the restrictive diffusion in the intercellular spaces enhances this role of the stratum corneum.

6.10 Transdermal Studies in Human and Animal Skin: Physiology and Anatomy Correlation

The three pathways by which transdermal permeation of drugs occurs have been discussed above: (1) through the intercellular lipid domains in SC; (2) through the skin appendages, and (3) through the keratin filled cells in the SC [1-5, 95, 96]. The lack of correlation in the transdermal permeation of molecules across species or from different application sites in the same donor is due to variations in the skin (or SC) thickness, the composition of intercellular SC lipids and the number of skin shafts. Netzlaff *et al.* [97] show that the amount of free fatty acids, triglycerides and the density of hair follicles are decisive factors for causing differences between the skin barriers among species. The majority of molecules permeate the SC by its lipid domain, so the composition of these regions is essential to correlate human and animal drug diffusion flow rates.

There are various transdermal essays performed to determine drug diffusion rates and doses, such as *in vitro*, *ex-vivo (postmortem)* and *in vivo*. The *in vitro* testing refers to the utilization of

reconstructed skin from keratinocytes cell line. The conduction of *in vitro* penetration studies allows quantifying the rate and extent of compound transport across the skin without considerable costs. Consequently, the diminished ability to predict *in vivo* skin penetration fluxes and doses from these data remains one of the pillars of scientific production in the transdermal area, because the use of fresh human skin is not likely due to accessibility, availability and/or ethical concerns [98-100]. Furthermore, intrinsic variability among human samples due to differences in gender, race, age, and anatomical location of the donor constitute a misleading factor [98-100].

Certainly, the most reliable skin absorption data comes from human studies; however numerous *ex-vivo* and *in vivo* animal models are employed to overcome the restrictions to access human skin [98, 99]. A wide range of animal models has been suggested as a suitable replacement for human skin and used to evaluate percutaneous permeation of molecules. These include primates, pig, mouse, rat, guinea pig and snake models (in order of resemblance to human skin physiology).

The use of primates in research is highly restricted [4], which places porcine skin as the most accessible animal model for human skin substitution. The high availability of porcine skin arises from abattoirs, and the general histological and biochemical properties are similar to human skin [98]. Porcine ear and abdominal skin are particularly well-suited for permeation studies and gives comparable results to human skin [98]. Studies examining thickness of various skin layers have shown that the SC thickness in pigs is 21–26 μm , which is comparable to human skin [97-98]. Also, the viable epidermis in porcine skin is 66–72 μm thick, which is remarkably similar to the average human epidermal thickness of 70 μm [97-98]. The follicular structure of pig skin also resembles that of humans, with an average of 20 hairs in 1 cm^2 of porcine skin to 14–32 hairs (except the forehead area) of humans [97]. Moreover, the vascular anatomy and collagen fiber arrangement in the dermis, as well as the contents of SC intercellular lipids are similar in man and in the domestic pig [96]. The most resembling pig gender is the *Goettingen* minipig [4, 96].

The availability from rodents skin (mice, rats and guinea pigs) represents the popular and common model to *ex-vivo* and *in vivo* drug diffusion studies because these animals are uncomplicated to handle (small size), ease to obtain and low cost. There is a number of hairless species (nude mice, hairless rats), in which the absence of hair coat mimics the human skin better than hairy skin [95]. In these animals, there is no need for hair removal (clipping or shaving) prior to the experiment, thus avoiding the risk of injure the cutaneous tissue (which can enhance the drug profile release). The main drawbacks, if compared with human skin reside in higher hair follicles density of the rodent and higher permeation rates [95-100].

Basic Concepts in Transdermal Drug Delivery

The latter observations result from differences in anatomic and physiological content of the layers composition (table 3-3). Therefore, drug diffusion studies in rodents are considered the first step in a path, with multiple levels, in the construction of complete product documentation for regulatory approval [91-96].

Table 3-3 – Thicknesses of skin layers in rat, mice, pig and human.

	SC / μm	Epidermis / μm	Dermis / mm
Rat	18	32	2,09
Mice	9	29	0,70
Minipig	10	63	1,47
Human	17	70	2,28

The most successful transdermal studies rely on diffusion studies with vertical diffusion cells, such as the Franz cells [101]. A typical study corresponds to the application of the transdermal formulation in the model skin between a receptor and donor compartment. The formulation diffuses the skin thickness, until it reaches the receptor fluid. The receiver compartment is at the skin temperature (usually 32°C), and samples containing the drug are collected at different time intervals (equal amount of the chosen receptor fluid is added after each collection). The quantification process makes use of analytical methodologies, such as the HPLC (high pressure liquid chromatography).

Additionally, other permeation studies can be done, such as the direct application of a formulation to the model skin. The objective is to reduce the time of incubation and perform a direct qualitative and quantitative analysis by visualization techniques or extraction procedures, respectively. These transdermal essays involve the application of the formulation in a predetermined area, the recovery of the drug by skin biopsy punches and its analysis.

7. References

- [1] B.W. Barry, Novel mechanisms and devices to enable successful transdermal drug delivery. *Eur. J. Pharm. Sci.*, 14, (2001) 101-114.
- [4] K.A. Walters, *Dermatological and transdermal formulations*, Marcel Dekker, New York, 2002.
- [5] M. Brown, G. Martin, S. Jones, F. Akomeah. *Dermal and transdermal drug delivery systems: Current and future prospects*. *Drug Delivery*, 13 (2006) 175-187.
- [10] M.R. Prausnitz, R. Langer, Transdermal drug delivery. *Nature Biotechnology*, 26 (2008) 1261-1268.
- [66] A. Nokhodchi *et al*, The enhancement effect of surfactants on the penetration of lorazepam through rat skin. *Int. J. Pharm.*, 250 (2003) 359-369.
- [67] M.A.B. Richard *et al*, *The Merck Manuals for Health Care professionals*, Merck Research Laboratories, 2008.
- [68] I.P. Kaur, R. Smith, Penetration enhancers and ocular bioadhesives: two new avenues for ophthalmic drug delivery. *Drug Dev. Ind. Pharm.* 28 (2002) 353-369.
- [69] D.C. Corbo, J.C. Liu, Y.W. Chien, Drug absorption through mucosal membranes: effect of mucosal route and penetrant hydrophilicity. *Pharm. Res.* 6 (1989)848-852.
- [70] K. Barnhart, Vaginal drug delivery. *I Drugs.* 2 (1999)756-759.
- [71] A. Hussain, F. Ahsan, The vagina as a route for systemic drug delivery. *J. Control. Release*, 103 (2005) 301-313.
- [72] *Transdermal Drug Delivery Technologies, Companies & Markets*, Jain PharmaBiotech Report, 2012.
- [73] M.R. Prausnitz, S. Mitragotri, R. Langer, Current status and future potential of transdermal drug delivery. *Nat Rev Drug Discov.*, 3 (2004) 115-24.
- [74] J.D. Bos, M.M.H.M. Meinardi, The 500 dalton rule for the skin penetration of chemical compounds and drugs. *Exp. Dermatol.*, 9 (2000) 165-169.
- [75] Naik, Y.N. Kalia, R. H. Guy, Transdermal drug delivery: overcoming the skin's barrier function, 3, (2000) 318-326.
- [76] W. Stein., *Transport and Diffusion Across Cell Membranes*, Academic Press, 1986.
- [77] G. Kasting, B. Shroot, H. Schaefer, *Skin Pharmacokinetics*, Karger, 1987.
- [78] R.O. Potts, R.H. Guy, Predicting skin permeability. *Pharm. Res.*, 9 (1992) 663-669.
- [79] R.H. Guy, R.O. Potts, Penetration of industrial chemicals across the skin: a predictive model. *Am. J. Ind. Med.*, 23 (1993) 711-719.
- [80] G.L. Flynn *et al*, Mass transport phenomena and models: theoretical concepts. *J. Pharm. Sci.*, 63 (1974) 479-510.

- [81] T Higuchi, Physical chemical analysis of percutaneous absorption process from creams and ointments. *J. Soc. Cosmet. Chem.*, 11 (1960) 85–97.
- [82] R.G. Stehle, T. Higuchi, Diffusional model for transport rate studies across membranes. *J. Pharm. Sci.*, 61 (1967) 1367-1368.
- [83] A. Davis, J. Hadgraft, Supersaturated solutions as topical drug delivery systems. *Pharmaceutical Skin Penetration Enhancement*, Marcel Dekker, 1993.
- [84] G.L. Flynn, O.S. Carpenter, S.H. Yalkowsky, Total mathematical resolution of diffusion layer control of barrier flux. *J. Phar. Sci.*, 61 (1972) 312-314.
- [85] I. Steinstrisser, H. P. Merkle, Dermal metabolism of topically applied drugs: Pathways and models reconsidered, *Pharmaceutics Acta Helvetiae*, 70 (1995) 3-24.
- [86] S. Riegelman, Pharmacokinetics. Pharmacokinetic factors affecting epidermal penetration and percutaneous absorption. *Clin. Pharmacol. Ther.*, 16 (1974) 873-883.
- [87] K. Kubota, A compartment model for percutaneous drug absorption. *J. Pharm. Sci.*, 80 (1991) 502-504.
- [88] K. Kubota, H.I. Maibach, A compartment model for percutaneous absorption: compatibility of lag time and steady-state flux with diffusion model. *J. Pharm. Sci.*, 81 (1992) 863-865.
- [89] R.H. Guy, J. Hadgraft, H.I. Maibach, A pharmacokinetic model for percutaneous absorption. *J. Int. Pharm.*, 11 (1982) 119-129.
- [90] E. Nakashima, P.K. Noonan, L.Z. Benet, Transdermal bioavailability and first-pass skin metabolism: a preliminary evaluation with nitroglycerine. *J. Pharmacokinet. Biopharm.*, 15 (1987) 423-437.
- [91] H.Y. Ando, N.F. Ho, W.I. Higuchi, Skin as an active metabolizing barrier I: Theoretical analysis of topical bioavailability. *J. Pharm. Sci.*, 66 (1977) 1525-1528.
- [92] B.W. Barry, *Dermatological Formulations: Percutaneous Absorption*. New York, Marcell Dekker, 1983.
- [93] F.D. Malkinson, E.H. Ferguson, Percutaneous absorption of hydrocortisone-4-¹⁴C in two human subjects. *J. Invest. Dermatol.*, 25 (1955) 281-283.
- [94] V.P. Shah *et al*, Bioequivalence of topical dermatological dosage forms – methods of evaluating bioequivalence. *Pharm. Res.*, 15 (1998) 167-171.
- [95] B. Godin, E. Touitou, Transdermal skin delivery: Predictions for humans from in vivo, ex vivo and animal models. *Advanced Drug Deliv. Reviews*, 59 (2007) 1152–1161.
- [96] J. Kanitakis, Anatomy, histology and immunohistochemistry of normal human skin. *Eur. J. Dermatol.*, 12 (2002) 390–397.
- [97] F. Netzlaff *et al*, Comparison of bovine udder skin with human and porcine skin in percutaneous permeation experiments. *Altern. Lab. Anim.*, 34 (2006) 499–513.

- [98] U. Jacobi *et al*, Porcine ear skin: an in vitro model for human skin. *Skin Res. Technol.*, 13 (2007) 19–24.
- [99] F.P. Schmook, J.G. Meingassner, A. Billich, Comparison of human skin or epidermis models with human and animal skin in in-vitro percutaneous absorption. *Int. J. Pharm.*, 14 (2001) 51–56.
- [100] M.J. Bartek, J.A. Labudde, H.I. Maibach, Skin permeability in vivo: comparison in rat, rabbit, pig and man. *J. Invest. Dermatol.* 58(3) (1972) 114-123.
- [101] T.J. Franz, Percutaneous absorption on the relevance of in vitro data. *J. Invest. Dermatol.*, 64 (1975) 190-195.

IV

**Transdermal Drug
Delivery Technologies**

1. Introduction

Transdermal drug delivery technologies generated tremendous interest among the leading pharmaceutical companies in the end of the 20th century. The advantages discussed earlier, such as (1) avoidance of liver first-pass metabolism, (2) prevention of exposure to chemical and biological conditions of the gastrointestinal tract, (3) reduction of adverse effects for diminishing the drug doses, (4) improvement of patient compliance, and (5) ability to provide controlled delivery of drugs with short half-lives were all attractive features to the pharmaceutical industry.

Nonetheless, excitement derived to disappointment, when the limitations of the existing transdermal technologies arise, and the numbers of effective drug candidates were limited to nitroglycerin, scopolamine, clonidine, estradiol, testosterone, nicotine and fentanyl [72].

Even so, the introduction of several transdermal products in the market signals its value in \$16 billion dollars worldwide, in 2011 [72]. The segmentation of this market comprises a dominant technology, transdermal patches, with total sales of \$10 billion and other miscellaneous technologies count the rest.

A list of the Federal Drug Administration (FDA, US) reports the approved drugs administered transdermally, with their commercial names and purpose (table 4-1) [72].

Table 4-1 – Commercially available drugs in the form of transdermal patches.

Drug	Commercial names	Purpose
Nitroglycerin	<i>Nitro-BID, Nitrol</i>	Chest pain
Scopolamine	<i>Isopto Hyoscine</i>	Motion sickness
Nicotine	<i>Nicorette, Nicotrol</i>	Smoking cessation
Clonidine	<i>Catapres</i>	High blood pressure
Fentanyl	<i>Sublimaze</i>	Pain Relief
Estradiol	<i>Alora, Climara, Fempatch</i>	Postmenstrual syndrome
Testosterone	<i>Testoderm TTS</i>	Hypogonadism in males

The limited success of transdermal systems included the following factors: (1) local skin irritation associated with certain drugs and formulations, (2) limitations on the drug dose, which could be delivered transdermally, (3) significant delay time in reaching the

bloodstream, and (4) variation of the drugs profile release based on site of application, skin type and patient age.

Without the interest of multinational pharmaceuticals and the funding partnerships that they provide, few transdermal drug delivery companies can sustain themselves without a large pipeline leading products to the market place. The table 4-2 presents the transdermal technologies in clinical use, or planned for clinical use. A discussion about the physical background and mechanisms of enhancing transdermal delivery is presented throughout this chapter.

Table 4-2 – Transdermal drug delivery technologies sorted by physical principle.

	Area	Transdermal Technologies
Passive Drug Diffusion	Formulations	Creams
		Gels
	Absorption Enhancers	
	Transdermal Patches	Drug-in-adhesive Reservoir Type
Active Drug Diffusion	Electric Assistance	Electroporation
		Iontophoresis
	Mechanical Processes	Jet Inject
		Skin Ablation
		Microneedles
	Acoustical Methods	Sonophoresis
Photomechanical waves		

2. Passive Drug Diffusion

The traditional systems for drug diffusion through the skin for treating skin disorders or local pain symptoms consist in the use of creams, gels or lotions. Their success in topical delivery is driven by the ability of promoting *in site* delivery of drugs, its emollient and protecting action, the satisfying cosmetic aspect (smell, texture and freshness) and the increased patient compliance [102].

The constitutions of these formulations consider unique or several excipients, mono or multiphasic systems, where the formulation scientist develops complex phase diagrams to obtain a final homogeneous mixture. The nature of these excipients determines the formulation behavior, and its modulation towards hydrophilicity or lipophilicity can be

done, according to the drug physicochemical properties and the passive diffusion flux maximization ($K_{SC/Veh}$ and C_{veh}). Additionally, the formulation can contain other excipients, such as antimicrobial agents, antioxidants, stabilizers, emulsifiers, thickeners and absorption enhancers [103].

2.1 Creams for Topical Delivery

Creams are semisolid cutaneous preparations that contain medicinal substances or cosmetic ingredients dissolved or suspended in their aqueous or oil phase [103]. These types of emulsions represent one of the most popular vehicles for topical delivery due to the range of advantages that they present:

- (i) Affinity and adhesiveness for the skin surface;
- (ii) Possibility of simultaneous incorporation of substances with hydrophilic and lipophilic characteristics;
- (iii) Prospect of developing vehicles with different textures, consistency and penetration competences;
- (iv) Richness in water grants hydration and emollient properties to the skin formulation;
- (v) Dual consistency with the lipophilic part draws attention to its action as cleaning agents.

A cream is defined as a heterogeneous system with multiple phases and constituted by a liquid, disperse in another. Its chemical nature appears of two types [104]:

- Oil/water (O/W), where the core phase consists of lipophilic substances immiscible in the external phase form by water and polar molecules.

The oil phase contains molecules of apolar nature with long carbon chains, in which their primary function is to increase the flexibility and gentleness (emollient) of the topical formulation. The most common compounds used are hydrocarbons, fatty acids and silicones.

- Water/oil (W/O), where the inner core has water and the outer layer apolar molecules.

The constitution of these types of creams considers purified water dissolved or dispersed in humectants, such as glycerin. The latter constituents function reduce or prevent water losses by evaporation. The presence of thickeners, such as polyacrylic acid and cellulose

derivatives can increase the gel consistency or provide antimicrobial and antioxidant functions. In both kinds of creams, the active substance should be dissolved in the adequate physicochemical phase. The formulation scientists' always consider another cream: the emulsion one [105]. They are adequate for molecules with amphiphilic nature (both hydrophilic and lipophilic), in which the self-assembly results in the reduction of the superficial tension - system stabilization and no phase separation.

The majority of the pharmaceutical and cosmetic creams are O/W emulsions because their penetration capability enhances drug diffusion on the lipophilic environment of the stratum corneum. Additionally, in the end of the treatment, the removal of these creams from the skin is straightforward upon water washing [102-105].

2.2 Gels for Topical Delivery

The definition of a gel is extremely broad, and applications are even broader. Gels are semisolid cutaneous preparations corresponding to a particular state of a colloidal solution [104], as it forms a tridimensional network of macromolecules (by gelification agents), in which a liquid containing the drug distributes itself. The adaptability and versatility of gels results in a system suitable for a wide range of pharmaceutical applications based in the following types of gelification polymers [102-105]:

- Natural polymers of animal origin (jelly and casein), vegetable (arabic and tragacanth gum), seeds (guar, starch gum) and algae (carrageenan and alginates);
- Synthetic polymers derive from cellulose ethers (methylcellulose, hydroxyethylcellulose and carboxymethylcellulose of sodium), vinyls (polyvinyl alcohols, polyvinylpyrrolidone and carboxyvinyls) and carboxyvinyls, such as the series of carbopol polymers.

According to the nature of the solvents, the gels can be classified as:

- Hydrogels, where its excipients are water, glycerin and propylene glycol containing gelification agents, such as starch, cellulose derivatives and carbopol type polymers.
- Oilgels, where its excipients are liquid paraffin mixed with polyethylene and fatty acids that swell upon colloidal silica, aluminum or zinc soaps application [105].

Gels are a cosmetic well accepted formulation by the patient due to advantages, such as:

- (i) Transparent aspect;
- (ii) Easiness of application and washable character;
- (iii) Production of a freshness feeling on the skin;
- (iv) Cost reduction and the potential for *in house* production,
- (v) Lack of irritability,
- (vi) Ability to apply to large skin areas.

However, the gels have shortcomings, mainly the tendency for desiccation [105]. The application of gels in cosmetic preparations extends from anti-cellulite, slimming, facial masks or anti-aging products. The scientific literature describes other types of topical formulations based on semisolid preparations, such as ointments, lotions and poultices that present the same performance as creams and gels: the viscoelastic and the non-Newtonian behavior (plastic, pseudoplastic or thixotropic ones). Other categories are essential to patient compliance and industrial efficacy, namely cosmetic aspect and penetration profile, which disregard them as the most prone to market utilization.

2.3 Absorption Enhancers

Among the myriad of strategies employed to increase both the amount of therapeutic agent traversing the skin and the range of drugs that can be effectively delivered through the skin, expectations were raised by the use of absorption enhancers (or penetration enhancers) [1].

These agents interact with the stratum corneum cells to facilitate and promote drug flux [106]. The application of these molecules dates centuries ago in the preparation of poultices and ointments for treating skin diseases, though it is only in the last four decades that the development of enhancers called the attention of science and industry [1, 4, 73]. However, the binomial relationship of cost/effectiveness for the absorption enhancers is unclear for a majority of these molecules because of irritability concerns and lack of evidence of the fundamental mechanisms of action (as required from a regulatory point of view) [75]. In this section, there is a description of the categories and mechanisms of action of the most investigated enhancers.

2.3.1 General Characterization of the Absorption Enhancers

Absorption enhancers have gained efficacy with the expanding knowledge of the lipid domains within the stratum corneum [107, 108], and have the advantage of the physician techniques of flexibility in the formulation and ease of application over a large area (>10 cm²) [108]. An ideal penetration enhancer should transiently reduce the barrier resistance of the SC without damaging the skin cells. Moreover, the ideal absorption enhancers should possess the following properties [106-107, 109]:

- (i) Pharmacologically inert;
- (ii) Nontoxic, nonirritating, and non-allergenic;
- (iii) Rapid onset of action with predictable and suitable duration of action for the therapeutic drug;
- (iv) Transient effect on the stratum corneum barrier;
- (v) Chemically and physically compatible, safe and stable with the delivery system;
- (vi) Readily incorporated into the delivery system;
- (vii) Inexpensive and cosmetically acceptable.

Substances reported to render the SC more permeable include alcohols, sulphoxides, pyrrolidones, fatty acids, terpenes, surfactants and phospholipids [106]. Their structural diversity is associated with multiple modes of action: enhancers, such as sulphoxides and alcohols increase the drug flux by inserting polar molecules into the polar headgroup regions of the lipid intercellular structure causing fluidization by diminishing the lipid lateral packing (table 4-3) [4]. Additionally, they may lead to lipid extraction from the SC (inducing disorganization and structure failure).

Others, such as phospholipids and surfactants (namely Azone, 1-n-Dodecyl Azacycloheptyl-2-Ketone and SEPA, 2-*n*-nonyl-1,3-dioxolane) are known to insert into the intercellular lipid tails causing their fluidization, as the structural organization collapses momentarily [108]. Fatty acids, such as oleic acid and isopropyl myristate are among the most effective absorption enhancers. The proposed mechanism of action for oleic acid (*cis*-9-octadecenoic acid) [106-107, 109] highlights its kinked structure (i.e., the bent *cis* configuration), which disturbs the intercellular lipid packing resulting in separation of the SC lipid domains, and thereby reducing their barrier function (table 4-3).

The use of terpenes enhances permeation effects of lipophilic drugs and hydrophilic drugs, such as testosterone and propranolol, respectively. Terpenes, such as menthol, cineole, and limonene gathers the main characteristics of absorption enhancers: safe, nonirritant and non-toxic to skin (table 4-3) [109].

Transcellular diffusion along the corneocytes is favored by ionic surfactants, such as dimethyl sulfoxide (DMSO) and urea, which interact with the keratin in the corneocytes and disrupts its protein structure (table 4-3) [4].

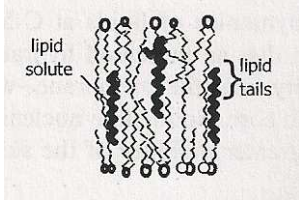
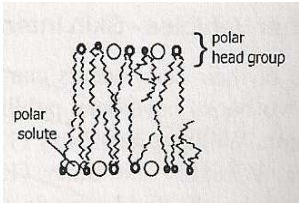
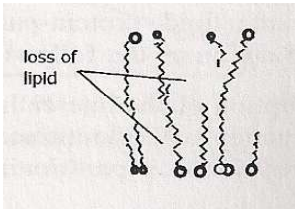
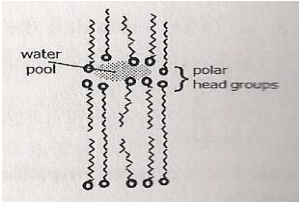
Synergistic effects between enhancers (e.g., Azone® or fatty acids) and polar co-solvents (ethanol, propylene glycol) facilitate the drug solubilization within the SC, thus amplifying the lipid disruptive effect [106, 110]. Sulphoxides and phospholipids mixtures are aggressive and generate significant structural perturbations, for example, keratin denaturation and the solubilization of skin components. The state of skin hydration has been considered by the scientific community, as one of most significant factors in drug diffusion across the skin layers [110]. Simple hydration (achieved by skin occlusion, i.e., interruption of the normal flux of water exit), which is a well-known strategy (but poorly understood) for promoting drug absorption by an effect on lipid bilayer conformation or spacing [111].

Many studies [4, 110] monitored the effect of hydration on the ceramides alkyl chains within the intercellular domains and found a change in neo-differentiated SC that led to an increase in lipid fluidity. Solid state nuclear magnetic resonance (NMR) has also been used to show greater mobility on the skin structure in the presence of increasing water levels.

Extensive knowledge about absorption enhancers focuses on their chemical structure, such as chain length, polarity and level of unsaturation, to understand the mechanisms of barrier function perturbation (table 4-3). Additionally, the enhancers' action can induce irritation and erythema in the skin, when their concentration surpasses a certain threshold [111].

Table 4-3 summarizes the classes of absorption enhancers and their contribution to the enhancement of transdermal drug delivery in a combination with effectiveness and diminished side effects [4, 72].

Table 4-3 – The effect, the diagrammatic representation and applications of the different types of absorption enhancers.

Solvent/Vehicle	Effect	Visualization	Industrial Applications
Fatty acids, Terpenes and Azone®	Insertion of solvent molecules into lipid tail regions causing fluidization in the structure		<i>Biphaxis™</i> (Helix Biopharma), <i>MenoRest®</i> (Novartis)
Polar Solvents	Insertion of polar molecules into polar headgroups regions causing fluidization of the extremely packed structure.		<i>ACROSS®</i> , <i>Antares Transdermal (ATD) Gel Technology</i>
Organic Solvents	Solubilization and extraction of the lipids present in the intercellular membranes.		<i>Every transdermal or topical formulation has ethanol or similar in its constituents</i>
Water and Sulphoxides	Formation of water “pools” around polar headgroups resulting in a channel through the intercellular domain.		<i>Pennsaid®</i> , <i>Estracomb TTS®</i>

Differential scanning calorimetry studies [4] demonstrated that the terpenes skin action, with oleic acid and dimethyl sulphoxide (DMSO) creates polar channels in the stratum corneum structure, so a relevant question comprises about the physical and biological consequences of these molecules. Some examples are depicted in figure 4.1 [4].

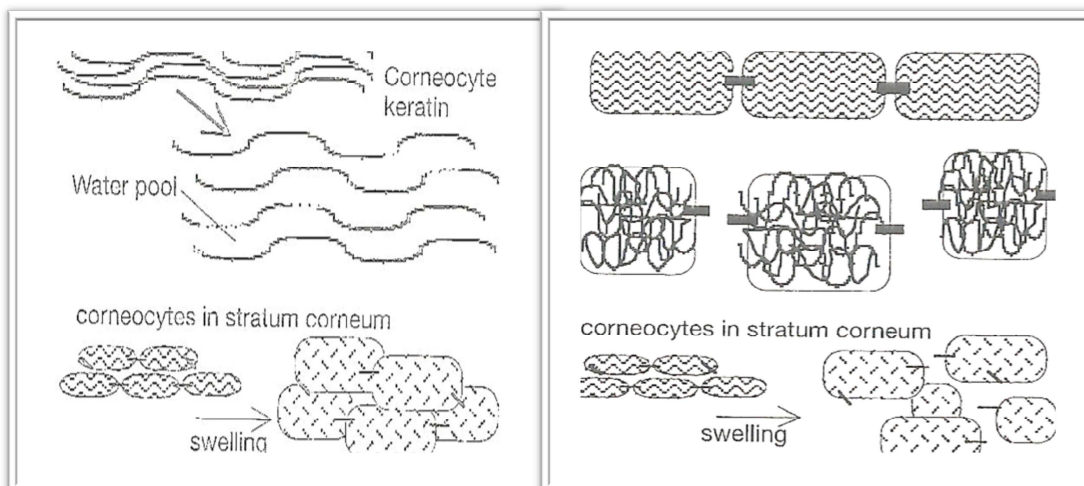


Fig. 4.1 – The effect of different absorption enhancers in the stratum corneum structure. The left side image represents the biological action of skin occlusive conditions as swelling takes place in the intracellular keratin of the corneocytes, which creates polar channels. The right image symbolizes the biological consequence of the SC fluidization as it develops in the corneodesmosomes.

2.4 Transdermal Patches

Transdermal patches (TP) are innovative passive transdermal delivery systems intended for achieving a systemic effect [107]. A transdermal patch is an adhesive placed on the skin to deliver a time-released dose of a drug to treat a systemic condition. Since the early 1980s, this dosage form has been available commercially [72]. This approach provides a significant improve in TDD and offers the possibility of synergetic action with other technologies:

- (i) Controlled release of the drug;
- (ii) Steady blood level;
- (iii) Improved efficacy over other dosage forms, such as tablets and injections;
- (iv) Reduced secondary effects (irritation or eczema);
- (v) User-friendly, convenient, painless and multi-day dosing.

The inconveniences of transdermal patches relate with the inconveniences of TDD: low therapeutic levels and size limitation delivery of large pharmaceuticals. Consequently, the transdermal therapeutic patches are of particular clinical significance for the prevention and long-term treatment of chronic diseases, such as hypertension, hormone replacement or smoke cessation [112].

The basic structure of standard skin patches is shown in figure 4.2. The major drawback of transdermal patches relates with the patch-skin adhesion, which may constrain everyday life activities [110-112].

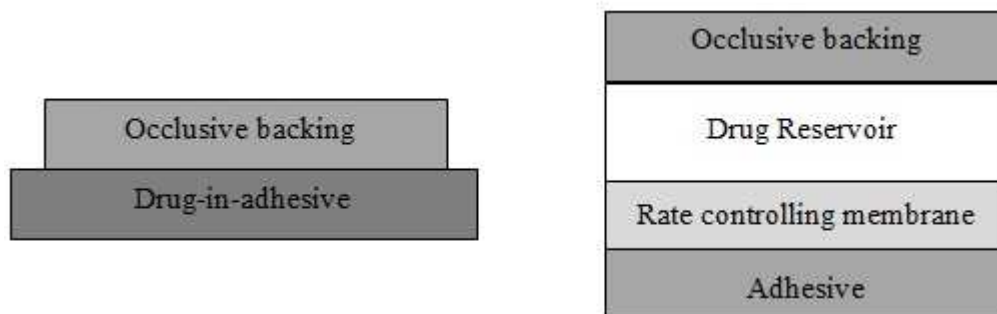


Fig. 4.2 – Basic structure of transdermal patches: drug-in-adhesive (left) and reservoir type (right).

The drug-in-adhesive skin patch incorporates the drug and other excipients into the organic solvent solution, mixed it and cast as a thin film. Afterwards, the resulting film is dried to evaporate the solvents leaving an adhesive film containing the drug. These types of patches can be matrix systems, where the adhesive part is sandwiched between the release container and the backing layer. Drug-in-adhesive patch may be single layer or multilayer. Some examples of suitable adhesives are polymers, such as polysiloxanes, polyacrylates and polyisobutylene. These systems are hydrophobic in nature, so the incorporation of drugs considers hydrophobic ones [4, 110].

In a reservoir transdermal patch, the drug solubilization occurs in a rate-controlling membrane. The membrane is a material placed between the drug formulation and the final layer of adhesive, which is sealed to the backing layer and forming a pocket to enclose the drug-containing medium. The reservoir patch is made of a homogenous dispersion of the drug, in an unleachable viscous liquid medium (silicon) to form a paste. This paste contains a suspension or a clear solution of drug in a releasable solvent (ethanol) [110-112].

The reservoir system is used when the compound to be delivered is of high molecular weight and, therefore, more difficult to deliver transdermally. A drug-in-adhesive system is of particularly useful when prolonged drug delivery is desired, such as nicotine patches. Table 4-4 exhibits comparative features of the main types of transdermal patches [72].

Table 4-4 – Comparative features of transdermal patches.

Drug-in-adhesive	Reservoir
2-3 layers (simple construction)	4-5 layers (complex construction)
Skin controlled release	Membrane controlled release
Low dose dumping potential	Dose dumping possible
Good skin conformability	Poor skin conformability

3. Active Drug Diffusion

Topical formulations with therapeutic purposes added more to popular folklore than to the clinical armamentarium and hypodermic needles remain the most relevant alternative to oral delivery regardless of pain, contaminations and waste issues. Chemical absorption enhancers may increase the permeability of the skin, but there are fundamental constraints in their design associated with the skin irritation potential and mechanistic issues. Transdermal patches are successful only for low molecular weight and lipophilic drugs. Consequently, the amplification of the TDDS requires the development of active techniques.

3.1 Electroporation

The stratum corneum is the main barrier to transdermal transport; thus the disruption of the stratum corneum can dramatically affect overall skin permeability [1-3]. Electroporation has been proposed to enhance transdermal delivery because the structure of the stratum corneum is particularly attractive for this technique [113]. The organization of the lipid bilayers within the stratum corneum shows parallel structures, which defines a characteristic electrical breakdown in the range of 30–100 V voltages. Subsequently, electroporation pulses are capable of interacting and disrupting the self-assembly of the SC lipids by applying 100 to 1500 V voltages [113]. This disruption generates open spaces promptly filled by water creating aqueous pathways through the stratum corneum. The electroporation mechanism of action reflects on the role of electrophoresis and thermal effects in enhancing molecular transport through the transiently permeabilized skin (figure 4.3) [114].

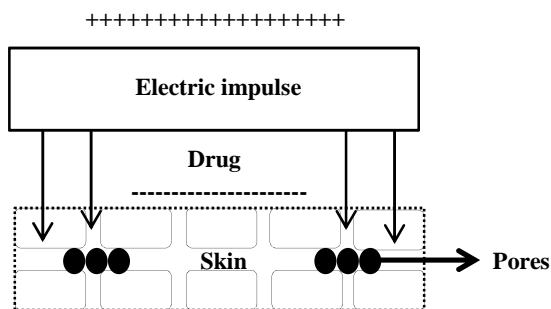


Fig. 4.3 – Schematic view of electroporation. The proposed mechanism of action [108-110] is based on the application of electrical pulses that crosses the lipid lamellae (open spaces) vacuuming it, so that a water influx arises to it (black circles).

The major drawbacks of this transdermal system rely on the unclear mechanism of action because evidences of these pores is still totally indirect, though its physical description characterizes them as small (<10 nm), sparse, and short-lived (μs to s) [115].

The parameters affecting the *in vivo* electroporation of drugs include electrical ones, physicochemical properties of the drug and formulation, as depicted in table 4-5.

Table 4-5- Parameters affecting skin electroporation.

Parameters	Increase in	Effect
Electrical parameters	Pulse voltage, number and length	Positive
	Charge	Positive
Physicochemical properties	Molecular weight	Negative
	Conformation	Unknown
	Lipophilicity	Negative
	Competitive ions	Negative
Formulation of drug reservoir	pH	Positive
	Viscosity	Negative

3.2 Iontophoresis

In the class of the electric assistance methodologies, iontophoresis represents the most popular physical system for transdermal delivery of drugs. This medical and social recognition probably derives from the change in the paradigm caused by the ancient and pioneer works of Pivati in 1747, which throughout the years paved the way to Le Duc experimental statements [72]. The latter demonstrated that the transport of ions to the skin occur by the action of continuous electrical current and proved that such transfer was dependent on the charge of the ion.

Iontophoresis refers to the delivery of drugs across the skin by means of a continuous electric current [116]. This technique represents a noninvasive methodology that uses the potential (<5V) of an electric current (0.1 to 1 mA/cm²) to produce, in a controlled way, an increase in the transdermal drug delivery [116]. The transdermal drug delivery by iontophoresis is available for commercial purposes in the skin anesthesia and anti-inflammatory action [117]. This technique has the largest medical implementation in the physical therapy area [117, 118].

The mechanisms involved in the transdermal transfer of drugs by iontophoresis are: (1) the electrorepulsion created by the interaction drug-electric field, (2) electroosmosis, which is the transdermal movement of part of the solvent with the neutral and ionic components diluted therein, and (3) the skin permeability induced by the application of an electrical flow (figure 4.4).

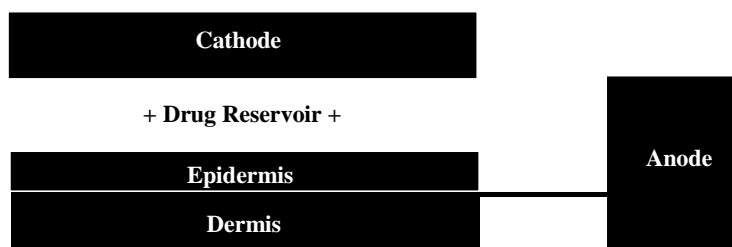


Fig. 4.4 – A schematic representation of a typical iontophoresis application to the skin. Two electrodes are placed in contact to the skin surface and a drug reservoir is positioned between the skin and the electrode of the same electric charge.

The skin characteristics relevant for iontophoresis are the high impedance associated with stratum corneum thickness, its low degree of hydration and the number of sweat glands and hair follicles [116, 117]. The main feature of the iontophoresis mechanism is the transient decrease of skin impedance, which drives to a constant flux of the ionized drug and a rapid recovery of the barrier function. This transient decrease occurs independently of the transferred solution and the amplitude and duration of the electrical stimuli. The electric doses provided in a clinical procedure vary between 0.1 to 1 mA *per* electrode area in square centimeters (cm²). In human clinical trials, the usual relation stands for 0.3 to 0.5 mA/cm² [117, 118].

3.3 Jet Inject

Jet injection is a ballistic method based on a local injection of a liquid by means of a device that uses high pressure to force microdroplets of a liquid drug to penetrate the skin

[1, 107]. Pressure can reach up to 4 bar, and the velocity of the droplets can range from 100 m/s to 200 m/s [119]. The advantage of using jet injection is to minimize patient discomfort due to the inexistence of an application time.

There are two types of jet injections: high volume (more than 100 μL) and low volume ones (20–30 μL). The low-volume method limits the target tissue to a small area (lower than 1 cm^2). Moreover, the efficiency of this method depends on the fluid velocity which contributes to the penetration into the skin, whereas the diameter of the jet and the injected volume limit the penetration depth of the solution [119].

The mechanism of action corresponds to the creation of holes at the skin's surface by the high pressure applied and, most likely, through the erosion or fracture of the skin [119]. The major advantage of jet injectors is the high rate of drug administration, where doses can be fired sequentially, allowing up to 1000 subjects to be medicated per hour [72]. However, contamination issues arise in 1980 and the US Department of Defense cancelled its *in vivo* application [72].

3.4 Skin Ablation

Skin ablation is a promising technology that uses thermal heating by an independent source, such as a laser, to remove the stratum corneum, while sparing deeper tissues by modulating the incoming deposit of energy and its delivery time [120]. The size of the disruptions generated by this method is believed to be of micrometer dimensions, which are large enough to allow transport of small drugs and, in some cases, macromolecules, but, in principle, small enough to prevent skin damage of clinical significance [121].

Skin ablation considers different heat sources to produce the SC elimination, such as pulsed lasers, arc discharge and short-duration resistive heating, which causes disruptions of the SC, as small as micrometer-sized holes [122]. The creation of an assortment of micropores arises by focusing thermal energy and scorching small micrometer-sized areas [122]. The tissue vaporization only occurs on the superficial layer of the skin by keeping a diminished exposure time, so, in principle; the epidermis and dermis do not experience a significant increase in their temperature, so that this methodology is reportedly painless [120-122]. However, additional studies are required to assess the cellular viability of the tissue.

The most efficient heat source for skin ablation is the application of microsecond pulsed lasers [122]. The mechanism of drug flow enhancement relates with the direct absorption of light by the skin, which causes the water from the outer layers to heat up and

evaporate. The resulting microexplosion induces tissue ablation with reduced risk to the epidermis because the laser pulse duration is smaller than the water time relaxation [120-122]. Table 4-6 summarizes different lasers used in clinical or pre-clinical studies [72].

Table 4-6 – Histological consequence of various lasers impinging in the skin.

Type of Laser	Tissue Interaction	Histological Consequence
CO ₂	Vaporization	Epidermal removal with dermal injury
Er:YAG	Ablation	Epidermal and dermal removal
Combined Er:YAG/CO ₂	Ablation followed by coagulation	Epidermal removal and dermal heating
Long pulse Nd:YAG	Nonablative techniques	Dermal injury (subsurfacing)

3.5 Microneedles

The mechanical assistance technologies evolved rapidly in the last decade, and the emergence of microscopic needles places transdermal drug delivery in a new dimension in the drug delivery market [72]. A microneedle is an array of a microstructured material coated with a drug or a vaccine, which upon application to the skin may produce a systemic or local effect. The microstructured material may be a metal, silicon or polymer, and their dimension does not exceed the 1 micrometer in diameter, though there is a thickness variation considering the biological target [123].

The technological development envisions the creation of large transportation routes of micrometer dimensions across the stratum corneum and viable epidermis, which should enhance transdermal drug delivery [124]. The pain and contamination issues arising from the hypodermic needles utilization is partially solved because of the reduced microneedles array diameter. Consequently, the process of insertion in the skin does not significantly stimulate nerve endings located in the superior dermis [124]; however, the micrometer-sized holes cause extensive TEWL during several hours (prolonged skin recovery).

The mechanism of insertion in the skin is of critical importance for a correct development of a microneedle based technology, as seen in figure 4.5 [123, 124]. This development must consider the mechanical properties of the skin, mainly the deformation strength. In consequence, the microneedles must have the correct geometry (shape and form) and strength to pierce the skin and fulfill an adequate insertion [124].

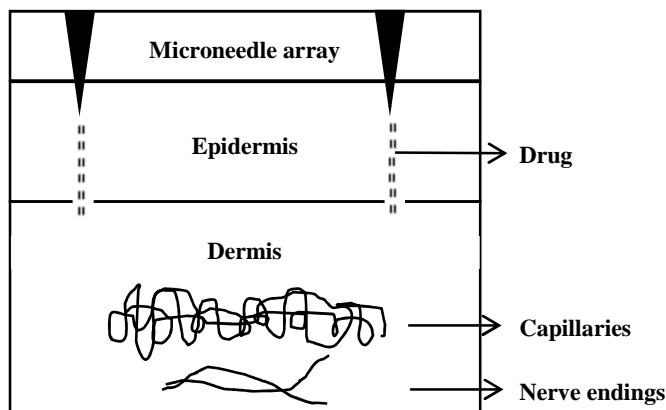


Fig. 4.5 – Schematic microneedle based technology. The microneedle array (black triangles) pierces the skin promoting drug diffusion (black dots).

The microneedle and skin ablation techniques may change the paradigms of transdermal drug delivery. The number of companies developing these new solutions has been growing dramatically [72].

3.6 Sonophoresis

The transdermal drug delivery recurring to ultrasound waves (USW) is known as sonophoresis or phonophoresis. An ultrasound wave is a longitudinal wave that propagates from a source and causes a local oscillatory motion of the particles that constitute the medium, in which it disseminates [125]. As a consequence, there is a particle displacement from its original position and a variation in the system pressure: increase or decrease in the medium pressure, conditional to the *in site* cycle of the wave felt by the medium (compression – high pressure – or a rarefaction – low pressure) [126]. The frequencies used in a clinical protocol range from 20-100 kHz (low-frequency sonophoresis) to 1-16 MHz (high-frequency sonophoresis), though the therapeutic conditions corresponds to ultrasound frequencies between 1-3 MHz and a pressure around 2 bar [127]. The most recent development in ultrasound based technologies follows the *in vivo* low-frequency sonophoresis to deliver high molecular weight drugs [127].

The mechanism of stratum corneum disruption relates with the acoustic cavitation of the coupling medium between the ultrasound source and the skin. Acoustic cavitation can be described as the growth and oscillation of microbubbles pre-existing in the medium when the driving acoustic field exceeds a certain threshold of energy [125]. This threshold is attained when the acoustic pressure amplitude is high enough to generate a tension in the liquid equal or greater to its tensile strength (peak of the rarefaction wave). The compression cycle of an USW raises the pressure outside the air bubble, which by

osmotic process increases the diffusion of gas out of the bubble (reduction in size). On the other hand, in the negative cycle of the USW, the pressure outside the bubble forces gas to diffuse into the bubble causing expansion. This cycle is known as rectified diffusion [125].

The mechanism of action of sonophoresis includes phenomenon such as stable and transient cavitation [126]. Stable cavitation refers to bubble growth under gentle pressure oscillations across its surroundings, which cause an accumulation of shear stress in its vicinities and membrane permeabilization [125-127]. Transient cavitation refers to the bubble burst after engaging a critical radius growth, in the negative cycle of the USW. This process has been considered the main mechanism of biological barriers perturbation [127] and its characterization comprises (1) a pressure variation, which forms gas bubbles within medium that collapse if the tensile strength is surpassed, and (2) small gas bubbles already present in the coupling medium grows without limit and explode. Bubble collapse produces a shock wave that propagates at supersonic speed and enhances SC permeability (figure 4.6) [127].

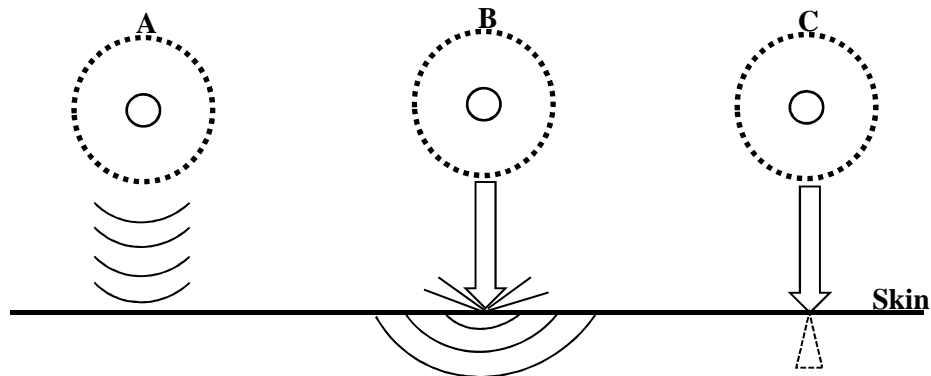


Fig. 4.6 – Three possible modes of ultrasound waves to permeabilize the stratum corneum intercellular lipids.

Cavitation phenomena might enhance stratum corneum permeability from different modes. Figure 4.6 A shows bubbles collapsing symmetrically and producing a shock wave that disrupts the SC ordered and packed structure. Figure 4.6 B shows the production of acoustic microjets after bubbles explosion that do not penetrate the SC, but may cause its disruption. Finally, figure 4.6 C shows the referred microjets impacting on the SC surface, being absorbed and physically disrupting the intercellular domains [127]. Ultrasound based technologies have been perennial in the clinical field because its utilization as a TDDS in physical therapy is broadly disseminated [117, 118].

3.7 Photomechanical Waves

The previous section shows that transdermal delivery with an external pressure is a technique that may contribute to further developments in drug delivery. The introduction of a novel transdermal system [128], which used the energy of a laser to generate pressure waves of high amplitude can be seen as a precursor of the work presented in this thesis.

The works of Doukas and Kollias [128-130] demonstrated a different way to induce the SC permeabilization using a pulsed laser to generate a photomechanical wave when the laser light is totally absorbed by a black polystyrene material (the nondirect irradiation of the skin), and effectiveness in the delivery of macromolecules. The term photomechanical wave refers to a pressure wave generated by a laser, which is characterized by high amplitude pressure transients, short rise times of the wave and broader wave bandwidths [130].

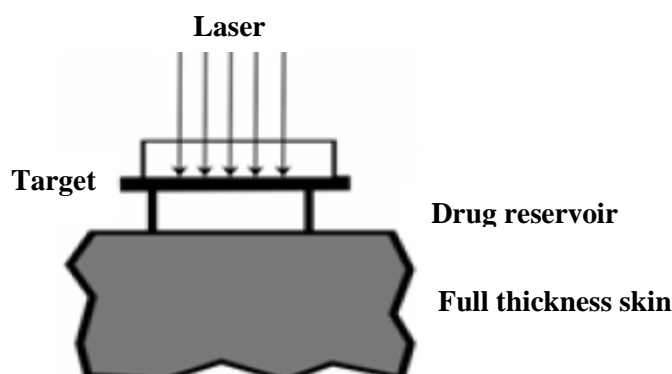


Fig. 4.7 – Schematic representation of the photomechanical waves based technology. The 10 J *per* pulse laser light is impinged and absorbed by a target material (black polystyrene, 1mm). The resulting pressure wave crosses a drug reservoir that also acts as a coupling medium and permeabilizes the upper skin layers. In consequence, the drug entrance in the skin is facilitated and a concentration gradient sustains the TDD, until the barrier function is fully recovered.

In this transdermal system, the application of highly intense Q-switch ruby lasers (nanosecond lasers with energy *per* pulse in the joules range) into an absorbing material causes material ablation and the generation of a pressure wave. The laser irradiation causes the decomposition of the target into small fragments, which move away from its surface at supersonic speed and the imparted recoil momentum is the origin of the high amplitude pressure transient [128].

These types of pressures waves are compressive ones, which eliminates the risks of tissue cavitation [127]. Their amplitude in the hundreds of bars range and its duration extends over hundreds of nanoseconds [128]. This characterization requires a different mechanism of interaction with the skin when compared with cavitation phenomenon associated with the ultrasound technique. The exact mechanism by which a pressure wave

permeabilizes the skin has not been clearly stated because the pressure acts on a very short time scale and structures, such as individual cells, tissues or orderly lipid lamellae will react differently concerning its typified tensile strength and shears modules [128-130]. Despite this fact, the current knowledge points to an expansion of the intercellular lipid lamellae, which provides an aqueous continuous pathway to deeper tissues [129]. Further biophysical explanations are unclear.

From a TDDS perspective, the photomechanical waves based technology demonstrated the *in vivo* deliver of large molecules, such as insulin. The recovery of the barrier function was not studied at the time, and standard procedures, such as the determination of TEWL and tritiated water fluxes were not considered [128-130].

4. Comparison of the Transdermal Drug Delivery Technologies

After the phenomenological and mechanistically review on the main transdermal drug delivery technologies, a summary of the characteristics of each one of them may help to rationalize the benefits and drawbacks (table 4-7).

Table 4-7 – Transdermal drug delivery technologies characteristics.

Variable	Topical delivery	Penetration enhancers	Transdermal patches	Electric assistance	Mechanical processes	Acoustical methods
Skin irritation	No	Yes	Yes	No	No	No
Cosmetic adequacy	No	No	No	Yes	Yes	Yes
Dosage flexibility	No	No	Yes	Yes	Yes	No
Range of applications	No	Yes	No	Yes	Yes	Yes
Product cost	Low	High	High	High	High	Low
Patient compliance	Yes	Yes	Yes	Yes	No	Yes

This table elucidates the changing paradigm that the mechanical processes and acoustical methods introduced in the field of transdermal drug delivery technologies [72]. However, there is room for further development in new transdermal systems because the binomial cost/effectiveness is not fully accomplished. Additionally, the physical methods available to actively deliver drugs through the skin have not yet fulfilled the need for safe, painless, efficient and affordable transdermal delivery of drugs [72].

5. References

- [1] B.W. Barry, Novel mechanisms and devices to enable successful transdermal drug delivery. *Eur. J. Pharm. Sci.*, 14, (2001) 101-114.
- [2] R. Wickett, M. Visscher, Structure and function of the epidermal barrier. *Am. J. Infect. Control*, 34 (2006) 98-110.
- [3] R. Paus, What is the 'true' function of the skin? *Exp. Dermatol.*, 11 (2002) 159-187.
- [4] K.A. Walters, *Dermatological and transdermal formulations*, Marcel Dekker, New York, 2002.
- [72] *Transdermal Drug Delivery Technologies, Companies & Markets*, Jain PharmaBiotech Report, 2012.
- [73] M.R. Prausnitz, S. Mitragotri, R. Langer, Current status and future potential of transdermal drug delivery. *Nat Rev Drug Discov.*, 3 (2004) 115-24.
- [75] Naik, Y.N. Kalia, R. H. Guy, Transdermal drug delivery: overcoming the skin's barrier function, 3, (2000) 318-326.
- [102] C. M. Burgess, *Cosmetic Dermatology*, Springer Science+Business Media, 2005.
- [103] *Farmacopeia Portuguesa VIII*, 2005.
- [104] K. Holmberg, B. Jönsson, B. Kronberg, B. Lindman, John Wiley & Sons, 2003.
- [105] A.O. Barel, M. Paye, H.I. Maibach, *Handbook of Cosmetic Science and Technology*, Marcell Dekker, 2001.
- [106] P. Karande, A. Jain, K. Ergun, V. Kispersky, S. Mitragotri, Design principles of chemical penetration enhancers for transdermal drug delivery. *Proc. Natl. Acad. Sc. USA*, 102 (2005) 4688-4693.
- [107] M.B. Brown, G.P. Martin, S.A. Jones, F.K. Akomeah, Dermal and transdermal drug delivery systems: Current and future prospects. *Drug Delivery*, 13 (2006) 175-187.
- [108] S. Andega, N. Kanikkannan, M. Singh, Comparison of the effect of fatty alcohols on the permeation of melatonin between porcine and human skin. *J. Control Release*, 77(2001) 17-25.
- [109] N. Kanikkannan, K. Kandimalla, S.S. Lamba, M. Singh, Structure-activity relationship of chemical penetration enhancers in transdermal drug delivery. *Cur. Med. Chem.*, 7 (2000) 593-608.
- [110] G. Chopda. <http://www.pharmainfo.net/reviews/transdermal-drug-delivery-systems-review> (accessed 06/04/2012).
- [111] S. Singh, An overview of transdermal drug delivery. *Drug Delivery Report*, (2005) 35- 40.

- [112] B.J. Thomas, B.C. Finnin, The transdermal revolution. *Drug Discovery Today*, 9 (2004) 697-703.
- [113] M. R. Prausnitz, The effects of electric current applied to skin: A review for transdermal drug delivery. *Advanced Drug Delivery Reviews*, 18 (1996), 395-425.
- [114] R. Vanbever, M.A. Leroy, V. Pr at, Transdermal permeation of neutral molecules by skin electroporation. *J. Control Release*, 54 (1998) 243-250.
- [115] A.R. Denet, R. Vanbever, V. Pr at, Skin electroporation for transdermal and topical delivery. *Advanced Drug Delivery Reviews*, 56 (2004) 659-674.
- [116] Y. N. Kalia, A. Naik, J. Garrison, R. H. Guy, Iontophoretic drug delivery. *Advanced Drug Delivery Reviews*, 56 (2004) 619– 658.
- [117] S. Dubey, Y.N. Kalia, Non-invasive iontophoretic delivery of enzymatically active ribonuclease A (13.6 kDa) across intact porcine and human skins. *J. Control. Release*, 145 (2010) 203-209.
- [118] S A. Saliba *et al*, Effect of Duration and Amplitude of Direct Current when Lidocaine Is Delivered by Iontophoresis. *Pharm.*, 3 (2011) 923-931.
- [119] S. Mitragotri, Current status and future prospects of needle-free liquid jet injectors. *Nature Rev. Drug. Disc.*, (2006) 543-548.
- [120] J.W. Lee, P. Gadiraju, J.-H. Park, M.G. Allen, M.P. Prausnitz, Microsecond thermal ablation of skin for transdermal drug delivery, *J. Control. Release*, 154 (2011) 58-68.
- [121] Y. G. Bachav, Effect of controlled laser microporation on drug transport kinetics into and across the skin. *J Control. Release*, 146 (2010) 31-36
- [122] M. Skorczakowski *et al*, Mid-infrared Q-switched Er:YAG laser for medical applications. *Laser Phys. Letters*. 7 (2010) 498-504.
- [123] P.M. Wang, M. Cornwell, J. Hill, M.R. Prausnitz, Precise Microinjection into Skin Using Hollow Microneedles. *J. of Invest. Dermatol.* 126 (2006) 1080–1087.
- [124] M.R. Prausnitz, Microneedles for transdermal drug delivery. *Advanced Drug Delivery Reviews*, 56 (2004) 581–587.
- [125] B.E. Polat *et al*, Ultrasound-mediated transdermal drug delivery: Mechanisms, scope, and emerging trends. *J. Control. Release*, 152 (2011) 330–348.
- [126] S. Mitragotri, D. Blankschtein, R. Langer, Transdermal Drug Delivery Using Low - Frequency Sonophoresis. *Pharm. Res.*, 13 (1996) 411-420.
- [127] S. Mitragotri, J. Kost, Low-frequency sonophoresis. *Advanced Drug Delivery Reviews*, 56 (2004) 589–601.

- [128] S. Lee, N. Kollias, D.J. McAuliffe, T.J. Flotte, A.G. Doukas, Topical Drug Delivery with a Single Photomechanical Wave. *Pharm. Res.*, 16 (1999) 1717-1721.
- [129] A.G. Doukas, T.J. Flotte, Physical Characteristics And Biological Effects Of Laser Induced Stress Waves. *Ultrasound Med. & Biol.*, 22 (1996) 151-164.
- [130] G. K. Menon, N. Kollias, A. G. Doukas, Ultrastructural Evidence of Stratum Corneum Permeabilization Induced by Photomechanical Waves. *J. Invest. Dermatol.*, 121 (2003) 104-109.

V

**Laser Generation
of Acoustic Waves**

1. Introduction

The use of lasers in a clinical environment has made an important impact in the practice of medicine [131]. This work highlights the generation of acoustic waves by pulsed laser irradiation of solids, which can be applied in the permeabilization of biological barriers. Lasers are a convenient way of producing high optical energies and powers over a small area, and stress waves can be generated following the light absorption by materials which present an efficient light-to-pressure conversion.

The laser irradiation can produce two main types of stress waves: dielectric breakdown and material ablation generates shock waves, which are characterized by a sudden discontinuous change in the material properties (melting) that propagates at a supersonic speed, and induces a tremendous rise in the pressure and temperature of the traversed medium [132]. Thermoelastic expansion involves the transient heating of the material surface, which propagates into the material at the speed of sound, with a moderate rise in the system pressure – photoacoustic waves [132].

Acoustic generation deals with the generation of acoustic waves in a solid, liquid or gaseous medium. The application of pulsed lasers into a material may cover a wide range of optical power densities, and encompass different types of mechanisms [132, 133]. In the absence of a change of state, the most relevant acoustic generation mechanisms are electrostriction, radiation pressure and thermoelastic expansion, with the latter representing the dominant mechanism. The utilization of higher optical powers densities in a region of the material and above a thermal threshold induces a change in the physical state of the medium. These mechanisms occur upon ionization and breakdown of the material – dielectric breakdown and material ablation, respectively [133].

The foundations of this work are in the generation of photoacoustic (PA) waves by pulsed lasers, and in the physical processes underlying the conversion of light into acoustic energy.

2. Mechanisms for Acoustic Waves Generation

The generation of acoustic waves by lasers was first revealed by White in solids [134] and Askar'yan in liquids [135], shortly after the invention of the Q-switched laser. The nature of the generation process depends on the intrinsic characteristics of the laser source, the medium material or boundary conditions.

Electrostriction reflects an intrinsic characteristic of molecules – polarizability. This phenomenon characterizes the movement of molecules into regions of different optical intensity due to their intrinsic polarizability [136]. These movements produce a density gradient, a temporal-spatial density change in the medium material: an acoustic wave. The acoustic gradient produced presents conversion efficiencies below 10^{-4} [133]. Several calculations suggested that the efficiency conversion of the light-to-acoustic energy of the previous mechanism was negligible, if compared to the thermal-expansion, material ablation and dielectric breakdown [133].

The destructive nature of the dielectric breakdown mechanism discourages its use in the clinical field because it occurs at laser intensities above 10^{10} W/cm², which can be obtained by focusing a pulsed laser [133]. Such high intensity promotes optical breakdown by two different paths: multiphoton ionization and avalanche/cascade ionization. Multiphoton ionization arises from *quasi*-simultaneous absorption of photons to reach the electron ionization energy [137]. Avalanche ionization develops in the presence of impurities of the medium, as ionized electrons interact with excited electrons of other atoms, consequently liberating them, and initiating a cascade of these events [137]. The efficiency of the light-to-acoustic conversion in dielectric breakdown can reach 30% [133].

The remaining acoustic generation mechanisms also result from the laser beam impinging on a material and its partial or total absorption [138] (figure 5.1). The material ablation and thermoelastic process differ in reason of the thermal properties of the medium, namely the meltdown threshold of the material. If the laser optical power is kept below this threshold, the material does not melt and the generation regime is called thermoelastic, figure 5.1 (a). If the optical power exceeds the melting threshold, the material undergoes melting reactions - ablation regime, figure 5.1 (b).

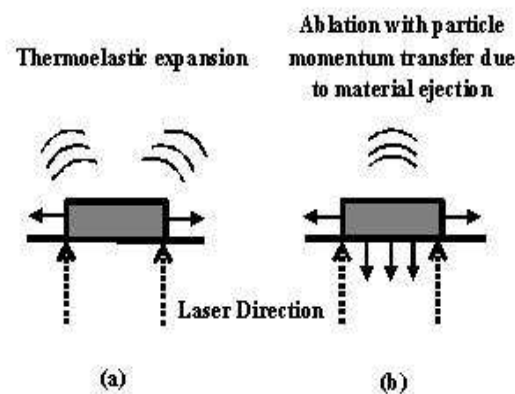


Fig. 5.1 – Principal mechanisms for laser generation of acoustic transients: (a) thermoelastic expansion and (b) ablation regime.

In the material ablation mechanism, it is postulated that when the laser energy density exceeds the strength of the material, there is a breakdown into small particles [139]. This phenomenon occurs due to the surpassing of the material thermal threshold, which

induces an explosion accompanied by the ejection of particles from the material surface, and formation of plasma in the material/air interface [140]. Consequently, there is a change in the physical state of the material, and this explosion produces a recoil stress that increases the peak amplitude of the acoustic wave [141]. This description corresponds to the photomechanical production of material ablation, although photothermal and photochemical processes can also be responsible for the acoustic generation. Photothermal refers to the decomposition of the medium by irradiation with very high temperatures (exceeding the boiling threshold), while the photochemical decomposition relates to the chemical interaction between molecules and laser photons, which promotes the fracture of chemical bonds (such as, amine bond breakdown in triazene polymers) [133, 142].

In figure 5.2⁶, a carbon dioxide (CO₂) laser of 50 J *per* pulse and pulse duration of 100 μ sec generates a power of $8 \cdot 10^7$ W/cm² over an area of $6 \cdot 10^{-3}$ cm² [143]. The formation of the acoustic wave in the graphite medium occurs after surpassing the melting threshold (right edge of the photograph). The directionality of the wave follows the direction of the impinging laser beam (but with opposite sense), and the plasma formed between the material/air interface contributes to the expansion and amplitude of the acoustic wave.

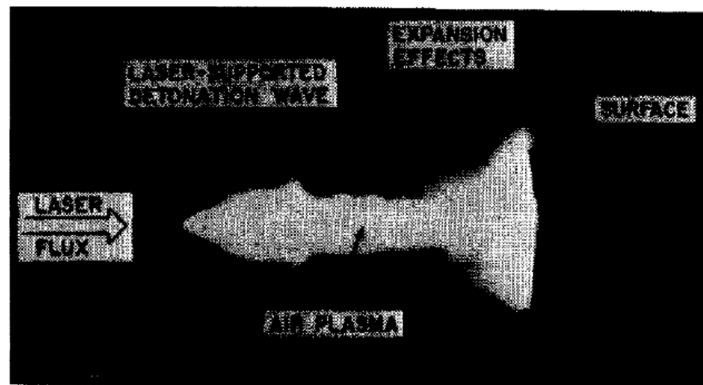


Fig. 5.2 – Plasma produced by a CO₂ laser after detonating a graphite medium.

The maximization of the acoustic generation in the ablation regime depends on several parameters [144]:

- Selection of the laser light wavelength with a minimum absorption depth in the material;
- Short laser pulse duration to maximize the acoustic wave peak pressure (PP in equation 5.1);
- High repetition rate of the laser pulse (diminishing loss of the incident energy to the surroundings);

⁶ A. N. Pirri, Theory for momentum transfer to a surface with a high-power laser. *Phys. Fluids*, 16 (1973) 1435-1440.

- High quality of the laser beam (brightness, focusability and homogeneity).

The efficiency of the acoustic conversion in the ablation regime is up to 1% [133], and can be estimated for polymers and metals by the coupling coefficient:

$$PP = b \frac{I^{0.7}}{(\lambda\sqrt{\tau_L})^{0.7}} \quad (5.1)$$

where PP is the peak pressure of the wave, b a proportionality constant which depends on the material properties, I the laser irradiance, λ the laser wavelength and τ_L the laser pulse duration. During the ablation process, only a small fraction of the laser energy is absorbed by the medium and converted into acoustic energy, so that designing stratified mediums (overlays) guarantees a recoil momentum increase: higher efficiency conversion and higher PP [145].

The thermoelastic expansion mechanism involves the transient heating of a restricted volume, in respect of the absorbed laser energy [133]. If the absorption coefficient of the medium is high, the absorption of the laser energy occurs near the surface of the material, and the thermal expansion circumscribes the acoustic generation to a volume resembling a thin disc ($\leq 10 \mu\text{m}$) [146]. Afterwards, the optical absorption causes a temperature rise in a localized volume of the medium, which expands to adjacent areas by heat conduction and resulting in a strain in the material that propagates as an acoustic wave [147]. In rigid boundaries, the enclosed heat is trapped, and consequently induces an increase in the system pressure [148]. The duration of the thermoelastic expansion is proportional to the pulse duration of the laser pulse, which translates that the center frequency and bandwidth of the acoustic wave is determined by the incident laser pulse [149, 150]. The light-to-acoustic conversion efficiency is considered very low (10^{-4}) [133].

3. Physics of Acoustic Wave Propagation

An acoustic wave is a mechanical wave resulting from the back and forth vibration of the medium particles through which the wave is traversing (figure 5.3). The particles motion is parallel (or anti-parallel) to the direction of the energy transport. The wave directionality characterizes it as a longitudinal one, and its wavelength represents the distance that the disturbance travels in one complete wave cycle [151]. A longitudinal

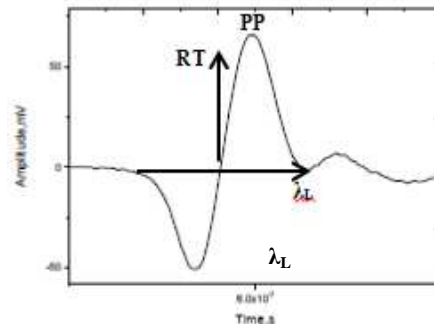


Fig. 5.3 – A typical photoacoustic wave: PP represents the peak pressure of the wave, RT symbolizes its rise time (10 to 90% of the PP) and λ_L the acoustic wavelength.

wave consists of a repeating pattern of compressions and rarefactions, respectively, high-pressure and low-pressure regions moving through a medium - a pressure wave. Consequently, the acoustic waves propagation can be described by the mathematical theory of waves [151, 152].

Acoustic waves can be generated in fluids and solids assuming a compressible, non-viscous fluid (i.e., no attenuation) with no shear strength and in equilibrium (i.e., no inertial forces). The displacements of the material propagate as an acoustic wave. Due to the lack of shear strength, localized deformations of the medium do not result in shear deformations but instead cause transient changes in the materials volume, as shown in figure 5.4.

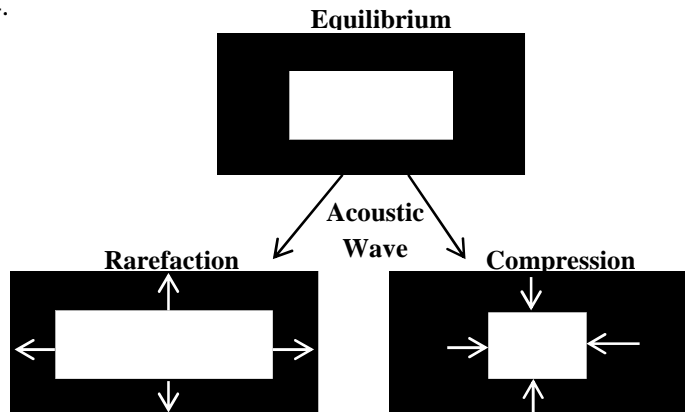


Fig. 5.4 – Material represented as rectangles that are disturbed by the action of an acoustic wave. The lower left depicts the rarefaction of the wave where the surrounding medium pushes the material into a larger volume, diminishing its density. The lower right depicts the compression of the material into a smaller volume, increasing the system pressure.

3.1 Hooke’s Law for Acoustics

Hooke’s law for the acoustic propagation in a material states that stress is linearly proportional to strain, for small strains. The one dimension example of this case is when a mass is connected to a spring that disturbs it from equilibrium:

$$F = -k_s \left(\frac{du}{l} \right) \hat{k} \tag{5.2}$$

where du is the displacement from equilibrium, k_s is the spring constant, l is the length of the spring in equilibrium and \hat{k} is the downward point unit vector. The ratio du/l is also known as the compressional strain of the spring model. In the equilibrium position there is no motion because the gravitational force balances the elastic force. In a three dimensional situation, the application of an acoustic wave to a material described by the Hooke’s Law states that the surrounding disturbed medium exerts a pressure on the face

of the material (P) that is linearly proportional to the corresponding volume change of the cube:

$$P = -k_B dV/V \quad (5.3)$$

where dV is the change in volume after the disturbance, V is the undisturbed material volume and k_B is the bulk modulus. The volume change term is the equivalent of the one dimensional displacement change, and the disturbance can be measured by,

$$\frac{dV}{V} = \frac{\partial u \partial y \partial z + \partial v \partial x \partial z + \partial w \partial x \partial y}{dx \partial y \partial z} + K \approx \frac{\partial u}{\partial x} + \frac{\partial v}{\partial y} + \frac{\partial w}{\partial z} \quad (5.4)$$

where K is a second term neglected for small displacements (valid for $dV/V < 10^{-4}$) and $V = dx \partial y \partial z$ is the material volume before the disturbance. Substituting equation 5.3 into equation 5.4 results in:

$$P = -k_B(x, y, z) \nabla \cdot \mathbf{u} + S(x, y, z, t) \quad (5.5)$$

where $\nabla \cdot \mathbf{u}$ are the Cartesian components of the displacement along the x , y , and z axes, and $S(x, y, z, t)$ is a time dependent term independent of the displacement field.

3.2 Newton's Law for Acoustics

The application of an external force into a material results in a non-zero gradient along the material axes. Consequently, a concomitant elastic force imposes upon the material, which is balanced by an inertial force, so that Newton's law states:

$$\text{Newton's Law: } \frac{\partial P}{\partial x} = -\rho(x, y, z) \partial^2 u / \partial t^2 \quad (5.6)$$

where ρ represents the density of the material. From the resolution equation 5.6 arises

$$[P(x + dx, y, z, t) - P(x, y, z) \partial y \partial z] \approx -[\rho(x, y, z) dx \partial y \partial z] \ddot{u}(x, y, z, t) \quad (5.7)$$

where the double dot corresponds to two time derivatives. Expanding the Hooke's Law in a Taylor series about the point (x, y, z) outcomes in:

$$\begin{aligned} & \left[P(x + dx, y, z, t) - P(x, y, z, t) + \frac{\delta P}{\delta x \partial x} + \text{High Order Terms} \right] \partial y \partial z \approx \\ & -[\rho dx \partial y \partial z] \ddot{u}(x, y, z, t) \end{aligned} \quad (5.8)$$

and dividing by $dx dy dz$ neglecting higher-order terms, the Newton's Law simplifies to:

$$\frac{\delta P(x,y,z)}{\delta X} = -\rho(x, y, z)\ddot{u}(x, y, z, t) \quad (5.9)$$

For an arbitrary force distribution, the general form of Newton's law is

$$\nabla P = -\rho(x, y, z)\ddot{u}(x, y, z, t) \quad (5.10)$$

where $\ddot{u}(x, y, z, t)$ is the particle acceleration vector.

3.3 Acoustic Wave Equation

The application of $(\partial^2 / \partial t^2, \nabla)$ to equation 5.5 and 5.10, respectively, and then dividing by $\rho(x, y, z)$ results in:

$$\ddot{P} = -k(x, y, z)\nabla * \ddot{u} + S(x, \ddot{y}, z, t),$$

$$\nabla * \left[\frac{1}{\rho(x,y,z)\nabla P} \right] = -\nabla * \ddot{u} \quad (5.11)$$

The above two equations are the first-order equations of motion in an acoustic medium. Substituting one in another yields the second order acoustic wave equation:

$$\nabla * \left[\frac{1}{\rho(x,y,z)\nabla P} \right] - 1/[k(x, y, z)\ddot{P} = S(x, y, z, t)]/k(x, y, z) \quad (5.12)$$

This equation is valid for arbitrary velocity and density distributions. Assuming negligible the density gradients, the above equation reduces to the following equation:

$$\nabla^2 P - c^{-2}\nabla^2 \partial P / \partial t^2 = -\rho(x, y, z)S(x, \ddot{y}, z, t)/k(x, y, z) \quad (5.13)$$

where c represents the compressional wave propagation velocity $c = \sqrt{k(x, y, z)/\rho(x, y, z)}$. For simplification purposes, the above equation is known as the inhomogeneous acoustic wave equation for negligible density variations, and expressed as,

$$\nabla^2 P - c^{-2} \partial^2 P / \partial t^2 = F \quad (5.14)$$

where $F = -S(x, y, z, \ddot{z}, t)/k(x, y, z)$ is the inhomogeneous external force term, which specifies the location and time history of the acoustic wave [151, 152].

3.4 Heat Equation

The overall thermoelastic generation of acoustic waves is governed by two equations: the acoustic wave equation and the heat equation. The heat conduction equation determines the temperature distribution in the perturbed medium by [146]

$$\frac{\partial T}{\partial t} = k_T \nabla^2 T + \frac{1}{\rho C_p} \delta \quad (5.15)$$

where k_T is the thermal diffusivity, ρ is the density of the medium, C_p is the specific heat capacity, and δ is the rate of energy deposited in the absorbing medium volume. The two parameters that characterize the heat influence in the generation of acoustic waves by a laser source are the thermal diffusivity ($k_T = \sqrt{\frac{2\alpha}{w}}$) and effusivity ($\varepsilon = \sqrt{k\rho C_p}$), where α is the thermal conductivity and w is the modulation frequency [146].

4. Theory for Laser induced Acoustic Waves

The thermoelastic expansion mechanism represents the basis of this work, and depends of the time, in which the laser energy is deposited in the medium (*ultrafast energy deposit*), i.e., the laser pulse (τ_L) is shorter than the time required for acoustic wave to traverse the absorption depth of the material [150]. The condition which maximizes the light-to-acoustic conversion is expressed by the following relation:

$$\tau_L c_s \mu_a \gg 1 \quad (5.16)$$

where μ_a is the linear absorption coefficient of the absorbing material and c_s is the longitudinal speed of sound. This relation postulates that a maximization of the medium absorptance will enhance the energy conversion, in the region where the optical energy is deposited. Consequently, the ultrafast increase in the local temperature takes place during the laser pulse, creating a stress in the medium, which propagates as an acoustic wave.

The linear acoustic wave equation may be used to describe this phenomenon, with the addition of a material term that describes the heated region. The full treatment and solution of equation 5.14 can be found in Paltauf et al. [153] and Gusev et al. [154]. A typical solution can be found as follows:

$$\nabla^2 P - c^{-2} \delta^2 P / \delta t^2 = \frac{\beta}{\rho C_P} S \quad (5.19)$$

where β is the thermal expansion coefficient, C_P is the specific heat at constant pressure and S is the heat generated per unit of volume and time. S can be described as an instantaneous heat deposition so that $S(r,t) = W(r) \delta(t)$, where $W(r)$ is the absorbed volumetric energy density and $\delta(t)$ is the Dirac delta. Following Paltauf and Gusev, it is possible to determine the compressional velocity from which the pressure can be calculated. Using an acoustic interface which approximates the laser energy deposition in the medium by an optical fiber, the following solutions appear,

$$p(z, t) = \frac{1}{2} \Gamma \mu_a H_0 (\exp[-\mu_a(z - ct)] + \exp[-\mu_a(z + ct)]) \quad (5.20)$$

where Γ is the unitless Grüneisen coefficient, which is the fraction of deposited energy that is available for acoustic energy conversion, μ_a the linear absorption coefficient of the medium and H_0 is the radiant exposure. The first term is the downward plane wave (tensile), while the second term is the upward plane wave (compression).

4.1 The Grüneisen Coefficient

The Grüneisen coefficient, Γ , is the ratio of laser energy that is available for thermoelastic conversion into acoustic energy, and for most solids a simple relation has been shown by Grüneisen to have experimental validity [155],

$$\Gamma = \frac{\text{Volume Coefficient of Thermal Expansion} * \text{Specific Volume}}{\text{Compressibility} * \text{Specific Heat (Constant volume)}} \quad (5.21)$$

The experimental values of Γ for most solids (namely polymers) lie between 1.5 and 2.5, and for living tissue mediums 0.11 to 0.5. The establishment of a theoretical basis for the Grüneisen constant was originated from the works of Slater [155], in his derivation of the Mie-Grüneisen equation of state $(P - P_0) * V = \Gamma * (E - E_0)$, where the subscripted values of pressure (P) and internal energy (E) are volume (V) dependent at zero kelvin. The rationalization of this works results in:

$$\Gamma = \frac{\alpha c_a^2}{C_P} \quad (5.22)$$

where α is the volumetric thermal expansion coefficient and c_a is the adiabatic speed of sound.

This thermal parameter of materials describes an important feature of the light-to-acoustic conversion, because an increase in its absolute value should maximize the peak pressure of the acoustic wave.

5. Generation of Photoacoustic Waves by the Thermoelastic Process

The transient permeabilization of biological barriers requires acoustic wave bandwidths with very higher frequency components (≥ 20 MHz) because pressure gradients must be produced in the sub-millimeter range to perturb the relevant biological structures and high frequencies are strongly absorbed by biological tissues [156]. Additionally, the avoidance of transient cavitation bubbles is a critical factor because otherwise that can cause permanent damage in biological tissues, as they expand to millimeter sizes and collapse. The mechanical index (MI) describes the likelihood of cavitation,

$$MI = \frac{P_{rmax}}{\sqrt{f}} \quad (5.23)$$

where p_{rmax} is the tensile peak pressure and f is the center frequency of the acoustic wave. In view of the deleterious effect of cavitation, the MI for ultrasound should be lower than 0.5 [157, 158]. Thus, the acoustic waves with $f_{US} > 100$ MHz can be used in a biological environment, if $p_{max} \leq 5$ MPa (≤ 50 bar). Moreover, a 2 minutes exposure time to 20 MHz, 8 ns laser pulses of 40 mJ/cm², gives a temporal average of the total exposure to ultrasound below 1 W/cm², which is less than the exposure level of physiotherapy. Although safe, such moderately intense acoustic waves present rise times of tens of bar/ns and acoustical wavelengths ($\lambda_L = 2c_s\tau_L$) of tens of microns, which may transiently perturb a biological barrier, as the skin, and consequently facilitate the transdermal drug delivery [144].

The design of an efficient photoacoustic converter of laser pulse energy must consider that the generation of the pressure wave, in the presence of a rigid boundary, leads to a higher pressure than in the case of a free boundary [133]. The acoustic constrain of the photoacoustic converter by quartz plates was shown to enhance the amplitude of 20 MHz photoacoustic waves by a factor of nearly 100 [159]. Moreover, in the case of an acoustic transient generated by thermoelastic expansion, the presence of a rigid boundary transforms a stress transient consisting of a compression followed by a tensile part into a unidirectional compressive impulse [160]. As a consequence, the effects of cavitation are minimized and mostly-compressive acoustic transients permeabilize the skin.

The irradiated areas of the light-to-pressure converters have limits for what can be considered the generation of a planar acoustic wave. The criterion is that the laser beam radius r must be chosen to meet the condition,

$$r \gg \sqrt{2c_s \tau_L z} \quad (5.24)$$

where z is the distance between the medium material surface and the final target of the wave. A structural support with $z = 1$ mm, with values of $c_s=2500$ m/s and $\tau_L=10$ ns, requires $r \gg 0.2$ mm. Hence, it is possible to focus a laser beam to a radius of 1 mm and still produce a planar acoustic wave. This configuration means that the laser apparatus required for an energy density of 10 mJ/cm^2 per pulse on an area of 0.03 cm^2 corresponds to a laser pulse of 0.3 mJ.

Another relevant aspect is that when a photoacoustic wave travels in one medium (medium 1) and encounters a boundary in a second medium (medium 2), it reflects and transmits (or refracts). Consequently, new acoustic waves are generated within the propagation path. The transmission coefficient is given by,

$$T_c = \frac{A_2}{A_1} = \frac{2\sqrt{Z_1 Z_2}}{Z_1 + Z_2} \quad (5.25)$$

where A_2 and A_1 are the initial amplitude in medium 1 and the final amplitude in medium 2, and Z_1 and Z_2 are the acoustic impedances in the two media. Complete transmission between the two mediums requires $Z_1=Z_2$. The presence of voids in this assembly is a major cause of inefficiency in the acoustic transmission. The presence of air with an acoustic impedance dramatically different from the other media of the assembly results in poor acoustic transmission and loss of efficiency of the conversion. Thus, it is necessary to insure a good acoustic coupling between the photoacoustic converter (where the photoacoustic wave is generated), and the final medium, the skin.

The acoustic impedance of the skin is $Z_{skin}=1.54 \text{ MRayl}$ [$1 \text{ MRayl} = 1 \times 10^6 \text{ kg}/(\text{m}^2 \text{ s})$], similar to that of water ($Z_{water}=1.48 \text{ MRayl}$), but dramatically different from that of metals ($Z_{Aluminum}=17 \text{ MRayl}$, $Z_{steel}=46 \text{ MRayl}$), although relatively close to those of plastics ($Z_{Teflon}=2.97 \text{ MRayl}$, $Z_{polyethylene}=1.76 \text{ MRayl}$, $Z_{polystyrene}=2.42 \text{ MRayl}$). Interesting materials for good acoustic coupling with the skin are paraffin ($Z_{paraffin}=1.8 \text{ MRayl}$), glycerol ($Z_{glycerol}=2.3 \text{ MRayl}$), graphite ($Z_{graphite}=2.7 \text{ MRayl}$), cellulose acetate ($Z_{cellulose}=3.2 \text{ MRayl}$) or acoustic scanning gel. Efficient delivery of acoustic waves to the skin requires the choice of materials with acoustic impedances close to Z_{skin} . The problem of acoustic impedance mismatch may also be solved by using multiple matching layers in series

where the optimum impedance for each layer is equal to the geometric mean of the impedance of the layers on either side.

The maximum pressure amplitude (P_{max}) generated by thermoelastic expansion after absorption of a laser pulse with the optical power density I_L is defined by [133]

$$P_{max} = \frac{\Gamma}{c_s} I_L \quad (5.26)$$

The average sound power density (rate of energy flow through a unit area perpendicular to the direction of propagation - I_s) is given by [161]

$$I_s = \frac{p^2}{\rho c_s} \quad (5.27)$$

when $p \ll \rho c_s^2$. This leads to an efficiency of light-to-pressure transduction that increases with the optical power density

$$\eta_{PA} = \frac{I_s}{I_L} = \frac{\Gamma^2}{c_s^3 \rho} I_L \quad (5.28)$$

Inspired by the tenets of photoacoustic calorimetry and the present rationalization, we designed light-to-pressure transducer materials (photoacoustic converters) that are very thin (thickness $< 100 \mu\text{m}$), strongly absorbing ($\mu_a > 50 \text{ cm}^{-1}$) and incorporate dyes with ultrafast radiationless decays ($< 1 \text{ ns}$ lifetimes). We name such materials “piezophotonic”. A polymeric piezophotonic material with $c_s = 2500 \text{ m/s}$ and $\mu_a = 500 \text{ cm}^{-1}$ is in the limit of generating a photoacoustic wave by thermal expansion within the time dependence of a laser pulse with $\tau_L = 8 \text{ ns}$. For example, a confined polystyrene target coated with a PA reference ($c_s = 2320 \text{ m/s}$, $C_p = 2 \text{ J/(g K)}$, $\Gamma = 0.70$ and $\alpha = 6.6 \times 10^{-7} \text{ K}^{-1}$ [155]) absorbing a 8 ns laser pulse with 32 mJ in 0.8 cm^2 ($I_L = 5 \text{ MW/cm}^2$) should be able to produce a maximum pressure of 146 bar. The equation 5.28 holds true below the ablation threshold, which is around $I_L = 15 \text{ MW/cm}^2$ for polystyrene [162], and the maximum light-to-pressure photoacoustic conversion efficiency attainable with this polymer is 0.5%. The maximization of the terms in equation 5.28 should promote an increase in the acoustic conversion, by the thermoelastic expansion mechanism, to levels unprecedented in the scientific literature. Biagi *et al* reported heavily absorbing films designed to maximize the value of η_{PA} and obtained a conversion efficiency of 10^{-5} [163]. This disappointing efficiency can be assigned to the low power densities employed: $I_L = 0.4 \text{ MW/cm}^2$ produced an acoustic wave with $p_{max} = 0.1 \text{ bar}$. Guo *et al* developed photonic crystal-metallic structures with a layer of an elastomer and operated in a total-internal-reflection geometry to obtain $p_{max} = 2.4 \text{ bar}$ with $I_L = 3 \text{ MW/cm}^2$ [164]. This is one of the highest

conversion efficiencies reported in the literature, although it did not make use of confinement by rigid interfaces. Higher conversion efficiencies can be expected from materials with high Grüneisen coefficients, but these coefficients must be calculated from appropriate thermodynamic quantities, namely taking into consideration all the modes of the material, for consistency with the specific heat [155, 165]. Silicone elastomers, such as Sylgard 184® are among the polymers with the highest Grüneisen coefficients, $\Gamma = 1.5$ [166], and making use of $c_s = 1100$ m/s and $\rho = 1010$ kg/m³ [167], we calculate a theoretical conversion efficiency of 59% at the ablation threshold of $I_L = 35$ MW/cm² [168]. However, the duration of the PA wave is only as short as an 8 ns laser pulse incident on a silicone elastomer when $\mu_a > 1100$ cm⁻¹.

6. References

- [131] W.W. Lou, R. G. Geronemus, Dermatologic Laser Surgery. Seminars in Cutaneous Medicine and Surgery, 21(2002) 107-128.
- [132] D.A. Hutchins, Ultrasonic generation by pulsed lasers, Phys. Acoust., 18 (1988) 21– 123.
- [133] M.W. Sigrist, Laser generation of acoustic waves in liquids and gases, J. Appl. Phys., 60 (1986) 83-121.
- [134] R. M. White, Generation of Elastic Waves by Transient Surface Heating. J. App. Phys. 34 (1963) 3559-3567.
- [135] Askar'yan *et al*, Excitation of Signals in a Negatively Charged Post of an Antenna under the Influence of an Unfocused Laser Beam. Sov. Phys. JETP Lett., 4 (1966) 122-123.
- [136] S.J. Daviest, C. Edwards, G.S. Taylor, S.B. Palmer, Laser-generated ultrasound: its properties, mechanisms and multifarious applications. J. Phys. D: Appl. Phys., 26 (1993) 329-348.
- [137] J.R. Sukovich, A. Sampathkumar, R.G. Holt, Pressure Dependence of Laser-Induced Dielectric Breakdown in Water. IEEE J. Quant. Electr., 47 (2011) 1297-1303.
- [138] W. W. Duley, Laser Processing and Analysis of Materials. Plenum, New York, 1983.
- [139] J.C. Miller, Laser Ablation-Principles and Application. Springer Series in Materials Science, Volme 28, Springer, New York, 1994.
- [140] R. Fabro *et al*, Physical study of laser-produced plasma in confined geometry. J. Appl. Phys., 68 (1990) 775– 784.
- [141] M. von Allmen and A. Blatter, Laser-Beam Interactions with Materials—Physical Principles and Applications, Springer Series in Materials Science: Springer, New York, 1995.
- [142] A. Harata *et al*, Laser-induced surface acoustic waves and photothermal surface gratings generated by crossing two pulsed laser beams. Appl. Phys. Lett., 57 (1990) 132–134.

- [143] A. N. Pirri, Theory for momentum transfer to a surface with a high-power laser. *Phys. Fluids*, 16 (1973) 1435-1440.
- [144] A.G. Doukas, N. Kollias, Transdermal drug delivery with a pressure wave. *Advanced Drug Delivery Reviews*, 56 (2004) 559–579.
- [145] T.W. Murray, J.W. Wagner, Laser generation of acoustic waves in the ablative regime. *J. App. Phys.*, 85 (1999) 2031-2040.
- [146] J.B. Spicer, A.D.W. McKie, J.W. Wagner, Quantitative theory for laser ultrasonic waves in a thin plate. *Appl. Phys. Lett.*, 57 (1990) 1882-1884.
- [147] L.M. Lyamsev, Optoacoustic sources of sound. *Sov. Phys. Usp.*, 24 (1981) 977–995.
- [148] D. Kim, M. Ye, C.P. Grigoropoulos, Pulsed laser-induced ablation of absorbing liquids and acoustic-transient generation. *Appl. Phys. A*, 67 (1998) 169-181.
- [149] F.A. Schaberle *et al*, Analytical solution for time-resolved photoacoustic calorimetry data. A survey of mechanisms common in photochemistry. *Photochem. Photobiol. Sci.*, 9 (2010) 812-822.
- [150] A.A. Karabutov, E.V. Savateeva, N.B. Podymova, A.A. Oraevsky, Backward mode detection of laser-induced wide-band ultrasonic transients with optoacoustic transducer, *J. Appl. Phys.*, 87 (2000) 2003-2014.
- [151] J.D. Achenbach, *Wave Propagation in Elastic Solids*, 1973, North-Holland/Elsevier, Amsterdam.
- [152] L. Kinsler, A. Frey, 1961, *Fundamentals of Acoustics*, Wiley and Sons, New York.
- [153] G. Paltauf and H. Schmidt-Kloiber, “Photoacoustic waves excited in liquids by fiber–transmitted laser pulses. *J. Acoust. Soc. Am.*, 104 (1998) 890–897.
- [154] V. E. Gusev, A. A. Karabutov, *Laser Optoacoustics*. AIP Press, 1993.
- [155] W.H. Childs, Thermomechanical properties of selected space-related materials, in, *The Aerospace Corporation*, Los Angeles, 2002.
- [156] V. Venugopalan, N.S. Nishioka, B.B. Mikic, Thermodynamic response of soft biological tissues to pulsed infrared-laser irradiation *Biophys. J.*, 70 (1996) 2981-2993.

- [157] R.E. Apfel, C.K. Holland, Gauging the likelihood of cavitation from short-pulse, low-duty cycle diagnostic ultrasound. *Ultrasound Med. Biol.*, 17 (1991) 179-185.
- [158] C.C. Church, A theoretical study of acoustic cavitation produced by “positive-only” and “negative-only” pressure waves in vivo. *Ultrasound Med. Biol.*, 29, (2003) 319-330.
- [159] R.J. von Gutfeld, R.L. Melcher, 20-MHz acoustic waves from pulsed thermoelastic expansions of constrained surfaces. *Appl. Phys. Lett.*, 30 (1977) 257.
- [160] E.F. Carome, N.A. Clark, C.E. Moeller, Generation of acoustic signals in liquids by Ruby laser-induced thermal stress transients. *Appl. Phys. Lett.*, 4 (1964) 95-97.
- [161] J.P. Simonin, On the mechanisms of in vitro and in vivo phonophoresis. *J. Controlled Release*, 33 (1995) 125-141.
- [162] H. Fukumura, N. Mibuka, S. Eura, H. Masuhara, Mass spectrometric studies on laser ablation of polystyrene sensitized with anthracene. *J. Phys. Chem.*, 97 (1993) 13761-13766.
- [163] E. Biagi, F. Margheri, D. Menichelli, Efficient laser-ultrasound generation by using heavily absorbing films as targets, *IEEE Trans. Ultraon., Ferroelect., Fre. Contr.*, 48 (2001) 1669-1680.
- [164] Y. Guo, H.W. Baac, S.-L. Chen, T.B. Norris, L.J. Guo, Broad-band, high-efficiency optoacoustic generation using a novel photonic crystal-metallic structure. *Proc. SPIE*, 78992 (2011) 78992C78991-78998.
- [165] I. Gilmour, A. Trainor, R.N. Haward, Calculation of the Grüneisen constant of glassy polymers from thermoelastic data, *J. Polym. Sci.*, 16 (1978) 1291-1295.
- [166] R.E. Winter, G. Whiteman, G.S. Haining, D.A. Salisbury, K. Tsembeles, Measurement of equation of state of silicone elastomer, in: M.D. Furnish, Y.M. Gupta, J.W. Forbes (Eds.) *Shock Compression of Condensed Matter - 2003*, American Institute of Physics, New York, 2004, pp. 679-682.
- [167] J.C.F. Millett, G. Whiteman, S.M. Stirk, N.K. Bourne, Shear strength measurements in a shock loaded commercial silastomer, *J. Phys. D: Appl. Phys.*, 44 (2011) 185403.

- [168] V.-M. Graubner, R. Jordan, O. Nuyken, T. Lippert, M. Hauer, B. Schnyder, A. Wokaun, Incubation and ablation behavior of poly(dimethylsiloxane) for 266 nm irradiation, *Appl. Surf. Sc.*, 197-198 (2002) 786-790.

VI

**Development of a
Photoacoustic Waves
based TDD System**

1. Introduction

This chapter discusses the theoretical and practical concepts underlying the photoacoustic (PA) waves based TDD system.

1.1 Background

Photoacoustic effects have been known since the 19th century [169] with the discovery by Bell of the effect of sunlight on a selenium cell, which rapidly modulated sunlight on gases. The practical development of photoacoustics began with the advent of lasers in the 1960's [134, 135], when researchers were able to exploit the short laser pulses for acoustic generation in solids and liquids. The photoacoustic phenomena described in this thesis results from a photothermal interaction consisting in the ultrafast optical energy conversion into thermal energy by a strongly absorbing material. In other words, thermalization of the energy in the irradiated volume is faster than the laser pulse [149, 150].

Thermoelastic expansion is considered an inefficient method to convert light into acoustic pressure [133]. However, it is often overlooked for optically thin materials that the peak pressures obtained by thermoelastic expansion scale with the reciprocal of the thickness (h) of the absorbing material, for the same amount of energy absorbed [170],

$$PP = \frac{\Gamma}{h} \Delta H_{th} \quad (6.1)$$

where ΔH_{th} is the thermal energy released per unit area and the dimensionless Grüneisen coefficient is $\Gamma = \alpha c_a^2 / C_p$ (α is the volumetric thermal expansion coefficient, c_a is the adiabatic speed of sound and C_p is the specific heat capacity) [155]. The physics for optically thin materials also apply to cases where the absorptance of the sample is approximately 1, if the bottom interface is totally reflecting and the light traverses twice the absorbing material [171]. The dependence between the amplitude of the photoacoustic wave and the thickness of the light absorbing material was also observed when heavily absorbing films are employed as targets of the laser pulse [163]. The maximum pressure produced by the thermoelastic process was found to increase as the thickness of the absorbing film is reduced, and this property was used in the design more efficient photoacoustic generators of acoustic waves [163].

The maximization of the conversion between laser and acoustic energy *via* the thermoelastic processes requires (1) a choice of materials that convert the laser pulse energy into heat within the duration of the laser pulse, (2) thin films (low h) with absorptances higher than unit, and (3) materials with large Grüneisen coefficients. Therefore, a technology aimed at the fast and efficient conversion of the energy of a laser pulse into a photoacoustic wave must incorporate in

a very thin layer a compound that strongly absorbs light at the wavelength of the laser pulse. Additionally, it should convert into heat all the energy absorbed during that laser pulse. Photoacoustic calorimetry (PAC) reference compounds meet these properties. The intensity of the photoacoustic wave may be further increased, if ultrafast structural volume changes accompany the radiationless decay occurring within the duration of the laser pulse, but in this case the material is damaged.

Two other relevant aspects are the time profile of the laser beam and material properties. The duration of the thermoelastic expansion, and hence the rise time of the photoacoustic wave (time from 10% to 90% of the peak pressure), depends on the rates of the processes taking place in the absorbing material [149, 150]. When this material incorporates dyes selected from photoacoustic references (species that convert all the absorbed light into heat in a time shorter than the laser pulse) and $\mu_a c_a \tau_L \gg I$, the duration of the PA is as short as that of the laser pulse, and the spectral band of the PA transient is determined by the spectral band of the laser pulse [149]. For example, the acoustic transient profile will follow that of a $\tau_L = 10$ ns laser pulse for a typical polymer ($c_s = 2500$ m/s) when $\mu_a \gg 400$ cm⁻¹. When sufficient quantities of PAC reference compounds are incorporated in appropriate supporting materials, such that the optical penetration depth ($\delta = 1/(2.3\mu_a)$) is smaller than 10 μ m, the duration of the nanosecond laser pulse and its peak power determine the bandwidth and intensity of the acoustic transient [172]. The amplitudes of the acoustic transients decrease when τ_L is significantly larger than the ratio of optical penetration depth to the velocity of the longitudinal waves, and the decrease of the acoustic transient amplitude with the increase in τ_L is more accentuated at high frequencies [163].

The fast and efficient conversion of the laser pulse energy generates very wide band acoustic transients, with bandwidths in the tens or hundreds of MHz, depending on the laser pulse width. For sufficiently short laser pulses, the center frequency of the generated wave is displaced to higher frequencies when the optical penetration depth of the absorbing material is decreased. For example, for Nd:YAG laser excitation at 1064 nm, graphite-based materials have optical penetration depths of 10 to 50 microns, whereas the optical penetration depth of aluminum is 10 nm, and this displaces the center frequency of the generated ultrasound from 2.1 to 12 MHz [173].

2. Photoacoustic Calorimetry Pathway to the Photoacoustic Waves Generation

Photoacoustic calorimetry (PAC) is based on the detection of the pressure wave produced by thermal or volume changes occurring after light absorption [174]. Photoacoustic calorimetry allows measuring the magnitude of non-radiative processes following the absorption of radiation. As an analytical technique, it allows the determination of quantum yields of formation

of the triplet state in molecules and organic polymers and in the study of kinetics and energetics of electron transfer reactions [175] among other processes [176].

The thermal induced pressure wave originates either from nonradiative decay of excited states or enthalpy change in photoinitiated reactions. Additionally, structural volume changes due to movements of the photoexcited molecules and/or the surrounding solvent or reaction volume changes, also contribute to the PAC signal. The transient pressure change can be written as [176, 177]

$$\Delta P = -\frac{1}{\kappa_T} \left(\frac{\Delta V}{V} \right)_T = -\frac{1}{\kappa_T} \left(\frac{\Delta V_{th} + \Delta V_e}{V} \right)_T \quad (6.2)$$

where ΔP is the pressure change, V the illuminated volume, and κ_T the isothermal compressibility. The signal produced in a pressure transducer should be linearly dependent on the amount of absorbed photons, n_{abs} :

$$n_{abs} = \frac{N_{ph}}{N_A} (1 - 10^{-A}) \quad (6.3)$$

where A is the absorbance of the solution at the excitation wavelength λ , N_A Avogadro's constant, and N_{ph} the number of incident photons. The total signal is given by

$$H^S = k_I n_{abs}^S \left(\phi \frac{\alpha}{c_P \rho} E_\lambda + \Delta V_e \right) = k_I n_{as} \left(\phi \frac{\Gamma}{c_a^2 \rho} E_\lambda + \Delta V_e \right) \quad (6.4)$$

where $E_\lambda = N_A h c / \lambda$ is the energy of 1 mol of photons of wavelength λ (= 1 Einstein), $\phi = \Delta H_{th} / E_\lambda$ is the fraction of the absorbed energy, E_λ , released as heat, Q , ΔV_e is the structural volume change per absorbed Einstein, and α the cubic thermal expansion coefficient of the solution.

In order to obtain α and ΔV_e , the instrumental constant (k_I) must be determined by comparing the signal of the sample with that of calorimetric reference. As described previously, a calorimetric reference represents a molecule which releases all the absorbed energy as heat, in a time shorter than the instrumental response. Photocalorimetric reference compounds are molecules which are non-fluorescent, show no transients with a lifetime longer than the laser pulse duration, are photochemically stable, and are 100% efficient in delivering the absorbed energy to the medium as heat, when the excited molecules return to their ground state. Several reference compounds have been identified for aqueous solutions and for organic solvents. In a photoacoustic calorimetry experiment, these molecules and the sample solutions should be measured under identical experimental conditions (solvent, temperature, excitation wavelength, and geometry).

With high temporal resolution, the signal for the calorimetric reference is given by

$$H^r = kn_{abs}^R \frac{\beta}{c_p \rho} E_\lambda \quad (6.5)$$

The determination of the heat decay can be obtained from the ratio of equation 6.4 and 6.5, using the amplitudes of the photoacoustic waves. For transient species with lifetimes within the transducer integration time, kinetic information is obtained by considering that the photoinduced acoustic wave generated by a given sample, $E_s(t)$, is the result of the convolution between the heat function $H(t)$, describing the kinetics of the photochemical processes in the sample, and the instrument response given by a calorimetric reference wave, $T(t)$. Numerical reconvolution is used to retrieve kinetic and enthalpic parameters.

2.1 Photoacoustic Calorimetry Cells

In a typical experiment, time-resolved photoacoustic calorimetry monitors the pressure changes induced in a liquid sample after excitation with pulsed laser. Fast piezoelectric transducers monitor the time evolution of the pressure pulse. In a right-angle arrangement the transducer is located in a plane parallel to the direction of the laser beam [178]. In front-face geometry, a dichroic mirror is placed between the sample solution and the transducer to avoid signals generated by direct absorption of the incident light by the transducer's surface. Only this geometry can be conveniently used for solid samples [179].

2.2 Photoacoustic Calorimetry with Solid Samples

Dyes in thin polymer films may have diverse potential technological uses, such as the development of molecular electronics, electrochromic windows, molecular based solar cells and a wide variety of sensors [180-182]. In view of these applications, the dynamical processes of the excited states of dyes adsorbed in solid polymer matrixes are an important subject of contemporary research.

Current photothermal methods with high time-resolution are suitable for studies of liquid samples. Such methods are, in principle, applicable also to optically transparent solid samples [178, 179]. The application of photoacoustic calorimetry to films using the front-face geometry provided new insights into the dynamical processes in excited states of dyes adsorbed to titanium dioxide (TiO₂) nanoparticles relevant for dye-sensitized solar cells [179].

The photoacoustic studies can be complemented with laser flash photolysis experiments on the solid films, in order to directly access the kinetics of the processes under study. Figure 6.1 shows the transient-transient absorption of CuTMeOHPP (Copper tetra-methoxy-tetraphenylporphyrin) and Mn-TPP (Mn^{III}5,10,15,20-tetraphenylporphyrinate) in cellulose acetate polymer matrix, in the nanosecond time range [183]. It is clear that no transient is seen with this time

resolution for the Mn-TPP sample. The CuTMeOHPP sample presents a depletion band at 420 nm and two wide bands for lower and higher wavelengths. By analogy with other porphyrins the observed transient is assigned to CuTMeOHPP triplet state [179].

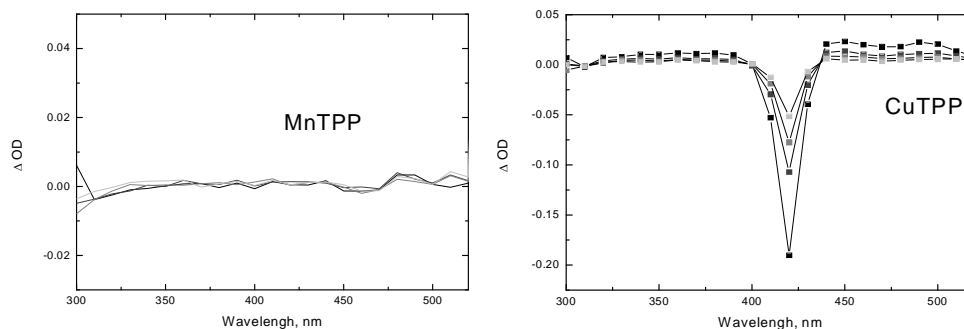


Fig. 6.1 - Nanosecond laser flash photolysis for: **left**) Mn-TPP film in cellulose acetate; **right**) CuTMeOHPP film in cellulose acetate.

The decay could be adjusted by a mono exponential, yielding a triplet lifetime of 90 ns (figure 6.2 left). The photoacoustic signals obtained for Mn-TPP and CuTMeOHPP in cellulose acetate are shown in figure 6.2 right. The signal obtained for CuTMeOHPP is lower in intensity and dephased from the signal obtained with Mn-TPP. The flash photolysis data indicates that under these circumstances, Mn-TPP behaves as a calorimetric reference. Under this assumption, we analyzed the obtained data, fitting the CuTMeOHPP photoacoustic signal with two sequential exponential decays [183]. The first decay yielded lifetime faster than the time resolution of the detector, and it was assumed as prompt heat released upon thermal deactivation of the excited singlet state formed after laser excitation. A second exponential decay characterized by a lifetime of 98 ns was obtained. Based on the flash photolysis experiment, this decay relates to the triplet state deactivation. A triplet quantum yield of 0.82 was obtained for CuTMeOHPP (considering that the fluorescence quantum yield is negligible and the triplet energy of 164 kJ mol⁻¹ [183]).

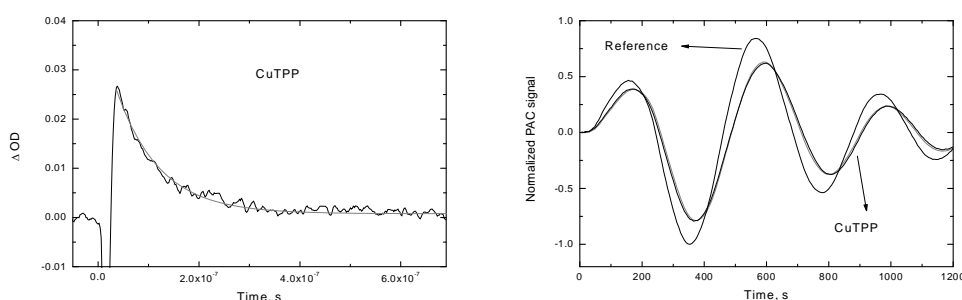


Fig. 6.2 - **Left**) transient absorption decay for CuTMeOHPP in cellulose acetate (450 nm). **Right**) PAC signals for CuTMeOHPP in cellulose acetate, with Mn-TPP in cellulose acetate as reference.

The results show that photoacoustic methods can be used not only to unravel the kinetics and thermochemistry of the nonradiative processes associated with the photoexcitation of sensitizer dyes dissolved in liquid solutions, but also adsorbed in solids matrixes. It also shows that

intense photoacoustic waves are produced when thin films of dye-polymer composites are irradiated by nanosecond laser pulses [183].

3. Laser System Suitable for PA Waves Generation

The scope of this thesis is to describe a laser-based photoacoustic waves system to permeabilize biological barriers. The laser is critical factor to determine portability, safety, cost and handling of the system. The condition $\mu_a c_a \tau_L \gg 1$ directs the choice of lasers to pulsed lasers with $\tau_L < 10$ ns, such as Q-switched ND:YAG lasers. The Q-switch technology allows the generation of high pulse powers and nanosecond pulse durations. The energy losses, quality factor Q of the laser resonant cavity is best defined as the ratio of energy stored in the resonant cavity to the energy loss per cycle: the higher the Q, the lower the energy loss. The generation of a Q-switched pulse can be termed as follows: (1) primarily, the resonator losses are kept at a high level causing the non-action of stimulated emission. Flashlamp continuously raises energy gain in the laser medium (accumulation) inducing an elevation in the energy levels of population inversion by several orders of magnitude. (2) Secondly, the losses are suddenly reduced to minimal values, so that an increase in the power of laser radiation forms in the resonator. (3) When the cavity power reaches the saturation energy of the gain medium, the laser medium reaches saturation. Consequently, the peak of laser pulse results from the energy equalizes between the gain and resonator losses.

The pulse duration of a nanosecond Q-switch ND:YAG laser corresponds to the back and forth trip of the radiation in the resonator, and its energy can range some milijoules (mJ) to a few hundreds joules (figure 6.3).

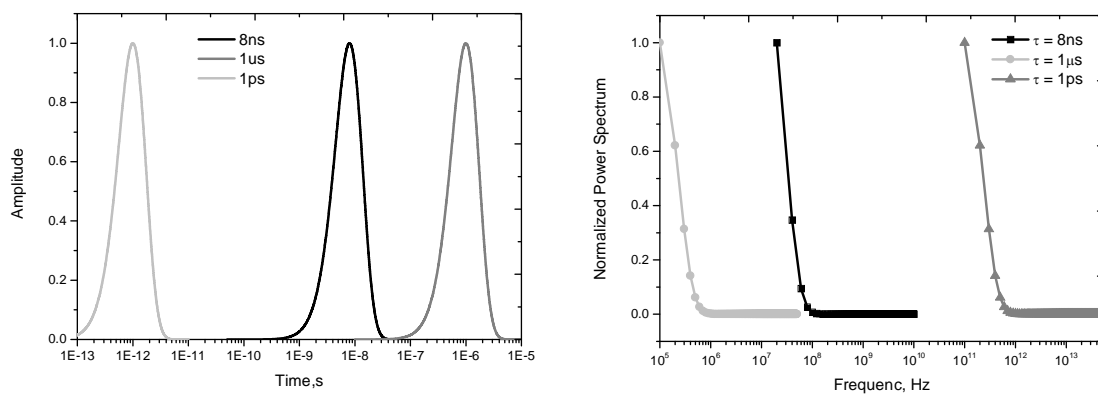


Fig. 6.3 - Simulated laser pulses of 1 μs, 8 ns and 1 ps time width (left) and respective bandwidths (right).

An 8 ns laser pulse bandwidths obtained by fast-Fourier transform (FFT) gives frequencies extending to ca. 100 MHz.

4. Construction of the Piezophotonic Materials

The development of materials, capable of rapidly and efficiently converting the energy in a laser pulse into high frequency broadband ultrasound using the photoacoustic effect, has been eluded by lack of fundamental understanding of the processes involved and by the inability to develop adequate chromophores and substrates. The nature of the converter was almost always a self-standing thin metallic film, or a metal evaporated into a transparent support [144]. Further evolution considered the use of metallic films evaporated onto the tip of optical fibers [164]. Only in the last decade alternative materials (mainly carbon-polymer composites) were described [163] and the importance of the thermoelastic properties and thickness [184] of the materials was revealed.

Doukas and co-workers [144] explored the principles of transdermal and intracellular drug delivery with pressure waves generated by laser pulses. They showed the critical relevance of generating a pressure transient with high peak pressure and high impulse (defined as the rate of pressure increase per unit of time). Their light-to-pressure transducers were 0.8 mm or 3 mm thick metal sheets or commercial plastics, respectively. The low energy-conversion efficiency of such commodities required laser pulses up to 10 J to permeabilize the biological barriers. With such high laser energies it is possible to produce ablation and consequently, intense pressure waves.

Achieving the same result with lower energies requires materials with design properties. Such materials did not exist previously to this work [184]. The fundamental physical characteristics of piezophotonic materials (*piezo* – mechanical stress/pressure, *photonic* – light) are recognizable in their name. The chemical properties of the piezophotonic materials ultimately determine their energy-conversion efficiency and the nature of the photoacoustic waves [184].

The relation between the radiationless process of the dye, the Grüneisen coefficient of the medium and the thickness of the converter were described by Arnaut et al [170]. Biaggi made use of the reciprocal dependence on thickness of the converter to improve conversion efficiencies of ultrasound generation [163]. However, it is necessary to use equation (6.2) in order to combine the properties that maximize the efficiency of light-to-pressure conversion. Table 6-1 summarizes the thermal and acoustic properties of polymeric and nanostructured candidates for the piezophotonic materials [185].

Table 6-1 – Thermal and acoustic properties for the piezophotonic materials substrates. PDMS stands for polydimethylsiloxane, PMMA for polymethylmethacrylate and PS for polystyrene. * Not applicable.

Substrates	Thermal conductivity W/(m*K)	Thermal expansion coefficient 10^{-6} K^{-1}	Specific heat capacity J/(g*K)	Acoustic impedances MRayl	Acoustic velocity m/s	Grüneisen coefficient
Air	0.025	*	1.00	$0.42 \cdot 10^{-3}$	340	*
Water	0.6	214	4.18	1.48	1480	7.6
Glass	1.1	5.9	0.84	12.1	5500	3.9
PDMS elastomer	0.17	$7e-4$	1.46	1.90	1100	1.5
PMMA	[0.17; 0.19]	7	1.48	3.23	2740	1.3
PS	0.12	6.6	2	2.42	2400	0.7
TiO ₂	11.7	9.20	0.69	[5.3; 7.2]	4140	5.5

This table reflects on the thermal and acoustic parameters which maximized the light-to-acoustic conversion – Grüneisen coefficient. The high acoustic impedance of PMMA undermines its utilization as a substrate in the piezophotonic materials construction, despite exhibiting an elevated Grüneisen coefficient. Consequently, a PDMS elastomer (Sylgard® 184), PS and TiO₂ will be used in the development of the light converters due to a high Grüneisen coefficient.

4.1 Photoacoustic References

Dyes for piezophotonic materials must have very high intersystem crossing rates, such as ultrafast nonadiabatic photoinduced intramolecular proton or hydrogen-atom transfers (e.g. ortho-hydroxybenzophenone), ultrafast metal-to-ligand and/or ligand-to-metal charge-transfer relaxation processes (e.g., the paramagnetic tetraphenylporphyrin complex, Mn-TPPCl), charge-transfer bands associated with ultrafast charge recombination (e.g., intervalence charge transfer bands), isomerizations returning to the ground state through conical intersections (e.g., β -carotene). This characteristics can also be found in non-toxic dyes used in food technology [186] (e.g., allura red, amaranth, brilliant black G, new coccine,) or near-infrared absorbing dyes known as molecular heaters that block laser light [187] (e.g., EPOLIGHT™). Following the incorporating large quantities of such dyes in polymers, thin films of piezophotonic materials can be produced by different physical techniques, such as (1) spin-coating gives films with thicknesses between a few tens of nanometers (nm) and 10 micrometers (μm) and (2) casting techniques with highly controlled thicknesses in the micrometer range. The most promising dyes for light-to-sound conversion should have a strong absorption at the wavelength of the laser pulse in a reduced thickness of a specific material ($\mu_a \leq 500 \text{ cm}^{-1}$) and a total conversion of the absorbed energy into heat during the laser pulse duration ($\leq 8 \text{ ns}$).

4.1.1 Porphyrins as Photocalorimetric References

Some classes of porphyrins meet the criteria for an effective photoacoustic waves generator, such as specific paramagnetic metal-porphyrin complexes [188]. These compounds exhibit different physico-chemical properties due to electronic transitions, after the absorption of light, in the visible spectrum of electromagnetic radiation.

4.1.1.1 UV-Visible Absorption Spectroscopy

The characteristic UV-visible spectrum of a porphyrin has a strong absorption band with a high molar absorptivity coefficient between 400-450 nm, followed by 4 bands of lower intensity around 500-650 nm (only valid for free base porphyrins). The electronic interpretation of these physical features was rationalized by Gouterman [188], in a simplified model of 4 orbitals. Gouterman theory states that absorption spectrum of the porphyrins relates to the electronic transitions between the energy levels of the 2 highest molecular orbitals occupied orbitals energy (HOMO), and the 2 lower energy unoccupied molecular orbitals (LUMO).

The free base porphyrins present a molecular symmetry of D_{2h} with its HOMO molecular orbitals being denominated a_u e b_b . For the case of metaloporphyrins (metal in the center of the porphyrin ring), the correspondent symmetry is D_{4h} with the HOMO orbitals being a_{1u} and a_{2u} . The LUMO orbitals are identified as e_{gx}^* and e_{gy}^* and b_{2g} and b_{3g} with respect of D_{4h} and D_{2h} . The a_u and b_{1u} HOMO orbitals pair and the b_{2g} and b_{3g} LUMO orbitals pair present very similar energy levels, so that they are considered degenerate. As a result, the transition $a_u \rightarrow b_{2g}$ and $b_{1u} \rightarrow b_{3g}$ shows a transition energy similar to that of $b_{1u} \rightarrow b_{2g}$ and $a_u \rightarrow b_{3g}$, and leads to a transition pair of low energy and intensity (Q_x, Q_y) and a (B_x, B_y) of high energy and intensity. Consequently, the absorption spectrum reveals a very intense band around 400 nm, known as Soret band (B_x, B_y – overlapping bands so just one appears in a absorption spectrum). The substitution of the 2 central hydrogen atoms from the macrocycle by a metallic ion changes the molecule symmetry to D_{4h} , with energy degeneration of the orbitals b_{2g} and b_{3g} (henceforth called e_g), which results in just one Q band [188]. The metaloporphyrins UV-visible spectrums can be classified according to the interaction between the metal and the π system of the tetrapyrrolic macrocycle. The metals which present a complete or empty valence layer (d^0 or d^{10}) do not interact extensively with π system, which results in little difference between the metal and free base porphyrin UV spectrum (except for the Q bands). The Zn(II)TPP is an example of this regular porphyrins because the Zn^{2+} ion has a d orbital complete (d^{10}). Otherwise, an extensive interaction between the π system and the metal is expected for d^n orbitals, $1 \leq n \leq 9$. In this case, there are two main effects for different metals: (1) a retro-donation of electrons from the d_{xy} and d_{yz} metal orbitals to the unoccupied π^* orbitals of the

macrocycle (spectrum deviated to the blue), and (2) charge transfer from the metal p orbitals to the unoccupied π^* orbitals of the porphyrin (d^6 - d^9 metals like Fe^{3+} , Mn^{3+} and Cr^{3+}) or from the π electrons of the porphyrin to the d orbital of the metal (Sn^{2+} and Pb^{2+}). For the complexes metal-porphyrins with Fe^{2+} , Co^{2+} , Ni^{2+} , Pd^{2+} and Cu^{2+} , as a central atom, it is also observed additional bands [188]. Figure 6.1 shows absorption spectra of manganese porphyrin in different support substrates.

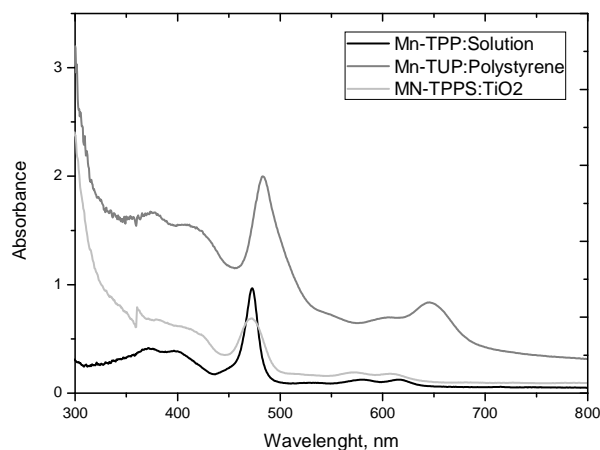


Fig. 6.4 – Absorption spectrums of MnTPP dissolved in toluene $\epsilon_{480\text{ nm}} \geq 10^5\text{ M}^{-1}\text{ cm}^{-1}$), Mn-TUP dispersed in polystyrene and Mn-TPPS adsorbed in TiO_2 .

4.1.1.2 Fluorescence Spectroscopy

The absorption of light by a porphyrin is a dynamic process where the intrinsic nature of the molecule will determine the exact pathway for the energy dissipation. The main processes involved in the deactivation of the excited states of an isolated molecule are the radiative and radiationless processes. The absorption of radiation by a molecule occurs “instantaneously” ($\leq 10^{-15}$ seconds) to the various electronic excited states and their vibrational levels, without the possibility of rearrangement of the nucleus positions (Franck-Condon principle) [189]. Immediately after follows the deactivation pathway from the high vibrational energy levels to the lowest vibrational level of the first excited electronic state, S_1 , because the energy difference between S_1-S_0 is generally larger than the difference between S_n-S_1 . Thus, in S_1 it is possible that the energy deactivation may follow three competitive pathways, fluorescence, internal conversion and intersystem crossing, which do not occur in deactivations of higher excited electronic states, where the internal conversion is much faster than the other processes. This kinetic competition explains the Kasha rule, which states that luminescence emission of light is independent of the excitation wavelength [189]. The vast majority of porphyrins obey to the Kasha rule and the transition from the lowest vibrational level of the excited state S_1 to the lowest vibrational level of the ground state S_0 leads to a more intense $Q(0,0)$ fluorescence band. The transitions to higher vibrational levels in the ground state originate $Q(0,n)$ bands, with n being the correspondent vibrational level ($n = 1,2,\dots$). Free base porphyrins, e.g. TPP, shows

fluorescence quantum yields with moderate absolute values ($\Phi_F = 0.10 \pm 0.01$ for deaerated solutions in toluene [190]) and fluorescence lifetime, τ_F , around 15 ns [190]. This means that free base porphyrins are not suited candidates for PAC references in the generation of PA waves. However, the introduction of a metal in the porphyrin macrocycle may change the dominant energy deactivation pathway to ultrafast internal conversion process [188]. The paramagnetic metaloporphyrins exhibit d orbital energies intermediate between the ring-centered HOMO and LUMO orbitals of the analogous free-base porphyrins, which offer an alternative path for radiationless deactivation.

The choice of manganese porphyrins for the light-to-acoustic conversion reflects their commercial availability and their ability to behave as photoacoustic references. Figure 6.5 gathers the chemical structure of the manganese porphyrins used throughout this work.

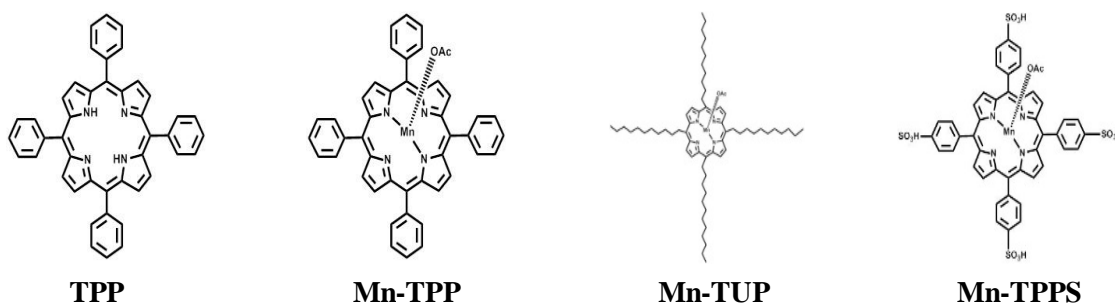


Fig. 6.5 – Chemical structure of the porphyrins used: TPP, *Mn-TPP*, *Mn-TUP* and *Mn-TPPS* are the tetraphenylporphyrinate, Mn^{III} 5,10,15,20-tetraphenylporphyrinate, Mn^{III} 5,10,15,20-tetraundecylporphyrinate and Mn^{III} 5,10,15,20-tetrakis(4-sulphonylphenyl) porphyrinateacetate.

4.1.2 Graphite as Photoacoustic References

Graphite has ultrafast photon-to-phonon conversions followed by cooling in picoseconds. Excitation of carbon (carbon black [191], graphite powder [192], carbon nanotubes [193]) dispersed in polymeric matrices absorb in the UV-visible (figure 6.6) and produce ultrasounds.

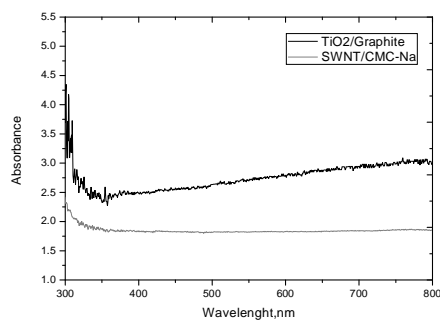


Fig. 6.6 – Absorption spectrum of graphite in a TiO_2 substrate and single wall nanotubes (SWN) dispersed in carboxyl methyl cellulose (Na).

4.1.3 Near Dyes as Photoacoustic References

Sunlight holds 50% of its radiation intensity in the near infrared region ranging from 700 nm to 2000 nm. Near-infrared (NIR) dyes have electronic transitions in this spectral region (figure 6.7). NIR absorbing dyes that can convert infrared radiation into heat, for instance by absorbing 1064 nm light of an Nd:YAG lasers [187], can be useful photoacoustic references in the NIR. The choice of appropriate NIR's for light-to-acoustic conversion is challenging because of the spectral, thermal and photochemical long-term stability requirements [187]. The NIR dye studied in this work was commercially available as an Epolight™ series (chemical structure not available). Epolight™ 1178 can be solubilized with the methodology developed in the production of the piezophotonic materials (good solubilization in toluene – chapter 12 for technical aspects).

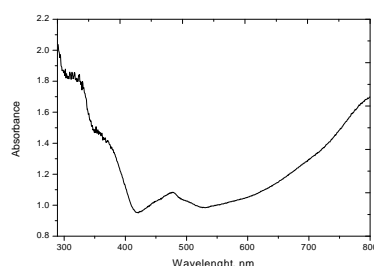


Fig. 6.7 – Absorption spectrum of Epolight™ 1178 in a polystyrene substrate.

4.1.4 Strongly Absorbing PAC References

Photoacoustic calorimetric (PAC) references are characterized to be (1) non-fluorescent molecules with no transients with a lifetime longer than a few nanoseconds, (2) photochemically stable, and (3) have unity efficiency in delivering the absorbed energy to the medium as heat, when the excited molecules return to their ground state. In addition, $\mu_a c_a \tau_L \gg 1$ is more easily met if the dye has a very high absorption coefficient in the visible or NIR. This is the case of dyes used in the food industry, which also have low toxicity. The commercial available Allura Red®, Amaranth®, New Coccine® (NC) and Brilliant Blue G® (BBG) show high water solubility, large absorptions over a broad range of wavelengths ($\geq 10^4 \text{ M}^{-1} \text{ cm}^{-1}$) and ultra-fast radiationless decays, which might classify them among suitable candidates to be incorporated in piezophotonic materials [186].

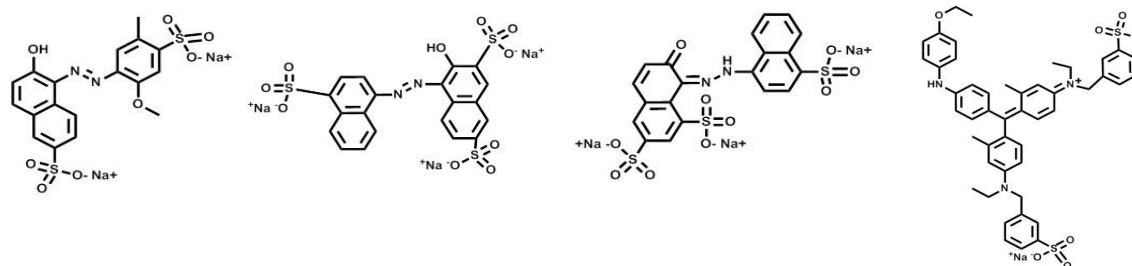


Fig. 6.8 – Chemical structures of the water based photoacoustic references: Allura red®, Amaranth®, New Coccine® and brilliant black G®.

5. Development and Optimization of Piezophotonic Materials

Various materials were tested to characterize their ability to convert light energy into a pressure wave, such a (1) manganese metaloporphyrins in polymer or nano-crystallized titanium dioxide substrates, (2) different types of graphite dispersed in polymer bases, (3) near-infrared dyes and (4) water soluble dyes in polystyrene substrates.

5.1 Metaloporphyrins and Carbon based Thin Films

The experimental arrangement employed in the characterization of piezophotonic materials was inspired in the front-face cell used in photoacoustic calorimetry (PAC) of solid films - figure 6.9 [179].

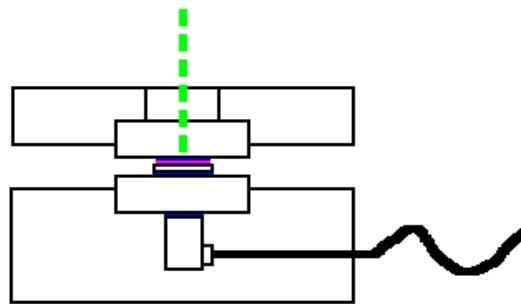


Fig.6.9 - PAC adapted arrangement for the irradiation of the piezophotonic films. The laser pulse first traverses a quartz window and the contact transducer is protected from the laser by a mirror. The film is between the window and the mirror. Good acoustic contact is maintained by adding silicone or ultrasound gel.

Fig. 6.10 shows the photoacoustic waves generated by:

- [A1] - Mn-TUP dissolved in a polystyrene substrate with various thicknesses ([400, 1000] μm);
- [A2] - Mn-TPPS in titanium dioxide (TiO_2) nano-crystalline matrix;
- [A3] - Graphite embedded in TiO_2 thin films with various thicknesses ([50, 100, 200] μm);
- [A4] - Solution of single wall nanotubes dissolved in carboxyl methyl cellulose - sodium, as the counter ion - ([50, 100, 200] μm);
- [A5] - Black polystyrene.

Figure 6.10 depicts the first front of the PA wave and their shape looks similar for all the dyes: a more intense compressive part followed by a lower intensity tensile part.

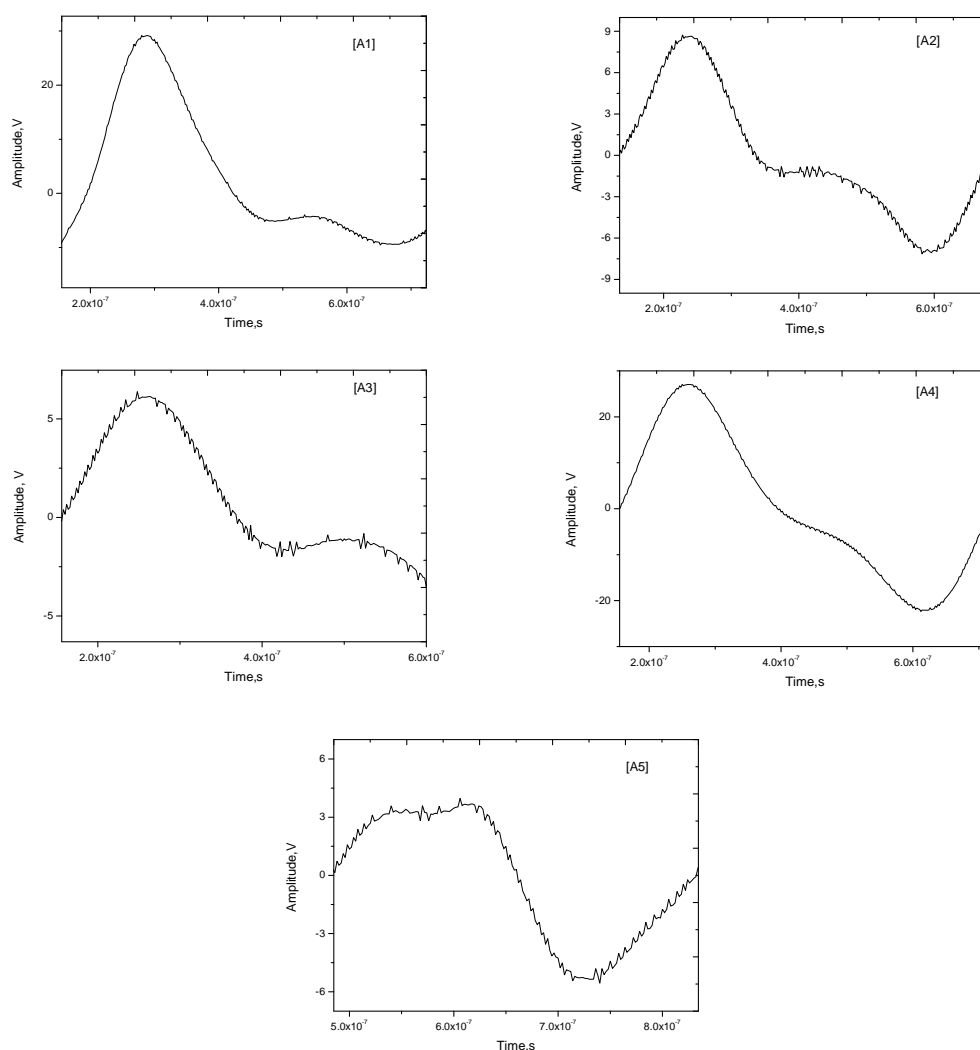


Fig. 6.10 – Representative photoacoustic waves as function of time. PA waves produced by [A1] with 400 μm , [A2, A3] with 50 μm , [A4] with 100 μm and [A5], upon pulsed laser excitation at 532 nm, with 10 mJ/cm^2 and measured by a 225 MHz contact transducer.

Samples [A1] through [A5] were subject to laser pulses of 10 mJ/cm^2 , which lead to the formation of photoacoustic waves with different amplitudes depending of the light-to-acoustic energy of each dye and the thermal properties of the substrate (Grüneisen coefficient). The Mn-TUP solubilized in polystyrene, [A1], as well as, the single wall nanotubes dissolved in a surfactant, [A4], present the highest amplitude of the PA waves. In both cases, different substrates were tested, which resulted in a clear dependence on the material thickness and linear absorption coefficients (table 6-2). The piezophotonic materials of Mn-TUP in polystyrene represent a clear example of the theoretical predictions: reducing the material thickness corresponds to a maximization of the light-to-pressure conversion, generating a more intense photoacoustic signal, for the optical and thermal properties. This rationalization was tested by the direct comparison of the acoustic signal between the piezophotonic materials and the materials used by Doukas et al [144] - [A5]. It is observed an increase of the amplitude of the PA waves by an order of magnitude. According to table 6-1, the manganese piezophotonic materials based on the adsorption to nano-crystalline substrates should present the most intense

pressure waves, also because it attains $\mu_a = 1600 \text{ cm}^{-1}$. However the experimental results show relatively low pressures. The same is true for the [A3] film; although a low concentration of graphite may actually be linked to titanium nanocrystals. In both cases, the low pressures obtained with TiO_2 substrates may be related to the generation of photoacoustic waves in nanostructures with challenging acoustic coupling.

Table 6-2 – Piezophotonic films characteristics and PA waves amplitude generated upon laser excitation. $I_{\text{Abs}}/I_0 = (1-10^{-\text{Abs}})$: I_{Abs} represents the fraction of incident light absorbed; I_0 represents the energy of incident light. * Not applicable.

PAC Reference	Substrate	Thickness μm	λ_{ex} nm	Abs	$\mu_a \text{ cm}^{-1}$	Amplitude mV	Amplitude / (I_{Abs}/I_0)
Mn-TUP	Polystyrene	400	532	0.48	12	29.09	43.49
	Polystyrene	400	532	0.42	10.5	23.04	37.17
	Polystyrene	1000	532	1.10	11	17.38	18.88
Mn-TPPS	TiO_2	1	532	0.16	1600	8.60	27.91
	TiO_2	50	532	0.27	54	4.45	9.61
Graphite	TiO_2	100	532	1.73	173	2.06	2.10
	TiO_2	200	532	2.70	135	3.09	3.10
	CMC-Na	50	532	0.12	24	6.1	25.27
SWNT	CMC-Na	100	532	0.83	83	27.02	31.71
	CMC-Na	200	532	1.81	90.5	13.32	13.53
	Black	Polystyrene	634	532	5	*	2.30

5.2 Metaloporphyrins and Activated Carbon based Thin Films

Fig. 6.11 collects experiments where the photoacoustic waves were generated by:

[B1] - Mn-TUP dissolved in a polystyrene substrate with a 200 μm of thickness;

[B2], [B3] - Activated carbon dispersed in epoxy glue.

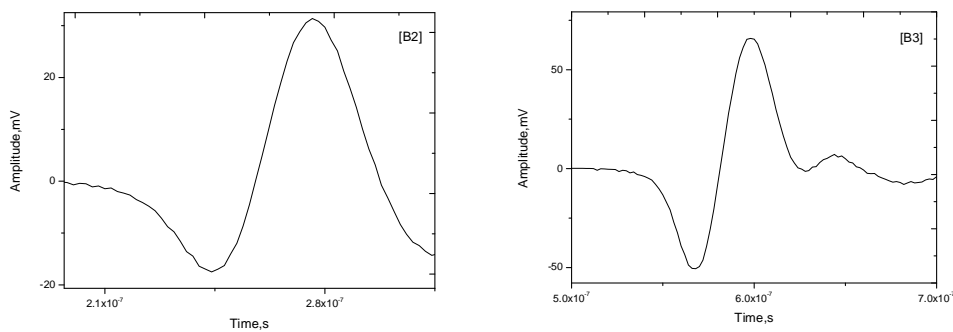


Fig. 6.11 – Representative photoacoustic waves as function of time. PA wave produced by [B2, B3] upon pulsed laser excitation at 505 nm, with laser energy of 76 mJ/cm^2 and measured by a 10 MHz contact transducer.

The use of carbon derivatives in the generation of acoustic transients with high amplitudes relied in the production of films [B2] and [B3], which touches upon a current controversy: carbon solubilization [193]. In these experiments, we could absorb solid particles dispersed in the film. It was not possible to determine a specific material thickness, and the linear absorption coefficients remain to be maximized (table 6-3). Nevertheless, the PA waves generated by these piezophotonic films have amplitudes comparable to those of Mn-TUP based films (30% more intense).

Table 6-3 – Piezophotonic films characteristics and PA waves amplitude generated upon laser excitation. $I_{\text{Abs}}/I_0 = (1-10^{-\text{Abs}})$: I_{Abs} represents the fraction of incident light absorbed; I_0 represents the energy of incident light. * Not applicable.

PAC Reference	Substrate	Thickness μm	λ_{ex} nm	Abs	μ_a cm^{-1}	Amplitude mV	Amplitude/ I_{abs}
Mn-TUP	Polystyrene	200	505	1.22	61	79.9	85.02
Activated	Epoxy Glue	*	505	5	*	60.7	*
Carbon	Epoxy Glue	*	505	5	*	29.6	*

5.3 Metaloporphyrins and Near-Infrared based Thin Films

Fig. 6.12 presents photoacoustic waves generated with a nanosecond ND:YAG laser upon excitation at 1064 nm.

[C1] – NIR dye (Epolight® 1178) dissolved in a 1:1 polystyrene substrate with a 200 μm of thickness;

[A5] - Black polystyrene.

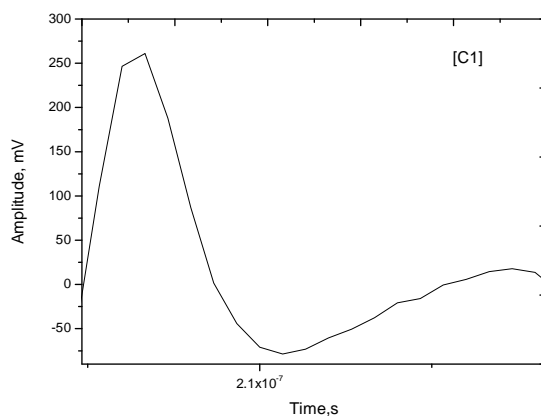


Fig. 6.12 – Representative photoacoustic waves as function of time. PA wave produced by [C1] with a thickness of 200 μm upon pulsed laser excitation at 1064 nm, with laser energy of 50 mJ/cm^2 and measured by a 15 MHz contact transducer.

Table 6-4 – Piezophotonic films characteristics and PA waves amplitude generated upon laser excitation at 1064 nm.

PAC Reference	Substrate	Thickness μm	λ_{ex} nm	Abs	μ_a cm^{-1}	Amplitude mV	Amplitude/ I_{abs}
Epilight 1178	Polystyrene	200	1064	*	*	261	*
Black	Polystyrene	634	1064	*	*	108	*

At this time, instrumental limitations to measure the absorbance at 1064 nm do not allow for a quantitative interpretation of this interesting observation.

5.4 Metalloporphyrins and NIR based Thin Films in Polystyrene and TiO_2

Fig. 6.13 collects a set of photoacoustic waves generated with laser light of 478 nm and laser energy of 31 mJ/cm^2 (at the maximum of the metalloporphyrins absorption spectra):

[D1, D2, D3, D4] – Diluted Mn-TPP solutions in 3:4, 1:2 and 1:4 polystyrene substrate with thicknesses of [37, 27, 25, 29] μm , respectively;

[D5] - Mn-TPPS linked to a nanocrystalline TiO_2 ;

[D6] - Mn-TUP dispersed in a polydimethylsiloxane matrix (PDMS) with a thickness inferior to 100 μm ;

[D7] – NIR dye (Epilight® 1178) dissolved in a 1:1 polystyrene substrate with a thickness of 33 μm .

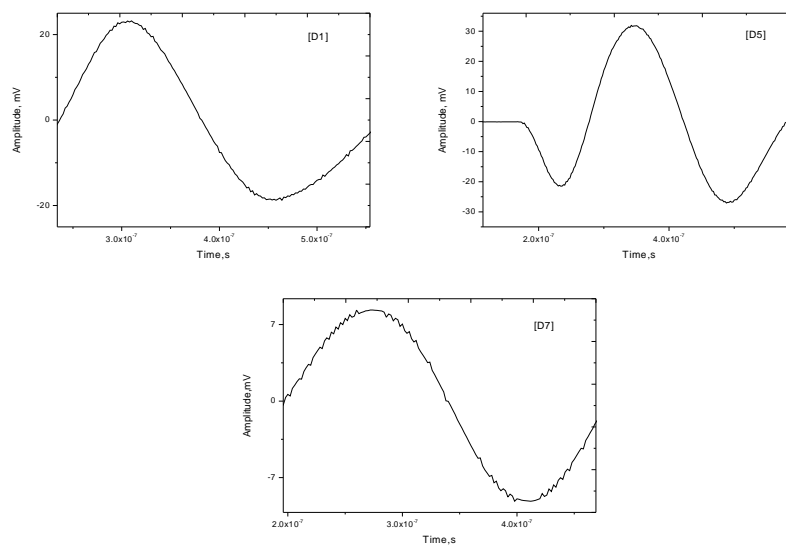


Fig. 6.13 – Representative photoacoustic waves as function of time. PA wave produced by [D1] with a 37 μm of thickness, [D5] with a thickness of 5 μm , [D7] with a thickness of 33 μm upon pulsed laser excitation at 478 nm, with laser energy of 31 mJ/cm^2 and measured by a 15 MHz contact transducer.

Samples [D1] through [D7] were subject to laser pulses of 31 mJ/cm^2 , which lead to the formation of photoacoustic waves with different amplitudes. We investigated the role of a long alkyl Mn-TPP derivative porphyrin (Mn-TUP) in the light-to-acoustic conversion comparing the intensity of the waves with those generated by Mn-TPP. The results shown in table 6-5 allow us to conclude that both dyes generate intense PA waves. This series of thin films exhibits a dependence on the μ_a , as the lower absorbance film has the lower PA waves amplitude.

For irradiation in the visible spectrum, the near-infrared dyes are not suited due to the reduced linear absorption coefficient (low absorbance). If compared to the results of films [A2, A4], we observed a dramatic increase in the PA waves intensity for the [D5] film, mainly due to better control of the dye deposition adsorption to nanocrystalline TiO_2 [179].

Table 6-5 – Piezophotonic films characteristics and PA waves amplitude generated upon laser excitation. $I_{\text{Abs}}/I_0 = (1-10^{-\text{Abs}})$: I_{Abs} represents the fraction of incident light absorbed; I_0 represents the energy of incident light. * Not applicable.

PAC Reference	Substrate	Thickness μm	λ_{ex} nm	Abs	$\mu_a \text{ cm}^{-1}$	Amplitude mV	Amplitude/ I_{Abs}
Mn-TPP	Polystyrene	37	478	5	1351	23.2	23.20
		27	478	3.9	1444	24	24.00
		25	478	4.5	1800	19.2	19.20
		29	478	3.1	1068	10.1	10.11
Epolight 1178	Polystyrene	33	478	1.1	333	6.9	7.50
Mn-TUP	PDMS	< 100	478	3.9	< 800	10.6	10.60
Mn-TPPS	TiO_2	< 5	478	0.5	1000	31	45.34

The photoacoustic wave produced by a Mn-TUP in a silicone substrate (PDMS) will only deposit the produced heat as a very fast transient, if the μ_a is maximized above 1100 cm^{-1} . That was not the case for [D6], despite high absorbance in the visible spectrum. The solubilization of Mn-TUP/silicone mixture limits the final outcome (figure 6.14).

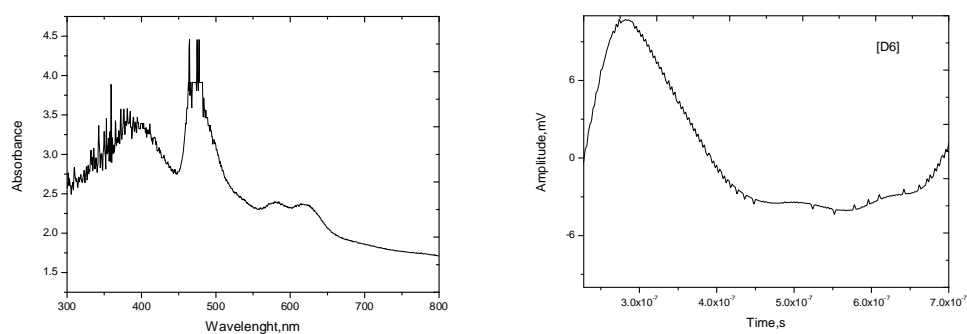


Fig. 6.14 – **Left**) Absorption spectrum of Mn-TUP dissolved in Sylgard® - silicone elastomer. **Right**) Photoacoustic wave generated [D6] film upon laser excitation at 478 nm with 31 mJ/cm^2 .

5.5 Metaloporphyrin based Thin Films *versus* Thick Black Polystyrene

Figure 6.15 compares the photoacoustic waves generated by the best piezophotonic materials developed so far, against the materials used by Doukas et al [144]:

[A1] - Mn-TUP dissolved in a polystyrene substrate with 400 μm of thickness;

[A5] - Black polystyrene;

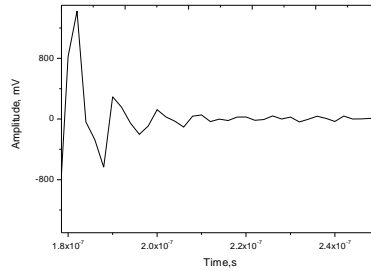


Fig. 6.15 - Representative photoacoustic waves as function of time. PA wave produced by [A1] upon pulsed laser excitation at 355 nm, with laser energy of 10 mJ/cm², and measured by a 225 MHz contact transducer.

The set of experiments collected in table 6-6 for different contact transducers shows that the Mn-TUP piezophotonic materials are capable of producing higher acoustic transients than the transients of Doukas materials, even for low linear absorption coefficients, μ_a . Interestingly, the Pa waves amplitude measured with 2.25 and 15 MHz transducers are only different by a factor of 2-3, when we compare Mn-TUP with the commercial black polystyrene, but that difference reaches one order of magnitude when we compare the amplitudes measured with a 225 MHz transducer. The difference reveals that the piezophotonic material generates PA waves with very high frequency components.

Table 6-6 – Piezophotonic films characteristics and PA waves amplitude generated upon laser excitation at 532 nm. $I_{\text{Abs}}/I_0 = (1-10^{-\text{Abs}})$: I_{Abs} represents the fraction of incident light absorbed; I_0 represents the energy of incident light. * Not applicable.

PAC Reference	Substrate	Thickness μm	Transducer MHz	Abs	μ_a cm^{-1}	Amplitude mV	Amplitude/ I_{Abs}
Mn-TUP	Polystyrene	400	2.25			1146	1446
			15	0.48	12	227	339
			225			29.09	43.49
	Polystyrene	400	2.25			1456	2349
			15	0.42	10.5	242	390
			225			23.04	37.17
Black	Polystyrene	634	2.25			607	
Black	Polystyrene	634	15	5	*	270	*
			225			2.30	

5.6 Bandwidths of the Piezophotonic Films based upon Metaloporphyrins

The thickness minimization of the piezophotonic materials reveals major increases in the PA waves amplitude (up to 5 times the black polystyrene material). In figure 6.16, we compare the bandwidths generated between those types of films:

[F1, F2, F3, F4] - Mn-TUP dissolved in a polystyrene substrate with various thicknesses ([38, 11, 19, 17] μm);

[A5] - black polystyrene.

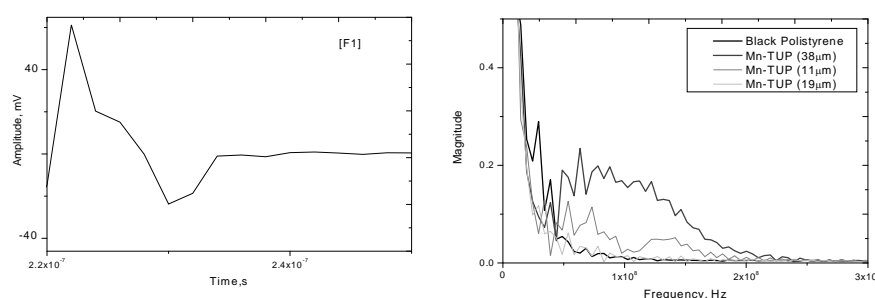


Fig. 6.16 – Left) Representative photoacoustic waves as function of time. PA wave produced by [F1] upon pulsed laser excitation at 484 nm, with laser energy of 50 mJ/cm^2 and measured by a 225 MHz contact transducer. Right) Respective bandwidth analysis of [F1, F2, F3] films.

The [F1, F2, F3, F4, A5] piezophotonic samples were subject to laser pulses of 50 mJ/cm^2 (table 6-7), which lead to the formation of photoacoustic waves correlated with the μ_a and thickness. This result confirms the theoretical prediction and the adequacy of Mn-TUP in the making of piezophotonic materials. Very high acoustic transients are obtained upon reducing the material thickness ($< 50 \mu\text{m}$) and very high concentrations of the PAC references are incorporated in those thin layers ($\mu_a > 500 \text{cm}^{-1}$).

Table 6-7 – Piezophotonic films characteristics and PA waves amplitude generated upon laser excitation. $I_{\text{Abs}}/I_0 = (1 - 10^{-\text{Abs}})$: I_{Abs} represents the fraction of incident light absorbed; I_0 represents the energy of incident light. * Not applicable.

PAC Reference	Substrate	Thickness μm	λ_{ex} nm	Abs	μ_a cm^{-1}	Amplitude mV	Amplitude/ I_{abs}
Mn-TUP	Polystyrene	38	484	2.45	644	53	53.19
		11	484	1.42	1291	40	41.60
		19	484	1.39	732	35	36.49
		17	484	2.18	1282	45	45.30
Black	Polystyrene	634	484	5	*	2.3	*

5.7 Water Based Piezophotonic Films

In the literature it has been claimed that some dyestuffs can be used as water-soluble PAC references: allura red [G1], amaranth [G2], new coccine [G3] and brilliant blue G [G4] [186]. We tested those dyestuffs using a 20 MHz needle hydrophone to obtain an absolute value for the pressure generated. The use of needle hydrophones is technically more challenging than contact transducers because they have to use water as the coupling medium and are very sensitive to the relative position of the hydrophone (subsequently, the laser beam as well). The differences between the dyestuffs in figure 6.17 may be related to the difficulties in keeping the experimental setup in the same geometry.

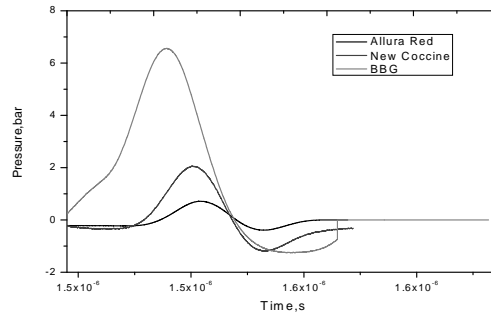


Fig. 6.17 - Measured photoacoustic waves as function of time. Normalized and representative PA waves produced by [G1, G3, G4] upon pulsed laser excitation at 532 nm, with laser energy of 50 mJ/cm² and measured by a 20 MHz needle hydrophone.

On the other hand, needle hydrophone gives the absolute peak pressure of the water-soluble dyes gives. The incurrent pressure observed was 6 bar for BBG, which implies an impulse of 0.6 bar/ns (table 6-8). This result lies in the limit of an effective permeabilization of biological barriers presented by Doukas: 1 to 50 bar/ns. The production of piezophotonic films with New Coccine and brilliant blue G was difficult to reproduce due to difficulties in the solubilization process (appearance of granules), and Amaranth was not possible to incorporate in the polystyrene substrates. Additionally, there is a degradation of the dyes after a few impinged laser shots into the piezophotonic films, accompanied by cracks in the surface of the films.

Table 6-8 – Piezophotonic films characteristics and PA waves amplitude generated upon laser excitation.

PAC Reference	Substrate	Thickness μm	λ_{ex} nm	Abs	μ_a cm ⁻¹	PP bar
Allura Red	Polystyrene	193	532	0.581	30.10	3.57±1.46
	Polystyrene	76	532	0.230	30.26	4.77±1.77
	Polystyrene	37	532	0.228	61.62	4.83±0.83
Amaranth	Polystyrene	260	532	1.527	58.73	4.40±0.46
	Polystyrene	74	532	0.619	83.65	5.37±0.51
NC	Polystyrene	55	532	0.433	78.72	2.47±1.38
	Polystyrene	219	532	0.910	41.55	2.57±0.35
BBG	Polystyrene	113	532	0.236	20.89	6.70±1.61

6. Summary of the Best Piezophotonic Materials

The development of piezophotonic materials capable of producing intense and very fast acoustic transients based upon the thermoelastic expansion phenomenon is summarized in table 6-9.

Table 6-9 – Summary of the best piezophotonic materials characteristics.

PAC Reference	Substrate	Thickness μm	λ_{ex} nm	Abs	μ_a cm^{-1}
Mn-TPP	Polystyrene	95	532	1.15	120
Mn-TUP		38	484 532	1.4 1.1	370 290
Mn-TPPS	TiO ₂	1.75 – 7.5	472	0.5	2860 - 670
Mn-TPP	Polystyrene	100	532	1.5	150
Mn-TPP		60	532	1.4	230
Mn-TUP		50	355	3.2	640
Mn-TUP		30	355	>1	>330

This table shows the properties of the best piezophotonic materials developed with the manganese porphyrins solubilized in polystyrene or adsorbed in TiO₂ nanoparticles. In the example of figure 6.18, the determination of the peak pressure of the film was achieved with a 20 MHz needle hydrophone, with a 40 mJ/cm² laser fluence, and using a 8 ns pulse at 532 nm. The photoacoustic wave produced a $p_{\text{max}} = 12$ bar. This value represents 8% of the theoretical efficiency (chapter 5), but nevertheless the conversion efficiency is 3 times higher than the highest efficiency reported in the literature [164]. The conversion efficiency could be easily improved increasing the laser power density in view of equation 6.2, but the purpose of this work was to generate PA waves capable of increasing the permeability of the skin with safe laser and ultrasound powers. Thus, we did not attempt to maximize pressures at the expense of high laser powers.

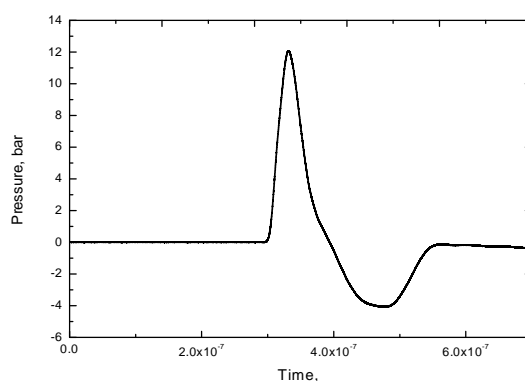
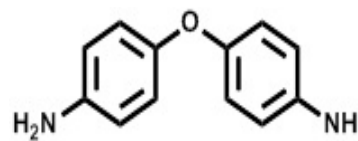


Fig. 6.18 – Representative photoacoustic wave as function of time. The wave was produced by irradiating a polystyrene film containing Mn-TPP, with $\mu_a = 640 \text{ cm}^{-1}$, $\Gamma=0.7$, $c_L= 2400 \text{ m/s}$, laser pulse duration of 8 ns, laser energy density of 32 mJ/cm², optical power density of 4MW/cm².

7. Characterization of Acoustic Waves Generated by Explosive Polymer Films

Ablation and plasma formation are efficient processes to produce acoustic transients, but they usually require high energy densities. However, low ablation threshold polymers have been made with thin triazene films (figure



6.19). Triazene polymers rapidly decompose into gaseous fragments with 355 nm laser pulses, therefore providing

Fig. 6.19 – Chemical structure of aryltriazene.

particle ejection at low laser fluences. An improved synthesis of aryltriazene polymers gives thin (15 to 500 nm thick) polymer films with low ablation thresholds [194], which may be convenient for biological work. This fact relates with the production of the shock waves by photochemical decomposition, at low laser fluencies, rather than by vaporization at high energies, which favours the viability of the cells [133]. When combined with the front-face design of photoacoustic cells [179], triazene films can produce large pressure transients at low energy densities. Ablation is an intrinsically destructive process, and the repetition of the laser pulses will not give reproducible pressure waves, above the ablation threshold. Otherwise, thermal expansion associated with the absorption of a laser pulse by a PAC reference dye can be repeated at high pulse frequencies without appreciable changes in the wave amplitude. Figure 6.20 shows that the switchover from thermoelastic to the ablation regimes for the triazenes molecules occurs at laser fluences lower than 50 mJ/cm². This switchover leads to an increase in the pressure wave amplitude by more than a factor of 5. Saturation of the signal did not allow for the measure of the peak amplitude of the pressure wave in this experiment.

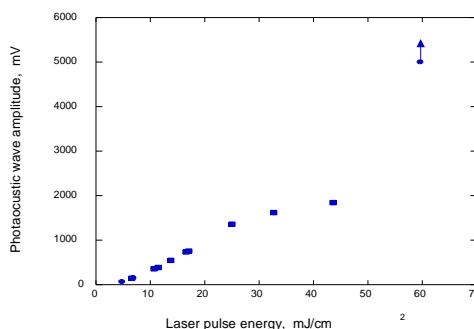


Fig. 6.20 - Pressure wave amplitudes measured with a 15 MHz contact piezoelectric transducer following the excitation of a triazene polymer films with increasing laser fluences (squares) compared with the amplitude measured with another triazene film at a higher energy (circle, only a lower limit for the shock wave amplitude could be measured in this experiment because it exceeded the range of the oscilloscope).

Another set of experiments using additional triazene polymer films with optical densities ca. 1 at the excitation wavelength (355 nm) is presented in figure 6.21. Samples 1 and 7 were subject to laser pulses of increasing laser energies. Both films lead to the formation of pressure waves with intensities increasing linearly until the laser pulse energy reaches ca. 20 mJ/cm². From that

laser intensity the pressure wave amplitude tends to stabilize or drop. The triazene film # 9 was only excited with three laser intensities. Two shots at very low laser intensity and then the laser was set to 50 mJ/cm^2 . With this laser intensity, the pressure wave intensity was extremely high. Good linearity with the laser energy was obtained with the linear part of sample 7. This behaviour was also observed with other samples of triazene polymer films.

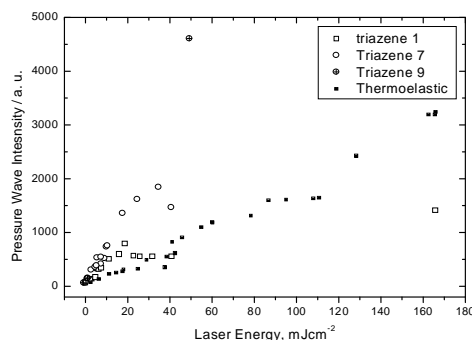


Fig. 6.21 - Thermoelastic generation of an acoustic wave by a thin polymer film containing a photoacoustic reference, compared with the shock wave generated by a thin triazene film.

Figure 6.21 also presents the pressure wave amplitudes obtained with a manganese porphyrin dispersed in a polystyrene film with that originates a thermoelastic pressure wave upon laser irradiation. The pressure wave intensities observed with this film increase linearly with the laser excitation energy. The intensities of photoacoustic waves were further studied with excitation by 30 ps FWHM Nd:YAG laser and detection with a 225 MHz transducer. Fig. 6.22 shows the pressure waves obtained. Considering the differences in amplitude and in laser energy, it is possible to determine that the ablation of the triazene polymer produces a pressure 50 times higher than thermoelastic expansion of photoacoustic reference polymers in photoacoustic cells with the front-face design, for the same incident laser energy (50 mJ/cm^2).

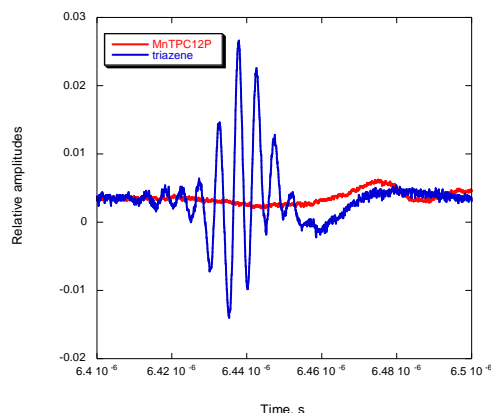


Fig. 6.22 - Same as previous figure but using additional triazene polymer films and a polystyrene film doped with a Mn-TUP (red).

8. Comparison between PA Waves, Ultrasound Waves and Shock Waves

Photoacoustic waves produced by piezophotonic materials are characteristically different from the ones generated by an ultrasound source or from laser-ablated materials. The main differences reside in the intrinsic features responsible for the waveforms typologies: the PA waves show a mostly unipolar compressive wave (positive pressures), while the ultrasound waves (UW) have continuous oscillations between positive and negative pressures [144]. The latter tensile component is accountable for the biological effects of cavitation [195, 196]. The shockwaves have high pressure peaks and rise times determined by the material ablation, while the PA waves show moderate pressure peaks and rise times as short as the laser pulses.

The optical energy deposition determines the initial acoustic wave profile. The acoustic transient generated by thermoelastic expansion within rigid boundaries consists in a compression followed by a rarefaction peak, but the unidirectional compressive PA wave dominates the tensile part of the wave [34].

Doukas and co-workers have shown that a single high-impulse pressure wave can increase the permeability of the skin to large drugs [144], including insulin [197]. It was emphasized that ablation of polystyrene targets by laser pulses with fluences up to 10 J/cm² can generate pressure waves with amplitudes between 300 and 1000 bar, which are much more effective in permeabilizing the stratum corneum than the pressure waves with amplitudes of 1 to 5 bar usually employed by ultrasound techniques. It was further observed that the onset of the permeabilization of the stratum corneum occurred at 350 bar [144]. Our Pa waves seem to be unable to reach the stated threshold for skin permeabilization because the amplitudes are below 12 bar (at a laser fluences of 50 mJ/cm²). This limitation is only apparent because the rise time of the shock waves generated by the ablation of polystyrene targets is larger than 200 ns, and the rate of pressure increase, or impulse, of the waves generated by Doukas and co-workers is usually between 1 and 50 bar/ns [144]. The rise time of a PA wave with an amplitude of 12 bar generated by a piezophotonic material obeying the condition $\mu_a c_s \tau_L > 1$ is the duration of the laser pulse (≤ 8 ns) implying an impulse superior to 1bar/ns, which is in the limit for the permeabilization of the skin. Table 6-10 presents typical peak pressures (PP), rise times (RT) and the concomitant impulse of the wave.

Table 6-10 –Shock, ultrasound and photoacoustic waves physical characterization.

	PP bar	RT ns	Impulse bar/ns
Shock	300-1000	200	2.5-50
UW	1-5		Up to minutes
PA	12	8	2

Additionally, the PA wave generated by the piezophotonic material has a larger bandwidth, with significant frequency components extending to the hundreds of MHz (figure 6.23 left). Such materials produce very high frequencies ultrasound, as expected from PA waves of very short duration. In the series of piezophotonic materials with Mn-TPPS incorporated in TiO₂ (table 6-9) with a constant absorbance and various thicknesses h , the peak pressures increase as the thickness of the material decreases (figure 6.23 right).

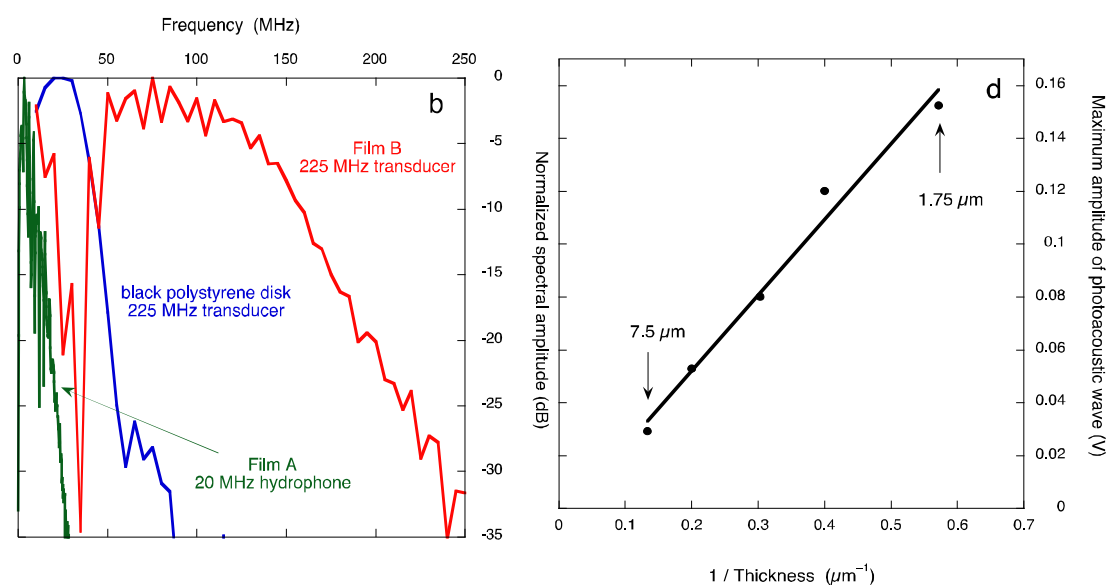
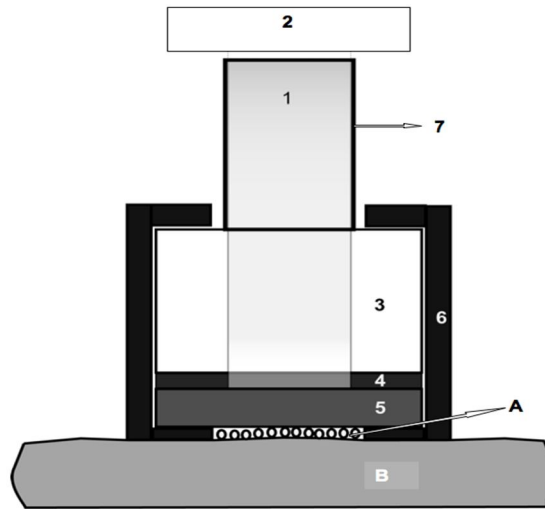


Fig. 6.23 – **Left)** FFT analysis of the pressure waves generated with Mn-TUP in polystyrene substrate versus the pressure wave generated by a black polystyrene disk (red and blue lines measured with a 225 MHz contact transducer. Mn-TTP in a polystyrene substrate measured by a 20 MHz needle hydrophone. **Right)** Dependence of the photoacoustic signal intensity on the thickness of the series of films of titanium dioxide with Mn-TTPS (matched absorbances) at the pulsed laser excitation wavelength of 472 nm, as measured by a 100 MHz contact transducer.

Figure 6.23 left shows that significant frequency components up to 200 MHz are only present in the signal generated by the piezophotonic material. Such materials produce ultrasound with very high frequencies, as expected from PA waves of very short duration [28].

9. Design of a PA Waves System based on Piezophotonic Materials

Figure 6.24 represents a schematic cross-section of an embodiment of the PA waves transdermal system to deliver compounds in a suitable pharmacological formulation (A) through biological barriers (B). The optical guide is connected to a laser pulse source that allows directionality to the piezophotonic material. The rigid window element is transparent to the wavelength of the laser pulse that is selectively absorbed by the PAC reference compound. The close contact between the window element (3), the support element (5) and the piezophotonic film is provided by a structural element – rigid boundaries.



Figs 6.24 – Schematic cross representation of the assembled PA waves transdermal system. A- formulation, B – biological barrier, 1 – laser pulse, 2 – laser box, 3 – window, 4 – piezophotonic material, 5 – mirror, 6 – structural element, 7 – optical guide.

10. References

- [28] C.R. Harding, The stratum corneum: structure and function in health and disease. *Dermatol. Therapy*, 17 (2004) 6-15.
- [34] L.M. Lieb, B.D. Brown, G.G. Krueger, A.P. Liimatta, R.N. Bryan, Description of the intrafollicular delivery of large molecular weight molecules to follicles of human scalp skin in vitro. *J. Pharm. Sci.*, 86 (1997) 1022-1029.
- [133] M.W. Sigrist, Laser generation of acoustic waves in liquids and gases, *J. Appl. Phys.*, 60 (1986) 83-121.
- [134] R. M. White, Generation of Elastic Waves by Transient Surface Heating. *J. App. Phys.* 34 (1963) 3559-3567.
- [135] Askar'yan et al, Excitation of Signals in a Negatively Charged Post of an Antenna under the Influence of an Unfocused Laser Beam. *Sov. Phys. JETP Lett.*, 4 (1966) 122-123.
- [144] A.G. Doukas, N. Kollias, Transdermal drug delivery with a pressure wave. *Advanced Drug Delivery Reviews*, 56 (2004) 559–579.
- [149] F.A. Schaberle et al, Analytical solution for time-resolved photoacoustic calorimetry data. A survey of mechanisms common in photochemistry. *Photochem. Photobiol. Sci.*, 9 (2010) 812-822.
- [150] A.A. Karabutov, E.V. Savateeva, N.B. Podymova, A.A. Oraevsky, Backward mode detection of laser-induced wide-band ultrasonic transients with optoacoustic transducer, *J. Appl. Phys.*, 87 (2000) 2003-2014.
- [155] W.H. Childs, Thermomechanical properties of selected space-related materials, in, *The Aerospace Corporation*, Los Angeles, 2002.
- [163] E. Biagi, F. Margheri, D. Menichelli, Efficient laser-ultrasound generation by using heavily absorbing films as targets, *IEEE Trans. Ultraon., Ferroelect., Fre. Contr.*, 48 (2001) 1669-1680.
- [164] Y. Guo, H.W. Baac, S.-L. Chen, T.B. Norris, L.J. Guo, Broad-band, high-efficiency optoacoustic generation using a novel photonic crystal-metallic structure. *Proc. SPIE*, 78992 (2011) 78992C78991-78998.
- [169] A. B. Bell, "On the production and reproduction of sound by light," *Am. J. Sci.*, 20, (1880) 305.
- [170] L.G. Arnaut, R.A. Caldwell, J.E. Elbert, L.A. Melton, Recent advances in photoacoustic calorimetry: theoretical basis and improvements in experimental design. *Rev. Sci. Instrum.*, 63 (1992) 5381.
- [171] G.V. Ostrovskaya, Optical-to-acoustic energy conversion efficiency upon interaction of pulsed laser radiation with a liquid: II. Conversion efficiency measurement by holographic interferometry upon acoustooptic interaction. *Tech. Phys.*, 47 (2002) 64-71.

- [172] M. Dubois, P.W. Lorraine, B. Venchiarutti, A.S. Bauco, R.J. Filkins, T.E. Drake, K.R. Yawn, Optimization of temporal profile and optical penetration depth for laser-generation of ultrasound in polymer-matrix composites, in: D. Thompson, D. Chimenti (Eds.) Review of Progress in Quantitative Nondestructive Evaluation, AIP Conf. Proc., (2000) 287.
- [173] S.R. Visuri, H.L. Campbell, L. Da Silva, Optically Generated Ultrasound for Enhanced Drug Delivery. The Regents of the University of California, USA, 2002.
- [174] S.E. Braslavsky et al, Photoprocesses in biliverdin dimethyl ester in ethanol studied by laser-induced optoacoustic spectroscopy (liao). *Tetrahedron*, 39, (1983) 1909-1913.
- [175] K. Heihoff, S. E. Braslavsky, Photoacoustic and Photothermal Phenomena. Springer, Heidelberg, 1987, 105-106.
- [176] S.E. Braslavsky, G.E. Heibel, Time-resolved photothermal and photoacoustics methods applied to photoinduced processes in solution. *Chem. Rev.*, 92 (1992) 1381–1410.
- [177] K.S. Peters, G.J. Snyder, Time-resolved photoacoustic calorimetry: probing the energetics and dynamics of fast chemical and biochemical reactions. *Science*, 241, (1988) 1053–1057.
- [178] T. Gensch, C. Viappiani, Time-resolved photothermal methods: accessing time-resolved thermodynamics of photoinduced processes in chemistry and biology. *Photochem. Photobiol. Sci.*, 2, (2003) 699–72.
- [179] C. Serpa *et al*, Photoacoustic Measurement of Electron Injection Efficiencies and Energies from Excited Sensitizer Dyes into Nanocrystalline TiO₂ Films, *J. Am. Chem. Soc.*, 130 (2008) 8876-8877.
- [180] N.S. Foster, J.E. Amonette, S.T. Autrey, J.T. Ho, Detection of trace levels of water in oil by photoacoustic spectroscopy. *Sens. Actuators, B*, 77, (2001) 620–624.
- [181] N.S. Foster, J.E. Amonette, S.T. Autrey, In situ detection of chromate using photoacoustic spectroscopy. *Appl. Spectrosc.*, 53, (1999) 735–740.
- [182] B. Schlageter *et al*, Development of an optoacoustic sensor module for pH and/or CO₂ determination in aqueous solutions, *Sens. Actuators, B*, 39 (1997) 443–447.
- [183] M. Pineiro *et al*, Photoacoustic measurements of porphyrin triplet state quantum yields and singlet oxygen efficiencies, *Chem. Eur. J.*, 4 (1998) 2299.
- [184] G. F. F. Sá, C. Serpa, L. G. Arnaut, *Device for efficient delivery of compounds to or through the skin or biological barriers, using light-absorbing thin films*, 2011 1000030526 Application number Pat., 2011 (PCT request done in June of 2012).
- [185] Polymer Data Handbook, 1999, Oxford University Press, Inc., edited by James E. Mark.
- [186] S. Abbruzzetti, C. Viappiani, D.H. Murgida, R. Erra-Balsells, G.M. Bilmes, Non-toxic, water-soluble photocalorimetric reference compounds for UV and visible excitation *Chem. Phys. Lett.*, 304 (1999) 167-172.

- [187] J. Fabian, Near-Infrared Absorbing Dyes. *Chem. Rev.*, 92 (1992) 1197-1226.
- [188] M. Gouterman, *Optical Spectra and Electronic Structure of Porphyrins and Related Rings*, 1978, edited by D. Dolphin: *The Porphyrins*, Volume 3, academic Press, New York.
- [189] Nicholas J. Turro, *Modern Molecular Photochemistry*, 1991, University Science Books, California.
- [190] S.L. Murov, I. Carmichael, G.L. Hug, *Handbook of Photochemistry*, 1993, Marcel Dekker, New York.
- [191] T. Buma, M. Spisar, M. O'Donnell, High-frequency ultrasound array element using thermoelastic expansion in an elastomeric film. *Appl. Phys. Lett.*, 79 (2001) 548-550.
- [192] E. Biagi, F. Margheri, D. Menichelli, Efficient laser-ultrasound generation by using heavily absorbing films as targets, *IEEE Transaction on Ultrasonics. Ferroelectrics and Frequency Control*, 48 (2001) 1669-1680.
- [193] H. W. Baac *et al*, Carbon nanotube composite optoacoustic transmitters for strong and high frequency ultrasound generation, *Appl. Phy. Lett.*, 97 (2010) 234104.
- [194] M. Nagel *et al*, Aryltriazene Photopolymers for UV-Laser Applications: Improved Synthesis and Photodecomposition Study. *Macromol. Chem. Phys.*, 208 (2007) 277–286.
- [195] NCRP, Exposure criteria for medical diagnostic ultrasound. II. Criteria based on all known mechanisms, in, National Council on Radiation Protection and Measurements. Bethesda MD, 2002, Report No.140.
- [196] M.H. Niemz, *Laser-Tissue Interactions*, 2007, Springer, Berlin.
- [197] A.G. Doukas *et al*, Photomechanical transdermal delivery of insulin in vivo. *Lasers in Surgery and Medicine*, 28 (2001) 282-285.

VII

**Understanding the
Interaction between
Photoacoustic Waves
and Skin**

1. Introduction

The available literature on mechanistic studies between pressure waves and the skin does not provide a complete insight on the physical processes occurring in the intercellular domains of the stratum corneum [144]. The works of Doukas *et al* focus on the macroscopical effect of pressure waves, specifically the expansion of the lacunar spaces within the intercellular regions of the stratum corneum. The biophysical mechanism of the molecular rearrangement of the intercellular lipids is unknown. Doukas *et al* have not clearly identified the mechanism by which these intercellular expansions occur; however they speculate that the incompressibility of water during the travel time of the shock waves should have a role. Furthermore, they recognize that water is the principal component of the newly expanded spaces [144].

The lack of biophysical information concerning the events occurring in the SC upon pressure waves application drove us to consider a simple model composed of dipalmitoylphosphatidylcholine (DPPC) vesicles, which resembles the long chain ceramides of the SC. The hydrophobic effect causes the spreading of lipids in water (with phosphate buffer solution, PBS, pH 7.4), which leads to the spontaneously formation of aggregates consisting of vesicles, such as DPPC phospholipids. The extensive literature concerning the biophysical features of DPPC vesicles inspire us to use it as a model to study the interaction with the photoacoustic waves. Therefore, it should be possible to unveil some features of the unknown biophysical pathways of the SC expansion.

2. Lipids Biophysical Nature

Lipids comprise a distinct family of naturally occurring molecules, which include fatty acids, phospholipids, triglycerides, sphingolipids, and sterols such as cholesterol, prenols and glycolipids. Their biological functions are particularly relevant for maintaining high levels of energy storage, signaling cells of external deregulations and as structural components of all biological barriers [198].

The amphiphilic nature of lipids is one of their key features. The backbone of this nature relies in the presence of two contrasting parts of molecules: a hydrophobic tail and a hydrophilic headgroup. The structure of lipids assembly depends on weak intermolecular forces, such as van der Waals forces, hydrogen bonding and electrostatic interaction between the headgroups and water. These forces are established between adjacent hydrocarbon chains.

The hydrophilic part of a lipid has an affinity to polar solutes, such as water; nevertheless the hydrophobic region is excluded from water due to the hydrophobic effect. In the presence of water, the hydrophobic repulsion drives a spontaneously assembly of the lipid parts towards the

most favorable energetic arrangement [199]. Consequently, the creation of self-assemblies, such as micelles, microemulsions or vesicles occurs if their concentration is superior to a certain threshold, called critical aggregation concentration (CAC). In general, the lipids apolar regions are predominant in terms of molecular weight, so that they aggregate with extremely low CAC (DPPC example in figure 7.1).

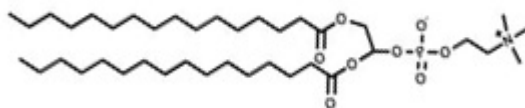


Fig. 7.1 – Chemical structure of DPPC.

The aggregate depends on three packing constrains: (1) the optimal area occupied by the polar interface (S_0), (2) the maximum length of the alkyl chain (l), and (3) the molecular volume of the hydrocarbon portion of the amphiphile (v). These parameters determine the critical packing parameter (CPP), which can be applied to predict, for a particular molecule, the preferential shape of the aggregate formed in aqueous solutions [200].

$$CPP = \frac{v}{lS_0} \quad (7.1)$$

The lipid bilayers form when the CPP is equal to 1.

2.1 Model Membranes

The main purpose in this chapter is to exploit the interaction of photoacoustic waves with lipids, and try to describe and explain undocumented features arising from it. Various model membranes could be used for studying this phenomenon, though the simplest model with pure lipids resembling the SC ones is the first step in that pathway. We should remark that the systems used in this study do not contain other lipids or proteins, which are present in the intercellular region of the stratum corneum. Consequently, these studies cannot mimic all the properties of that biological barrier, but the main biophysical and biochemical features are nevertheless preserved because of the similarity between DPPC and the SC ceramides. After a full biophysical description of this mixture, we intend to increase the complexity of such system, namely with other SC components, such as cholesterol or keratin.

2.1.1 Liposomes

Liposomes are spherical lipid vesicles formed by a unilamellar or multilamellar bilayers, enclosing small volumes of aqueous solution inside the vesicle [200]. Their classification depends on the size and number of lamellae, which originates multilamellar vesicles (MLV),

giant unilamellar vesicles (GUV), large unilamellar vesicles (LUV) and small unilamellar vesicles (SUV) [200].

The MLV include several lipidic bilayers and their diameters can be up to centimeters. These vesicles are structurally poorly-defined systems, so that their use as biophysical models has been neglected in favor of unilamellar vesicles. One prominent liposome attribute is the curvature of the self-assembled lipids. Bilayer curvature depends on the liposome diameter, with SUVs ($\emptyset < 50$ nm) having the highest curvature. For LUV (\emptyset around 50-500 nm), the average bilayer curvature is practically the same as for planar membranes, when considering curvature at a molecular level [201]. For a liposome composed of one lipid species, the bilayer packing defects are highest for small vesicles.

2.2 Lipid Dynamics: Phase Transition

Lipid dynamics depends on many factors, such as alkyl chain length, number of *cis*-double bonds, temperature and pressure, degree of hydration, free volume and lipid content [198, 201]. One of the most pertinent properties of a bilayer is how the lipid dynamics changes with temperature, known as bilayer phase behavior.

At a certain temperature, a lipid bilayer can exist in either a liquid (L_α), a solid phase (S_o) or a coexistence of both phases (phase transition temperature, PTT). At this precise temperature, all lipids undergo a melting process, which leads the system into a more fluid and disorder state (L_α) [202]. In detail, conformational studies indicate that, below the phase transition temperature, the lipids have uniform and all-trans configuration chains, whereas, above that temperature, the additional available degrees of freedom induce the rotation of carbon-carbon bounding into a gauche configuration [201]. Despite the changes around phase transition temperatures (PTT), the hydrophobic effect still remains virtually unchanged, and the reason for structural organization even at the chaotic PTT state [201].

An important feature to address at the PTT is the lipid elastic response to external stimuli. At this state, a strong mechanical stress can induce distortions and structural disarrangement, which can change along each bilayer with the duration of the stimuli and its localization. The events promoted by this stress accounts for bilayer compression, distension or stretch, which may promote lipid fusion or other membrane deformations. Parameters, such as compressibility modulus (k_M), and the tension required for rupture (τ_c) may be used to characterize these events [202].

Papahdjopoulos *et al* [203] found that during lipid phase transition, there was a maximum leakage of radioactive sodium ions, indicating that the bilayer permeability changed at this

temperature. These authors suggest that the increase in membrane permeability relates with the creation of gel to fluid boundaries. [204]. Other studies propose that, at the phase transition, the membrane suffer significant changes in the lateral compressibility, which are intrinsically related to the increase in membrane fluctuations [205].

DMPC (1,2-dimyristoyl phosphocholine) vesicles, which undergo a transition temperature at 23°C, provide another conspicuous example of membrane behavior at the PTT [206]. At room temperature, the heterogeneities in DMPC vesicles arise from the coexistence of the fluid and gel phases [206], which can be understood as a local variation in the lipid stacking inside the membrane. This results in cross membrane pores allowing solvents of finite sizes to leak in or out of the vesicles [206].

The membrane heterogeneities presented at the PTT were both phases coexist, promote an increase in membrane fluctuations and hence amplify lipid permeability [202]. At this temperature, the membrane barrier function is weakened, so it is the ideal temperature to initiate the study of interaction of photoacoustic waves and lipids. Furthermore, if no visible change is detected by the induction of PA waves in membranes, at this temperature, then it will be difficult to see changes far from this point.

The selection of DPPC also relied on the fact that it is a widely studied lipid, so most of the phase behavior is well understood and established. Furthermore, it presents a gel to liquid PTT (41 °C) near a biological body temperature (37°C), though the skin temperature is around 32 °C. Concentration and temperature dependence studies of a binary mixture of DPPC and POPC (1-palmitoyl-2-oleoyl phosphocholine) performed by Shoemaker *et al* [207] emphasized their resemble with the stratum corneum lipids. This system shows a significant decrease of the tension required to break its vesicles with increasing temperature. At the coexistence phase around 41 °C, the system undergoes further reduction on its assembly tension (in a degree of 40%) if compared to the initial vesicles.

3. Fluorescence Anisotropy Studies in the DPPC:DPH System

A current methodology to study the effect of an external stimulus, such as the application of acoustic energy, in the structure and dynamics of a lipidic system is based on the use of fluorescent probes [207, 208]. The selection of different dyes relates to the target in the bilayer, which is supposed to vary according to the physico-chemical properties of the probe, such as lipophilicity and charge.

The vesicles are characterized by unique properties due to its vertical heterogeneity: the backbone structure with headgroup regions containing charged and polar groups near the interface, and a more apolar area in the lipid acyl tails. The separation between the backbone areas presents a small distance (2 nm), which implies two entirely different chemical-physical media with distinct properties [200].

The disturbing events occurring in the phase transition temperature relate to the melting of the alkyl chains [202], so a molecular probe that solubilizes and locates in the inner core of the bilayers should inform on this process. There is a variety of molecular probes suited for this purpose, namely pyrene, trans-parinaric acid and diphenylhexatriene (DPH – figure 7.2) [212]. However, the latter is the appropriate hydrophobic probe, because is readily soluble in the lipid tail area, does not induce significant variations in the PTT (0.1-0.2 °C) and has a large anisotropy and fluorescence quantum yield [208].

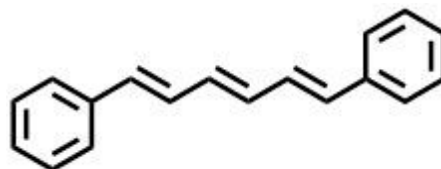


Fig. 7.2 – Chemical structure of DPH.

The events occurring at the phase transition temperature can be monitored by fluorescence anisotropy due to the rotational motion of DPH in a free-movement state [208]. In fluorescence anisotropy, the light emitted by a fluorophore has unequal intensities along different axes of polarization. Anisotropy measurements may provide information on the size and shape of the fluorophore or the rigidity of a molecular environment based on the photoexcitation of a fluorescent dye by polarized light [208]. In homogeneous solutions, the dyes orientation is random, but upon excitation with polarized light, one selectively excites the molecules that have absorption transition moments oriented along the electric vector of the excitation light [208]. This photoselection results in a polarized fluorescent population that decays along a fixed axis of the dye. The angle between the two transition states and the molecule rotation during the excited state determines the measured anisotropy (r), so that its definition is $r = I_{\parallel} - I_{\perp} / I_{\parallel} + 2I_{\perp}$, where I_{\parallel} and I_{\perp} is the fluorescence intensity of horizontal and vertical polarized emission [208].

The interaction between a photoacoustic wave and a vesicle is expected to change the rigidity of the lipidic system. The experimental design consists (1) in measuring a regular and stable anisotropy signal of the DPH in the DPPC:DPH system, (2) to apply the photoacoustic waves produced by irradiation of Mn-TUP piezophotonic materials and (3) to follow the recovery of the signal to determine the kinetic profile. Experimentally, it was decided to characterize the anisotropy signal at 40, 41 and 42 °C and to apply photoacoustic waves during 0.5, 1, 2 and 5 minutes.

3.1 DPPC:DPH System at 40°C subject to PA Waves

The photoacoustic waves laser assembly applied in these experiments is depicted in figure 7.3.

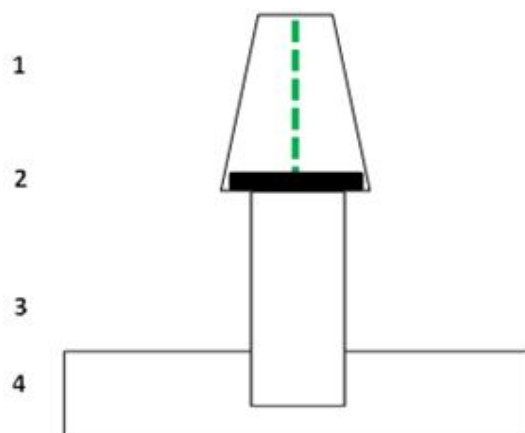


Fig. 7.3 - Laser assembly (1) for the irradiation of the polymer film. The laser pulse (green) impinges into the piezophotonic material (2), which produces a PA wave that traverses a quartz cell (3) until it reaches the DPPC:DPH solution. The anisotropy signal is followed by a Cary Eclipse fluorescence spectrophotometer (4) equipped with a thermostatic multicell holder (3). Acoustic contact is maintained by an ultrasound gel.

The anisotropy signal of DPH, at 40 °C, shows significant changes, as portrayed in figure 7.4. The DPPC:DPH system instability depends of the exposure time to the photoacoustic waves because a 5 minutes interaction induces a 0.020 decrease of the anisotropy signal, and a 2 minutes application period is responsible for a 0.01 reduction. For smaller contact times, (0.5 and 1 minute of PA waves), the system maintains its conformational structure. The anisotropy variation of 0.5 minutes PA waves finishes after 500 seconds.

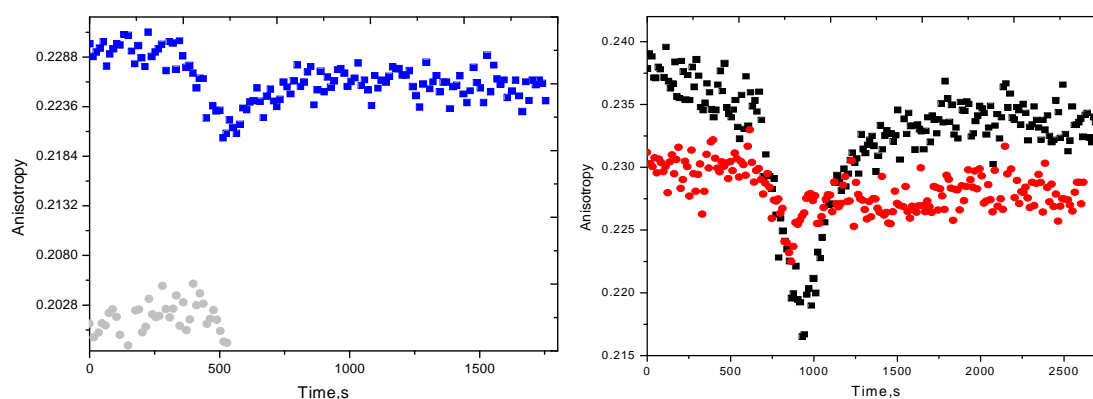


Fig. 7.4 – Changes in DPH fluorescence anisotropy after PA waves application on the DPPC:DPH system (100:1) at 40 °C. Vesicles were exposed to PA waves for 0.5 minutes (gray) and 1 minute (blue) in the left image and 2 minutes (red) and 5 minutes (black) in the right image. The PA waves were produced by irradiating a polystyrene film containing tetraphenyl porphyrin of manganese, with $\mu_a = 640 \text{ cm}^{-1}$, $\Gamma = 0.7$, $c_L = 2400 \text{ m/s}$, laser pulse duration of 8 ns, laser energy density of 50 mJ/cm^2 , optical power density of 6.25 MW/cm^2 .

3.2 DPPC:DPH System at 41 °C subject to PA Waves

The phase transition temperature of the DPPC:DPH system is 40.7 °C [206], so the expectation is that the anisotropy variation at 40 and 41 °C, upon PA waves application, should be maximized. The result observed in figure 7.5 describes this maximization, even for reduced PA waves application times. Interestingly, 2 minutes of PA waves interaction produce a larger variation in the anisotropy than the exposure to PA waves for 5 minutes (0.020 versus 0.010), which may suggest a saturation effect. For shorter exposure times we see assist to a less effective induced-instability of the anisotropy signal (≤ 0.01).

This physical effect clearly disturbs the lateral compressibility of the lipid system, which at the PTT is even more sensible to external forces [202, 206].

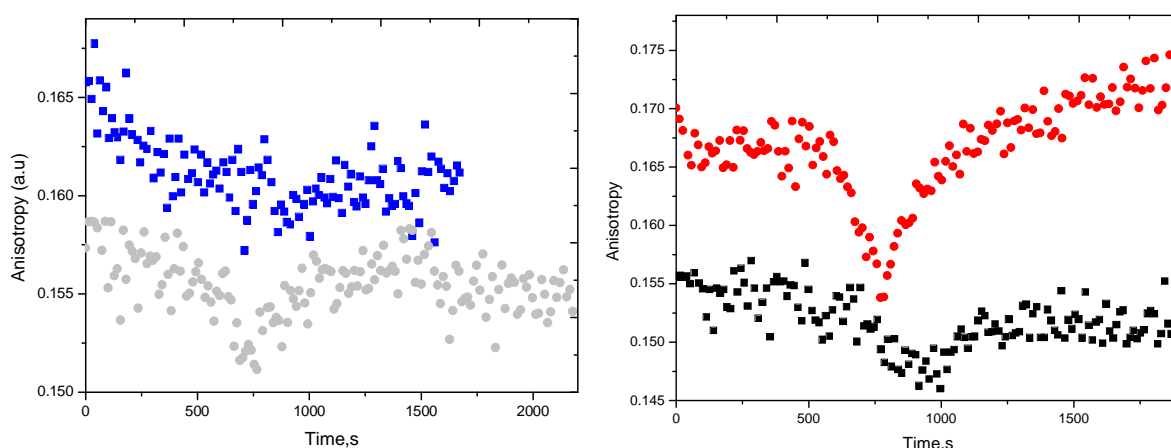


Fig. 7.5 – Changes in DPH fluorescence anisotropy after PA waves application on the DPPC:DPH system (100:1) at 41°C. Vesicles were exposed to PA waves for 0.5 minutes (gray) and 1 minute (blue) in the left image and 2 minutes (red) and 5 minutes (black) in the right image. The PA waves were produced by irradiating a polystyrene film containing tetraphenyl porphyrin of manganese, with $\mu_a = 640 \text{ cm}^{-1}$, $\Gamma = 0.7$, $c_L = 2400 \text{ m/s}$, laser pulse duration of 8 ns, laser energy density of 50 mJ/cm^2 , optical power density of 6.25 MW/cm^2 .

3.3 DPPC:DPH System at 42 °C subject to PA Waves

Above the phase transition temperature, where the lipid system has a distinct single phase structure (liquid), the photoacoustic waves does not induce a perturbation in the anisotropy signal (figure 7.6). Only for the 5 minutes application period, we note to a 0.05 variation in the anisotropy signal, which does not recover the initial vesicle conformation. This result was predictable because the fluorescence anisotropy measurements are more sensitive to changes in the arrangements of nonfluid systems [208].

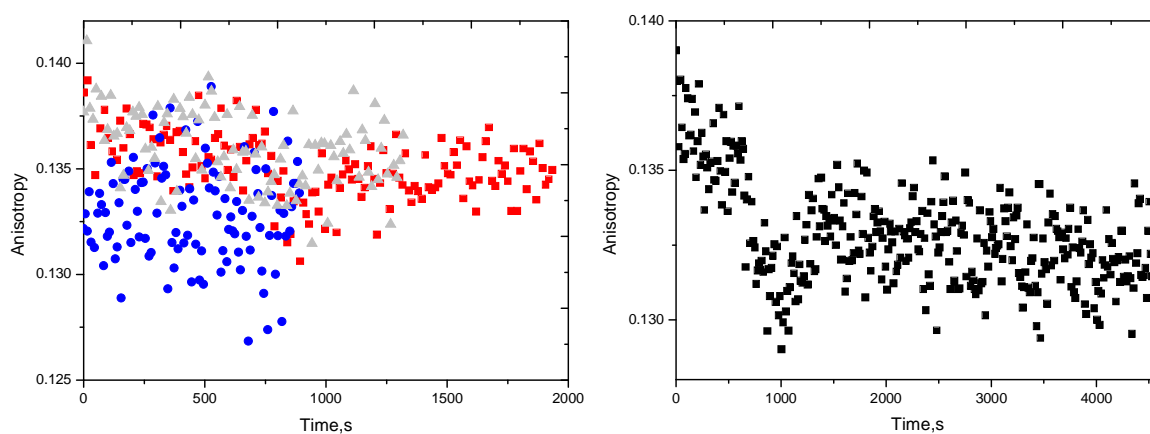


Fig. 7.6 – Changes in DPH fluorescence anisotropy after PA waves application on the DPPC:DPH system (100:1) at 42 °C. Vesicles were exposed to PA waves for 0.5 minutes (gray), 1 minute (blue) and 2 minutes (red) in the left image and 5 minutes in the right image. The PA waves were produced by irradiating a polystyrene film containing tetraphenyl porphyrin of manganese, with $\mu_a = 640 \text{ cm}^{-1}$, $\Gamma = 0.7$, $c_L = 2400 \text{ m/s}$, laser pulse duration of 8 ns, laser energy density of 50 mJ/cm^2 , optical power density of 6.25 MW/cm^2 .

4. Conclusions

The anisotropy studies indicate that the photoacoustic waves perturb the DPPC:DPH vesicles by increasing the molecular fluidity around the phase transition temperature. Despite this increase, the system is flexible enough to recover its original form. The recovery kinetic profile was adjusted for each PA waves experiments by a single exponential fit (figure 7.7).

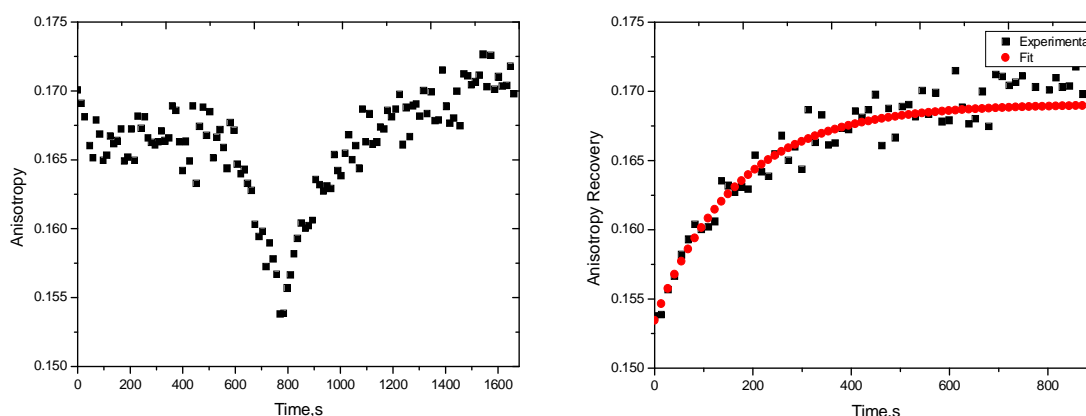


Fig. 7.7 – Change in anisotropy after PA waves application (left). The DPPC:DPH was exposed to 2 minutes of PA waves at 41°C. Anisotropy recovery was fitted with a single exponential represented by the red line with $\tau = 1.70 \times 10^2 \text{ s}$ (right).

In table 7-1, there is a summary of the kinetic constants calculated for the experiments with a distinct variation in the system anisotropy. The PA waves generate a transient effect in the rigidity of the DPPC: DPH system with a recovery time between 2 or 3 minutes. The increase in fluidity induced by the pressure increase may offer the opportunity of molecules of larger sizes to diffuse across the vesicles, which may be relevant for gene transfection therapies if the same

principles apply to the cell membranes. Future work will be directed towards a more complex lipid system, to simulate the stratum corneum intercellular regions.

Table 7-1 – Recovery kinetic parameters for a single exponential decay.

T (°C)	Δt (min)	k (10^{-3} s^{-1})	τ (10^2 s)
40	0.5	-----	-----
	1	5.0	2.0
	2	25	0.4
	5	6.4	1.6
41	0.5	-----	-----
	1	6.4	1.6
	2	5.9	1.7
	5	5.9	1.7
42	0.5	-----	-----
	1	-----	-----
	2	3.0 ³	3.3
	5	1.8	5.5

The barrier imposed by the stratum corneum to the diffusion of small and lipophilic solutes is due, at least in part, to the intercellular lipids [1-3]. Thus, physico-chemical properties, such as the skin temperature, should influence and/or disturb the physiological organization of those lipids. It is established that a rise in skin temperature increases the penetration of drugs [209-212]. The temperature enhanced diffusion was associated with phase transitions of the lipids, which resulted in augmented fluidity (rotational disorder) of the intercellular lipids [212].

Recent studies concluded that relevant temperature lipid transitions occur in the human stratum corneum [212]. These transitions represent a reversible solid-to-fluid phase changes at [35, 65, 80, 95] °C [212], which reflect the lipid entanglement of the SC, namely the uniformly distributed phases with different lattice packing (i.e, orthorhombic, hexagonal and liquid crystalline phase). The natural immiscibility of these phases due to the imbalances in their hydrophobic and hydrophilic interactions [209, 210] should be enhanced upon heating, and therefore, impact in the skin permeability. The structure and function of the SC at 32 °C ensures the skin barrier function properties, nevertheless the promotion of a phase separation state at 35 °C can transiently disrupt the skin barrier [212].

The exertion of an external and localized pressure in a medium produces a movement from the equilibrium position of adjacent particles. The propagation of high frequency ultrasound waves in solutions or tissues is strongly attenuated by the medium. This means that the mechanical

energy of the wave is dissipated in terms of heat (or kinetic energy) taken up by the particles of the medium. The changes observed in our lipid model should at least be partly assigned to a rise in the lipid temperature. The temperature effect in the lipid organization involves an increased fluidity of the system [209-212], which is in agreement with our observations.

The acoustic wavelength of the photoacoustic waves generated by the metaloporphyrins based piezophotonic materials is ca.15 μm . This is much larger than the size of the DPPC:DPH vesicles, which is around 100 nm (see chapter with experimental details). The radiation force exerted by the acoustic waves is diminished because of the difference in sizes and the pressure gradient across a vesicle is relatively small. Nevertheless, this pressure gradient can be an additional factor in the perturbation of the vesicle fluidity manifested by the transient changes in anisotropy.

5. References

- [1] B.W. Barry, Novel mechanisms and devices to enable successful transdermal drug delivery. *Eur. J. Pharm. Sci.*, 14, (2001) 101-114.
- [2] R. Wickett, M. Visscher, Structure and function of the epidermal barrier. *Am. J. Infect. Control*, 34 (2006) 98-110.
- [3] R. Paus, What is the 'true' function of the skin? *Exp. Dermatol.*, 11 (2002) 159-187.
- [144] A.G. Doukas, N. Kollias, Transdermal drug delivery with a pressure wave. *Advanced Drug Delivery Reviews*, 56 (2004) 559–579.
- [198] A. Blume, G. Cevc, Ed.; Marcel Dekker. *Dynamic Properties. In Phospholipids Handbook: New York*, 1993.
- [199] K.D. Collins, Charge density-dependent strength of hydration and biological structure. *Biophys J.*, 72 (1997) 65-76.
- [200] W.L.C. Vaz, *Properties of Lipid Bilayers*. 2008, Wiley Encyclopedia of Chemical Biology.
- [201] R.B. Gennis, *Biomembranes*. 1989, New York. Springer-Verlag.
- [202] J.F. Nagle, Theory of the Main Lipid Bilayer Phase Transition. *Am. Rev. Phys. Chem.*, 31 (1980) 157-195.
- [203] D. Papahadjopoulos, K. Jacobson, S. Nir, T. Isac., 311 (1973) 330-340.
- [204] L.C. Hansson, J.H. Ipsen, O.G. Mouritsen. *Biochim Biophys Acta*, 979 (1989) 166-176.
- [205] J.F. Nagle, H.L. Scott., *Biochimica et Biophysica Acta* 513 (1978) 236-243.
- [206] F. Tokumasu, A.J. Jin, J.A. Dvorak. *J. Electron. Microsc.*, 51 (2002) 1-9.
- [207] S.D. Shoemaker, T.K. Vanderlick, Material Studies of Lipid Vesicles in the L_{α} and L_{α} -Gel Coexistence Regimes. *Biophys J.*, 84 (2003) 998–1009.
- [208] J.R. Lakowicz, *Principles of Fluorescence Spectroscopy*. 1999, Kluwer Academics/Plenum Publishers (2nd Edition), New York.
- [209] S.M. Al-Saidan, B.W. Barry, A.C. Williams, Differential scanning calorimetry of human and animal stratum corneum membranes. *Int. J. Pharm.*, 168 (1998) 17-22.
- [210] G.M. Golden *et al*, Lipid thermotropic transitions in human stratum corneum. *J. Invest. Dermatol.*, 86 (1986) 255-259.
- [211] T. Ogiso, H. Ogiso, T. Paku, M. Iwaki, Phase transitions of rat stratum corneum lipids by an electron paramagnetic resonance study and relationship of phase states to drug penetration. *Biochim. Biophys. Acta*, 1301 (1996) 97-104.
- [212] C.L. Gay *et al*, Characterization of Low-Temperatur (i.e., <65 °C) Lipid Transitions in Human Stratum Corneum. *J. Invest. Dermatol.*, 13 (1994) 233-239.

VIII

**Safety Issues of the
Photoacoustic Waves
Transdermal System**

1. Introduction

The molecule of water can cross the skin barrier in a controlled way, in a process highly relevant for body temperature regulation [213-216]. Transepidermal water loss (TEWL) is a measure of the amount of water exchanged between the skin and the outside environment. This biophysical measure correlates well with the barrier function efficacy to drug diffusion, and fluctuations in its value can relate to external stimuli or cellular damage [217-219].

The development of the photoacoustic wave transdermal system requires safety tests, which can be related with the recovery of the skin barrier function and skin damage/irritation. The barrier function ensured by the singular stratum corneum physiology may be disrupted with physical methods, which creates channels that enhance the water flow to the exterior environment. Consequently, a sudden increase in water flux is correlated with a barrier function disruption [215]. On the other hand, skin irritation is a reversible inflammatory reaction that can lead to erythema, which is provoked by structural damage of cellular organelles [4, 217-219]. Many chemical substances act as skin irritants and the primary body response of this process is the production of cytokines by keratinocytes (signalling proteins for cellular damage and infections). Activated Langerhans cells also secrete cytokines, but in a lesser extent [4, 219].

The barrier disruption and skin damage can be evaluated by noninvasive biophysical techniques, such as transepidermal water loss and reflectance spectroscopy, respectively. Skin irritation can be determined by measuring the skin contents of melanin (superficial damage) and hemoglobin (erythema dissemination). When erythema occurs, there is an increase in skins' superficial blood flow, which increases the levels of hemoglobin, and, consequently, allows assessing the extent of biological damage [217-219]. The analysis and quantification of this parameter can be obtained by using an absorption probe, Mexameter® MX18 (Courage+Khazaka), which emits light of defined wavelengths for melanin and hemoglobin detection and reads out the reflected light by the skin. The positions of emitter and receiver probes guarantee that only scattered light by skin is measured (figure 8.1⁷).

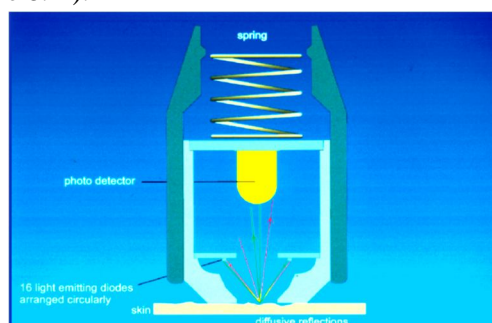


Fig. 8.1 – Schematic representation of Mexameter® MX 18. The melanin and hemoglobin content is determined at 568, 660 and 870 nm, respectively.

⁷ Image available at <http://www.courage-khazaka.de/index.php/en/all-downloads/downloads-en/file/29-brochmx18cl400e> (downloaded 25/05/2012)

The skin barrier function stability is examined by measuring the differences in water flux between untreated and treated skin [220]. The determination of the water flux is based upon the Fick's Diffusion Laws [80], and represents the basis of the open chamber measurements of transepidermal water loss (figure 8.2⁸).

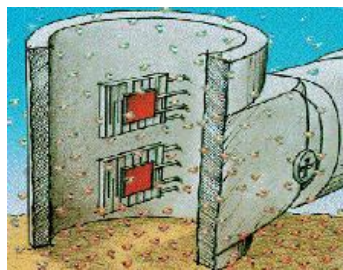


Fig. 8.2 – Schematic representation of the Tewameter® TM 300.

The temperature and water sensors (red panels in figure 8.2) are located inside the cylindrical probe head, which assures environmental protection against air moisture. The temperature sensors should be at skin's temperature (32 °C), to provide an accurate and reproducible measurement (pre-heating).

2. PA Waves Application in Animal Models

The first safety tests employed animal models that resemble the human skin, namely minipigs [94]. The TEWL measurements rely on the water content reading before and after the PA waves application (figure 8.3). All the TEWL measurements were performed in collinear skin sites in the minipigs dorsum to eliminate regional variations, in the stratum corneum physiology. The production of PA waves relied in the utilization of piezophotonic materials with Mn-TUP solubilized in polystyrene and the laser fluence set at 50 mJ/cm² (6.25 MW/cm²). The experiments were performed in a surgery room with controlled temperature and humidity (20°C and 40-50%, respectively).

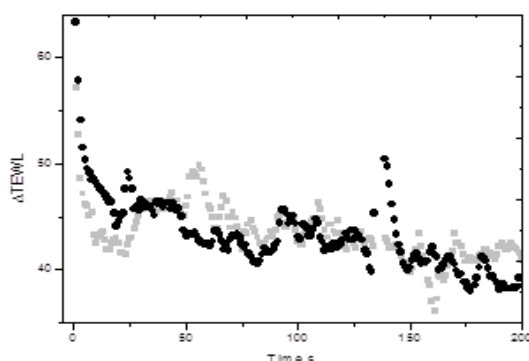


Fig. 8.3 - Changes in transepidermal water loss after PA waves application (black) and after occlusion (gray) in different minipigs skin sites. The minipig skin was exposed for 20 seconds of PA waves produced upon laser irradiation (50 mJ/cm², 6.25 MW/cm²) in Mn-TUP incorporated in polystyrene, and the change is the TEWL after the exposure to the PA waves minus the initial TEWL.

⁸ Image available at <http://www.courage-khazaka.de/index.php/en/all-downloads/downloads-en/file/50-brochtm300e> (downloaded at 25/05/2012)

In figure 8.3, the exposure of the minipig dorsum to PA waves results in an TEWL increase in an excess of $66 \text{ g}/(\text{m}^2 \text{ hr})$, although occlusion with the laser OFF changed the TEWL by $58 \text{ g}/(\text{m}^2 \text{ hr})$. These values show a strong growth, if compared to basal TEWL values of the minipig dorsum (figure 8.4). The high values of TEWL drifts by the use of a hydrophilic acoustic coupler, which increases the water content at each experimental site. Nonetheless, the subsequent recovery of the TEWL is longer for the skin site subject to the PA waves, denouncing a more intense perturbation of the barrier function, if compared to the simple entrapment of water by occlusion. In figure 8.4 right, the recovery to basal values after the PA waves interaction has a delay of 47 minutes, while, after occlusion, the recovery lasts 20 minutes (figure 8.4 left). The PA waves perturbation can be quantified to be around $8 \text{ g}/(\text{m}^2 \text{ hr})$.

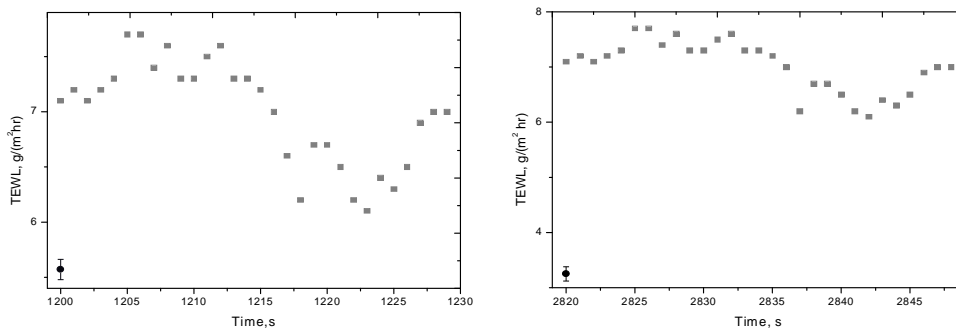


Fig. 8.4 – Left) Transepidermal water loss (\pm SEM) in normal skin (black) and after occlusion (gray) without the PA waves. **Right)** Transepidermal water loss (\pm SEM) after in normal skin (black) and after (gray) 30 seconds PA waves application. SEM symbolizes the standard error of the mean.

Figure 8.5 shows the increase in TEWL after subjecting the skin of a minipig to 1 minute of PA waves. The control experiment of occlusion was performed with the same formulation and device than previous, but with the laser OFF. The PA waves effect on TEWL is visible during 150 seconds, after the measure started. The remaining TEWL relaxation to basal values results from the utilization of a hydrophilic acoustic coupling medium. We tested increasing PA waves application times, 1 and 5 minutes (figure 8.5 and 8.7, respectively), with laser pulses of $50 \text{ mJ}/\text{cm}^2$ at 532 nm .

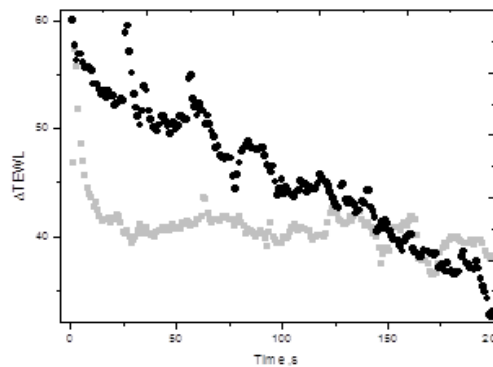


Fig. 8.5 - Changes in transepidermal water loss after PA waves application (black) and after occlusion (gray) in different minipigs skin sites. The minipig skin was exposed for 1 minute of PA waves produced upon laser irradiation ($50 \text{ mJ}/\text{cm}^2$, $6.25 \text{ MW}/\text{cm}^2$) in Mn-TUP incorporated in polystyrene, and the change is the TEWL after the exposure to the PA waves minus the initial TEWL.

The 1 minute PA waves interaction with minipig skin promotes an increase of $15 \text{ g}/(\text{m}^2 \text{ hr})$ more, than the effect of occlusion. Additionally, the recovery time after the PA waves is now distinctively slower than in the control (figure 8.6).

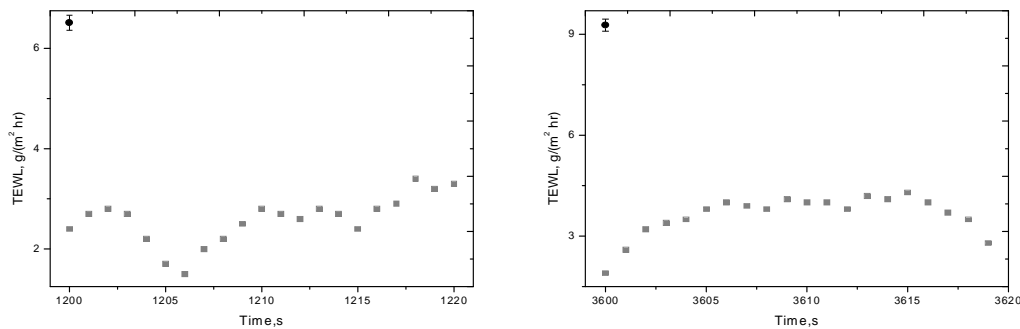


Fig. 8.6 – Left) Transepidermal water loss (\pm SEM) in normal skin (black) and after occlusion (gray) without the PA waves. **Right)** Transepidermal water loss (\pm SEM) after in normal skin (black) and after (gray) 1 minute

We also test an experimental design with a presumable overdose time, in order to assess the safety of the PA waves interaction with living tissues. Figure 8.7 presents the results obtained for an exposure time of 5 minutes, equivalent to more than 5000 PA waves.

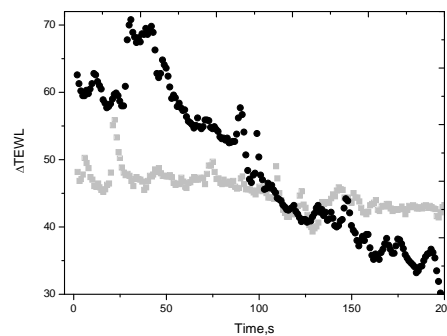


Fig. 8.7 - Changes in transepidermal water loss after PA waves application (black) and after occlusion (gray) in different minipigs skin sites. The minipig skin was exposed for 5 minutes of PA waves produced upon laser irradiation ($50 \text{ mJ}/\text{cm}^2$, $6.25 \text{ MW}/\text{cm}^2$) in Mn-TUP incorporated in polystyrene, and the change is the TEWL after the exposure to the PA waves minus the initial TEWL.

The extended exposure to the photoacoustic waves produces a significant increase in the minipig TEWL: nearly $20 \text{ g}/(\text{m}^2 \text{ hr})$ more than the occlusion site (figure 8.7). Despite this significant increase in the minipig TEWL, the skin recovers from the PA waves effect within 1 minute. The remaining TEWL relates to the utilization of an acoustic coupling medium with a high percentage of water ($> 80\%$). Figures 8.8 depict the recovery to TEWL basal values after occlusion and PA waves.

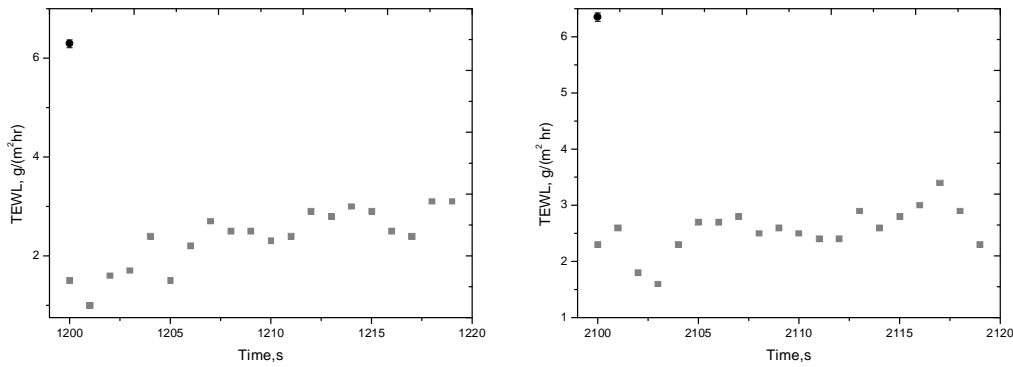


Fig. 8.8 – Left) Transepidermal water loss (\pm SEM) in normal skin (black) and after occlusion (gray) without the PA waves. **Right)** Transepidermal water loss (\pm SEM) after in normal skin (black) and after (gray) 5 minutes

2.1 Conclusions for the Animal Studies

The experimental design of the animal safety tests informs on the minimum photoacoustic waves exposure times required to produce a significant increase in the TEWL, in comparison with the TEWL of the minipig skin due to occlusion. The results show that both techniques enhance the TEWL of the minipig, however a more pronounced effect was observed using the PA waves. The increase in TEWL of 8, 15 and 20 $\text{g}/(\text{m}^2 \text{ hr})$ follows the increase of the exposure times: 0.5, 1 and 5 minutes.

This experimental observation correlates with the expected increase in the water loss due to the perturbation of the function barrier by the use of PA waves. The increase of water flow from the skin occlusion sites is related to water entrapment in the skin surface [220]. The use of hydrophilic ultrasound gels, as an acoustic coupling media undermines a complete rationalization of the results, nevertheless the TEWL curves shows that the additional water content induced by the PA waves recovers within 1 minutes (the following relaxation time results from the ultrasound gel).

3. PA Waves Application in Human Volunteers

In humans, the value of transepidermal water loss (TEWL) changes with the anatomical site, environmental conditions and, to some extent, with the equipment employed in the measurement [214-216]. TEWL measurements often involve the ventral forearms of healthy volunteers, and values between 5 and 14 $\text{g}/(\text{m}^2 \text{ hr})$ have been reported in the scientific literature [214-216]. This should not be interpreted as lack of precision of the measurements, but rather as warning against comparison between absolute measurements performed in different laboratories. The precision of the measurements in a given setting is usually high, e.g., 6.4 $\text{g}/(\text{m}^2$

hr) with a standard deviation of $2.08 \text{ g}/(\text{m}^2 \text{ hr})$ or $14.5 \pm 3.2 \text{ g}/(\text{m}^2 \text{ hr})$ [221]. This is valid providing that the same equipment is used with the same protocol and under the same environmental conditions.

After safety tests in minipigs, 21 healthy volunteers (18-25 years of age) from a population of medicinal chemistry students of the University of Coimbra gave their informed consent to participate in blind TEWL measurements before and after the application of PA waves, in their ventral forearms for 2 minutes. One measurement was made in one forearm of the volunteer with the laser OFF and another one in the other forearm the laser ON (figure 8.9). Piezophotonic materials containing Mn-TUP and Mn-TPP solubilized in polystyrene were used in the volunteers, the laser fluence per pulse was set at $50 \text{ mJ}/\text{cm}^2$ ($6.25 \text{ MW}/\text{cm}^2$), and silicone was used as acoustic coupler (nonaqueous medium).

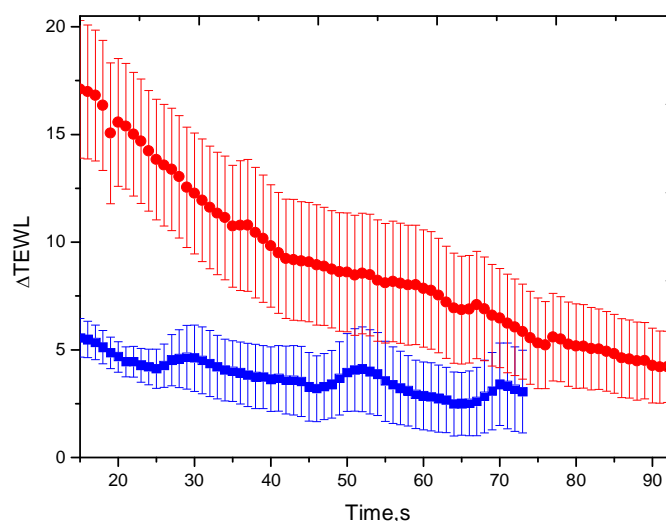


Fig. 8.9 - Changes in transepidermal water loss (average \pm s.e.m.) of the right (in red) and left (in blue) ventral forearms of volunteers. The right ventral forearms were exposed for 2 minutes to PA waves generated by Mn-TUP piezophotonic films in polystyrene although subject to $50 \text{ mJ}/\text{cm}^2$ laser pulses at 20 Hz, and the change is the TEWL after the exposure to the PA waves minus the initial TEWL. The TEWL of the left ventral forearms was measured with the same protocol but with the laser off. The transient change in this case comes from near-surface water trapped by occlusion.

The average (\pm s.e.m.) TEWL increase for 22 volunteers upon exposure to PA waves was $17 \pm 3 \text{ g}/(\text{m}^2 \text{ hr})$, although simple occlusion with the laser OFF changed the TEWL by $5.4 \pm 0.9 \text{ g}/(\text{m}^2 \text{ hr})$, which is a statistically significant difference (t probability < 0.005). TEWL returned exponentially to basal values with a half-life of $\tau_{1/2} = 40 \text{ s}$, figure 8.9. Considering that the first TEWL measurement was made 15 s after lifting the piezophotonic material from the skin, to allow for the cleaning of the silicone with absorbing paper, and assuming the same exponential relaxation in the first 15 s, we obtain an initial TEWL increase of $22 \text{ g}/(\text{m}^2 \text{ hr})$, and $6 \text{ g}/(\text{m}^2 \text{ hr})$ of which are due to the occlusion. Erythema measurement at the site of the PA waves exposure

unveils an increase from 254 ± 8 to 324 ± 15 (t probability < 0.0001), but the effect quickly fades out a few seconds later. This observation relates to the PA waves application because upon pressing the skin for two minutes can cause blanched skin. The normal blood flow is interrupted, which depending of the person blood circulation health may cause a local color change in the skin [222]. The same procedure but with the laser OFF reveals no change in the erythema measurement (262 ± 50 and 263 ± 56), nevertheless the variability of these results (high SEM) can explain the erythema results upon PA waves exposure because some volunteers report blanched skin, and others an increase in the redness at the application site. This effect is a temporary one, which confirms that the PA waves interaction with the skin does not induce any skin damage or irritation.

The assessment of pain associated with the PA waves application represents a critical factor in the development as a transdermal system. This parameter can be measured using a visual analogue scale, which rates the pain from 0 (no pain) to 10 (worst pain ever). All the volunteers reported scores of 0 to 2 with the laser OFF and 18 volunteers reported this range with the laser ON (figure 9.10). Two volunteers reported a score of 3 and one a score of 5. The TEWL of the latter volunteer increased by $40 \text{ g}/(\text{cm}^2 \text{ hr})$ and was the second highest registered. The volunteers reported a gently warming sensation at the end of the PA waves application time.

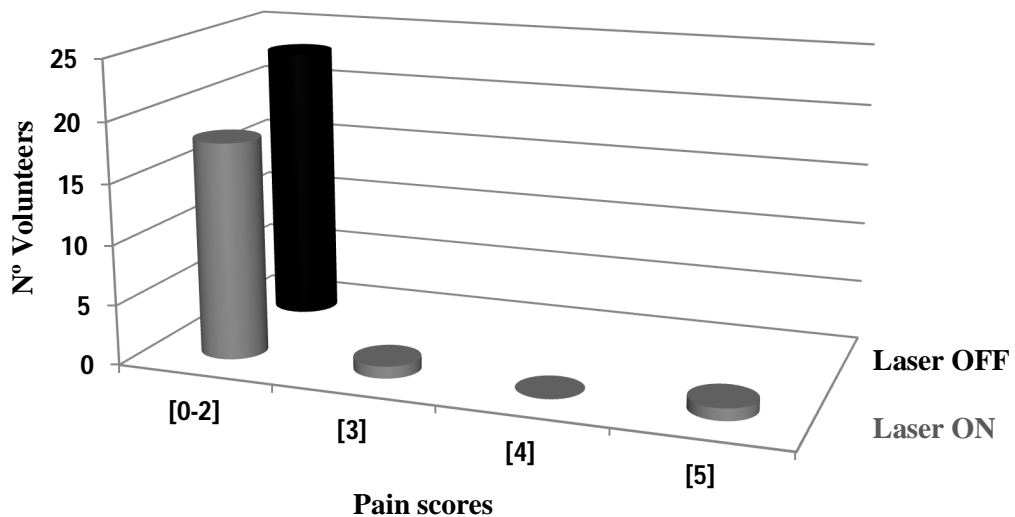


Fig. 8.10 – Box chart graphic describing the pain felt by the volunteers after the PA waves application.

4. Overall Conclusions

The experimental protocol followed for minipigs and human volunteers was similar, nevertheless it differs in the nature of the coupling medium. The higher TEWL minipig values relates to the utilization of ultrasound gel as coupling medium that has a water content greater than 80%). The results reveal that the “water factor” introduces an absolute TEWL value five

times higher, than the baseline in the human experiments because this was avoided by the use of silicone, as an acoustic coupler to human skin. However, even under this condition, the absolute TEWL is higher after the application of the photoacoustic waves, for all the application times, when compared to the occlusion site in the minipig skin. The recovery of the barrier function to the TEWL measured with the laser OFF takes only a few minutes (up to 150 seconds), both in human and minipig experiments (figure 8.3, 8.5 and 8.7). Erythema is not visible in the minipig skin, even after the application of an excess of 5000 photoacoustic waves. In the experiments with volunteers, a similar increase in the absolute value of the TEWL (a factor of three) is reported for 10x sequential tape stripping with D-Squame® tapes [223], and microneedles studies [223]. These values remained elevated, for at least two hours in the tape stripping studies, and also in the use of metal microneedle arrays with needles lengths of 200-400 μm and diameters of 200-300 μm [223]. The increases in TEWL with such microneedles did not reach a factor of two and were associated with longer skin recovery times, typically more than two hours [223]. Iontophoresis applied for 3 h at a current density of 250 $\mu\text{A}/\text{cm}^2$, which corresponds to a total delivery current higher than usual for this transdermal delivery technique, showed that the effect of iontophoresis on TEWL is not as pronounced as the effect of single occlusion [224]. Additionally, erythema was observed in all the volunteers of this study and occasionally edema.

The application of photoacoustic waves to the skin of volunteers reports an increase by a factor of 3 in the TEWL values, followed by a complete recover of skin barrier function in 2 minutes, leaving no signs of damage (negligible erythema and fast fading one), and causing a gentle warming sensation (no pain). The enhancement of skin permeability without causing discomfort or irreversible effects has obvious implications in the transdermal delivery of drugs.

5. Rationalization of the PA Waves Interaction with the SC Intercellular

Lipids

The stratum corneum physiology is an arrangement of packed cells, consisting in a pattern of polygonal dead cells [1-3]. The intercellular spaces consist of lipid bilayers, such as ceramides and cholesterol, alternating with water layers, with a repeating distance around 65-100 \AA and a continuous hydrophilic pathway of only 10 \AA wide [37, 38]. The propagation of an acoustic transient with a very high impulse favours a mechanism based on the radiation pressure exerted in skin interfaces with different acoustic impedances [161]. Contrary to conventional scientific wisdom [133, 161], cavitation is not the primary mechanism because the photoacoustic waves produced has low tensile parts and frequency rich phases, which results in mechanical index

below 0.5 [195, 196]. The radiation pressure mechanism was originally discarded on the basis of calculations of radiation pressures of μbar [133, 161], but here we employ PA waves with pressures changing by more than one bar across a single cell (figure 8.11). The radiation pressure mechanism was rejected on the basis that the wavelength of an acoustic wave is far greater than the corneocyte and intercellular lipid areas to produce local mechanical strains. This is no longer the case of the very high impulse photoacoustic waves because its acoustic wavelength is around $15\ \mu\text{m}$, which implicates a direct interaction with the SC structure.

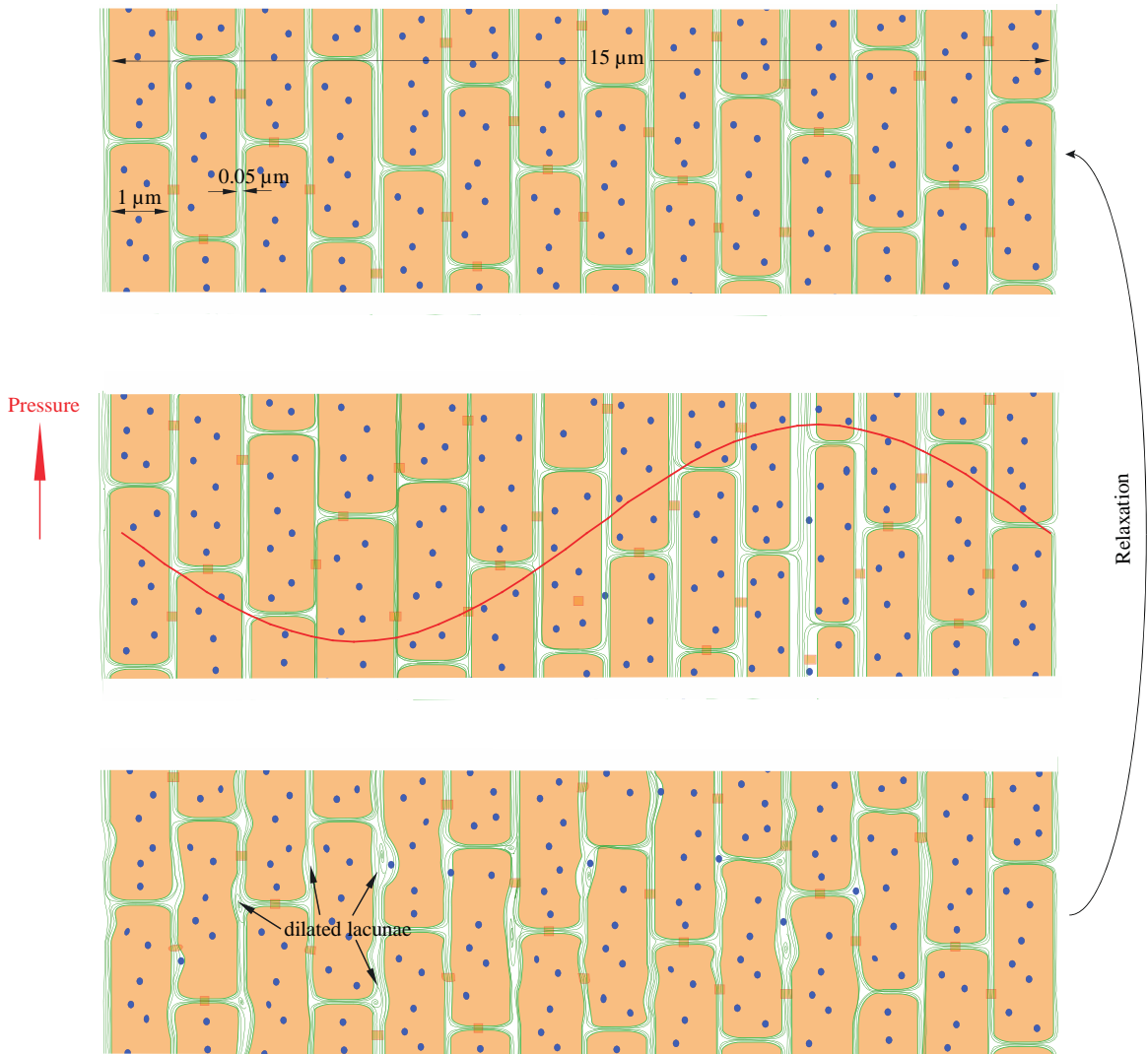


Fig. 8.11 - Rationalization of the increased skin permeability following the application of photoacoustic waves with frequencies above 100 MHz. Top: unperturbed stratum corneum, shown as 14 layers of tightly packed corneocytes with hydrophilic domains (blue) separated by intercellular lipid lamellae (green), where the diameter of the corneocytes ($40\ \mu\text{m}$) is not represented to the scale. Middle: Compressive front and rarefaction tail of a high-impulse photoacoustic wave traversing the stratum corneum and producing very fast pressure changes. Bottom: perturbed stratum corneum with expansion of the lacunar spaces where the organization of the lipid matrix is changed but takes some time to relax to the original structure, which facilitates the diffusion of drugs through the expanded spaces.

An acoustic wave propagating across media (corneocyte and intercellular space) with different acoustic impedances results in multiple reflections and changes in its shape, which, at a given point, may displace the regions of the medium connected by the weaker intermolecular forces. If we focus on one spatial location, the multiple reflections across the SC may sum up as an strong displacement gradient, which may exceed the tensile strength that keeps the lipid arrangement in the intercellular spaces [195, 196]. The PA waves interaction with skin lipids result in mechanical displacements in the SC intercellular organization, which arise from subtle changes, such as a phase shift in one bilayer, because two acoustics waves have passed in the local structure. Although, the biophysical mechanism remains largely unknown at this time, the work presented here clearly identifies the increase in the lipid fluidity in a single lipid model (by the temperature effect), upon photoacoustic waves application. Additionally, the radiation pressure mechanism can explain the results of Doukas et al [144], where electronic microscopy studies unveiled lacunar expansions of the intercellular spaces of the SC.

The path through the intercellular lipids can be facilitated by expanding the intracellular domains of the stratum corneum, and the transdermal delivery of large drugs may be enhanced with such an expansion [144]. High-impulse shock waves are believed to use this mechanism to increase the permeability of the skin [144], though, the current scientific knowledge in this area is ambiguous, and this work represents the first approach to clear out the exact mechanism of acoustic energy interaction with SC lipids.

6. References

- [1] B.W. Barry, Novel mechanisms and devices to enable successful transdermal drug delivery. *Eur. J. Pharm. Sci.*, 14, (2001) 101-114.
- [2] R. Wickett, M. Visscher, Structure and function of the epidermal barrier. *Am. J. Infect. Control*, 34 (2006) 98-110.
- [3] R. Paus, What is the 'true' function of the skin? *Exp. Dermatol.*, 11 (2002) 159-187.
- [4] K.A. Walters, *Dermatological and transdermal formulations*, Marcel Dekker, New York, 2002.
- [37] M. Ponc, A. Weeheim, P. Lankhorst, P. Wertz, New acylceramide in native and reconstructed epidermis. *J. Invest. Dermatol.*, 120 (2003) 581–588.
- [38] I. Hatta, N. Ohta, S. Ban, H. Tanaka, S. Nakata, X-ray diffraction study on ordered, disordered and reconstituted intercellular lipid lamellar structure in stratum corneum. *Biophys. Chem.*, 89 (2001) 239-242.
- [94] V.P. Shah et al, Bioequivalence of topical dermatological dosage forms – methods of evaluating bioequivalence. *Pharm. Res.*, 15 (1998) 167-171.
- [133] M.W. Sigrist, Laser generation of acoustic waves in liquids and gases, *J. Appl. Phys.*, 60 (1986) 83-121.
- [144] A.G. Doukas, N. Kollias, Transdermal drug delivery with a pressure wave. *Advanced Drug Delivery Reviews*, 56 (2004) 559–579.
- [161] J.P. Simonin, On the mechanisms of in vitro and in vivo phonophoresis. *J. Controlled Release*, 33 (1995) 125-141.
- [195] NCRP, Exposure criteria for medical diagnostic ultrasound. II. Criteria based on all known mechanisms, in, National Council on Radiation Protection and Measurements. Bethesda MD, 2002, Report No.140.
- [196] M.H. Niemz, *Laser-Tissue Interactions*, 2007, Springer, Berlin.
- [213] Carlos Serpa, G. F. F. Sá, Luis G. Arnaut, Intense, high-frequency pressure waves produced with low laser fluences. *Proc. SPIE*, 8207A, 12 (2012) 1-6.
- [214] I.H. Blank, J. Moloney, A.G.E.I. Simon, C. Apt, The diffusion of water across the stratum corneum as a function of its water content. *J. Invest. Dermatol.* 82 (1984) 188-194.
- [215] K.P. Wilhelm, A.B. Cua, H.I. Maibach, Skin aging. Effect on transepidermal water loss, stratum corneum hydration, skin surface pH, and casual sebum content. *Arch. Dermatol.* 127 (1991) 1806-1809.
- [216] Y.N. Kalia, I. Alberti, N. Sekkat, C. Curdy, A. Naik, R.H. Guy, Normalization of stratum corneum barrier function and transepidermal water loss in vivo. *Pharm. Res.* 17 (2000) 1148-1150.

- [217] M. Heenen, P.U. Giacomoni, P. Golstein, Erythema, a link between UV-induced DNA damage, cell death and clinical effects?. *Compreh. Series Photosciences*, 3 (2001) 277-285.
- [218] P. Simonen *et al*, Do inflammatory processes contribute to radiation induced erythema observed in the skin of humans. *Radiotherapy and Oncology*, 46 (1998) 73-82.
- [219] C.S. Hamilton, Underprediction of human skin erythema at low doses per fraction by the linear quadratic model. *Radiotherapy and Oncology*, 40 (1996) 23-30.
- [220] J. Levin, H. Maibach, The correlation between transepidermal water loss and percutaneous absorption: an overview. *J. Control. Resease*, 103 (2005) 291-299.
- [221] J. Pinnagoda, R.A. Tupker, T. Agner, J. Serup, Guidelines for transepidermal water loss (TEWL) measurement. *Contact Dermatitis*, 22 (1990) 164-178.
- [222] P. Holstein, P.E. Nielsen, J.P. Barras, Blood Flow Cessation at External Pressure in the Skin of Normal Human Limbs. *Microvascular Research*, 17 (1979) 71-79.
- [223] S.M. Ball, J. Caussin, S. Pavel, J.A. Bouwstra, In vivo assessment of safety of microneedle arrays in human skin. *Eur. J. Pharm. Sc.*, 35 (2008) 193-202.
- [224] G.L. Li *et al*, Cutaneous side-effects of transdermal iontophoresis with and without surfactant pretreatment: A single-blinded, randomized controlled trial. *Br. J. Dermatol.*, 153 (2005) 404-412.

IX

**Transdermal Drug
Delivery**

1. Introduction

The ideal drug candidates for passive transdermal delivery meet the following criteria: relatively small molecular weight (< 500 Da), octanol-water partition constant K_{OW} of moderately lipophilic molecules ($1 < \log K_{OW} < 3$), and a small number of pendant groups capable of hydrogen bonding (5) [1, 225]. The physical action of a photoacoustic wave with a high rate of pressure increase *per* laser pulse should improve transdermal drug delivery independently of molecular size. However, the exposure of the lipid lamellae to the pressure increase results in a rapid recovery of the barrier function (chapter 7 and 8), which means that the passive diffusions laws will govern the diffusion and distribution into deeper layers [1, 73]. The enhancement effect of the PA waves, in transdermal drug delivery was evaluated using photosensitizers and a large protein (Green Fluorescence Protein - GFP).

The photosensitizers currently used in photodynamic therapy (PDT) are porphyrin derivatives with molecular weights higher than 500 Da (> 1000 Da), and are not expected to diffuse extensively and rapidly through the skin. Nevertheless, the treatment of skin cancers, such as actinic keratosis or basal cell carcinoma does not require the penetration of the drug through all the skin (including the dermis) [226]. In fact, for such conditions, an intradermal delivery, rather than a transdermal delivery, is sought. The novel sensitizers developed by M.M. Pereira and Luis G. Arnaut [227-229] include stable bacteriochlorins with extremely high absorption in the visible and near-infrared. These new molecules offer an opportunity for the photoacoustic waves system to enhance the skin delivery of molecules not expected to permeate with high fluxes through the skin. This goal is preceded of extensive work on the development of suitable formulations that serve a dual objective: good acoustic coupling between the skin and the distal end of the PA waves system and to maximize the transdermal delivery. These studies include formulation optimization method (factorial design), different absorption enhancers and multiple observation techniques (fluorescence microscopy and steady-state fluorescence). Consequently, the experimental design considers an *ex-vivo* skin delivery, in which several laser energies and the best piezophotonic materials were tested to determine the limits of the enhancement effect of the sensitizers transdermal delivery. Furthermore, the application of these protocols to an *in vivo* model of human skin (the minipig) gives a perspective of the value of the PA waves transdermal system. The size restriction in transdermal delivery challenges the development of effective transdermal technologies, and is related to the limited size of the available intercellular spaces of the stratum corneum. The formation of transient channels in the SC by the PA waves should

facilitate the diffusion of large molecules. This hypothesis is tested with a fluorescent protein, GFP, because it is easy to follow its diffusion in the skin by fluorescence microscopy.

2. Formulation Optimization of the Photosensitizers

The aim of the present study is to select an appropriate vehicle to enhance percutaneous absorption of the sensitizers developed by M.M. Pereira and Luis G. Arnaut [227-229]. This screening should assess the ability of different solvents to enhance the permeation of these molecules across the skin of the selected animal model: the minipig.

The ability of absorption enhancers, such as DMSO, oleic acid and Azone (in combination with propylene glycol - PG) to improve the *ex-vivo* skin diffusion of the sensitizers was screened using the factorial design technique. The selection of Azone and oleic acid was based on their penetration enhancing properties, mechanism of action and the synergistic effect demonstrated in other studies with PG [230-237]. The Azone ability to partition into the lipid lamellae of the SC relates with a fluidizing effect responsible for the drug permeation enhancement [233]. Oleic acid acts directly on the lipid regions of the SC, promoting phase separation of the intercellular lamellae, thus improving drug pathways [230-232]. DMSO inserts near the polar head regions of the intercellular lipids causing a perturbation in their packing, and an extraction/removal of the ceramides [231]. The choice of these absorption enhancers takes into account their action in the skin and literature reports, as well as their physicochemical properties, namely the lipophilicity (octanol/water partition coefficient – K_{OW}). Azone is a notable lipophilic enhancer ($\log K_{OW} > 6$), oleic acid a moderate one ($\log K_{OW} \sim 2$) and DMSO a highly hydrophilic one ($\log K_{OW} = -1.35$). Consequently, they offer a wide range of formulation properties to maximize passive permeation (table 9-1).

Table 9-1 – Excipients percentage in the sensitizer formulations (A to H) produced for the factorial design experiments.

Constituents (% w/w)	Gel code							
	A	B	C	D	E	F	G	H
Sensitizer	0.1	0.3	0.1	0.3	0.1	0.1	0.3	0.3
Ethanol	9	10.8	9	8.8	11	11	8.8	10.8
Propylene Glycol	32	32	36	36	32	36	32	36
Enhancer (Azone)	4	2	4	4	2	2	4	2
Distilled water	6	6	0	6	0	6	0	0
Gel base	44.9	44.9	44.9	44.9	44.9	44.9	44.9	44.9
Viscosity/ Pa.s	$1.8 \cdot 10^5$	$1.0 \cdot 10^5$	$6.6 \cdot 10^4$	$6.5 \cdot 10^4$	$6.8 \cdot 10^4$	$1.2 \cdot 10^5$	$5.9 \cdot 10^4$	$1.3 \cdot 10^5$

Remark: in the preparation of gels with DMSO and oleic acid we notice that no gel phase was formed with more than 2% of these enhancers. For A, C, D and G we use 2% and for B, E, F and H we use 0,5%. The compensation was done in the ethanol percentage.

Propylene glycol acts as cosolvent of drugs and absorption enhancer [230] in dermatological formulations. Its action increases the permeation fluxes of drugs alone or in combination with other molecules [230]. The mechanism of PG action in the intercellular spaces consists in its incorporation within the head group of the lipids by replacing bound water [230] or by inducing a keratin conformational change, which would alter its crystalline state and enhance the transcellular pathway [234].

The porphyrin derivatives are not expected to permeate extensively across the stratum corneum without help. As a result, a prolonged incubation time (2 hours) assures a sufficient amount of the compound for subsequent analysis. The interpretation of the DMSO, oleic acid and Azone effect in the sensitizer's flux across skin was assessed by the factorial design. The use of factorial design in the optimization of topical formulations enables the simultaneous evaluation of the influence of various factors and their respective interactions [238-242]. A mathematical equation derived from the experimental can be used to predict the response of a combination of factors not tested experimentally, inside the experimental domain [240]. This model can also be used to build response surfaces [240, 242] that enable us to visualize how the variables influence the overall response (*EF* represents the *enhancement factor*). In a first step, various formulations were prepared with different absorption enhancers and different concentration of the main formulations excipients (sensitizer, water and PG) – table 9-1. The assessment of sensitizer diffusion across the minipig epidermis relies in fluorescence microscopy.

The experimental design considers the fluorescence signal of the sensitizer in the skin layers as the overall response. The modulation of the main excipients concentration, water, propylene glycol and sensitizer corresponds to a three level of independent variables. From the response surface of those three variables, 3^2 factorial design, a non-linear quadratic model can be extracted and calculated according to [240, 242]:

$$y = \beta_1x_1 + \beta_2x_2 + \beta_3x_3 + \beta_{12}x_1x_2 + \beta_{13}x_1x_3 + \beta_{23}x_2x_3 + \beta_{123}x_1x_2x_3 + \varepsilon \quad (9.1)$$

where y is the response variable, $x_{1,2,3}$ are the independent variables (concentration of water, sensitizer and enhancer), and ε and $\beta_{1,2,3}$ the regression coefficients corresponding to the constant, the main effects, quadratic terms and interaction, respectively.

2.1 Results and Discussion

A 3^2 factorial design allows the evaluation of the excipients effect (water, sensitizer and propylene glycol), but also the contribution of the three absorption enhancers, DMSO,

oleic acid and Azone (table 9-1). This design results in an optimized formulation capable of delivering a high amount of sensitizer across the skin and to promote a good acoustic coupling between the PA waves transdermal system and the skin. Based on table 9-1 and 9-2, eight formulations were prepared by varying each factor individually, for each level. A 4% concentration of DMSO and oleic acid is incompatible with the formation of a gel, and their concentrations were reduced to half. The viscosity of a transdermal formulation should be between $[10^3, 10^5]$ Pa*s for assuring adhesion and remaining in the skin upon topical application [4, 243, 244].

Table 9-2 - Dependent and independent variables and respective levels used in the construction of a partial 3^2 factorial design.

Variables	Levels	
	Low (-1)	High (+1)
Concentration of Water (%)	34%	40%
Concentration of Sensitizer (%)	0.1%	0.3%
Concentration of PG (%)	32%	36%
Response	Fluorescence Microscopy	

The performance of the *ex-vivo* permeation studies results in the fluorescence microscopy images, such as those of figure 9.1 to 9.3. A grading system was established to create the surface response using a grading scale (see details in chapter 12). The scale clarifies the sensitizer permeation from 0 (no permeation) to 5 (maximum permeation) considering the amount of sensitizer delivered through the minipig epidermis and its distribution across the epidermis.

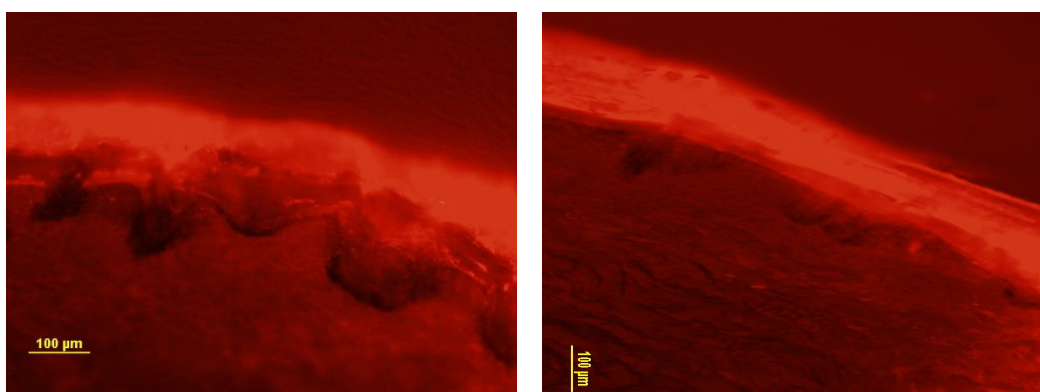


Fig. 9.1 – Representative fluorescence microscopy images of the sensitizer distributed in the minipig epidermis for 2 hours, when various formulations containing DMSO as absorption enhancer is used.

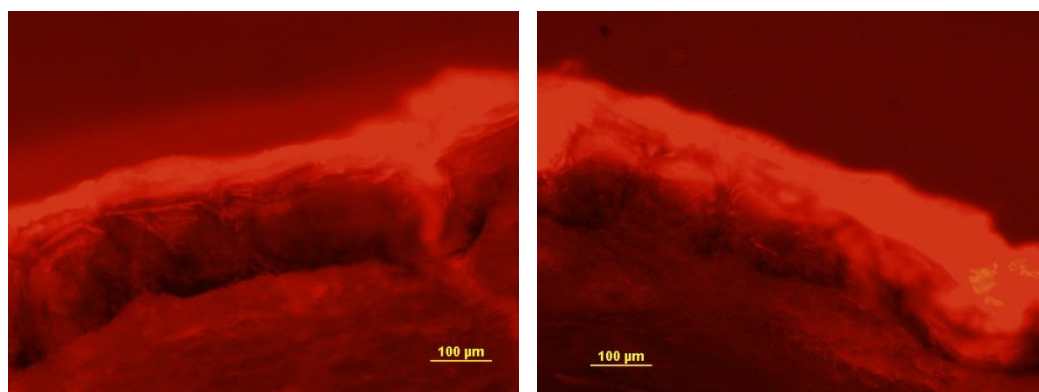


Fig. 9.2 – Representative fluorescence microscopy images of the sensitizer distributed in the minipig epidermis for 2 hours, when various formulations containing oleic acid as absorption enhancer is used.

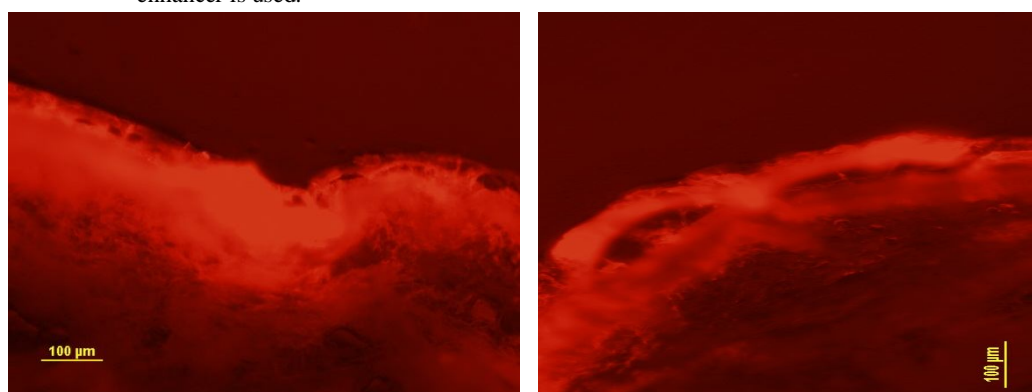


Fig. 9.3 – Representative fluorescence microscopy images of the sensitizer distributed in the minipig epidermis for 2 hours, when various formulations containing Azone as absorption enhancer is used.

The application of a grading scale to the fluorescence microscopy images allowed the determination of the response surface models depicted in figures 9.4 to 9.6, for the DMSO, oleic acid and Azone, respectively. These surfaces are constructed using a standard approach [240, 242], as a function of the water, sensitizer and propylene glycol concentrations with the following factorial design equations derived from the grading scale:

$$\begin{aligned}
 Y_{\text{DMSO}} &= 2.4+0.1[\text{PG}]-0.9[\text{H}_2\text{O}]-0.2[\text{Sens}]-0.2[\text{PG}][\text{H}_2\text{O}]-0.5[\text{PG}][\text{Sens}]-0.3[\text{H}_2\text{O}][\text{Sens}]-0.02[\text{PG}][\text{H}_2\text{O}][\text{Sens}] \\
 Y_{\text{Oleic Acid}} &= 4.9+0.61[\text{PG}]+0.07[\text{H}_2\text{O}]-0.2[\text{Sens}]-0.1[\text{PG}][\text{H}_2\text{O}]+0.8[\text{PG}][\text{Sens}]-0.2[\text{H}_2\text{O}][\text{Sens}]+0.3[\text{PG}][\text{H}_2\text{O}][\text{Sens}] \\
 Y_{\text{Azone}} &= 3.3+0.6[\text{PG}]-0.2[\text{H}_2\text{O}]-0.3[\text{Sens}]+0.2[\text{PG}][\text{H}_2\text{O}]+0.4[\text{PG}][\text{Sens}]-0.3[\text{H}_2\text{O}][\text{Sens}]-0.09[\text{PG}][\text{H}_2\text{O}][\text{Sens}] \quad (9.2)
 \end{aligned}$$

In this design, the use of the coded levels -1 and $+1$ of the independent variables (minimum and maximum values of the excipients concentration) allows obtaining the related regression coefficients for all the types of prepared formulations [240, 242].

Additionally, this methodology facilitates the interpretation of the results by relevance and without misleading deductions from the experimental results [239].

The polynomial equations show the quantitative effect of the excipients concentration on the permeation enhancement of the sensitizer and indicate how their interactions affect the overall skin diffusion. The coefficients with only one variable represent the main effect of the concentration variation itself, and the association of more than one coefficient represents how the response varies with multiple excipients concentration. A positive sign specifies an increase in the response produced by that independent variable or a synergistic effect produced by the combination of two or more independent variables. An absolute term with a high value gives an indication of a higher importance of the excipient in the permeation enhancement of the sensitizer [238-242].

In the surface response figures (figure 9.4 to 9.6), the representation of the water content relates to the water percentage in the gel base for facilitating the graphic visualization. The water percentage in the final transdermal formulations varies from 34 and 40% (details in the experimental section).

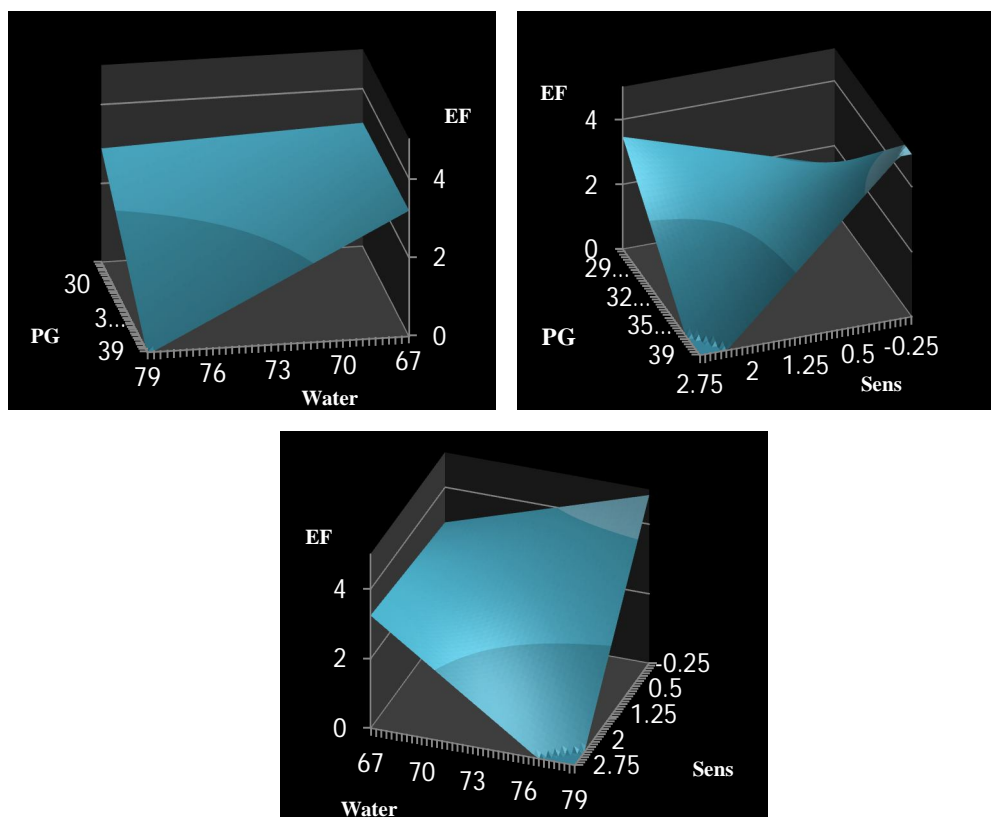


Fig. 9.4 – Estimated response surface illustrating the effect of water, sensitizer and propylene glycol concentrations in the accumulation of the sensitizer in the minipig epidermis when a formulation containing DMSO is used. EF stands for enhancement factor.

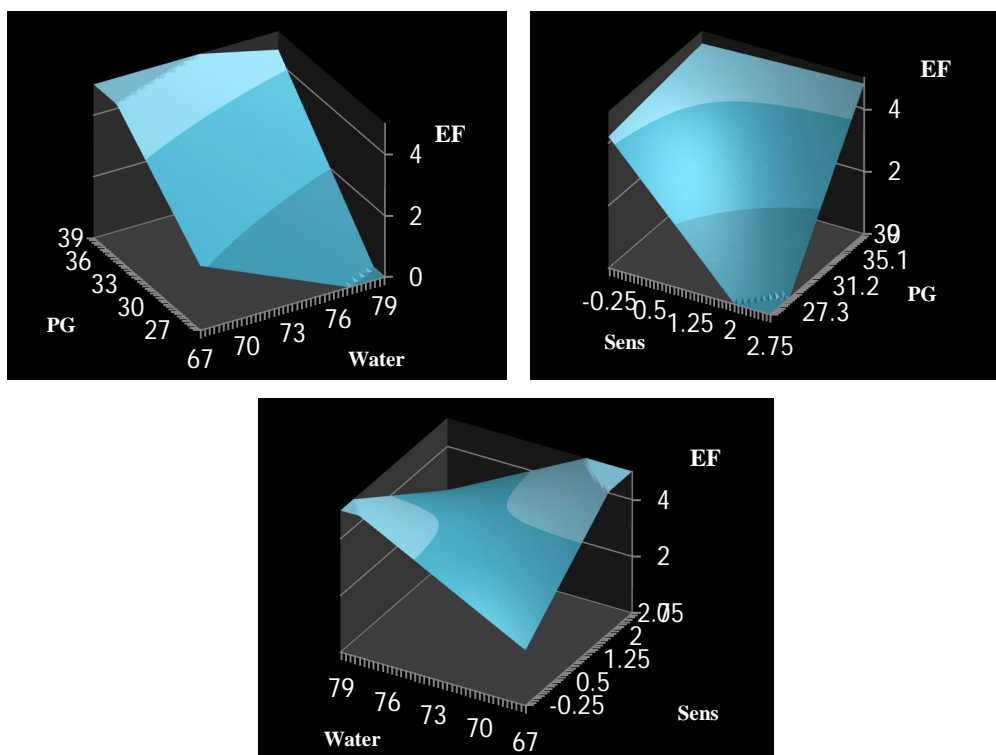


Fig. 9.5 – Estimated response surface illustrating the effect of water, sensitizer and propylene glycol concentrations in the accumulation of the sensitizer in the minipig epidermis when a formulation containing oleic acid is used.

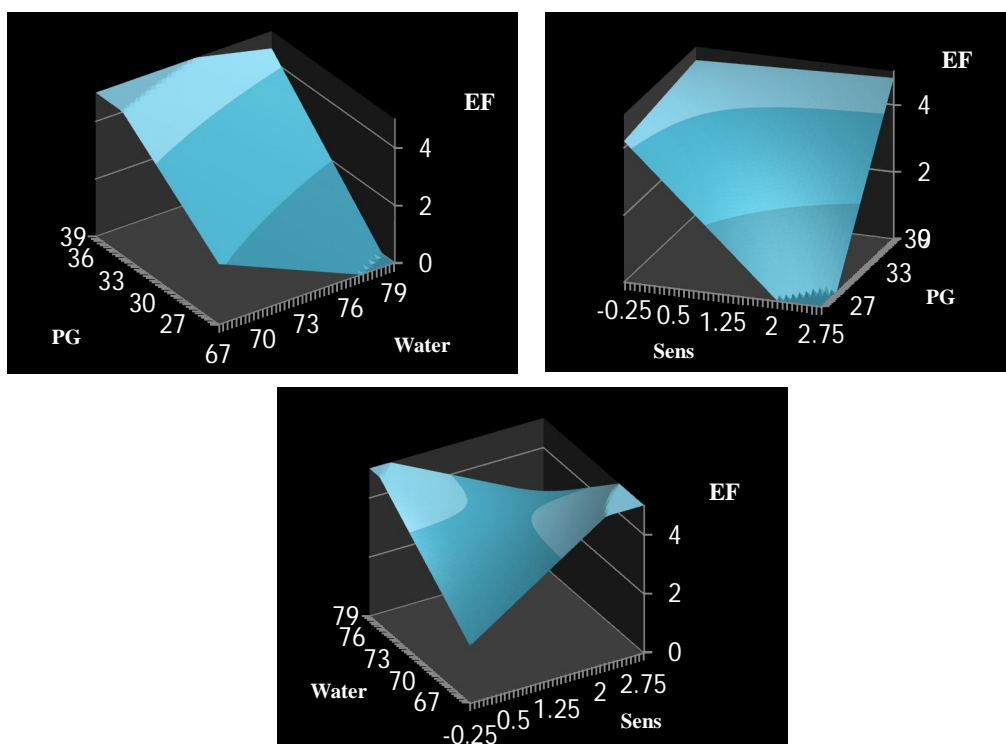


Fig. 9.6 – Estimated response surface illustrating the effect of water, sensitizer and propylene glycol concentrations in the accumulation of the sensitizer in the minipig epidermis when a formulation containing Azone is used.

From the analysis of the polynomial equations and the response surfaces, it is clear that the PG action by itself is capable of enhancing sensitizer drug delivery. This result is in agreement with previous results because this sensitizer is of moderate lipophilicity, $\log K_{O/W}$ around one [245]. This implicates favorable formulation-skin interactions for moderate lipophilic absorption enhancers, such as PG, because it facilitates the accumulation in the lipid environment of the stratum corneum. The regression coefficients for water exhibit a decrease in the sensitizer delivery for the formulations containing Azone and DMSO, highly lipophilic and hydrophilic absorption enhancers, respectively. This also confirms that formulations with moderate lipophilicity are more suitable for delivering amphiphilic drugs. The sensitizer regression coefficients do not provide a clear insight on its role; however, we can observe from the surface responses that high water content plus the sensitizer maximize the permeation (unfavorable hydrophilic environment in the formulation should enhance drug transport to the skin). The combination of independent variables leads to some conclusions, namely that [PG][H₂O] increases the sensitizer delivery in lipophilic formulations (Azone and oleic acid), and the opposite in the DMSO formulations.

The ability to fluidize the lipid lamellae of SC and, in that way, increase the drug permeation through the skin is reported for oleic acid and Azone with moderate lipophilic compounds ($\log K_{O/W} < 3$) [1]. For highly hydrophilic enhancers (DMSO), the partition to the SC is extremely small, which reduces the extraction or disruption of the intercellular regions and negatively affects the sensitizer transport across it. The polynomial equations and the surface response curves confirm these findings because there is a reduction in the sensitizer permeation across the minipig skin correlated to a more favorable environment in the formulation. This fact derives from the negative term [PG][Sens], in the DMSO polynomial equation. Furthermore, it is not clear that the sensitizer concentration itself maximizes or reduces its diffusion and distribution across the minipig skin.

The rationalization of the sensitizer permeation enhancement relates with the vehicles transport (of the formulations excipients) to the intercellular spaces within the stratum corneum. The results presented here confirm that formulations with moderate lipophilicity are capable of enhancing sensitizer diffusion in a larger extent. The qualitative analysis by fluorescence microscopy is particularly useful to evaluate the sensitizer distribution across the minipig skin. Nevertheless, a quantitative approach should provide further insight, on how the formulation manipulation may be optimized. For this quantitative approach, we developed a specific extraction procedure for the sensitizers considering the difficulties on separating a pure sample arising from the skin, upon topical application (details in chapter 12). The characteristic absorption and

fluorescence of these sensitizers, in the near-infrared region of the electromagnetic spectrum, allows for their quantification using steady-state fluorescence emission.

In figure 9.7, there is a graphic representation of the sensitizer amounts *per* cm², after the application of the transdermal formulations containing DMSO, oleic acid and Azone (table 9-1). The quantification of sensitizer recovered from the *ex-vivo* testing derives from the extraction method developed with after the calibration curve (figure 9.7 left).

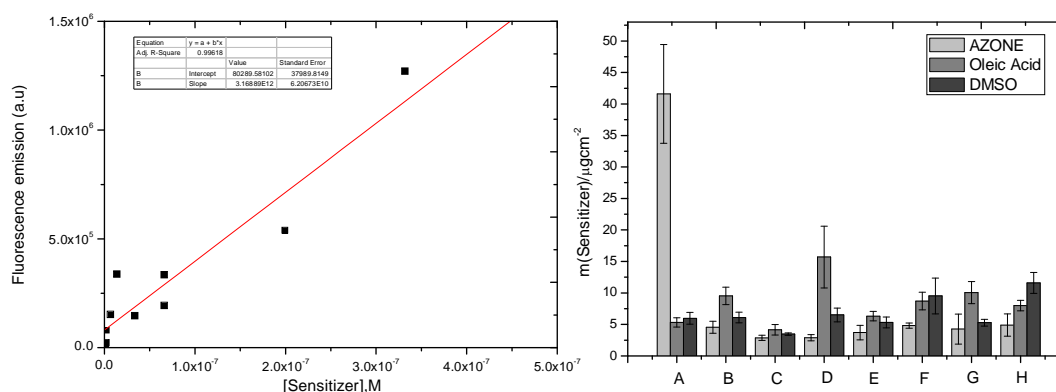


Fig. 9.7 – **Left)** Fluorescence calibration curve of the sensitizer in dichloromethane. **Right)** Amount of sensitizer extracted from the 1 cm² of minipig skin after 2 hours for the formulations containing DMSO, oleic acid and Azone. All essays were repeated 4 times.

The fluxes of sensitizer determined by the extraction procedure confirm the factorial design qualitative analysis because the more lipophilic formulations (Azone and oleic acid) enhance drug delivery by a factor of 2 (in average), if compared to the DMSO formulations. In detail, the formulations with the maximum concentration of PG are the most effective vehicles for the sensitizer delivery; except for formulation G, where the sensitizer concentration compensates the lower content of PG (this confirms the conclusion $[PG][Sens] > 0$ of the factorial design). In clear correspondence to the qualitative results, the water concentration does not play a significant role in the enhancement of sensitizer permeation, at these concentrations. A more substantial variation in the water concentration is not possible because otherwise the formulation would not be suited for TDD (viscosity between $[10^3, 10^5]$ Pa*s – table 9-1). Additionally, figure 9.7 right shows that the formulations containing 0.3% of sensitizer maximize its diffusion across the SC, despite variations in the formulations excipients, which clarifies a remaining doubt from the factorial design qualitative analysis.

The use of the factorial design technique and of the extraction method leads to the conclusion that the best formulation for the sensitizer transdermal delivery contains the lipophilic absorption enhancers (Azone and oleic acid) and a maximum propylene glycol and sensitizer concentrations (irrespective to the water content).

3. *Ex-Vivo* Transdermal Sensitizer Delivery by the PA Waves

The *ex-vivo* evaluation of the enhancement of transdermal drug delivery due to the application of photoacoustic waves was performed using the formulation D, with 0.3% of sensitizer, 40% of water, 36% of propylene glycol and 4% of Azone. The piezophotonic material used in these experiments was Mn-TUP incorporated in a polystyrene substrate with a linear absorption coefficient of 290 cm^{-1} . The laser impinged in the piezophotonic material for 2 minutes at 532 nm, with 3 sub-ablation energies: [10, 25, 50] mJ/cm^2 (figure 9.8).

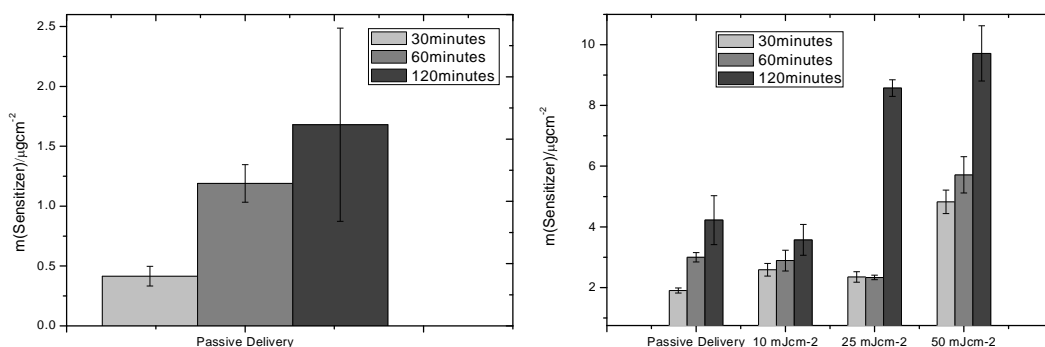


Fig. 9.8 – Left) Passive delivery of the sensitizer with formulation D and an incubation time of [30, 60 and 120] minutes repeated 6 times. **Right)** Amount of sensitizer extracted from the minipig skin with formulation D when passive delivery and PA waves delivery experiments were done in collinear skin sites for reporting the same SC barrier. The laser impinged in a Mn-TUP piezophotonic material of polystyrene with 290 cm^{-1} for 2 minutes at 532 nm. All essays were repeated 4 times.

The passive delivery of the sensitizer (figure 9.8 left) results in the accumulation of a few tenths of micrograms in the minipig epidermis. For an incubation time of 120 minutes, this quantity increases to $1.5 \mu\text{g}/\text{cm}^2$. In figure 9.8 right, the photoacoustic waves transdermal delivery leads to an increase in the recovered sensitizer mass, if compared to the passive delivery studies, of 4 to $10 \mu\text{g}/\text{cm}^2$ (at 120 minutes). A direct comparison between the passive delivery studies presented in figure 9.8 left and right reveals the importance of performing the experiments, in collinear skin areas, to maintain the same SC barrier and physiology. The passive delivery in figure 9.8 left was performed in a different minipig skin sample, while all the experiments in figure 9.8 right were done in another skin sample, but in collinear regions. The application of photoacoustic waves enhances sensitizer delivery, specifically for laser energies of $50 \text{ mJ}/\text{cm}^2$, where the enhancement reaches a 3 to 4 fold, if compared to the passive delivery, for all the

incubation times. These results demonstrate that the laser energy is a relevant factor for enhancing the sensitizer skin delivery because the generation of acoustic transients with higher pressure amplitudes increases the sensitizer delivery. The duration of the application of the PA waves application, 2 minutes, was selected on the basis of the results reported in chapter 7 and 8.

3.1 Qualitative Study of the Best Energy in the PA Waves Delivery

The extraction procedure supported that the energy required for the generation of photoacoustic waves capable of dramatically enhance the sensitizer delivery is 50 mJ/cm^2 . Confocal microscopy offers the possibility to visualize the sensitizer diffusion after 20 minutes following passive delivery or active delivery with 50 mJ/cm^2 , with the same piezophotonic material and an application time of 2 minutes (figure 9.9).

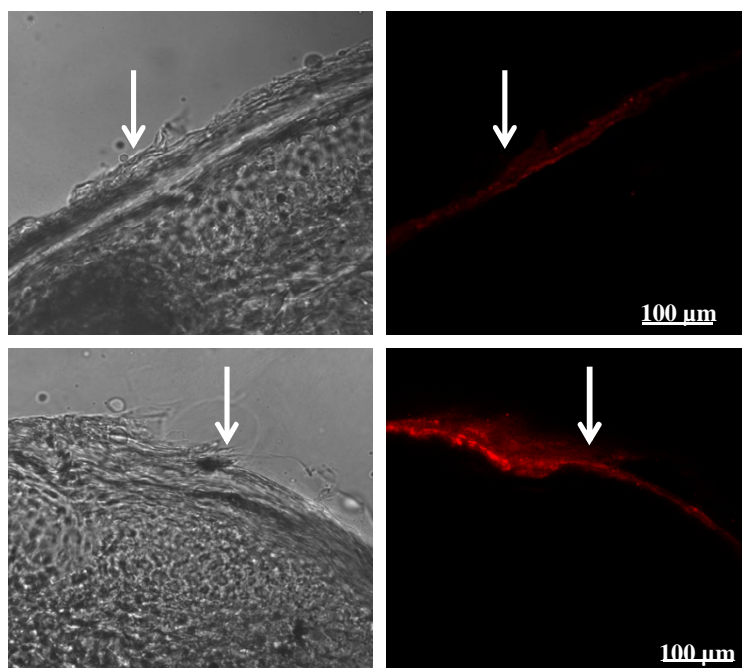


Fig. 9.9 – Representative confocal fluorescence images for the passive delivery of the sensitizer (top) and PA waves active delivery (down). The confocal fluorescence images have a transmission (left) and a fluorescence (right) image. The incubation time was 20 minutes after the laser impinged in a Mn-TUP piezophotonic material of polystyrene with $\mu_a = 290 \text{ cm}^{-1}$, at 532 nm with 50 mJ/cm^2 and for 2 minutes.

The depth of the sensitizer distribution, in the minipig epidermis, increases substantially after the PA waves delivery ($\sim 50 \mu\text{m}$), if compared to the passive delivery ($10 \mu\text{m}$ – restricted to the SC). Also, there is an increase in the sensitizer fluorescence intensity from the passive to the PA waves transdermal delivery. The results presented in this section illustrated the use of photoacoustic waves generated by Mn-TUP incorporated in a polystyrene substrate to promote transdermal sensitizer delivery. The following study

clarifies the use of manganese derivatives photoacoustic references incorporated in titanium dioxide to promote the sensitizer delivery with the same transdermal formulation.

3.2 Transdermal Delivery by the PA Waves using TiO₂ Substrate

The characterization of the photoacoustic waves, in chapter 6 showed the efficacy of the manganese porphyrin in transforming the laser light into acoustic energy, for both the polystyrene substrate and titanium dioxide. Figure 9.10 evaluates the benefit introduced by the reduced thickness of TiO₂ (7.5 μm) in the ex-vivo sensitizer transdermal delivery with formulation D (20 minutes of incubation time). The PA waves were generated by the absorption of 12 laser pulses of 355 nm laser light of 10 mJ/cm^2 by the photoacoustic reference Mn-TPPS.

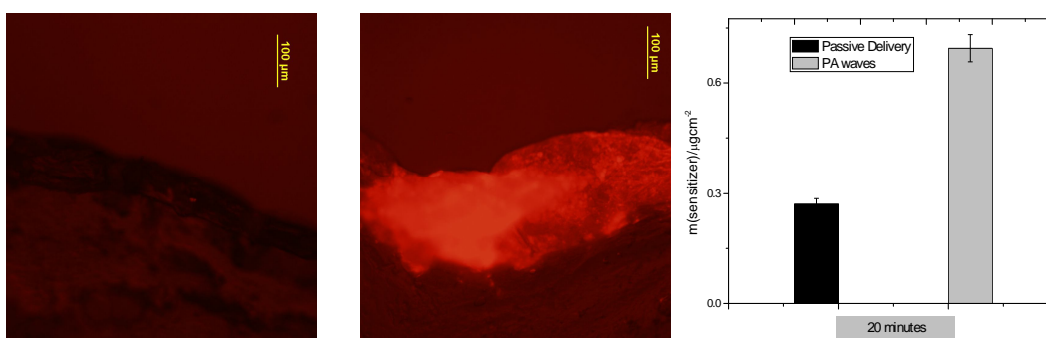


Fig. 9.10 – Representative microscopy fluorescence images for the passive delivery of the sensitizer (left) and PA waves active delivery (right). The PA delivery was produced with Mn-TPPS piezophotonic film in TiO₂ ($\mu_a = 670 \text{ cm}^{-1}$ – thickness of 7.5 μm) with 12 laser pulses at 355 nm with laser fluences of 10 mJ/cm^2 , and an incubation time of 20 minutes. In the extraction figure (right), the essays were repeated 4 times.

In figure 9.10 A right, the depth of the sensitizer diffusion and distribution extends over the entire minipig epidermis after PA wave delivery ($\sim [70, 100] \mu\text{m}$), whereas the passive delivery does not lead to observable sensitizer diffusion into the skin. These results confirm the importance of the reduced thickness of the piezophotonic materials, in the magnitude of the acoustic transients. In figure 9.10 B, the sensitizer mass extracted from the skin corroborates the previous results, with an enhancement factor up to 3 times, using the Mn-TPPS piezophotonic materials based in nanoporous titanium dioxide, as a photoacoustic reference.

4. *Ex-Vivo* Transdermal Sensitizer Delivery by PA and Shock Waves

The pressure waves generated by ablation of aryltriazenes polymers are 50 times higher than those of piezophotonic materials (chapter 6). Nevertheless, the previous results indicate that the sensitizer permeation, across the stratum corneum, was enhanced by photoacoustic waves. The experimental plan described in table 9-3 was designed to evaluate the effect of shock waves, under similar conditions to the PA waves transdermal system, in the sensitizer diffusion in the minipig skin. The sensitizer delivery used optimized formulation D.

Table 9-3 – *Ex-vivo* transdermal sensitizer delivery by the PA and shock waves.

Objective	Passive	Parameters	PA Waves	Shock Waves
Quantitative (Extraction) and Qualitative (Microscopy) analysis	20 minutes of incubation time	Thickness/ μm	38	< 5 μm
		$\lambda_{\text{exc}}/\text{nm}$	355	355
		Abs	1.4	1.1
		μ_a/cm^{-1}	368	2200
		Laser Fluence/ mJcm^{-2}	[10,15,50]	[10,15,50]

The sensitizer delivery using the photoacoustic waves and shock waves did not reveal significant differences in the amounts extracted from the skin after 20 minutes of incubation (figure 9.11). Both deliveries present an enhancement factor up to 3 times, when compared to the passive delivery ($0.38 \mu\text{g}/\text{cm}^2$). Moreover, in the case of shock waves, there is a reduction in the sensitizer skin permeation, at higher laser energies. This fact may relate to the aryltriazene ablation threshold because, after its surpass ($20 \text{ mJ}/\text{cm}^2$ – chapter 6), there is a visible destruction of the polymer structure, which should reduce the shock waves intensity (destructive nature of ablative methods for generating acoustic transients [133, 144]).

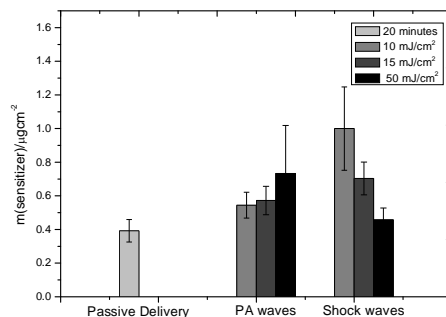


Fig. 9.11 – Sensitizer extraction after passive delivery with formulation D at incubation time of 20 minutes compared with 20 minutes of incubation time of PA waves and shock waves essays. All essays were repeated 4 times. The PA waves were generated upon irradiation of Mn-TUP incorporated in polystyrene with $\mu_a = 368 \text{ cm}^{-1}$, with light of 355 nm for 2 minutes. The shock waves used the aryltriazenes polymers with $\mu_a = 2200 \text{ cm}^{-1}$ and with laser light of 355 nm for 2 minutes.

4.1 Qualitative Analysis of the Transdermal Sensitizer Delivery

From the fluorescence microscopy analysis, significant differences emerge after the transdermal sensitizer delivery with the PA waves and the shock waves (figure 9.12 to 9.14). The following images are in excellent agreement with the extraction results, where the permeation with the 50 mJ/cm² PA waves gave the best sensitizer diffusion and distribution. These results confirm that the transdermal sensitizer delivery using shock waves does not correlate with the shock wave peak increase (chapter 6).

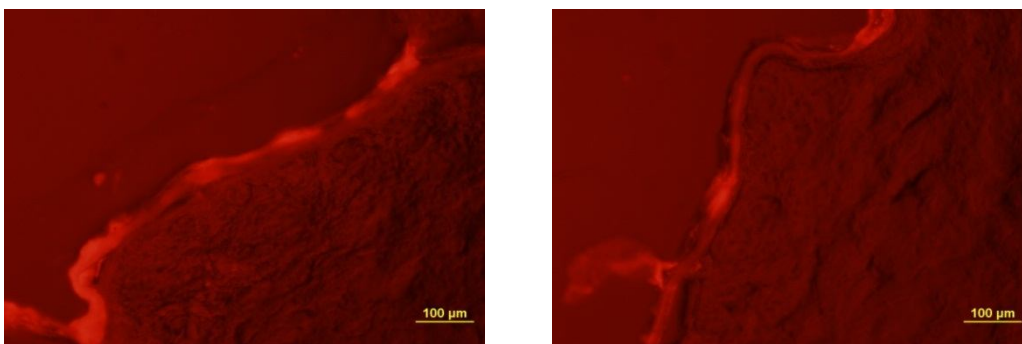


Fig. 9.12 – Representative fluorescence microscopy images of the 20 minutes sensitizer distributed in the minipig epidermis after passive delivery with formulation D.

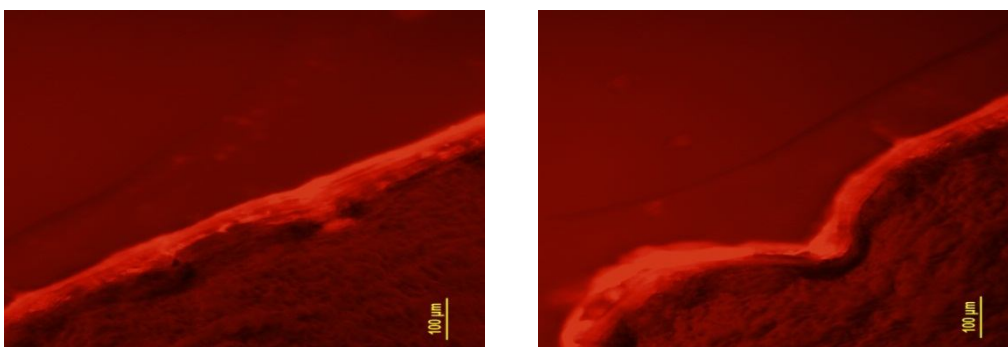


Fig. 9.13 – Representative fluorescence microscopy images of the 20 minutes sensitizer distributed in the minipig epidermis after active delivery with PA waves using formulation D. Laser energy at 50 mJ/cm² with 355 nm.

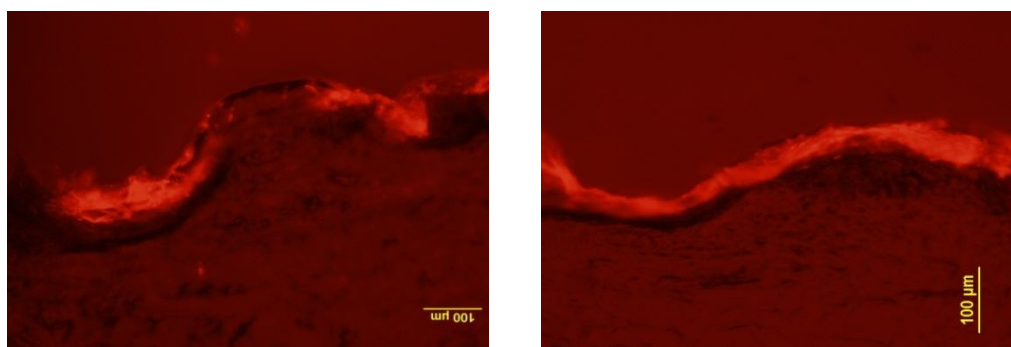


Fig. 9.14 – Representative fluorescence microscopy images of the 20 minutes sensitizer distributed in the minipig epidermis after active delivery with shock waves using formulation D. Laser energy at 10 mJ/cm² at 355 nm.

5. *In Vivo* Transdermal Sensitizer Delivery by the PA Waves

The stratum corneum represents the main barrier to transdermal drug delivery. Consequently, various dermatological studies are focused on the removal of this layer. Tape stripping [246] represents a minimal invasive procedure to remove the SC using adhesive tapes, for both *in vivo* and *ex-vivo* permeation studies in animal models [247]. In the *in vivo* transdermal sensitizer delivery, the PA waves sensitizer flow is compared to the tape stripping flow, in order to determine the enhancement factor between passive, tape stripping (also passive) and PA waves delivery.

5.1 Results and Discussion

The sensitizer used in the *in vivo* experiments is a more potent candidate for photodynamic therapy [245], which obligates to a new fluorescence calibration curve, to determine the amounts of compound delivered into the skin (figure 9.15).

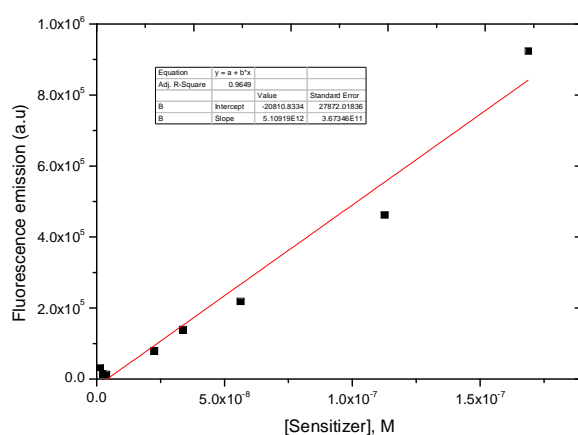


Fig. 9.15 – Fluorescence calibration curve, in dichloromethane, for the sensitizer used in the *in vivo* experiments.

The application of the sensitizer to the dorsum of the minipig employed the best absorption enhancers selected from the *ex-vivo* studies, either oleic acid or Azone (using formulation D as the basis). The piezophotonic materials used contain Mn-TUP and Mn-TPP incorporated in a polystyrene matrix, $\mu_a = 640$ and 230 cm^{-1} , respectively. The PA waves were generated upon irradiation of these materials with 532 nm light of 25 and 50 mJ/cm^2 for 2 minutes. The extraction of the sensitizer and its quantification is reported in tables 9.4 and 9.5, for oleic acid and Azone, respectively. In order to potentiate the transdermal delivery, the percentage of sensitizer in some formulations was increased to 0.5% or 5%, although the formulation D of the *ex-vivo* experiments was taken as the basis for the formulations employed *in vivo*.

Photoacoustic Waves for Transdermal Drug Delivery

Table 9-4 - Quantification of the sensitizer by steady-state fluorescence after extraction from the minipigs, using oleic acid as absorption enhancer. *TS* stand for tape-stripping. *NO* symbolizes passive delivery. Each essay was repeated 2 times or performed without repetition. PA waves were generated with Mn-TUP in polystyrene ($\mu_a = 640 \text{ cm}^{-1}$) upon laser irradiation with 532 nm light of 50 mJ/cm^2 for 2 minutes.

Sensitizer % / Method	Incubation Time	Fluorescence Intensity 751 nm	Mass extracted $\mu\text{g/cm}^2$
0.1% / TS	30 min	1.12E+04	0.10
	1 h	8.40E+03	0.08
	2 h	8.29E+03	0.08
	3 h	8.01E+03	0.07
	4 h	7.56E+03	0.07
	5 h	4.82E+03	0.05
	6 h	8.07E+03	0.08
	7 h	1.00E+04	0.09
0.5% / NO	30 min	8.83E+03	0.08
	1 h	9.49E+03	0.09
	2 h	1.55E+04	0.15
	3 h	1.30E+04	0.12
	4 h	1.93E+04	0.18
0.5% / TS	30 min	2.91E+04	0.27
	1 h	3.40E+04	0.32
	2 h	1.22E+04	0.11
	3 h	1.34E+04	0.13
	4 h	1.49E+04	0.14
5% TS	30 min	1.57E+04	0.15
	1 h	1.71E+04	0.16
	2 h	3.09E+04	0.29
	3 h	7.02E+03	0.07
	4 h	7.48E+03	0.07
	5 h	2.10E+04	0.20
	6 h	8.22E+03	0.08
0.5% / PA 25 mJ/cm^2	2 h	2.12E+04	0.20
	3 h	2.20E+04	0.21
	4 h	3.95E+04	0.37
	5 h	4.10E+04	0.39
	6 h	2.54E+04	0.24
0.5% / PA 50 mJ/cm^2	7 h	2.62E+04	0.25
	15 min	2.14E+04	0.20
	30 min	2.05E+04	0.19
	1 h	1.97E+04	0.19
	2 h	3.20E+04	0.30
0.5% / PA 50 mJ/cm^2	3 h	7.86E+04	0.74
	4 h	1.71E+04	0.16
	5 h	5.03E+04	0.47
	6 h	2.25E+04	0.21
	7 h	4.11E+04	0.39
0.5% / PA 50 mJ/cm^2	8 h	1.97E+04	0.18
	9 h	1.18E+04	0.11
	10 h	1.21E+04	0.11

Figure 9.16 describes the data obtained after passive permeation as a function of time. The formulation with 0.1% sensitizer leads systematically to lower amounts of compound extracted, but the formulations with 0.5% and 5% of sensitizer cannot be distinguished. This may relate to a solubilization problem with the 5% formulation because there was an excess of insolubilized sensitizer in the formulation. Consequently, it does not produce an additional enhancement in the sensitizer permeation across the minipig skin.

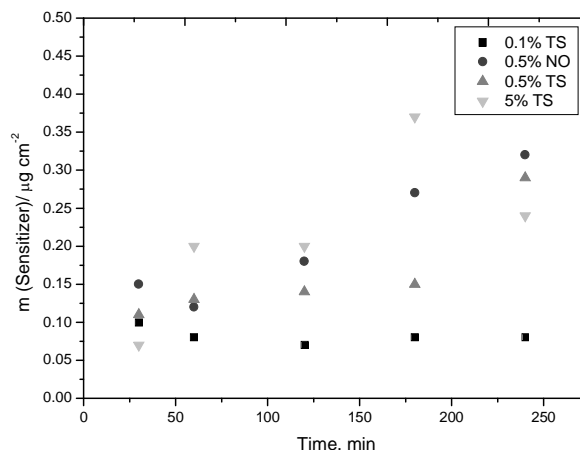


Fig. 9.16 - Quantification by fluorescence of the sensitizer extracted from minipig following passive permeation, when oleic acid was employed as absorption enhancer.

The sensitizer extraction after the PA waves transdermal delivery (table 9-4) reveals an enhancement factor up to 4, when comparing with the passive delivery results, for 30 minutes of incubation. Additionally, the enhancement of PA waves transdermal delivery is maximized for the 50 mJ/cm² laser energy. Figure 9.17 compares the average data for the passive formulation after the sum of the 0.5% and 5% sensitizer formulation, with the average data for PA waves permeation - PA waves (sum) - between 15 and 60 minutes.

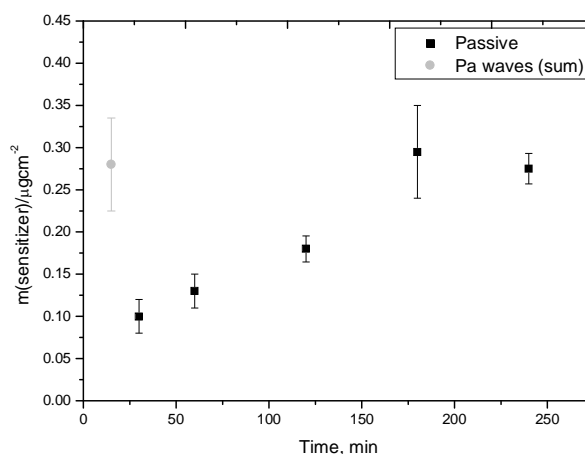


Fig. 9.17 - Mass of sensitizer extracted from minipig following PA waves (average data of the sum for 0.5 and 5% formulation – 15 to 60 minutes) or passive permeation, when oleic acid was employed as absorption enhancer. PA waves were generated with Mn-TUP in polystyrene ($\mu_a = 640 \text{ cm}^{-1}$) upon laser irradiation with 532 nm light of 25 and 50 mJ/cm² for 2 minutes.

Figure 9.17 reveals that the PA waves lead in ca. 30 min to the same amount of sensitizer delivery (0.30 $\mu\text{g}/\text{cm}^2$) as 180 minutes of passive delivery.

Table 9-5 and figure 9.18 compare the sensitizer permeation of a supersaturated formulation containing Azone. Figure 18 summarizes the PA waves sensitizer delivery, as an average of the data collected between 5 and 16 minutes or between 27 and 34 minutes.

Table 9-5 - Quantification by fluorescence of the sensitizer extracted after biopsy punches in minipigs, using Azone as absorption enhancer. PA waves were generated with Mn-TPP in polystyrene ($\mu_a = 230 \text{ cm}^{-1}$) upon laser irradiation with 532 nm light of 50 mJ/cm^2 for 2 minutes.

Sensitizer % / Method	Incubation time	Fluorescence intensity 751 nm	Mass extracted $\mu\text{g}/\text{cm}^2$
5% / NO	1 h	8.04E+03	0.08
	2 h	1.69E+04	0.16
		1.28E+04	0.12
	3 h	1.36E+04	0.13
		1.26E+04	0.12
5% / PA 50 mJ/cm^2	1.35E+04	0.13	
	5 min	1.48E+04	0.14
	6 min	1.63E+04	0.15
	10 min	7.67E+04	0.71
	11 min	5.89E+04	0.56
	15 min	1.69E+04	0.16
	16 min	9.75E+04	0.92
	27 min	1.89E+04	0.17
	28 min	4.30E+04	0.41
	29 min	1.97E+04	0.19
	30 min	2.00E+04	0.19
	31 min	2.20E+04	0.21
	32 min	1.77E+04	0.17
	33 min	3.82E+04	0.37
34 min	4.41E+04	0.41	

The *in vivo* transdermal sensitizer delivery using Azone shows that the passive flow stagnates over time. Nonetheless, its delivery is maximized using oleic acid as a permeation enhancer (0.38 $\mu\text{g}/\text{cm}^2$), when compared with Azone (0.13 $\mu\text{g}/\text{cm}^2$), in 3 hours of passive delivery. This is consistent with the role of the enhancers action in the extracellular domains of the stratum corneum because the oleic acid (OA) molecules reduces the diffusional resistance of skin by interacting and intercalate with the lipid structure – fluidization. Additionally, infrared studies concluded that OA exists in a liquid state in the SC which indicates a phase separation of the local lipid structure [235]. Azone also appears to reduce the diffusional barrier of the SC by inserting within the lipid continuum [233]. Its chemical structure (a ring at the end of a long alkyl chain) exhibits a $\log K_{O/W}$ superior to 7, which anticipates a superior accumulation in the SC, if compared to the OA ($\log K_{O/W} > 2$). Consequently, the percutaneous absorption of OA is better than Azone, which may correspond to an increment in drug diffusion rates, sufficient to elicit a pharmacological effect. This rationalization is in agreement for the passive diffusion results of the sensitizer delivery.

The sensitizer passive permeation does not depend of the tape stripping method, in the conditions employed with these minipigs; thus this flow occurs essentially in intact skin (table 9-4). The passive delivery results show a 2 fold increase in the sensitizer concentration after 4 hours, if compared to the 30 minutes incubation time (0.5% formulation for tape stripping and no tape stripping). The *in vivo* experiments show the efficiency of oleic acid in promoting the transdermal delivery of this sensitizer. Tables 10-4 and 10-5 also show that PA waves delivery increases the sensitizer delivery across the minipig epidermis. The images on figure 9.19 represent the sensitizer distribution in the minipig skin, upon its passive diffusion using a 0.5% formulation.

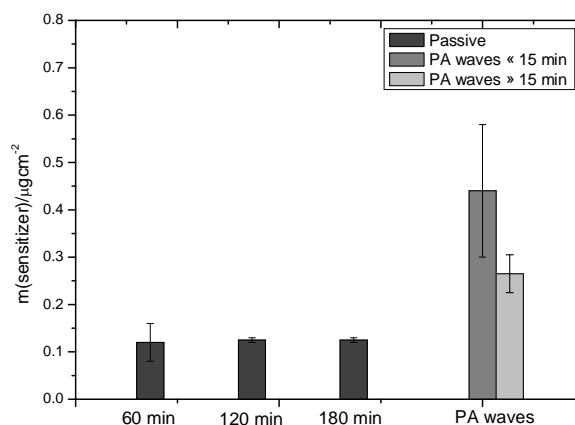


Fig. 9.18 – Sensitizer extracted from the skin after PA waves application and passive delivery when Azone is used as absorption enhancer. PA waves were generated with Mn-TPP in polystyrene ($\mu_a = 230 \text{ cm}^{-1}$) upon laser irradiation with 532 nm light of 50 mJ/cm^2 for 2 minutes.

These images show that, after 2 hours of passive permeation, the sensitizer penetrated $15 \mu\text{m}$ in the skin. It remains in the minipig stratum corneum, which confirms its importance as a reservoir of highly lipophilic molecules, such as the porphyrin derivatives sensitizers.

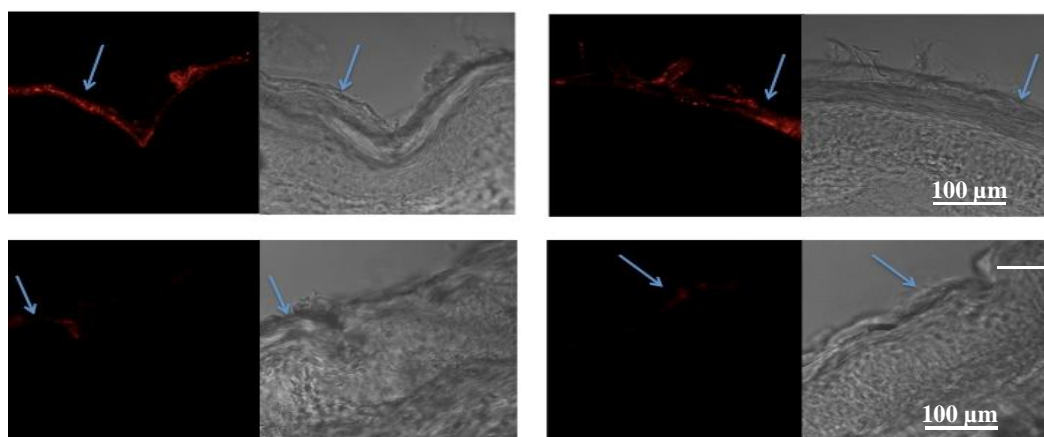


Fig. 9.19 - Representative confocal microscopy images of sensitizer located in the SC of the minipig following a 2 hours passive permeation when oleic acid is employed as absorption enhancer.

The PA waves application promotes an increase in the sensitizer flow through the minipig skin to $0.3 \mu\text{g}/\text{cm}^2$ in the first 30 minutes. The amount that permeated actively in 30 min is comparable and equivalent to the amount that permeated passively in 3 and 4 hours, both using Azone and oleic acid (tables 9-4 and 9-5). The increase in active flow represents an increase up to 4 fold in the first 30 minutes, when compared with passive delivery. This conclusion is concomitant with the comparison between figures 9.19 and 9.20. These figures present representative confocal microscopy images of passive and PA waves permeation, after 30 min of contact of the 0.5% formulation with the minipig skin. The confocal microscopy images of the PA waves permeation show more sensitizer in the skin samples and a deeper and more homogeneous distribution than with passive permeation, consistent with the results of extraction. The penetration depth estimated for active permeation in 30 min is 45 to 60 μm .

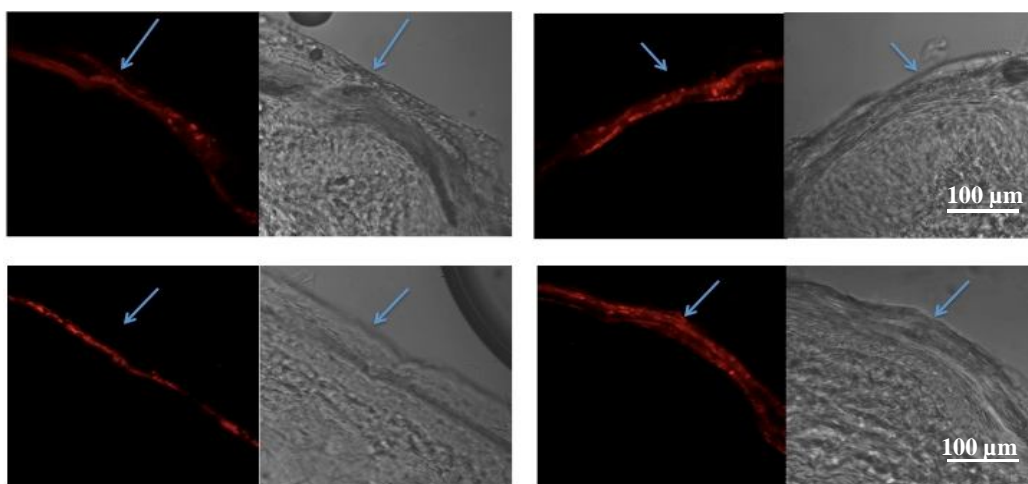


Fig. 9.20 - Representative fluorescence microscopy images of sensitizer located in the SC of the minipig following a 30 minutes incubation time with PA waves application ($\mu_a = 640 \text{ cm}^{-1}$, 532 nm light of $50 \text{ mJ}/\text{cm}^2$ for 2 minutes), when oleic acid is employed as absorption enhancer.

5.2 Conclusion

The control of skin permeability without causing discomfort or irreversible effects has obvious implications in the transdermal delivery of drugs, especially in the case of large molecules ($>500 \text{ Da}$). The extraction of the sensitizer from minipig skin biopsies collected after 30 minutes of contact of the topical formulation with the skin gave a passive flow of $0.1 \pm 0.02 \mu\text{g}/\text{cm}^2$. A similar procedure but applying the PA waves with piezophotonic materials of Mn-TPP in polystyrene and 8 ns laser pulses (fluences of 25 or $50 \text{ mJ}/\text{cm}^2$), at 20 Hz for 2 minutes (application time), increased the flow to $0.54 \pm 0.14 \mu\text{g}/\text{cm}^2$ in the first 15 min. It is not surprising that the PA waves produce a higher increase in the skin permeability to a larger molecule than in the transepidermal water

loss (a factor of 5 vs. a factor of 3). Indeed, this conclusion suggests that photoacoustic waves may be effective in promoting the diffusion of large molecules. Passive delivery with the absorption enhancers' did not induce dramatic increases in the sensitizer permeation flow, though oleic acid gives better results. It is particularly remarkable that confocal microscopy of biopsies revealed that the depth of diffusion increased from 15 μm for passive diffusion in 2 h, to 45-60 μm in 30 min with the application of photoacoustic waves. This is consistent with the role of the high-impulse pressure in disturbing the stratum corneum temporarily [144], and with the ability of the molecules to diffuse more easily through the epidermis.

6. *Ex-Vivo* and *In Vivo* Topical Delivery of GFP by PA Waves

Following the successful administration of a large molecule with the photoacoustic waves (> 1100 Da), the size restriction of this transdermal system was challenged with the topical delivery of Green Fluorescence Protein (GFP of 27 kDa in molecular weight). The topical formulation of GFP suffered minor alterations from the sensitizer formulations. The formulation included 0.1% of GFP in a gel base containing 4% of Azone. The *in vivo* passive delivery experiments failed to reveal any GFP fluorescence in skin fluorescence images (figure 9.21 left). On the other hand, after the generation of the PA waves with the piezophotonic materials, extensive GFP distribution was found in the epidermis, after 20 min of contact of the same formulation with the skin (figure 9.21 middle and right). The minipig skin was subjected to 12 PA waves (*in vivo* delivery – fluorescence microscopy) or 6 PA waves (*ex-vivo* delivery – confocal microscopy). The SC remained intact after all the experiments.

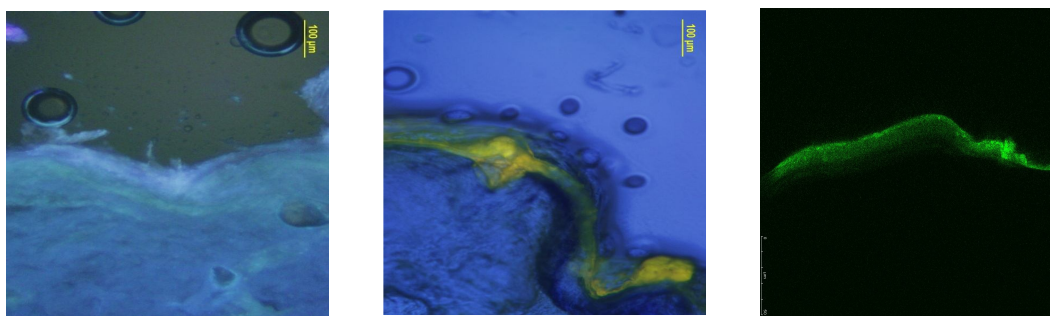


Fig. 9.21 – Representative fluorescence image for the *in vivo* passive delivery of GFP (left). *In vivo* topical delivery of GFP with 12 PA waves active delivery (middle) and *ex-vivo* 6 PA waves GFP delivery (right). Experimental conditions of the piezophotonic materials PA waves generation: $\lambda_{\text{exc}} = 355 \text{ nm}$, $\mu_a = 640 \text{ cm}^{-1}$ and $\mu_a = 330 \text{ cm}^{-1}$ for the Mn-TUP incorporated in a polystyrene substrate.

7. References

- [1] B.W. Barry, Novel mechanisms and devices to enable successful transdermal drug delivery. *Eur. J. Pharm. Sci.*, 14, (2001) 101-114.
- [4] K.A. Walters, *Dermatological and transdermal formulations*, Marcel Dekker, New York, 2002.
- [73] M.R. Prausnitz, S. Mitragotri, R. Langer, Current status and future potential of transdermal drug delivery. *Nat Rev Drug Discov.*, 3 (2004) 115-24.
- [133] M.W. Sigrist, Laser generation of acoustic waves in liquids and gases, *J. Appl. Phys.*, 60 (1986) 83-121.
- [144] A.G. Doukas, N. Kollias, Transdermal drug delivery with a pressure wave. *Advanced Drug Delivery Reviews*, 56 (2004) 559–579.
- [225] Lipinski C., *et al.*, Experimental and computational approaches to estimate solubility and permeability in drug discovery and development settings, *Advanced Drug Delivery Reviews*, 2001, Volume 46, p. 3–26.
- [226] I. Zalaudek *et al.*, Dermatoscopy of facial actinic keratosis, intraepidermal carcinoma, and invasive squamous cell carcinoma: A progression model. *J. Am. Acad. Dermatol.*, 66 (2012) 589-597.
- [227] L. G. Arnaut, M. M. Pereira, S. J. Formosinho, S. Simões, G. Stochel, K. Urbanska, *Process for Preparing Chlorins and their Pharmaceutical Uses* Universidade de Coimbra. UK Patent Application no. 0819594.3, 24 de Outubro de 2008. PCT/PT2009/000057, 22 de Outubro de 2009. WO/2010/047611.
- [228] M. M. Pereira, L. G. Arnaut, S. J. Formosinho, C. J. P. Monteiro, *Nouveaux dérivés de porphirine, notamment chlorines et/ou bactériochlorine, et leurs applications en thérapie photodynamique*. Universidade de Coimbra Patente francesa n° 0412149 de 16 de Novembro de 2004. PCT/EP/012212, de 10 de Novembro de 2005. WO/2006/053707.
- [229] C.J.P. Monteiro *et al.*, Synthesis of amphiphilic sulfonamide halogenated porphyrins: MALDI-TOFMS characterization and evaluation of 1-octanol/water partition coefficients. *Tetrahedron*, 64 (2008) 5132-5138.

- [230] H.K. Vaddi, P.C. Ho, S.Y. Chan, Terpenes in propylene glycol as skin-penetration enhancers: permeation and partition of Haloperidol, Fourier Transform Infrared Spectroscopy, and Differential Scanning Calorimetry. *J. Pharm. Sci.*, 91 (2002) 1639-1651.
- [231] V.R. Sinha, M.P. Kaur, Permeation enhancers for transdermal drug delivery. *Drug Dev. Ind. Pharm.*, 26 (2000) 1131-1140.
- [232] Y. Takeuchi *et al*, Effects of fatty acids, fatty amines and propylene glycol on rat stratum corneum lipids and proteins in vitro measured by fourier transform infrared/attenuated total reflection (FTIR/ ATR) spectroscopy. *Chem. Pharm. Bull.*, 40 (1992) 1887-1892.
- [233] J.E. Harrison, A.C. Watkinson, D.M. Green, J. Hadgraft, K. Brain, The relative effect of Azone and Transcutol on permeant diffusivity and solubility in human stratum corneum. *Pharm. Res.*, 13 (1996) 542-546.
- [234] S.B. Shabat, N. Baruch, A. C. Sintov, Conjugates of Unsaturated Fatty Acids with Propylene Glycol as Potentially Less-Irritant Skin Penetration Enhancers. *Drug Dev. and Ind. Pharm.*, 33 (2007) 1169–1175.
- [235] P. Karande, A. Jain, K. Ergum, V. Kispersky, S. Mitragotri, Design principles of chemical permeation enhancers for transdermal drug delivery. *Proc. Natl. Acad. Sci. USA*, 102 (2005) 4688-93.
- [236] S.A. Ibrahim, S.K. Li, Effects of chemical enhancers on human epidermal membrane: Structure-enhancement relationship based on maximum enhancement (E_{max}). *J Pharm Sci.*, 98 (2009) 926-944.
- [237] J. Hadgraft, J. Peck, D.G. William, W.J. Pugh, G. Allan, Mechanisms of action of skin permeation enhancers/retarders: Azone and analogues. *Int J Pharm.*, 141 (1996) 17-25.
- [238] P.J.S. Gomes, C.M. Nunes, A.A.C.C. Pais, T.P. Melo, L.G. Arnaut, 1,3-Dipolar cycloaddition of azomethine ylides generated from aziridines in supercritical carbon dioxide. *Tetrahedron Letters* 47 (2006) 5475-5479.
- [239] A.F. Peixoto, M.M. Pereira, A.A.C.C. Pais, Maximization of regioselectivity in hydroformylation of vinyl-aromatics using simple factorial design. *J. Molecular Catalysis A: Chemical* 267(1-2) (2007) 234-240.

- [240] N.A. Armstrong, *Pharmaceutical Experimental Design and Interpretation*, CRC press, Boca Raton, FL, 2006.
- [241] G.G. Agyralides, P.P. Dallas, D.M. Rekkas, Development and in vitro evaluation of furosemide transdermal formulations using experimental design techniques. *Int. J. Pharm.*, 281 (2004) 35-43.
- [242] G.A. Lewis, D. Mathieu, R.P. Tan-Luu, *Pharmaceutical Experimental Design*, Marcel Dekker, New York, 1999.
- [243] J.S. Yuan *et al*, Linker-based lecithin microemulsions for transdermal delivery of lidocaine. *Int. J. Pharm.*, 349 (2008) 130-143.
- [244] A. Misra *et al*, Formulation of a transdermal system for biphasic delivery of testosterone. *J. Control. Release*, 39 (1996) 1-7.
- [245] M.M. Pereira *et al*, Synthesis and photophysical characterization of a library of photostable halogenated bacteriochlorins: An access to near-infrared chemistry. *Tetrahedron*, 66 (2010) 9545-9551.
- [246] J. Lademann *et al*, the tape stripping procedure – evaluation of some critical parameters. *Eur. J. Pharm. Biopharm.*, 72 (2009) 317-323.
- [247] M.H. Qvist, U. Hoeck, B. Kreilgaard, F. Madsen, S. Frokjaer, Evaluation of Göttingen minipig skin for transdermal in vitro permeation studies. *Eur J Pharm Sc.*, 11 (2000) 59-68.

X

**Prospects in
Gene Therapy**

1. Introduction

Gene therapy consists in the use of DNA as a pharmaceutical agent to prevent or treat diseases [248, 249]. The physical endeavor comprises on supplementing or altering genes within the cell to overcome systematic or random protein expression errors, which may lead to diseases or body malfunctions. Gene therapy involves delivering deoxyribonucleic acid (DNA), which encodes a therapeutic gene that replaces a mutated one.

In order to be used in the clinical practice, gene therapy demands reliable and safe methods to deliver efficiently DNA to the human body cells. Those methods include two primary classes: viral vectors and nonviral methods [248, 249].

Viral vectors methods consist in the use of viruses that effectively bind to hosts and introduce their genetic patrimony into the cellular apparatus. The main idea in these technologies comprises the removal of viral DNA and the use of its capsule, as a vehicle to deliver the therapeutic DNA. The main drawbacks relate with safety, mainly mutagenesis, unexpected immune responses and inadequate targeting considering tissue specificity. Non-viral methods, such as electroporation [250] and ultrasound [251] receive much attention for the possibility of large scale production and reduced immunogenicity.

Gene transfection promoted by laser-induced pressure waves represents an attractive alternative method [252] with potential *in vivo* application, because laser light can be delivered to the human body through an optical fiber with high spatial controllability. Pressure waves generated by laser pulses can permeabilize biological barriers, such as the skin or cellular membranes, with a reversibility that allows the skin to recover its protective function and cells to remain viable. Doukas and co-workers [144, 252] explored the principles of transdermal and intracellular drug delivery with pressure waves generated by laser pulses, and showed the critical relevance of generating a pressure transient with high peak pressure and impulse. Their light-to-pressure converters were typically 0.8 mm or 3 mm thick metal sheets or commercial plastics (polystyrene), respectively. However, their low energy-conversion efficiency required nanosecond laser pulses up to 10 J to affect biological barriers, which is unfeasible in the clinical environment.

More recently, Terakawa *et al* [253] successfully achieved gene transfer into mammalian cells promoted by nanosecond lasers induced pressure waves. They suggest that the transfection efficiency depends on the pressure applied integrated over time (impulse) rather than on the stress gradient (defined as peak pressure divided by wave rise time).

The optimized conditions for transfection used irradiation with twenty laser pulses in a black rubber disk with a fluence of 1.3 J cm^{-2} . Under these conditions, the cellular viability remains of about 80%, and the light absorber medium was destroyed after several pulses (ablation – destructive technique [133]).

2. Gene Transfer with Acoustic Waves

The human genome project and advances in molecular biology led to the identification of various genes, with useful application in many therapeutic conditions [248, 249]. Consequently, gene therapy opened a new therapeutic window for managing and possible treat an array of complex diseases. For this purpose, cost-effective and safe cellular delivery systems must be sought.

2.1 Background

Gene transfer met considerable difficulties in the first regulatory phases due to delays in clinical trials and frustrating proof of viability and safety [248, 249, 254]. Practical examples confirm this status for viral and nonviral systems: a fatal accident occurred during adenoviral gene therapy [255], and chronic problems associated with leukemia can be found in the literature [256]. This background motivates a redirection of the investigations to nonviral technologies, such as microinjections, electroporation or ultrasound [256, 257], despite their lower transfection efficiency when compared to the viral ones, and technical problems related to the human application. The nonviral gene therapy shortcomings reside in the design of an appropriate, accurate, effective and safe gene transfer system for the *in vivo* application. The systems discussed in the introduction do not fulfill all the requirements of regulatory approval for clinical use [256, 257].

The most similar technology to the photoacoustic waves system discussed in this work is the ultrasound-mediated transfection (UMT). The progresses in this field highlights the noninvasive character, the 2 to 5 orders of magnitude in the ultrasound efficiency if compared to 1980's Feicheimer efficiencies [256, 257] and the definition of the mechanism by which ultrasound enhances gene delivery occurs (cavitation) [256, 257]. Ongoing work may clarify the exact contributions from different types of cavitation to UMT and give indications for its optimization in a clinical environment.

As explained for the ultrasound-mediated transdermal drug delivery in the chapter 4, cavitation represents the pivotal mechanism on perturbing the lipid packing of the

biological barriers. When periodic positive and negative pressures traverse a system, the negative part may promote the disturbance of the membrane assembly [125-127], if it encounters air bubbles in the surroundings. The pressure acts as an insufflating engine increasing the bubble size until it bursts, which destroys the lipid packing in membranes.

There are two types of cavitation: in stable cavitation, the applied pressure does not possess sufficient intensity to promote changes in the bubbles size and shape, so vibrations effects are responsible for the perturbation [125]. The stable oscillation across an acoustic field creates local shear forces and microstreaming [125-127]. In transient cavitation, bubbles expand and contract during unusually high pressure cycles, and suddenly the system does not support the applied forces and explodes. This phenomenon may be accompanied of localized increase in temperature and pressure, which may promote free radical generation [126].

The likelihood of cavitation is described by a mechanical index (MI), as stated in previous chapters. This concept defines that cavitation should increase with raising ultrasound power, but decrease with its frequency. Nowadays, the scientific literature considers the MI as a safety feature and defines that an equivalent pressure of 5 atmospheres (with a broadband centered in 1 MHz) of the wave peak is injury free [195, 196]. The biological effect of ultrasound results in the formation of pores, which are continuous pathways across the biological barriers [125-127]. The scientific literature provides compelling information on the reliability of UMT for gene therapy (table 10-1).

Table 10-1 – Gene transfection efficiency in ultrasound-mediated systems.

Reference	Microbubbles	Ultrasound	Transfection efficiency	Target
Greenleaf [258]	Albunex	1 MHz 0.32-0.41 MPa	43%	<i>In vitro</i> human chondrocytes
Frenkel [259]	Albumin bubbles	1.3 MHz 1.6 MI	41	<i>In vitro</i> 293 cell line
Taniyama [260]	Optison (75%)	1 MHz 2.5 W cm ⁻²	10-fold	<i>In vivo</i> rat ischemic muscle
Nakashima [257]	Optison (5-10%)	1 MHz 0.5 W cm ⁻²	50%	<i>In vivo</i> dental pulp stem cells

3. Cellular Viability Experiments

In order to use the photoacoustic waves with no safety restraints in gene transfection, the viability of living cells after being exposed to such waves must be clearly stated. The human osteosarcoma cell line (MNNG/HOS) was exposed to the PA waves produced with the laser irradiation of three distinct films (Table 10-2). The films were produced with the most efficient light-to-pressure piezophotonic materials dispersed in polystyrene: film 1 and 2 with Mn-TPP and film 2 with New Coccine (ease to produce and nondegradable upon laser irradiation). The irradiation of the piezophotonic materials employed laser pulses at 20 Hz of 532 nm light during 30 and 120 seconds, yielding 600 to 2400 laser pulses of 50 mJ cm^{-2} (figure 10.1).

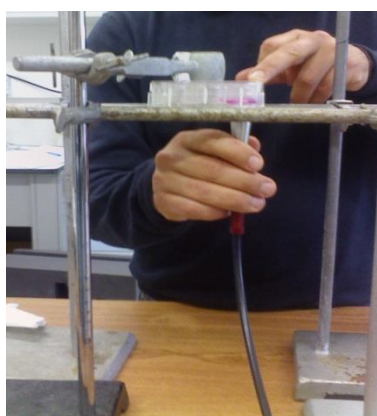


Fig. 10.1 – Typical set-up conditions for the cellular viability and gene transfection essays. A fiber optic guide 532 nm nanosecond laser light into the piezophotonic material that produces the photoacoustic waves. The PA waves are transmitted to the culture well using silicone as an acoustic coupling medium and its application is exerted from the bottom of the well.

The cellular viability upon photoacoustic waves application is depicted in table 10-2. The cellular viability essays ensure the safety of PA application, especially for high absorbing Mn-TPP/polystyrene piezophotonic materials. The material described as film 2 (Mn-TPP/Polystyrene with a thickness of $417 \mu\text{m}$) has a cellular survival rate undistinguishable from the control. With film 1 (Mn-TPP/polystyrene with similar absorbance but with a thickness of $115 \mu\text{m}$), the survival rate diminished as a function of the linear absorption coefficient (μ_a), although the survival rates remained high [255-260]. With both films, the results do not show distinct differences between 30 seconds and 120 seconds of PA waves exposure, which may indicate that the perturbation induced in the cells, is not sufficient to reduce their viability.

The New Coccine dye dispersed in polystyrene (film 3), with a thickness of $377 \mu\text{m}$, has the lower survival rate when exposed to an excess of 2400 laser pulses. However, even

for this essay, the survival rate is higher than 70%, which corresponds to survival percentages of ultrasound and electroporation application into cells [250, 255-260].

Table 10-2 – Cellular viability assays: piezophotonic materials, PA waves contact time, linear absorption (μ_a) and determined cell viability (CV). * Not applicable.

Piezophotonic Material	Application Time	Abs	μ_a (cm⁻¹)	CV (%)
Film1 of MnTPP/Polystyrene	30 sec	1.423	81	89.2
	120 sec			85.8
Film 2 of MnTPP/Polystyrene	30 sec	1.089	383	97.9
	120 sec			100
Film 3 of New Coccine/Polystyrene	120 sec	1.20	314	71.1
Control	*	*	*	100

The use of an excessive number of photoacoustic pressure waves did not compromise the cellular viability of human osteosarcoma cells (application time of 120 seconds – 2400 laser pulses). This shows that thermoelastic generation of PA waves through the irradiation of piezophotonic materials with low intensity lasers meets the safety requirements for gene transfection. A straightforward comparison with the ablation studies of Terakawa [253] demonstrates a higher cellular survival promoted by one fold less laser energy. Additionally, the piezophotonic materials can be reutilized in subsequent experiments. These results imply that the maximization of the light-to-energy conversion by the thermoelastic mechanism can transiently perturb the biological barrier function, without promoting cellular death.

4. *In Vitro* Gene Transfer with Photoacoustic Waves

The most resembling studies in gene transfer to the PA waves system have been produced by Visuri *et al* [173, 261], where they use diode-pumped frequency-doubled Q-switched Nd:YAG laser, which emits pulses of 532nm light with 90 ns of duration. The laser radiation was coupled to an optical fiber and delivered to an absorbing media of 1% of Amaranth red dye (water/volume). The laser energy exiting the optical fiber ranged from 100 to 350 μ J. The resulting optical power varied up to 500 mW, but typically was in the

Photoacoustic Waves for Transdermal Drug Delivery

range of 150-300 mW. Repetition rate of the laser was variable up to 5 kHz. Further developments of this methodology are not expected because their acoustic conversion is very low (use of exceptionally low laser energies): tensile part of the waves and rise times bellow the feasible minimum for disrupting biological barriers ($0.1 \text{ bar/ns} < 1 \text{ bar/ns}$) [144, 252].

Considering the physical features of the photoacoustic waves and the induced-cellular viability in the safety tests, the application of PA waves is expected to have a rate of pressure increase appropriately to promote a successful gene transfer. The experimental design to examine the prospects of PA waves application in gene therapy is described in table 10-3.

Table 10-3 – Experimental design for the application of PA waves in gene transfection essays. The gwizGFP and pEGFPC3 are notations for DNA plasmids used in different concentrations (5, 10, 50, 100 µg/ml). The PA waves exposure time ranged from 1.5 to 3 minutes.

Controls	Photoacoustic Waves Application				
Positive Control (5 µg gwizGFP DNA + lipofectamine 2000)	gwizGFP DNA 50 µg/ml PA time = 1.5 min	gwizGFP DNA 50 µg/ml PA time = 1.5 min	gwizGFP DNA 100 µg/ml PA time = 1.5 min	gwizGFP DNA 100 µg/ml PA time = 1.5 min	gwizGFP DNA 100 µg/ml PA time = 3 min
Negative control (gwizGFP DNA)	gwizGFP DNA 50 µg/ml PA time = 1.5 min	gwizGFP DNA 50 µg/ml PA time = 1.5 min	gwizGFP DNA 100 µg/ml PA time = 1.5 min	gwizGFP DNA 100 µg/ml PA time = 1.5 min	gwizGFP DNA 100 µg/ml PA time = 3 min
Positive Control (0,5 µg pEGFPC3 DNA + lipofectamine 2000)	pEGFPC3 DNA 5 µg/ml PA time = 1.5 min	pEGFPC3 DNA 5 µg/ml PA time = 1.5 min	pEGFPC3 DNA 10 µg/ml PA time = 1.5 min	pEGFPC3 DNA 10 µg/ml PA time = 1.5 min	pEGFPC3 DNA 10 µg/ml PA time = 3 min
Negative Control (pEGFPC3 DNA)	pEGFPC3 DNA 5 µg/ml PA time = 1.5 min	pEGFPC3 DNA 5 µg/ml PA time = 1.5 min	pEGFPC3 DNA 10 µg/ml PA time = 1.5 min	pEGFPC3 DNA 10 µg/ml PA time = 1.5 min	pEGFPC3 DNA 10 µg/ml PA time = 3 min

Negative controls are used to confirm the existence of a barrier to the transport of large molecules, in the cell membrane (figure 10.2 A). Positive controls performed with

lipofectamine transportation permits to compare, a traditionally effective method to deliver these large entities, with the photoacoustic waves systems (figure 10.2 B and C). Lipofectamine is a polycationic synthetic lipid mixed with an amine-group that forms DNA-lipid complexes due to ionic interactions between the head group of the lipid (positive charge) with the negative charge of the DNA phosphate groups. The mixture of lipid-DNA results in the formation of structures that fuse and pass across the cellular membrane [262, 263].

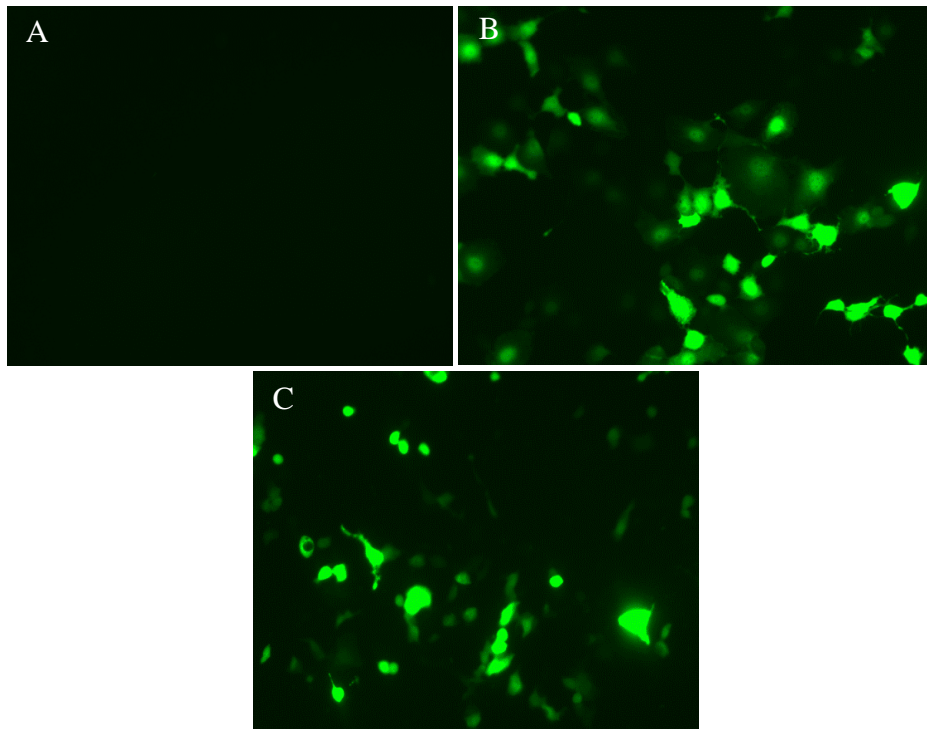


Fig. 10.2 – **A** – Representative image for negative controls essays performed for both plasmids. **B** – Representative image for the positive control with gwizGFP DNA delivered with lipofectamine. **C** – Representative image for the positive control with pEGFPC3 DNA delivered with lipofectamine.

The diffusion and exchanges of substances from the extracellular environment to the intracellular one is limited by the molecular size. Large entities, such as Green Fluorescence Protein plasmids accounting for hundreds of Dalton in molecular weight, are not capable of traversing the plasma membrane as illustrated by figure 10.2 A.

Figures 10.2 B and C show that lipofectamine is capable of transporting GFP plasmids across the cell membrane (fig 10.2B and C). The efficiency of this technique can be assessed by the number of transfected cells with GFP and its fluorescence intensity. In that extent, the gwizGFP plasmid proves to be slightly more effective.

DNA plasmid delivery with PA waves was attempted with different DNA concentrations and different exposure times, at the maximum pressure possible that the film 2 is capable of producing (figure 10.3). This piezophotonic material was chosen according to its physical features, maximum optical to pressure conversion and lower rise times, and the smallest fraction of cellular dead (table 10-2).

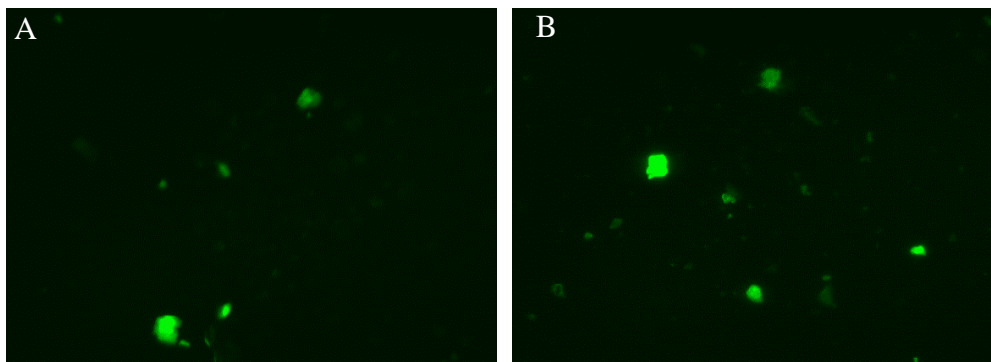


Fig. 10.3 – **A** – Representative image of the pEGFPC3 delivery by the PA waves with an application time of 1.5 minutes. **B** – Representative image of PA waves essays for an application time of 3 minutes with gwizGFP plasmid.

The images in figures 10.3 A and B indicate a significant number of cells expressing GFP upon exposure to the photoacoustic waves, showing evidence that these system can be used to promote DNA transfection. These preliminary results are extremely encouraging because there is a proof-of-concept of the PA waves potential in gene transfection. In further studies, this work will be pursued.

5. References

- [125] B.E. Polat et al, Ultrasound-mediated transdermal drug delivery: Mechanisms, scope, and emerging trends. *J. Control. Release*, 152 (2011) 330–348.
- [126] S. Mitragotri, D. Blankschestein, R. Langer, Transdermal Drug Delivery Using Low- Frequency Sonophoresis. *Pharm. Res.*, 13 (1996) 411-420.
- [127] S. Mitragotri, J. Kost, Low-frequency sonophoresis. *Advanced Drug Delivery Reviews*, 56 (2004) 589–601.
- [133] M.W. Sigrist, Laser generation of acoustic waves in liquids and gases, *J. Appl. Phys.*, 60 (1986) 83-121.
- [144] A.G. Doukas, N. Kollias, Transdermal drug delivery with a pressure wave. *Advanced Drug Delivery Reviews*, 56 (2004) 559–579.
- [173] S.R. Visuri, H.L. Campbell, L. Da Silva, *Optically Generated Ultrasound for Enhanced Drug Delivery*. The Regents of the University of California, USA, 2002.
- [195] NCRP, Exposure criteria for medical diagnostic ultrasound. II. Criteria based on all known mechanisms, in, National Council on Radiation Protection and Measurements. Bethesda MD, 2002, Report No.140.
- [196] M.H. Niemz, *Laser-Tissue Interactions*, 2007, Springer, Berlin.
- [248] A.B. Moseley, C.T. Caskey, Human genetic disease and the medical need for somatic gene therapy. *Adv. Drug Deliv. Rev.*, 12 (1993) 131-142.
- [249] M. Hiratsuka, T. Sasaki, M. Mizugaki, Genetic testing for pharmacogenetics and its clinical application in drug therapy. *Cli. Chim. Acta*, 363 (2006) 177-186.
- [250] S. Somiari *et al*, Theory and in vivo application of electroporative gene delivery. *Mol. Ther.*, 2 (2000) 178.
- [251] Y. Taniyama *et al*, Development of safe and efficient novel nonviral gene transfer using ultrasound: enhancement of transfection efficiency of naked plasmid DNA in skeletal muscle. *Gene Ther.*, 9 (2002) 372.
- [252] D.J. McAuliffe, S. Lee, T.J. Flotte, A.G. Doukas. Stress-wave - assisted transport through the plasma membrane in vitro. *Laser in Surgery and Medicine*, 20 (1997) 216-222.

- [253] M. Terakawa *et al*, In vitro gene transfer to mammalian cells by the use of laser-induced stress waves: effects of stress wave parameters, ambient temperature, and cell type. *J. biomed. Opt.*, 11 (2006) 014026.
- [254] G. Cevc, U. Vierl, Nanotechnology and the transdermal route. A state of the art review and critical appraisal. *J. Control. Release*, 141 (2010) 277-299.
- [255] C.M.H. Newman, T. Bettinger, Gene therapy progress and prospects: Ultrasound for gene transfer. *Gene Therapy*, 14 (2007) 465–475.
- [256] T. Nozaki *et al*, Ultrasound-mediated gene transfection: problems to be solved and future possibilities. *J. Med. Ultrasonics*, 33(2006) 135–142.
- [257] W.D. Jr. O'Brien, Ultrasound-biophysics mechanisms. *Prog. Biophys. Mol. Biol.*, 93 (2007) 212–255.
- [258] J.F. Greenleaf *et al*, Optimization of ultrasound-mediated gene transfer: comparison of contrast agents and ultrasound modalities. *Eur. Heart J.*, 24 (2003) 1690–1698.
- [259] P.A. Frenkel *et al*, Ultrasound-targeted microbubble destruction can repeatedly direct highly specific plasmid expression to the heart. *Circulation*, 108 (2003) 1022–1026.
- [260] Y. Taniyama *et al*, An efficient gene transfer method mediated by ultrasound and microbubbles into the kidney. *J. Gene Med.*, 7 (2005)108–116.
- [261] S. R. Visuri, N. Heredia, Opto-Acoustic Cell Permeation. *Photonics West Symposium*, San Jose, California, (2000) 23-29.
- [262] N. Wang, J. Ragoussis, The effect of neogaro-oligosaccharides on lipofectamine-mediated transfection. *Tech. Tips*, 3 (1998) 23-26.
- [263] J. Ou *et al*, AP-4F, antennapedia peptide linked to an amphipathic α helical peptide, increases the efficiency of Lipofectamine-mediated gene transfection in endothelial cells. *Bioche. Biophys. Research Comm.*, 305 (2003) 605-610.

XI

Concluding Remarks

1. Conclusion

The complexity of skin structure and the factors governing transdermal and topical diffusion of drugs limits the development of safe, painless and effective delivery systems. These three features must be present in novel transdermal drug delivery system in order to satisfy the standards of scientific discovery and obtain the authorization for introduction in the market by regulatory agencies.

The use of acoustic energy to permeabilize biological barriers was a concept introduced by Doukas *et al* [144] that met some success for a large scope of drugs and medical conditions, such as the treatment of insulin-dependent mice [197]. The generation of pressure waves with this technology was based on the ablation of materials with high-energy lasers (up to 0.5 J per pulse), and established the limits of effective membrane permeabilization in terms of pressure waves with rise times between 1 and 50 bar/ns. The path through the intercellular lipids can be facilitated expanding the extracellular domains of the stratum corneum, which enhances the transdermal delivery of large drugs with such an expansion [144]. High-impulse shock waves use this mechanism to increase the permeability of the skin [144]. However, this technology never entered the clinical practice probably because of the use of expensive and sophisticated lasers, as well as safety issues.

Our work describes the transient permeabilization of skin using photoacoustic (PA) waves generated by thermoelastic expansion of materials with efficient and ultrafast conversion of light into pressure using optical power densities of portable pulsed lasers (<10 MW/cm² per pulse). The scientific literature considered thermoelastic expansion an inefficient method to convert light into pressure, and optical-to-acoustic energy conversion efficiencies, $\eta_{PA} = E_S/E_L$, were determined to be lower than 10^{-4} [133]. The efficiency of the process increases when the absorbing medium is confined by rigid boundaries [133]. Additionally, taking into consideration that the peak pressures obtained by thermoelastic expansion scale with the reciprocal of the thickness of the absorbing material for the same amount of energy absorbed [164], we showed how to increase the conversion efficiency to unprecedented values. Moreover, the duration of the thermoelastic expansion, and hence the rise time of the photoacoustic wave, intrinsically depends on the rates of the processes taking place in the absorbing material [149, 150]. The duration of the PA wave is as short as that of the laser pulse (τ_L) when the following conditions are met: (i) $\mu_a c_s \tau_L \gg 1$ where μ_a is the linear absorption coefficient of the absorbing material and c_s is the longitudinal

speed of sound, (ii) the absorbing materials convert all the absorbed light into heat in a time shorter than τ_L .

The materials which take full advantage of these conditions are denominated piezophotonic materials, and the spectral band of its PA transient is determined by the spectral band of the laser pulse, when these two conditions are fulfilled [150]. The relations below the material ablation threshold, which maximize the light-to-pressure photoacoustic conversion efficiency involves the dependence with the Grüneisen coefficient and the absorption characteristics of these materials (μ_a). Our work demonstrates that the selected light-to-pressure conversion materials chosen and the laser sources employed are suitable for the generation of acoustic transients that permeabilize biological barriers [144]. These materials are very thin (thickness $< 100 \mu\text{m}$) and strongly absorbing ($\mu_a > 100 \text{ cm}^{-1}$), and incorporate calorimetric references with ultrafast radiationless decays ($< 1 \text{ ns}$ lifetimes). A polystyrene-based piezophotonic substrate with $\mu_a = 500 \text{ cm}^{-1}$ is in the limit of generating a PA wave with the time dependence of a laser pulse with $\tau_L = 8 \text{ ns}$.

The biophysical mechanism of acoustic waves interaction with the skin presented by Doukas *et al* [144], does not provide a complete insight on the physical processes responsible for the expansion of the lacunar spaces within the SC intercellular regions. Our approach to this problem started by considering model lipids resembling the SC lipid lamellae. The results show an increased fluidity of the lipids assembly upon PA waves exposure, which recover to its initial conformation in 2 to 3 minutes after the end of the perturbation. The pressure increase transiently disturbs the rigidity of the lipid environment, which should result in the appearance of membrane pores allowing molecules of finite sizes to diffuse across its structure. In this work we employ photoacoustic waves with 12 bar of peak pressures and center frequencies of 100 MHz to transiently perturb the stratum corneum. We show that the dynamic acoustic radiation force mechanism can explain the perturbation induced by the photoacoustic waves. Indeed, 15 bar pressure gradients across 5 corneocytes (approximately $5 \mu\text{m}$ wide) are expected to perturb their structure (acoustic wavelength of $15 \mu\text{m}$).

Any new transdermal drug delivery system must be evaluated in terms of its safety, including the generation of pain. To address the question of the photoacoustic waves interaction with living tissues, animal and human tests were performed based upon transepidermal water loss and erythema measures. The painless perspective was analyzed by using a visual analogue scale in human volunteers. The transepidermal water loss (TEWL) is recognized as a measure of the skin permeability to the

Concluding Remarks

enhancement of percutaneous absorption of drugs [220]. This parameter relates to the PA waves safety because the recovery time to TEWL basal values defines the transient or non-transient effect on the skin barrier function. Our results demonstrate that TEWL of healthy human volunteers' increases by a factor of 3, in two minutes of PA waves exposure, then the skin recovers its protective function in 2 minutes leaving no signs of damage (negligible erythema and quickly fading one), and causing mostly a gentle warming sensation (no pain).

The transdermal delivery of molecules for photodynamic therapy, photosensitizers, illustrates the potential of the PA waves to enhance drug delivery because they increase the drug flux by a factor of 5 relative to the passive flux, in only 15 minutes (0.1 ± 0.02 to $0.54 \pm 0.14 \mu\text{g cm}^{-2} \text{ h}^{-1}$). Moreover, the depth of diffusion increased from 15 μm , for passive diffusion in 2 h, to 35 μm in just 30 minutes with the application of photoacoustic waves. Following the successful administration of a large molecule (> 1000 Da) with the PA waves, the transdermal delivery of Green Fluorescent Protein (> 27 kDa) was attempted. The passive delivery failed to lead measurable GFP in minipig both *postmortem* and *in vivo*, but on the other hand, PA waves induced extensive GFP distribution across the minipig epidermis, after just 20 minutes. Based on these results, it is possible to claim that high-impulse photoacoustic waves open a new window for the painless transdermal delivery of a wide range of drugs. The enhancement of skin permeability without causing discomfort or lasting effects has obvious implications in the market of transdermal delivery.

Our foundational work in gene delivery demonstrates effective drug delivery across the cellular membrane, which certifies the use of PA waves based delivery system. The transient permeabilization of the cellular membrane allows the GFP expression, in a moderate extent.

2. PA Waves Vision in Transdermal Drug Delivery

The concept behind the development of photoacoustic waves for transdermal drug delivery is based on insight from photoacoustics and material chemistry. From the clinical point of view, the generation and use of intense acoustic transients has advantages, such as:

- Painless;
- Easy to use, reliable and robust;

- Safe handling;
- Cost Effective.

Painless administration: The administration of the photoacoustic waves with impulses around 5 bar/ns do not interact with the pain terminations. The deposition of pressure to living tissues creates a gentle warming in the volunteers.

Easy to use, Reliable and Robust: Nanosecond ND:YAG lasers suitable for the specifications of this transdermal system are ease to handle, portable, though, reliable and robust. They may encourage the compliance of the patients to the treatments and satisfy the clinicians.

Safe Handling: The overall characteristics of the photoacoustic waves make than safe to handle with a minimum training, just like diagnostic ultrasound.

Cost Effective: The laser technology employed is affordable and the piezophotonic materials can be produced at a very low cost and are recyclable. Additionally, the cost associated with the disposal and contaminations of hypodermic needles is not present in this technology.

3. References

- [133] M.W. Sigrist, Laser generation of acoustic waves in liquids and gases, *J. Appl. Phys.*, 60 (1986) 83-121.
- [144] A.G. Doukas, N. Kollias, Transdermal drug delivery with a pressure wave. *Advanced Drug Delivery Reviews*, 56 (2004) 559–579.
- [149] F.A. Schaberle *et al*, Analytical solution for time-resolved photoacoustic calorimetry data. A survey of mechanisms common in photochemistry. *Photochem. Photobiol. Sci.*, 9 (2010) 812-822.
- [150] A.A. Karabutov, E.V. Savateeva, N.B. Podymova, A.A. Oraevsky, Backward mode detection of laser-induced wide-band ultrasonic transients with optoacoustic transducer, *J. Appl. Phys.*, 87 (2000) 2003-2014.
- [197] A.G. Doukas *et al*, Photomechanical transdermal delivery of insulin in vivo. *Lasers in Surgery and Medicine*, 28 (2001) 282-285.
- [220] J. Levin, H. Maibach, The correlation between transepidermal water loss and percutaneous absorption: an overview. *J. Control. Release*, 103 (2005) 291-299.

XII

**Instrumentation,
Materials and Methods**

1. Instrumentation

The development of the photoacoustic waves transdermal system implies extensive laboratorial work concentrated in three main areas: the physics of the thin piezophotonic films, biophysical measurements of the skin and fluorescence quantification of drugs delivered through the skin. All the mathematical and graphic operations were performed with Excel® and Origin® software.

1.1 Absorption Spectroscopy

The absorption spectrums were collected using a double beam Shimadzu (UV-2100) UV-visible spectrophotometer. All measurements were performed in quartz cells with optical paths of 1 cm.

1.2 Emission Spectroscopy

The samples fluorescence was detected with a Spex Fluoromax 3.22 spectrofluorimeter using a Xenon lamp of 450 W and a detection system with a monophotonic count.

1.3 Photoacoustic Calorimetry

The photoacoustic calorimetry experiments were done using a front face irradiation photoacoustic cell of own manufacturing [179]. This allows enhancing the sensibility of the very fast heat depositions of short-lived acoustic transients. The configuration used allows the detection of transient species with lifetimes between 10 ns to 1 μ s.

The photoexcitation was obtained by irradiating the sample with a 484 nm and 472 nm light derived from an EKSPLA OPO model PG-122 pumped by an EKSPLA NL301G Nd:YAG laser delivering 4-6 ns pulses. A fraction of the laser beam is detected by a photodiode (Gentec, ED-200) to produce a trigger signal to the oscilloscope.

The photoacoustic signal is detected by a means of transducer (such as, the Panametrics, 0.25; 2.25, 15, 225 MHz transducers) placed at the bottom of the cell. This signal is amplified by an amplifier (Panametrics, model 5676) and then transferred DPO7254 Tektronix digital oscilloscope. A personal computer is used for the control of the oscilloscope.

Peak pressures and amplitude measurements were made with a calibrated needle hydrophone (model MH28 from Force Technologies) or with Panametrics contact

piezoelectric transducers (100 MHz and 225 MHz transducers, Olympus®), connected to the DPO7254 Tektronix digital oscilloscope.

1.4 Microscopy Analysis

The confocal fluorescence of the bacteriochlorin was measured with a LSM 510 Meta (Carl Zeiss, Jena, Germany) confocal microscope, with a x63 oil immersion objective (Plan-Apochromat, 1.4 NA; Carl Zeiss), using $\lambda_{\text{ex}} = 514 \text{ nm}$, $\lambda_{\text{em}} \geq 650 \text{ nm}$, laser power at 5% and an amplification 40x.

The fluorescence of GFP in skin samples from in vivo experiments was measured with an Olympus BX51M fluorescence microscope equipped with a UV mercury lamp (100 W Ushio Olympus). The 470-495 nm excitation cube and the 510-550 nm emission were employed to obtain the GFP fluorescence. The images were processed in a personal computer by an Olympus Digital DP70 video camera, and analysed with Olympus DP Controller 2.1.1.176 and DP Manager 2.1.1.158 software. Confocal GFP fluorescence in skin slices from experiments with *post mortem* minipig skin was visualized under a Leica TCS Sp5 confocal microscope. The microscopy is inverted (DMI6000) with a water apochromatic objective of 63 \times and numeric aperture of 1.2. Before connecting the confocal mode, the samples are observed with a sodium lamp, as the radiation source, and with Rhod-DOPE, as a fluorescent filter. The 3D projections were obtained using the analysis software of Leica®. All observations were done at 22 °C.

Figure 12.1 includes representative images used to construct the visual analogue scale of chapter 9. The scale starts with no sensitizer permeation (figure 12.1 A) and ends with the maximum amount of sensitizer accumulated and distributed across the minipig epidermis (figure 12.6).

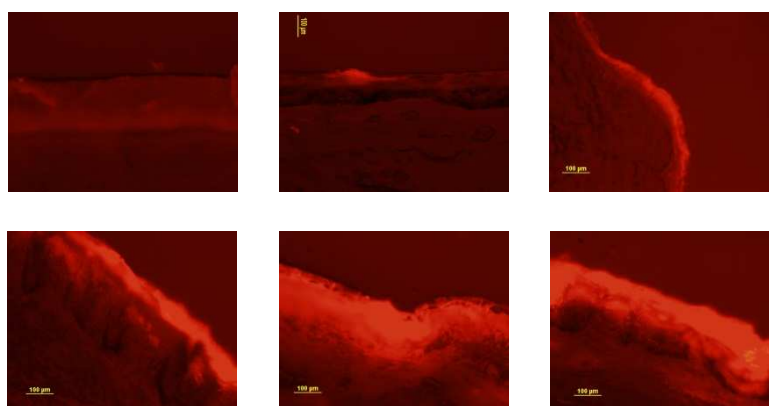


Fig. 12.1 – Representative fluorescence images of the sensitizer permeation used for constructing the visual analogue scale in the factorial design experiments. These images typify an evaluation of the amount of sensitizer and its distribution across the minipig epidermis (0 – no permeation; 5 – maximum permeation).

2. Materials

Mn^{III}5,10,15,20-tetraphenylporphyrinate (Mn-TPP), Mn^{III}5,10,15,20-tetraundecylporphyrinate (Mn-TUP) and Mn^{III}5,10,15,20-tetrakis(4-sulphonylphenyl) porphyrinate acetate (Mn-TPPS) were gently given by Prof. Dr. M. M. Pereira. Polystyrene (Mr. 20 kDa), Allura Red, Amarante, New Coccine, Propylene glycol, Methanol and Triethanolamine and Brilliant Blue G were purchased from Sigma-Aldrich. EpolightTM 1178, 1117, 1151 and 3072 were purchased from Epolin, INC. Triazenes were a gently gift from Thomas Lippert group. The commercial black polystyrene used in chapter 6 was recycled out-of-the-shell from a disk. Oleic acid (OA) and ethanol absolute were purchased from Merck. Dimethylsulfoxide (DMSO) and oleic acid were purchased from Fisher Scientific. Azone[®] (with the commercial name Laurocapram) was purchased from NetQem. Glycerin was purchased from Pronolab. DPPC (Dipalmitoylphosphatidylcholine) and DPH (1,6-Diphenyl-1,3,5-Hexatriene) were purchased from Avanti Polar Lipids, INC. Carbopol 940 was purchased from Molecular Probes[®]. Water was distilled on the laboratory. The sensitizers were a gift from Luzitin SA. GFP were purchased from Merck Milipore[®], with a molecular weight 28 kDa. GFP plasmid (gWizGFP) was purchased from Aldevron, Fargo, ND. The pEGFPC3 DNA plasmid was gently given by José Ramalho, Centro de Oftalmologia e Ciências da Visão, FMUC and lipofectamine purchase from InvitrogenTM.

3. Methods

3.1 Production of Piezophotonic Materials

The light-to-pressure transducer films were casted from a mixture of polystyrene and either Mn^{III}5,10,15,20-tetraphenylporphyrinate (Mn-TPP) or Mn^{III}5,10,15,20-tetraundecylporphyrinate (Mn-TUP) using an Elcometer 3505 cube film applicator. Polystyrene and toluene were mixed and stirred until complete solubilization of the polymer. The PAC reference compound was then added to polystyrene/toluene solution and all the mixture was stirred until the dye was completely dissolved. Air bubbles resulting from stirring were eliminated placing the polystyrene/toluene/dye in an ultrasonic bath for 2 minutes. Finally, the mixture was poured into the mold and spread on a clean glass lamina. The film deposited by casting was dried at room temperature and then removed from the lamina. The thicknesses of the films were measured with a digital micrometer.

Nanoporous titania films were prepared from a TiO₂ sol (HT/SP from Solaronix®). The colloidal thin films, [1.75; 2.5; 3.25] μm, were distributed in a screen printing previously acquired with required thicknesses. The larger films [5; 7.5] μm were made using the squeegee print method. The colloid was distributed with a glass rod sliding over a rim circle made of Scotch Magic adhesive tape (3M). After air drying, the films were sintered in an oven at 500 °C for about 90 minutes. Mn^{III}5,10,15,20-tetrakis(4-sulphonylphenyl) porphyrinate acetate (Mn-TPPS) was adsorbed to the surface of nanoporous titania by immersing glass slides coated with TiO₂ in an ethanolic solution of the dye for the period of time required to attain the desired absorptivity. The absorbances at 471.5 nm were matched at 0.5. These methods produce a uniform titania layer with a homogenous monolayer of dye adsorbed onto it [179]. The production of the piezophotonic materials were done at 22 °C.

3.2 Generation of Photoacoustic Waves

The generation of the PA waves with excitation at 484 nm and 472 nm employed an EKSPLA OPO model PG-122 pumped by an EKSPLA NL301G Nd:YAG laser delivering 4-6 ns pulses. Exploratory work with minipigs and the delivery of GFP employed a Spectra Physics Quanta Ray 130 Nd:YAG laser to generate the photoacoustic waves. The delivery of the bacteriochlorin and the work with volunteers used a portable Quantel Big Sky Ultra 50 Nd:YAG laser attached to a second harmonic generator (532 nm wavelength output, 8 ns pulse duration) to generate the photoacoustic waves. In the latter case, the laser pulse was directed to an optical fiber that delivered the light to the light-to-pressure converter. This material was confined between an optical window and a mirror using silicone as acoustic coupler. The mirror reflected the light back to the piezophotonic material and protected the skin from the laser light. The photoacoustic waves were transmitted to the skin by physical contact with the back of the mirror (acoustic coupling with silicone or ultrasound gel).

3.3 Large Unilamellar Vesicles Preparation

The DPPC (Dipalmitoylphosphatidylcholine) and the fluorescent probe, DPH (1,6-Diphenyl-1,3,5-Hexatriene), were mixed in the form of large unilamellar vesicles (LUV) prepared by evaporation of DPPC and DPH solution, in the azeotropic mixture of chloroform and methanol (87:13, V:V) at a final lipid:probe ratio of 1:100. The vesicle film hydration was prepared by solubilization in an aqueous buffer (PBS, pH = 7.4, molarity of 0.1mM), and the final LUV's arise from extrusion (Extruder from Lipex Biomembranes, Vancouver, British Columbia, Canada) through 100 nm pore size filters

(Nucleopore, Whatman, Springfield Hill, U.K.) at 55 °C [198, 200]. All the experimental solutions were kept above the DPPC gel-liquid melting temperature (41 °C) and the anisotropy measurements performed at the final lipid concentration of 0.1 mM. The experimental design relates different PA waves application times, 0.5, 2 and 5 minutes, and DPPC transition temperature, 40, 41 and 42 °C. The delivery of the photoacoustic waves to the lipid solutions used a portable Quantel Big Sky Ultra 50 Nd:YAG laser attached to a second harmonic generator (532 nm wavelength output, 8 ns pulse duration) with the piezophotonic being produced from a polystyrene/ Mn-TPP mixture.

The fluorescence anisotropy measurements were done in a Cary Eclipse fluorescence spectrophotometer (Varian®) equipped with a thermostatted multicell holder. UV-visible absorption spectral analysis was performed in a Unicam UV530 spectrophotometer (Cambridge, UK). Data was analysed using Microsoft Excel® and Solver®. The DPH quantification was made by absorption spectroscopy at 359 nm ($\epsilon = 91,000 \text{ cm}^{-1} \text{ M}^{-1}$) [264].

3.4 Transepidermal Water Loss (TEWL) Experiments

Healthy volunteers gave their informed consent to participate in the measurement of TEWL in both of their forearms, before and after the application of photoacoustic waves. They were informed that the application of the laser-generated photoacoustic waves took 2 minutes, and that they could ask to interrupt the experiment at any time. Subjects with a history of atopic dermatitis, asthma, contact dermatitis or allergy were excluded from the study. Each subject was tested in both forearms with the same procedure, except that in the first procedure the laser shutter was kept closed (laser OFF). The subjects were not informed that the first exposure was a control experiment. It was planned to exclude from the study, the volunteers reporting any discomfort in this first exposure (laser OFF), but this case was not observed and all the participants finished the experiment. The TEWL measurements were made with the following procedure, in a temperature-controlled room (20 °C and 40-50% of relative humidity), only in the presence of one volunteer and, occasionally a second one for acclimatization, and two investigators: 1) A circular area with 1 cm diameter was marked in each forearm and cleaned with medical cotton. 2) The erythema in this area was measured. 3) One investigator measured the TEWL in this area for at least 1 minute after stabilization of the measurements. 4) A thin layer of silicone was spread over the selected area. 5) The investigator pressed gently the device generating the photoacoustic waves against the selected area for 2 minutes – the volunteer did not know of the existence of a laser shutter. 6) The selected area was cleaned with medical cotton in ca. 15 seconds. 7) One investigator measured the TEWL in this area for

at least 1 minute after stabilization of the measurements. 8) The erythema in this area was measured again. Transepidermal water lost (TEWL) was measured using a Courage + Khazaka open chamber probe, model Tewameter® TM 300. Erythema was measured using a Courage + Khazaka probe, model Mexameter® MX 18.

The pain associated with each PW application was determined using a visual analogue scale where the volunteers were asked to situate the rating pain, from 0 (no pain) to 10 (worst pain ever).

In the case of the animal experiences, the methodological approach was adapted concerning the handling of the minipig and its anatomic profile, but the overall description remains the same.

3.5 Tissue Preparation

Female minipig skin was obtained following abdomnoplasty from a single donor. Immediately after excision, the skin was wrapped in aluminium foil and stored at -20 °C. Under these conditions, the skin is stable over 6 months, regarding penetration of drugs, as well the thickness of the stratum corneum [1-3]. In the night previous to the experiment, the skin is defrosted at +4 °C. Afterwards, we collect the fat tissue, the skin samples for the transdermal drug delivery of the sensitizers were cut in 2x2cm squares, and an adhesive tape with 4mm of diameter was placed on the skin. A cylindrical roll was used to assure adhesion between the tape and skin.

Concerning the fluorescence microscopy experiments, the skin samples collected require tissue fixation [4, 6]. The first step in the fixation process involved immersion in paraformaldehyde (4% in aqueous solution) for at least 24 h. Next, the samples were transferred to a 25% sucrose solution for at least 48 h. Following this treatment, the skin samples become denser than the sucrose solution and the tissue is considered immobilized. After the transdermal delivery studies, the skin samples for microscopy analyses were extracted with a 4 mm biopsy punch, frozen in dry ice and then mounted in a holder with Tissue-Tek O.C.T. Compound (Sakura Finetek Europe B.V., Zoeterwoude, The Netherlands). The skin slices are selected to be of 25 to 100 µm of thickness by a cryostat. The skin slices are kept refrigerated until fluorescence microscopy and confocal microscopy analyses.

3.6 Preparation of the Transdermal Formulations

The photosensitizers' uptake into the skin was performed using a Carbopol type gel with high water percentage. The gel preparation was done in three steps. First, the solvents of the gel base were introduced in the following order and stirred magnetically at 2400 rpm: 6% of glycerin, 1.35% of triethanolamine, 1% of carbopol 940, 15% of ethanol absolute and 76.65% of distilled water. Next, the sensitizers were dissolved in the following solvent mixture (% w/w): ethanol (10.8%), propylene glycol (36%), Azone (4%), distilled water (6%), and subject to 1 minute of ultrasound to assure complete solubilization. Finally, this solution was added to the gel base. The final concentration of the sensitizers in the gel was 0.1-0.3 %. To avoid degradation and maximize polymer swelling, the gels were prepared 24 hours before the experiment and kept at +4 °C. The determination of the formulations viscosities was done using a Rheometer (*StressTech*®).

Green Fluorescence Protein (GFP) formulation was prepared in the gel base receipt. GFP was dissolved in water and then the other components of the gel base were added, together with Azone (4%). The final concentration of the GFP in the gel base was 0.1%, and this was the topical GFP formulation employed in this work.

3.7 Transdermal Drug Delivery Studies

The photosensitizers' application in each skin punch was performed with an insulin needle. 0,2 mL of gel was applied and kept on the skin for the desired contact time for releasing purposes, with occlusion (*Tegaderm*® and aluminium foil). The remaining gel is removed with a spatula and the surface cleaned with cotton soaked in ethanol. The skin site is excised, frozen and the penetration profiles are obtained by examining the skin with microscopy analysis or the quantitative approach (extraction).

3.8 Extraction Procedure

In order to evaluate the quantities of the sensitizers delivered to the skin, a specific quantification method was developed. A 4 mm biopsy punch was taken from the skin experiment site and sectioned in the smallest pieces possible with a scalpel. These pieces were transferred to a cup glass along with a certain volume of dichloromethane and crushed with a shredder, *YSTRAL Micro Shaft 6G*. Afterwards, the remaining shredded skin undergoes an extraction procedure for 6 hours with a suitable solvent. For these sensitizers, dichloromethane represents the correct choice taking in account its lipophilicity and the one from skin. Fluorescence calibration curves 10^{-6} - 10^{-9} M were performed in the extractor solvent to validate the methodology used. Finally, the mass

delivered onto the skin was determined for each essay substituting its fluorescence in the calibration curve. The sensitizers used are particularly appropriate for these fluorescence determinations because they present a very characteristic fluorescence with a peak at 646 and 752 nm.

3.9 Transdermal Delivery in Minipigs

In vivo tests employed minipigs obtained from IMIDRA (Instituto Madrileño de Investigación y Desarrollo Rural, Agrario y Alimentario) - Aranjuez (Madrid). They were aged 6-8 months, white with brown spots, and with weights ca. 60 kg. They were received at INRB (Instituto Nacional de Recursos Biológicos), Vale de Santarém, Portugal, where they were accommodated in individual boxes with 1.5 m², feed with a standard diet for pigs and water *ad libidum*, for an acclimation period of three weeks. The study was performed in accordance to the Portuguese ethical guidelines on a license granted by *Direcção de Serviços de Saúde e Protecção Animal*, ref. 0420/000/000/2007. Access to food was suspended 24 h hours before treatment. The backs of the animals were shaved 24 h prior to the *in vivo* application of the dermatological formulations. The production of the transdermal formulations, laser system (Big Sky ND:YAG nanosecond laser) and piezophotonic materials (Mn-TUP and Mn-TPP based thin films in polystyrene) employed in these experiments were described previously. All procedures were carried out under anaesthesia. The pre-medication employed 30 min in advance was: Azaperone (Stresnil® - Veterinaria ESTEVE – Spain), 2 mg/kg intramuscular injection + atropine sulphate, 50 mg SC. The induction was done with ketamine (Clorketam® - Vétoquinol, France), 20 mg/kg by intramuscular injection. The anaesthesia was maintained with endotracheal intubation, using spontaneous ventilation with 2-3 l/min of oxygen + 3% isoflurane (Isoflo® - Veterinária ESTEVE, Spain). The skin biopsies were collected under the anaesthesia described above. After the collection of the biopsies, the animals were killed with an overdose of sodium thiopental (25 mg/kg) + 20 ml of 7.5% potassium chloride.

The transdermal delivery and skin biopsies were made with the following procedure in a temperature-controlled room (20 °C and 40-50 % relative humidity) in the presence of the investigators and two veterinary surgeons: i) The back of the minipig was cleaned with ethanol soaked in medical cotton and allowed to dry. ii) Square areas with 1 cm size was delimited on the back of the minipig using adhesive tape, resulting in 15 different squares in each animal. iii) The formulation containing bacteriochlorin or GFP, described above, was applied in the designated area with a spatula, leaving a uniform 1 mm layer of the formulation. iv) The device to generate photoacoustic waves, described above, was

gently pressed against the formulation and the laser was fired. v) The device was removed and more formulation was added to reform the 1 mm layer of formulation. vi) The formulation was occluded with Tegaderm[®] and aluminium foil for the desired amount of time. vii) At the end of the desired contact time, the Tegaderm[®] and aluminium were removed and the formulation was thoroughly cleaned with absorbing paper and then with ethanol soaked in medical cotton. viii) Skin biopsies were collected from each area.

3.10 Cell viability and Cells Transfection Experiments

The cell viability experiments used Human Osteosarcoma cell line (MNNG/HOS) and were analysed using the 3-(4,5-Dimethylthiazol-2-yl)-2,5-Diphenyltetrazolium Bromide (MTT) colorimetric assay. This assay enables the quantification of viable cells based on the reduction of the yellow tetrazolium salt to purple formazan crystals by the mitochondrial enzyme, succinate dehydrogenase of metabolic active cells. The amount of formed formazan crystals can be measured after dissolution with acidified isopropanol. The resulting purple solution is measured spectrophotometrically using an ELISA microplate reader. The cells were exposed to photoacoustic waves through the bottom of a cell culture well (using piezophotonic materials of Mn-TUP, Mn-TPP and New Coccine based thin films in polystyrene). After exposition the cell culture medium was removed and 200 μ L of MTT solution 0.5 mg/mL (M2128, Sigma-Aldrich[®]) were added to each well. The cells were further incubated at 37 °C, in the dark, during 4 hours. Then, 200 μ L of acidified isopropanol (0.04 M HCl) were added to dissolve the formazan crystals. Finally, 300 μ L of the solubilized products were transferred to a 96-well plate (Orange Scientific) and the absorbance was read using an automatic ELISA microplate reader at 570 nm with a reference filter of 620 nm (SLT Spectra-IITM - Austria). The results were expressed as percentage of viable cells in relation to the controls (untreated cells).

For *in vitro* gene delivery into cells, COS-7 cells were cultured in Dulbecco's Modified Eagle Medium with 10% bovine serum and antibiotics (penicillin/streptomycin), in a cell culture incubator at 37°C under an atmosphere of 5% CO₂ in air. After reaching 90% confluence, cells were harvested, seeded in culture dishes and incubated at 37°C for 24 h. Before PA waves exposition, aqueous solution of plasmid DNA coding GFP (gWizGFP and pEGFPC3) was added to the culture medium, making 100 μ g/mL of concentration. Twenty-four hours after laser irradiation, the expression of GFP in the cells was observed by use of fluorescence microscope (DMIRE200 Leica). Cells were visualized using bright field.

Photoacoustic Waves for Transdermal Drug Delivery

The cultured cells were exposed to several experimental conditions, changing the photoacoustic waves intensity and physical characteristics. Diverse laser fluences, irradiation times and piezophotonic materials were used. Distinct plasmid DNA concentrations were tried.

All photoacoustic waves were obtained by irradiating the piezophotonic materials with the output of a portable Quantel Big Sky Ultra 50 Nd:YAG laser attached to a second harmonic generator (at 532 nm). The 8 ns pulse width output was connected to an optical fiber that conducted the light into the light-to-pressure material. This material was confined between an optical window and a mirror using silicone as acoustic coupler. The same acoustic coupler or ultrasound gel was used to couple the produced PA to human or mini pig skin or to the bottom of a cell culture well (in the cell viability and transfection experiments).

4. References

- [1] B.W. Barry, Novel mechanisms and devices to enable successful transdermal drug delivery. *Eur. J. Pharm. Sci.*, 14, (2001) 101-114.
- [2] R. Wickett, M. Visscher, Structure and function of the epidermal barrier. *Am. J. Infect. Control*, 34 (2006) 98-110.
- [3] R. Paus, What is the 'true' function of the skin? *Exp. Dermatol.*, 11 (2002) 159-187.
- [179] C. Serpa *et al*, Photoacoustic Measurement of Electron Injection Efficiencies and Energies from Excited Sensitizer Dyes into Nanocrystalline TiO₂ Films, *J. Am. Chem. Soc.*, 130 (2008) 8876-8877.
- [198] A. Blume, G. Cevc, Ed.; Marcel Dekker. Dynamic Properties. In *Phospholipids Handbook*: New York, 1993.
- [200] W.L.C. Vaz, Properties of Lipid Bilayers. 2008, Wiley Encyclopedia of Chemical Biology.
- [264] R.B. Cundall, I. Johnson, M.W. Jones, E.W. Thomas, Photophysical properties of DPH derivatives. *Chem. Phys. Lett.*, 64 (1979) 39-42.

